The Biochemical and Biophysical Characterisation of $p47^{phox}$ Activation

Farah Hussain

Division of Molecular Structure

The National Institute for Medical Research

London, NW1 1AA, UK

January 2008

A thesis submitted in part fulfilment of the requirement of University College London for the degree of Doctor of Philosophy

ProQuest LLC
789 East Eisenhower Parkway
P.O. Box 1346
Ann Arbor, MI 48106-1346

DECLARATION

I, Farah Hussain, declare that the work described in this thesis was, except where otherwise indicated in the text, entirely my own.

I have not submitted any portion of the work referred to in this thesis in support of any other qualification at this or any other institute of higher learning.

Farah Hussain, January 2008

(Dedicated to my mother Kaneez Hussain)

ABSTRACT

The multi-component enzyme NADPH oxidase plays a central role in host defence against microbial infection, due to its ability to support the production of reactive oxygen species. The enzyme is dormant in resting cells where its six hetero-subunits are separated into cytoplasmic and membrane compartments. Activation and assembly of the NADPH oxidase is a complex process that is regulated, in large part, by changes in protein-protein and protein-lipid interactions. An important step in the activation process is the phosphorylation-induced translocation of the cytoplasmic $p40^{phox}$-$p67^{phox}$-$p47^{phox}$ complex to the membrane-bound heterodimeric $p22^{phox}$-$gp91^{phox}$ complex (flavocytochrome b_{558}). This interaction is prevented in the resting state due to an intramolecular interaction in $p47^{phox}$ that maintains the protein in an auto-inhibited conformation. Phosphorylation of eight serine residues in $p47^{phox}$ is essential for enzyme activation, of which five are located in the polybasic region and are known to relieve the auto-inhibition. Glutamate mutants were made to mimic phosphoserine residues, and various biochemical and biophysical techniques were used to demonstrate that phosphorylation of the remaining three serine residues, located in the C-terminal region, do not contribute to the release of auto-inhibition, and hence do not promote binding to $p22^{phox}$. Instead, they weaken the interaction with $p67^{phox}$. Based on these data, a new model for phosphorylation-induced changes in NADPH oxidase assembly is proposed.

Binding of the polybasic region and $p22^{phox}$ to the tandem SH3 domains of $p47^{phox}$ occurs with high affinity. This affinity is mediated through the formation of a 'superSH3 domain', which is largely dependent on two structural features: the covalent SH3-SH3 linker and a 'GWW' motif located in the n-Src loops of either SH3 domain. Mutant proteins were made and quantitative binding assays were performed to demonstrate that the chemical nature of the linker is more important for the intramolecular interaction with the polybasic region in the auto-inhibited state, than for an intermolecular interaction such as that with $p22^{phox}$ in the active state. Furthermore, it was shown that the tryptophan residues of the GWW motif play different roles in the stabilisation of the superSH3 domain conformation. Their precise role depends on whether additional interactions between the superSH3 domain and its target can occur outside of the conserved ligand binding site, as observed in the auto-inhibited state. These data suggest that the sequence requirements for the formation of a superSH3

domain are relatively flexible, making it more likely that other proteins containing multiple SH3 domains may also form a superSH3 domain.

ACKNOWLEDGMENTS

Firstly, I would like to thank Dr. Katrin Rittinger who gave me the opportunity to carry out this project. She has been an excellent supervisor, guiding and supporting me throughout. I also thank the Medical Research Council for funding this project.

A special thank you goes to my lab colleagues, I especially thank Dr. Karine Lapouge and Dr. Yvonne Groemping who helped me during the early stages of my PhD, Dr. Daniela Jozic and Dr. Sujit Dutta for humour, insults and helping me keep my sanity.

I also acknowledge all those people at the NIMR who have helped me in someway or another. My particular thanks to Dr. Phillip Walker for being the 'rock' of the division, Dr. Stephen Martin for help with CD spectroscopy, Dr. Simon Pennell for his patience and kindness in the critical reading of this thesis, the photographics department, and the NIMR library. I would also like to thank my friends at the NIMR and all the members of the Molecular Structure group who have made working here such a pleasant experience. I further acknowledge Dr. Roger Williams (MRC-LMB Cambridge) for his help with the lipid sedimentation work.

I extend my gratitude to my family, especially my mother for her undying love, support and encouragement. Finally, where would I be without my very patient and tolerant partner, to him thanks for his emotional support, and always keeping my spirits high during the writing of this thesis.

CONTENTS LIST

FIGURES LIST

TABLES LIST

ABBREVIATIONS LIST

ΔG	Gibbs free energy
ΔH	Enthalpy
ΔS	Entropy
λEX	Excitation wavelength
λEM	Emission wavelength
3C	3C-precision protease
aa	Amino acid
b.p.	Base pairs
BSA	Bovine serum albumin
CD	Circular dichroism
CG	Cathepsin G
CGD	Chronic granulomatous disease
DPI	Diphenylene iodonium
DTT	Dithiothreitol
EDTA	Ethylenediamine tetra-acetic acid
FAD	Flavin adenine dinucleotide (oxidised form)
fMLp	N-formylated peptide
GST	Glutathione S-transferase
H_2O_2	Hydrogen peroxide
HOCL	Hypochlorous acid
IL	Interleukin
IPTG	Isopropyl β-D thiogalactoside
ITC	Isothermal titration calorimetry
K_a	Association constant
K_d	Dissociation constant
LB	Luria-Bertani media
MAC	Membrane attack complex
MBL	Mannose-binding lectin
MPO	Myeloperoxidase
MWCO	Molecular weight cut off
n	Stoichiometry
NADPH	Nicotinamide-adenine dinucleotide phosphate (reduced)

NE	Neutrophil elastase
NKT	Natural killer T
nrdb	Non-redundant data base
$O_2^{\cdot-}$	Superoxide radical
$OH^{\cdot}$	Hydroxyl radical
PA	Phosphatidic acid
PC	Phosphatidylcholine
PCR	Polymerase chain reaction
PDB	Protein data bank
PE	Phosphatidylethanolamine
phox	Phagocytic oxidase
pI	Isoelectric point
PKC	Protein kinase C
PMA	Phorbol myristate acetate
PMN	Polymorphonuclear leukocytes
PR	Proline-rich
PS	Phosphatidylserine
PtdIns	Phosphoinositide
PX	Phox homology
ROS	Reactive oxygen species
rpm	Revolutions per minute
RT	Room temperature
SDS-PAGE	Sodium dodecyl sulphate polyacrylamide gel electrophoresis
SH3	Src-homology domain
SOD	Superoxide dismutase
SPR	Surface plasmon resonance
TB	Terrific broth
TCA	Trichloroacetic acid
TLR	Toll-like receptor
TPR	Tetratricopeptide repeats
UV	Ultraviolet
WT	Wild-type
°C	Centigrade
K	Kelvin

hr	Hour
min	Minute
sec	Second
kDa	kilo Dalton
Kb	Kilo base
Å	Angstrom (0.1 nm)
mg	Milligram (10^{-3} grams)
mm	Millimetre (10^{-3} metre)
ml	Millilitre (10^{-3} litre)
mM	Millimolar (10^{-3} molar)
µg	Microgram (10^{-6} grams)
µl	Microlitre (10^{-6} grams)
nm	nanometre (10^{-9} metres)

SYMBOLS FOR AMINO ACIDS

A	Ala	Alanine
B	Asx	Asparagine or aspartic acid
C	Cys	Cysteine
D	Asp	Aspartic acid
E	Glu	Glutamic acid
F	Phe	Phenylalanine
G	Gly	Glycine
H	His	Histidine
I	Ile	Isoleucine
K	Lys	Lysine
L	Leu	Leucine
M	Met	Methionine
N	Asn	Asparagine
P	Pro	Proline
Q	Gln	Glutamine
R	Arg	Arginine
S	Ser	Serine
T	Thr	Threonine
V	Val	Valine
W	Try	Tryptophan
Y	Tyr	Tyrosine
Z	Glx	Glutamate

CHAPTER ONE

1.0 Introduction

The human immune system is complex set of mechanisms, which protects the host against infection by invading pathogens such as bacteria, viruses, fungi and multicellular parasites. The system involves a whole range of proteins, cells, tissue and organs, which work in a dynamic manner, discriminating between self and non-self molecules to effectively clear the infection. The human immune system is composed of two distinct pathways; the innate immune system and the adaptive immune system. The former is directed against a wide variety of pathogens and is the first line of defence against microorganisms. However, it does not confer protective or long-lasting immunity to the host and in some instances infections cannot be resolved by innate immunity alone. The later, although slower to respond is extremely specific and in most cases the response provides life long immunity against re-infection from a specific pathogen. However, due to the slow response of the adaptive immune system (4-7 days) it is the innate immune response, which is critical in controlling infection in the early stages of infection. Together, the innate and adaptive immune responses act in concert to provide an effective system capable of preventing and clearing established infections (Chaplin, 2006; Hoebe et al., 2004; Janeway, 2001).

1.1 The innate immune response is the first line of defence

The first line of defence in the innate immune system involves physical barriers such as skin and mucosal linings (section 1.1.1). However, if this immediate defence mechanism is overcome by the pathogen then non-specific cellular and chemical responses are activated for the destruction of invading pathogens. There are two key cellular components which mediate an innate immune response; macrophage and mast cells (section 1.1.4.2) (Galli, 2000; Gordon, 1995). Both of these cell types are widely distributed within the body and respond immediately when physical barriers are penetrated by pathogens. Macrophages possess various functions but in innate immunity its major role is to recruit other effector cells to the site, and in particular phagocytic neutrophils. Phagocytosis and pathogen destruction by neutrophils is the central defence weapon in cell mediated innate immunity (Scapini et al., 2000). Mast cells on the other hand are involved in stimulating local inflammation by releasing a cocktail of

inflammatory mediators, and enhancing inflammation by recruiting further leukocytes to the site of injury. A further key component in the innate immune system is the complement system; a family of proteins which react with one another on the surface of pathogens to aid their clearance. Complement activation not only enhances phagocytosis and inflammation but can also induce cell lysis of targets directly (section 1.1.5) (Morgan et al., 2005; Muller-Eberhard, 1988; Reid, 1986; Reid and Day, 1989; Tomlinson, 1993). All of these key components involved in the innate immune response are described in more detail below (Figure 1).

1.1.1 Surface barriers and mucosal immunity

The body is protected by epithelia tissue such as skin and the mucosal linings of gastrointestinal, respiratory and urogenital tracts. The skin is the fist line of defence and provides a barrier against invading pathogens, and unless this barrier is compromised most pathogens cannot penetrate it. Epithelia also actively inhibit microbial growth through the secretion of microbicidal and microstatic compounds (Braff and Gallo, 2006). Oily sebum produced by sebaceous glands in the skin contains lactic acid and fatty acids which are toxic to some pathogens. In addition, these substances regulate the skins acidic nature (pH < 7.0) which inhibits bacterial growth. Furthermore, the presence of microbial flora on the surface of skin prevents pathogens from colonising the tissue, by competing with pathogens for nutrients and by producing bacteriocins that inhibit their growth (Kitano and Oda, 2006). The mucosal lining of gastrointestinal, respiratory and urogenital tracts produce mucous which trap invading pathogens and prevent them from adhering to the epithelium (Boyton and Openshaw, 2002). Mucous also contains various proteins such as lysozyme which is capable of destroying bacterial cell walls by targeting peptidoglycans, and the iron binding protein lactoferrin. Iron is required by all pathogens and the presence of lactoferrin competes for free iron, thereby depriving the pathogen of the mineral (Levay and Viljoen, 1995; Rogan et al., 2006). In addition, the mucociliary escalator of the respiratory tract continually moves mucous out from the lungs allowing microorganisms and debris to be removed by coughing and sneezing mechanisms. Other ejection mechanisms include perspiration, nasal secretions, saliva and tears. At this point if a pathogen is successful in overcoming the physical barriers of the innate immune system then non-specific chemical and cellular responses are triggered. These can include inflammation, various cells of the innate immune response, and activation of complement, phagocytosis and destruction of the pathogen.

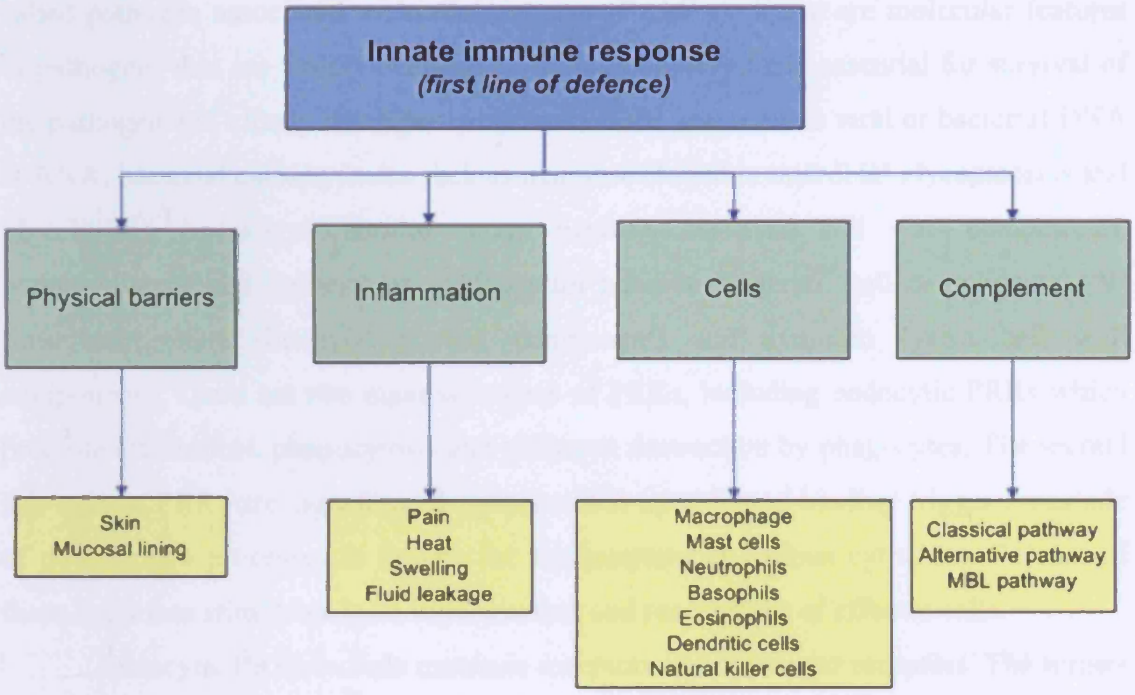

Figure 1: Overview of the innate immune system. The innate immune system is the first line of defence against invading pathogens. It involves physical barriers such as the skin and mucosal linings. If these barriers are breached or irritated by pathogens, then non-specific chemical and cellular responses are activated. These include inflammation which serves to prevent the spread of infection, to destroy the pathogen and to subsequently aid in the repair and healing of damaged tissues. Importantly, innate immunity depends on a wide variety of cell types which i) mediate inflammation and ii) mediate the destruction of pathogens. Moreover, both of these processes can be triggered as a result of complement activation. Some of the cell types involved in innate immunity are also involved in triggering an adaptive immune response, which provides a more specific defence and results in a life long immunity (Janeway et al., 2001).

1.1.2 Pattern recognition receptors (PRRs) and pathogen-associated molecular patterns (PAMPs)

One of the major problems of the innate immune system is how to distinguish between 'self' and 'non-self'. To solve this problem phagocytic cells have evolved a range of receptors called pattern recognition receptors (PRRs), which recognise so-called pathogen associated molecular patterns (PAMPs). These are molecular features of pathogens that are widely distributed, highly conserved and essential for survival of the pathogen and clearly distinguishable from 'self' and include viral or bacterial DNA or RNA, bacterial carbohydrates such as mannose (found in microbial glycoproteins and glycolipids), lipopolysaccharides (gram negative bacterial cell wall component), peptidoglycans and lipoteichoic acids (gram positive bacterial wall components), N-formylmethionine (bacterial protein component) and zymosan (yeast cell wall component). There are two main sub-types of PRRs, including endocytic PRRs which promote attachment, phagocytosis and pathogen destruction by phagocytes. The second sub-type of PRRs are signalling receptors which upon ligand binding trigger a cascade of downstream processes to initiate the transcription of various cytokines. Release of these cytokines stimulates local inflammation and recruitment of effector cells.

Endocytic PRRs include mannose receptors and scavenger receptors. The former belong to the family of Ca^{2+}-dependent lectin family, which bind via their carbohydrate binding domains to pathogen cell wall sugars such as mannose and fucose (Ezekowitz et al., 1990). These domains are fixed in a specific orientation and bind to residues which are found in correct spacing on the surface of a wide range of pathogenic microbes (Apostolopoulos and McKenzie, 2001; Stahl and Ezekowitz, 1998). Scavenger receptors are known to bind low density lipoproteins and various negatively charged ligands on gram negative and gram positive bacteria, for example lipoteichoic acid on *Staphylococci* and *Streptococci* (Dunne et al., 1994).

The group of signalling PRRs include the family of toll-like receptors (TLRs), the glycoprotein CD_{14}, and the family of nucleotide-binding oligomerization domain (NOD) receptors. At least eleven different TLRs exist of which some are expressed extracellularly and others within endosomes. TLRs recognise a broad range of microbial products including peptidoglycans, lipopollysaccharides, bacterial lipopeptides and various others (Aderem and Ulevitch, 2000; Hayashi et al., 2003; Takeda and Akira, 2005). Different TLRs can recognise different microbial components. For example

TLR-4 is important for the recognition of lipopolysaccharides (Poltorak et al., 1998), where as TLR-2 recognise a wider range of microbial components including peptidoglycans and lipoteichoic acid (Schwandner et al., 1999; Takeuchi et al., 1999). On the other CD14 can recognise both lipopolysaccharides and peptidoglycans (Antal-Szalmas, 2000). In contrast, NOD receptors are cytosolic proteins and recognise for example intracellular peptidoglycan components (muramyl dipeptides) of gram negative and gram positive bacteria (in the case of NOD1 and NOD2) (Bertin et al., 1999; Inohara et al., 1999; Ogura et al., 2001).

Secreted PRR proteins also play an important role in activating the innate immune response. One of the most important is the serum protein, mannan binding lectin (MBL) (Ma et al., 2004). MBL recognises mannose containing residues found on the surface of pathogens, which activates the MBL complement pathway to produce C3b complement proteins. These bind to the surface of pathogens thereby opsonising them for phagocytosis (refer to section 1.1.5 for details on the MBL complement activation pathway).

1.1.3 Inflammation

Inflammation is the first response to local injury and microbial invasion, which occurs to localise infection, to destroy the pathogen, and to aid in the repair of damaged tissues. Mast cells play a central role in inflammation as degranulation of these cells release inflammatory mediators such as histamine and prostaglandins to induce localised vasodilatation; the precursor effect of inflammation. Vasodilatation causes an increase in blood flow (which is associated with the redness and heat observed), which increases the delivery of phagocytes such as neutrophils and complement proteins to the injured tissue. The delivery of these components and their actions is associated with the pain observed with inflammation. Vasodilatation also causes capillaries to stretch and separate thereby increasing permeability, allowing plasma to escape to surrounding areas to induce swelling of the affected area. During this process plasma proteins and chemotactic factors also escape, further recruiting phagocytes such as neutrophils to the site of injury. Tissue based phagocytic macrophages also play a role in inflammation as they secrete various chemokines, which attract further phagocytes to the injured site.

1.1.4 Cells of the immune system

The cells of blood derive from the same progenitor/precursor stem cells of the bone marrow. Pluripotent hematopoietic stem cells can differentiate into cells that are involved in the immune system, which can be further divided into two types; the lymphoid progenitor cells and the myeloid progenitor cells (Figure 2). The lymphoid lineage gives rise to lymphocytes such as B cells and T cells that are primarily involved in the adaptive immune system. The myeloid lineage gives rise to monocytes/macrophage, mast cells, polymorphonuclear leukocytes (PMN's) and dendritic cells; which are involved in the innate immune response although some are also linked with the adaptive immune system (Dexter and Spooncer, 1987; Golde, 1991).

1.1.4.1 Cellular barriers of the innate immune system

A whole variety of cells are involved in the innate immune system for the effective clearance of infection. One of the most important cell types are phagocytes such as macrophage (Gordon, 1995) but more importantly neutrophils (Scapini et al., 2000). These cells patrol in search of invading pathogens, engulfing foreign particles and destroying them. Briefly a pathogen is engulfed into a phagosome, which then fuses with a lysosome. These lysosomes possess granules that contain a cocktail of destructive enzymes, and it is the combined action of a respiratory burst producing highly reactive oxygen species and the release of these granular enzymes, which ultimately destroys the phagocytosed pathogen. Other cell types important in innate immunity include those that mediate inflammation such as mast cells and basophils (Galli, 2000), and those that activate the adaptive immune response such as macrophage and dendritic cells (Banchereau et al., 2000; Palucka and Banchereau, 1999) for longer term defence. All of these cell types are discusses in more detail below.

1.1.4.2 Macrophage and mast cells

Monocytes continuously circulate the blood and migrate to tissues where they differentiate into macrophage. Macrophages are phagocytic and although they represent

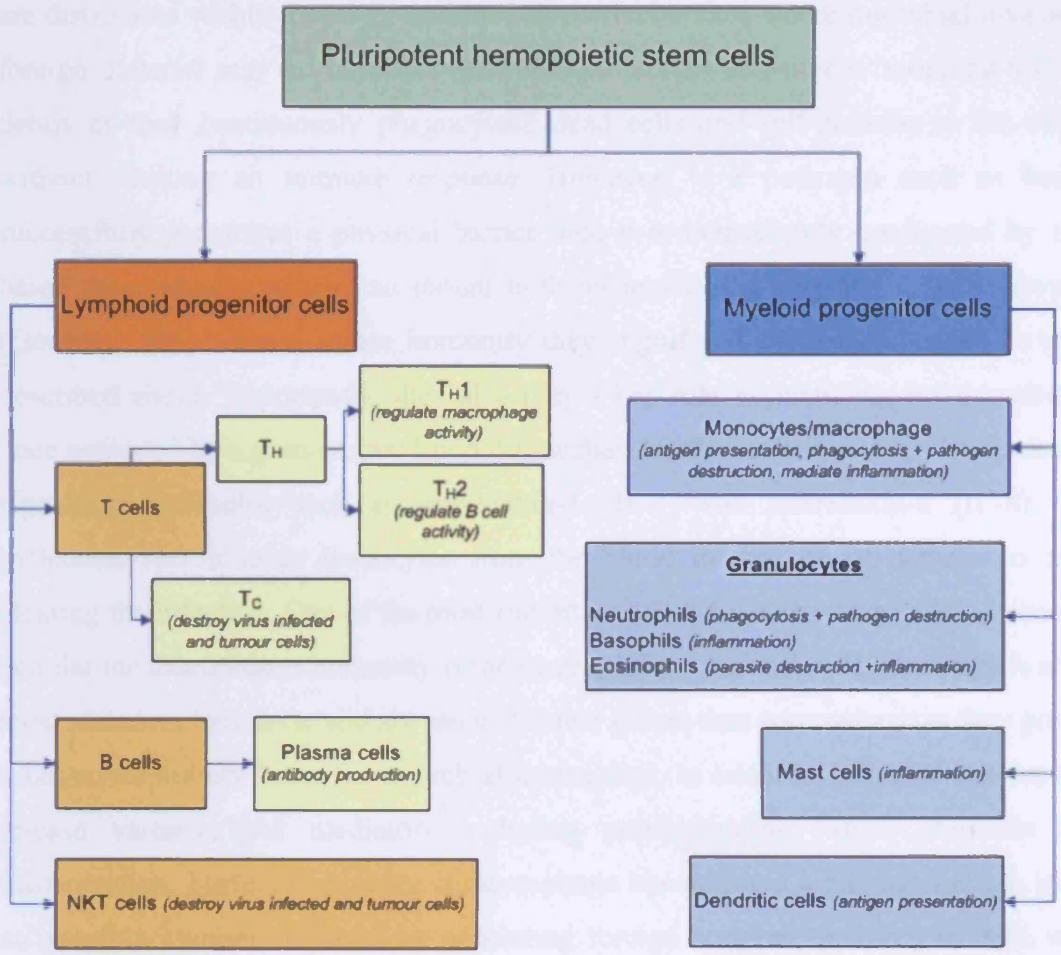

Figure 2: The cellular elements of blood involved in the immune system. Pluripotent hematopoietic stem cells give rise to lymphoid progenitor cells and myeloid progenitor cells. Lymphoid progenitor cells proliferate and differentiate into T lymphocytes and B lymphocytes which are involved in the adaptive immune response. One type of T lymphocyte (T_c) directly destroys pathogens where as the other (T_H) activates other effector cells such as macrophage or B cells for pathogen destruction. Although natural killer (NK) cells derive from the lymphoid lineage they are involved in the innate immune response. Myeloid progenitor cells proliferate and differentiate into granulocytes, mast cells, dendritic cells and macrophages, all of which are involved in the innate immune response and some of which are involved in regulating the adaptive immune response (adapted from Janeway et al. 2001).

less than 10 % of total leukocytes, they are extremely versatile in their function. They are distributed within the body stationed in particular sites where microbial invasion or foreign material may accumulate. Macrophages act as scavengers 'mopping-up' local debris as they continuously phagocytose dead cells and self-proteins in the vicinity without evoking an immune response. However, if a pathogen such as bacteria successfully penetrates a physical barrier then it is immediately confronted by tissue based macrophages which can mount both an innate and adaptive immune response (Gordon, 1995). During innate immunity they engulf and destroy pathogens as briefly described above. Importantly, they also play a key role in mediating inflammation, as once activated by e.g. microbial lipopollysaccharides they release a complex cocktail of signalling molecules such as interleukin-1 (IL-1) and interleukin-8 (IL-8). Such molecules recruit more leucocytes from the blood to the site of damage to aid in clearing the infection. One of the most important cell types to be recruited and central to cellular mediated innate immunity is the neutrophil (section 1.1.4.3). Neutrophils are the most abundant leukocyte and are more efficient killers than macrophage as they produce a larger respiratory burst for microbial destruction. In addition activated macrophages release various lipid mediators including prostaglandins, which stimulate local inflammation. Furthermore, once a macrophage has digested a pathogen it can initiate an adaptive immune response by presenting foreign antigens to T helper cells, which stimulate B cells for antibody production. Together this makes the macrophage an extremely versatile cell type, linking the innate and adaptive immune responses together (Gordon, 1995).

Mast cells mature in tissues and are widely distributed within the body. They possess granules which store a whole host of inflammatory mediators such as histamine and prostaglandins, thus play a key role in stimulating inflammatory responses (section 1.1.3). Mast cells can be activated to release these mediators through various means including physical/mechanical trauma, and the binding of anafylatoxins such as C5a to specific cell surface complement receptors (section 1.1.5). Once activated, mast cells release chemokines that recruit other leukocytes to the injured site such as eosinophils and basophils (1.1.4.3) to further stimulate the inflammatory response (Galli, 2000; Galli et al., 1991; Plaut et al., 1989; Wodnar-Filipowicz et al., 1989). Together macrophages and mast cells act as effector cells in first line of host defence.

1.1.4.3 The polymorphonuclear leukocytes

The polymorphonuclear leukocytes (PMN's) include neutrophils, eosinophils and basophils, all of which circulate the body until they are recruited to sites of infection and inflammation for pathogen destruction. Examples of recruitment signals for these cell types include N-formylated peptides e.g. fMetLeuPhe (by products of bacterial sections), cytokines such as IL-1 and IL-8 released by macrophages, histamine released by mast cells and basophils, and C3a/C5a produced during complement activation (Fernandez et al., 1978; Ryan and Hurley, 1966). The name PMN's originates from the fact that these cells contain many (poly) differently shaped (morpho) nuclei. These cells are also referred to as 'granulocytes' due to the presence of granules within their cytoplasm.

Neutrophils are the major cellular component of the innate immune system and play a fundamentally important role in eliminating non-viral infections. They are the most abundant leukocyte making up approximately 70 % of all leucocytes, and are one of the first cells type to be recruited to sites of damage (Scapini et al., 2000). Neutrophils are professional killers which recognise, phagocytose and destroy ingested microorganisms or particles through the action of oxygen dependent mechanisms and oxygen independent mechanisms. The oxidative pathway involves the activation of the enzyme, Nicotinamide-adenine dinucleotide phosphate (NADPH oxidase) (refer to section 1.3) which produces a respiratory burst of superoxide radicals ($O_2^{\cdot-}$), and the non-oxidative pathway involves the action of neutrophil granule proteins. More recently it has been shown that these two pathways may in fact merge into one for effective microbial killing, as discussed in greater depth in sections 1.2 and 1.3.

Eosinophils make up less than 5 % of total leukocytes and are predominantly involved in eliminating parasites. Once recruited to sites of infection they bind C3b opsonised parasites (C3b produced during alternative pathway complement activation by the parasite), which activates them to release their granule contents. These include cationic proteins, major basic protein (MBP), histaminase, arylsulphastase B and peroxidase, which together damage the parasite membrane. Eosinophils are phagocytes although not very effective ones as many parasites are too large to be engulfed, hence the reason why degranulation takes place outside the eosinophil. Eosinophils are also associated with inflammation as their granular proteins can damage host tissues (Capron, 1991).

Basophils on the other hand play more of a role in stimulating inflammation, and in contrast to neutrophils and eosinophils they are non-phagocytic. Basophils can be recruited to and activated at sites of damage through complement proteins, or by chemokines released by tissue based mast cells. Activation causes them to release their granular contents such as histamine into their surrounding which stimulates inflammation. Basophils, mast cells and eosinophils are also associated with allergic responses as they carry Fc receptors for IgE. Upon exposure to an allergen, allergen specific IgE are produced which bind to these receptors, and upon re-exposure the specific allergen binds to IgE on the surface of the leukocyte, inducing degranulation and inflammation (Galli, 2000; Galli et al., 1991; Plaut et al., 1989; Wodnar-Filipowicz et al., 1989).

1.1.4.4 Dendritic cells and Natural killer cells

Immature dendritic cells migrate from the blood and reside in most tissues, particularly in the skin and mucosal epithelium where they are referred to as Langerhan's cells. Dendritic cells are specialised antigen presenting cells, which initiate an adaptive immune response, making them a central component in linking innate and adaptive immune responses together. Dendritic cells can bind both bacterial and viral particles, and similar to macrophage, they engulf and intracellularly degrade pathogens. They then rapidly mature and migrate through lymph to lymph nodes where they display foreign antigens to cytotoxic T cells for direct killing, and to helper T cells to stimulate B cells for antibody production. In addition to being phagocytic dendritic cells are macropinocytic; a receptor independent mechanism which allows the cell to take up large volumes of fluid and concentrate the macrosolutes within. In doing so the dendritic cell is able to engulf e.g. encapsulated bacteria and virus particles, which do not carry common cell surface molecules for phagocytosis by macrophage or neutrophils. Upon engulfment dendritic cells expose pathogenic cell surface features allowing the dendritic cell to mature and display the antigen to T cells (Banchereau et al., 2000; Palucka and Banchereau, 1999).

Natural killer (NK) cells derive from the lymphoid lineage and are a form of cytotoxic lymphocyte that can destroy viral infected and cancer cells. They carry inhibitory receptors such as killer cell immunoglobulin-like receptors (KIR) and CD94/NKG2A heterodimers. These recognise cells missing MHC class I expression which can occur due to cancer or viral infection, and which are normally expressed on

most normal cells (Lanier, 1998). NK cells also recognise stress signals such as IFNα released from viral infected cells. The cytotoxic activity of NK cells derives from their cytoplasmic granules, which contain various cytotoxic compounds such as perforin and granzymes (proteases). Upon activation of NK cells these compounds are released where perforin forms holes within cell membranes of target cells, allowing granzymes to enter and induce apoptosis of the target. NK cells serve to contain viral infections while an adaptive immune response generates cytotoxic T cells that are antigen specific to clear the infection (Seino and Taniguchi, 2004; Van Kaer and Joyce, 2005).

1.1.5 Complement activation enhances phagocytosis and inflammation

The complement system is composed of a family of proteins that react with the surface of the pathogen to aid its clearance. The system is composed of a large number of plasma proteins, mainly produced by hepatocytes, which circulate in the plasma as inactive molecules. Complement activation functions to attract effector cells such as neutrophils (which carry complement receptors) to the site of infection via a concentration gradient, and to opsonise pathogens for phagocytosis, to stimulate an inflammatory response and to directly induce cell lysis of pathogens by creating pores within their membranes (membrane attack complex) (Morgan et al., 2005; Muller-Eberhard, 1988; Reid, 1986; Reid and Day, 1989; Tomlinson, 1993).

Complement can be activated via three different pathways; the alternative pathway, the classical pathway and the mannose-binding lectin (MBL) pathway (Figure 3). The alternative pathway is triggered spontaneously by microbial cell surface molecules such as lipopolysaccharides on gram negative bacteria, zymosan from yeast and fungal cell walls, and some parasitic cell wall molecules. Antigen-antibody complexes typically activate the classical pathway however, it can also be activated by some gram negative bacteria, making it an important link between adaptive and innate immune responses. The MBL pathway is initiated by the binding of the serum protein 'mannose-binding lectin' to mannose containing residues found on the surface some pathogens (binding of MBL to host membrane residues is prevented by the coverage of specific sugar groups such as sialic acid).

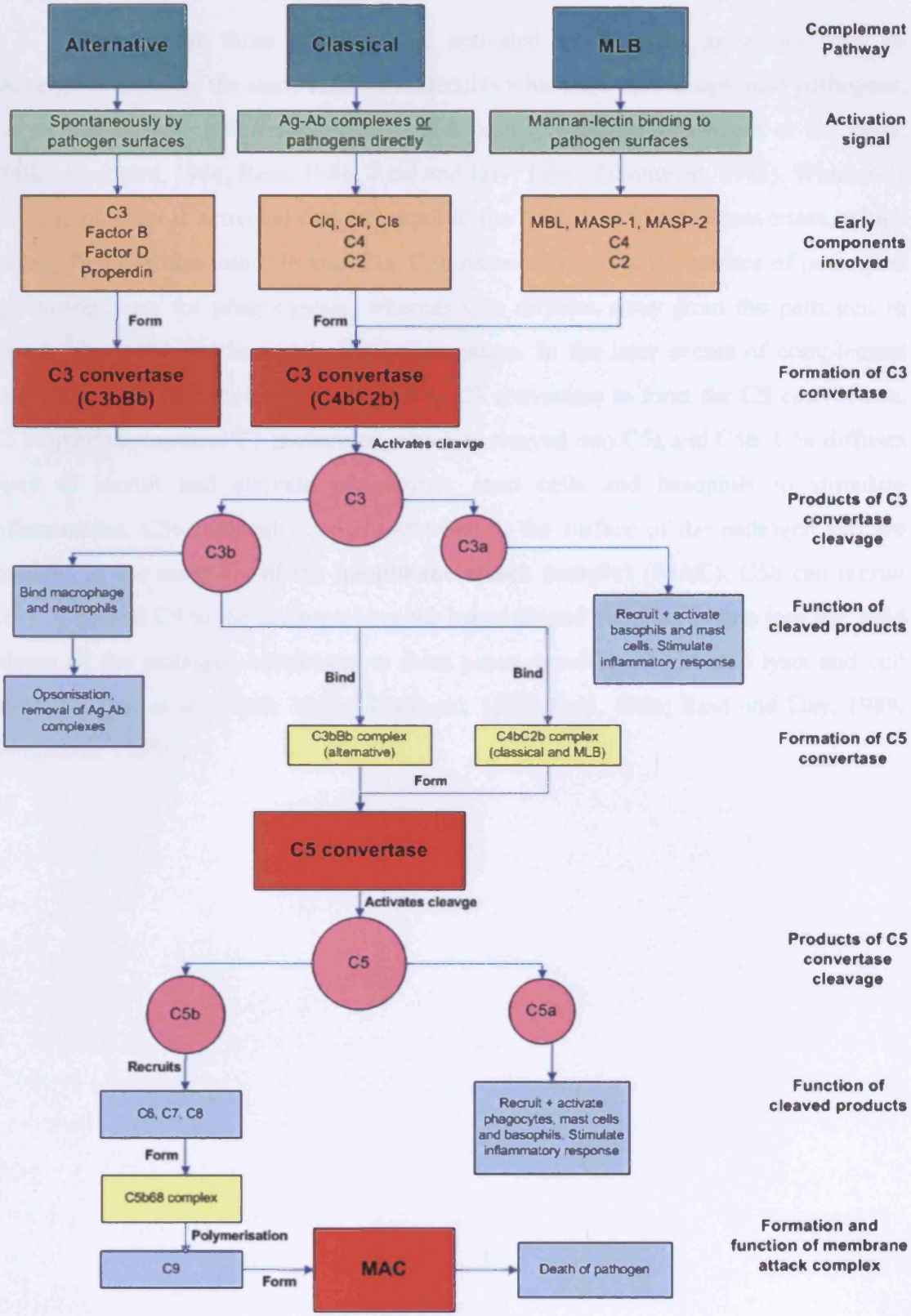

Figure 3: **Overview of complement activation.** The three pathways through which complement can be activated are the alternative, the classical, and the MBL pathways. Although these pathways can be activated by different molecules they all converge to produce the same effector molecules to opsonise, recruit and activate inflammatory cells and ultimately aid in destroying invading pathogens (adapted from Janeway et al., 2001).

Although the three pathways are activated by different molecules they all converge to generate the same effector molecules which are used to opsonise pathogens, recruit and activate inflammatory cells, and destroy pathogens (Morgan et al., 2005; Muller-Eberhard, 1988; Reid, 1986; Reid and Day, 1989; Tomlinson, 1993). Whichever way complement is activated they all result in the formation of a C3 convertase, which splits C3b molecules into C3b and C3a. C3b remains bound to the surface of pathogens opsonising them for phagocytosis, whereas C3a diffuses away from the pathogen to recruit mast cells and basophils for inflammation. In the later events of complement activation some C3b molecules can bind to C3 convertase to form the **C5 convertase**. C5 convertase captures C5 molecules, which is cleaved into C5a and C5b. C5a diffuses away to recruit and activate phagocytes, mast cells and basophils to stimulate inflammation. C5b molecules remain attached to the surface of the pathogen and are involved in the assembly of the **membrane attack complex (MAC)**. C5b can recruit C6, C7, C8 and C9 to the surface where the barrel shaped structure inserts into the lipid bilayer of the pathogen membrane to form pores, resulting in osmotic lysis and cell death (Morgan et al., 2005; Muller-Eberhard, 1988; Reid, 1986; Reid and Day, 1989; Tomlinson, 1993).

1.2 Phagocytosis and microbial destruction

Phagocytes were first recognised by Elie Metchnikoff whilst studying transparent starfish larvae. He observed that when splinters and carmine dye particles were introduced into the body of these larvae, they would become surrounded and engulfed by wandering mesodarmal cells (Metchnikoff, 1905). He discovered that these cells were phagocytic; a process which plays a central protection mechanism in the immune response, particularly that by neutrophils. The importance of microbial destruction by neutrophils is highlighted in a disease called chronic granulomatous disease (CGD). Individuals who suffer from CGD have dysfunctional neutrophils due to mutations in NADPH oxidase, which exposes them to recurrent and often life threatening bacterial and fungal infections (Thrasher et al., 1994; Winkelstein et al., 2000) (CGD is described in more detail in section 1.2.7).

The process of phagocytosis is split into several stages; chemotaxis, recognition plus adherence, ingestion (pseudopodium formation, phagosome formation, phago-lysosome formation), which is then followed by destruction of the engulfed pathogen (Figure 4). The stage of chemotaxis involves the migration of neutrophils up a gradient of chemotactic factors produced at the site of infection. As described earlier these molecules can include complement components such as C5a, bacterial factors such as fMetLeuPhe and various chemokines such as IL-8 (Fernandez et al., 1978; Ryan and Hurley, 1966; Schiffmann et al., 1975). Once neutrophils have been delivered to the injured site they are able to recognise and bind the pathogen, which is mediated through an array of pattern recognition receptors (refer to section 1.1.2), and it is this process which initiates ingestion of the pathogen. Ingestion of the pathogen involves the protrusion of the membrane to form pseudopodia which folds around the microbe, enclosing it within a vacuole known as a phagosome. The phagosome then migrates deeper into the cytoplasm where it collides and fuses with cytoplasmic granules to form a phagolysosome. The deadly contents of the granules are released into the vacuole and it is within the phagolysosome structure that destruction of the engulfed pathogen takes place (Moore et al., 1978; Stuart and Ezekowitz, 2005).

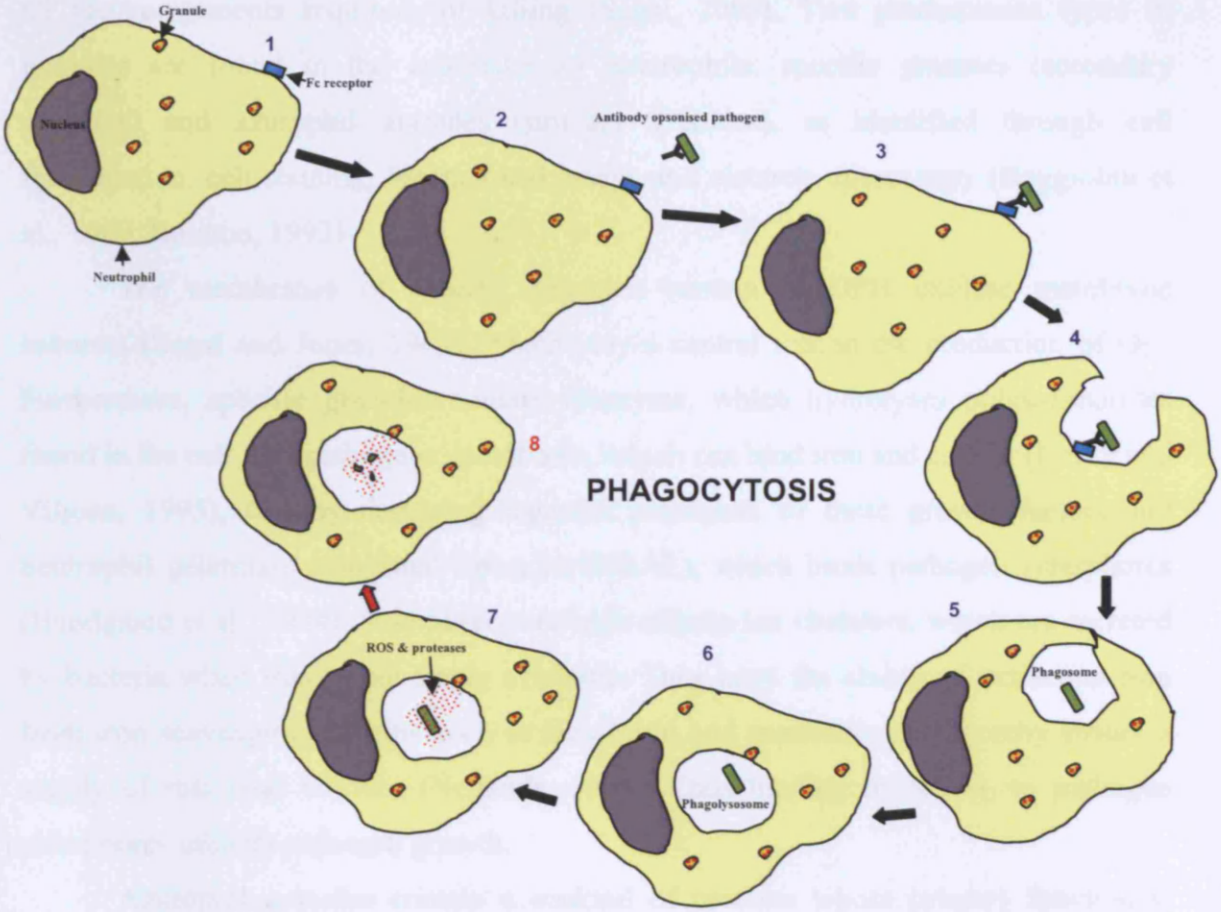

Figure 4: **The process of phagocytosis.** Illustration showing that phagocytosis takes place in several stages. 1) The surface of neutrophils is endorsed with receptors such as the Fc receptor. 2-3) The Fc receptor recognises and binds IgG opsonised pathogens. 4-5) Ingestion of the pathogen is initiated. The membrane protrudes out to form pseudopodia which fold around the pathogen to form a phagosome. 6) As the phagosome moves deeper into the cytoplasm, neutrophil granules fuse to form a phagolysosome. 7-8) Degranulation takes place, releasing various antimicrobial agents that destroy the enclosed pathogen.

1.2.1 Neutrophil granules play a central role in microbial killing

Neutrophil granules play a central role in microbial destruction as they contain all the components required for killing (Segal, 2005). Two predominant types of granules are found in the cytoplasm of neutrophils: specific granules (secondary granules) and azurophil granules (primary granules), as identified through cell fractionation, cell staining, biochemical assays and electron microscopy (Baggiolini et al., 1969; Bainton, 1993).

The membranes of specific granules contain NADPH oxidase membrane subunits (Segal and Jones, 1979), which play a central role in the production of $O_2^{\cdot-}$. Furthermore, specific granules contain lysozyme, which hydrolyses polysaccharides found in the cell wall pathogens, lactoferrin, which can bind iron and copper (Levay and Viljoen, 1995), thereby depriving ingested pathogens of these growth factors and neutrophil gelatinase-associated lipocalin (NGAL), which binds pathogen siderphores (Bundgaard et al., 1994). Siderphores are high affinity ion chelators, which are secreted by bacteria when iron is not freely available. They have the ability of extracting iron from iron scavenging proteins such as lactoferrin and transferrin and thereby ensure a supply of this vital nutrient (Neilands, 1995). Thus binding of NGAL to pathogen siderphores inhibits pathogen growth.

Azurophil granules contain a cocktail of proteins whose primary function is microbial destruction. These include defensins, which are small antimicrobial peptides that are capable of forming pores in pathogen membranes to allow efflux. Other granule contents include a) proteinases (cathepsin G, elestase and proteinase 3) which hydrolyse pathogen proteins, b) lysozyme and c) bactericidal/permeability increasing protein (BPI) which can bind lipopolysaccharides of gram negative bacteria. This causes membrane damage and results in growth arrest of the pathogen (Elsbach, 1998). A major characteristic component of azurophils is myeloperoxidase (MPO) which makes up approximately 25 % of the granule protein. This particular protein has interested researcher for many years, as MPO-mediated halogenation has long been believed to be one of the major killing system in neutrophils (Klebanoff, 1967a; Klebanoff, 1967b; Klebanoff, 1968; Klebanoff and White, 1969) as discussed is more detail in section 1.2.3.1. MPO activity, along with a diverse set of reactive oxygen species (ROS) is thought to be the primary source for microbial destruction. However more recently this mechanism of killing has been challenged by work from Segal and co-workers, who argue that ROS are generated to activate granule proteases. Their data suggest that it is

these activated proteases which destroy the engulfed pathogen, not the direct action of ROS or MPO activity (Ahluwalia et al., 2004; Reeves et al., 2002). These mechanisms and proposals for microbial destruction are discussed in more detail in section 1.2.4 and onwards.

1.2.2 The respiratory burst and ROS

Phagocytosis was first connected with oxygen in 1933 by Baldridge and Gerard who observed an increase in oxygen consumption when *cocci* were mixed with canine leucocytes, and smears of these leucocytes showed that they were loaded with the microorganism (Baldridge and Gerard, 1933). Based on these findings it was proposed that the increase in oxygen consumption in a 'respiratory burst' was related to an increase in energy demand for the process of phagocytosis to take place, and this energy derived from mitochondria. However in 1959 this theory was proven incorrect by Sbara and Karnovsky. Whilst studying phagocytosis of *T. bacilli* by monocytes and neutrophils, these authors reported that treatment of mitochondria with inhibitors such cyanide and azide did not inhibit the sudden increase in oxygen consumption (Sbarra and Karnovsky, 1959). This thereby suggested that the respiratory burst may be involved in some other process.

It wasn't until 1964 when Rossi and Zatti showed that granular fractions from phagocytosing genuine pig PMN's exhibited a dramatic increase in both NADH and NADPH oxidase activities. However granular fractions from resting neutrophils did not, and thus it was proposed that NADPH oxidase was responsible for the respiratory burst (Rossi and Zatti, 1964). In 1973 Babior and colleagues reported that the function of the respiratory burst was to produce $O_2^{\cdot-}$. This was shown through mixing human leucocytes with latex particles and cytochrome *c*, and measuring cytochrome *c* reduction at 550 nm. Reduction was abolished by superoxide dismutase (SOD) verifying that $O_2^{\cdot-}$ generation indeed took place (Babior et al., 1973).

The respiratory burst relies on the enzyme NADPH oxidase for which the core component; flavocytochrome b_{558} is present in both the neutrophil plasma membrane and the membrane of specific granules (Segal and Jones, 1979). Localisation of the cytochrome was determined by resolving neutrophil homogenates, along with organelle markers by analytical fractionation on sucrose gradients. Two sucrose fractions were found to absorb at 430 nm and 560 nm in dithionite difference spectra, thus suggesting that the cytochrome may be located in two separate compartments. One of these peaks

coincided with the peak activity of the specific granule markers; lactoferrin and vitamin B_{12} binding protein, thus suggesting that cytochrome *b* is found in specific granules. The second peak coincided with the light membranous organelles, thus suggesting that it may be located in the plasma membrane. The presence of cytochrome *b* was further confirmed when upon addition of pyridine, a sharp shift from 560 nm to 557 nm was observed in the spectrum (characteristic of a *b*-type cytochrome) (Segal and Jones, 1979).

Upon phagocytosis the cytochrome is incorporated into the vacuole through which electrons are pumped from NADPH in the cytosol, and donated to molecular oxygen at the other side in the vacuole. This one electron reduction generates superoxide anions ($O_2^{-\cdot}$) (Babior et al., 1973), which can be inter-converted by SOD to generate hydrogen peroxide (H_2O_2) (Iyer et al., 1961). From here potentially a whole host of other ROS can be generated, for example hypochlorous acid (HOCl) may be produced in the presence of Cl^-, MPO and H_2O_2. Hydroxyl radicals (OH•) can potentially be generated from the combination of H_2O_2 and $O_2^{-\cdot}$, which requires the presence of Fe^{2+} or Cu^{2+}. It is clear that both $O_2^{-\cdot}$ and H_2O_2 are produced by neutrophils, however whether the other ROS described above are also generated is controversial and is described in more detail later.

The importance of the respiratory burst in host defence, generated by the NADPH oxidase was highlighted in 1967 by Holmes and colleagues. These authors examined the metabolic changes that took place during the phagocytosis of latex particles by leucocytes of CGD patients (Holmes et al., 1967). They reported that the increase in oxygen consumption by phagocytosing CGD leucocytes was significantly lower than normal cells, as determined using an oxygen monitor. They also reported that glucose metabolism in CGD leucocytes was abnormal, as determined by the absence of a normal increase in the formation of $^{14}CO_2$ from glucose-3,4-^{14}C. In addition they showed that production of H_2O_2 was absent in CGD leucocytes, as determined by measuring the production of ^{14}C from the oxidation of formate-^{14}C by H_2O_2 (Holmes et al., 1967). Based on these results the authors proposed that the defective microbicidal activity of neutrophils in CGD patients was associated with the absence of a respiratory burst to produce ROS. This led researchers to believe that ROS were directly involved in promoting microbial destruction, which was further supported by the finding that destruction of aerobic organisms such as *S. aureus*, *E. coli* and *K. pneumoniae* by neutrophils under anaerobic condition was compromised (Mandell, 1974).

1.2.3 The initial proposal – ROS and MPO activity are directly involved in microbial destruction

ROS are toxic as they can react with biological molecules such as DNA, RNA and lipids, and thus exposure to excessive amounts can cause significant structural and functional damage. Sources for ROS include environment factors such as herbicides, radiation and cigarette smoke. Fortunately, the body's antioxidant defences which include superoxide dismutase, glutathione, catalases, vitamin C and E scavenge such free radicals to help combat free radical damage. However the ROS to which we are exposed do not all derive from environment factors, but are also generated as a natural byproduct of normal metabolism (mitochondrial respiration). Importantly, some free radicals are generated for signalling processes and others are produced deliberately by phagocytes for microbial clearance (Finkel, 2003).

Originally it was believed that $O_2^{\cdot-}$ generated by neutrophils was directly involved in pathogen destruction. Babior and colleagues reported that incubating *S. epidermidis* or *E.coli* with xanthine oxidase; an enzyme which can produce $O_2^{\cdot-}$, resulted in death of these organisms (Babior et al., 1975) (as determined by the pour pate method). However these experiments were conducted in the absence of the substrate xanthine. Moreover, killing was not abolished in the presence of superoxide dismutase (SOD), suggesting in fact that the organisms were destroyed *via* some other mechanism and not $O_2^{\cdot-}$. Since then various other studies have come to surface, which have shown that $O_2^{\cdot-}$ is not directly involved in pathogen killing. For example, Klebanoff showed that adding SOD to a reaction mixture containing *E.coli*, xanthine, xanthine oxidase, Cl^- and MPO did not inhibit killing of the organism (Klebanoff, 1974).

However, although $O_2^{\cdot-}$ itself may not be particularly bactericidal, it acts as a precursor for the generation of other, much more reactive oxygen species. Indeed, already in 1961 Iyer and colleagues showed that the respiratory burst produced a large amount of H_2O_2 (measured the production of ^{14}C from the oxidation of formate-^{14}C by H_2O_2) and that a product of this respiratory burst was implicated in antimicrobial activity (Iyer et al., 1961).

1.2.3.1 MPO and H_2O_2 mediated killing

Based on the following points Klebanoff proposed that MPO may play a key role in the killing process: i) the primary function of neutrophils is phagocytosis plus

microbial destruction, ii) H_2O_2 is implicated in microbial killing and iii) H_2O_2 can be a potential substrate for MPO. Klebanoff tested this hypothesis *in vitro* in collaboration with Hirsch (1961-1962). However, their results were at first rather disappointing. They found that mixing *E.coli* with MPO and H_2O_2 at pH 5.0 had no effect on cell viability, as determined by the pour plate method. However theoretically it was possible that MPO may kill organisms indirectly by converting a substance with little microbicidal effect to one with a higher microbicidal effect. Indeed in 1967 Klebanoff reported that when H_2O_2 and iodide (a non-toxic ion present at low concentrations in the plasma) were added to the reaction mixture, an extensive microbicidal effect was observed. He reported a reduction in bacterial viability from 6.2×10^6 to zero. Based on these results, Klebanoff proposed that MPO and H_2O_2 are required to oxidise iodide for the formation of the antibacterial agent iodine, which then prompted him to investigate iodination of *E.coli* by the MPO system (Klebanoff, 1967a). Iodination experiments involved measuring iodine incorporation into a trichloroacetic acid (TCA)-precipitable form, where a typical reaction mixture (pH 5.0) consisted of *E.coli*, I^{131}, MPO and H_2O_2. Klebanoff reported that significant iodination (36.1 mμmoles) of *E.coli* took place in the presence of MPO and H_2O_2, in contrast little or no iodination was observed in the absence of either component (0.1 mμmoles and 0.2 mμmoles; respectively) and in the absence of both components simultaneously (0.6 mμmoles). Under similar conditions he also investigated iodine incorporation by neutrophils that had phagocytosed *L. acidophilus*. He reported that iodine fixation was apparent in these smears but was absent in smears where *L. acidophilus* was not included. Based on these results Klebanoff proposed that MPO and H_2O_2 are required for iodine incorporation which may be important for pathogen destruction by neutrophils (Klebanoff, 1967a). This report was soon followed by another in 1968 where Klebanoff showed through similar *in vitro* experiments, that although iodide was the most bactericidal against *E. coli*, other halides such as bromide and chloride were also inhibitory (Klebanoff, 1968). Chloride is the most abundant of the three anions in biological fluids and oxidation of this halide can produce the highly reactive agent hypochlorous acid (HOCl), an agent typically found in household bleaches. Many researchers believe that the major function of neutrophil MPO-mediated halogenation of bacteria is to produce HOCl for microbial killing.

The role of MPO mediated destruction by neutrophils was further supported by the finding that that MPO-mediated halogenation was defective in CGD patients (Klebanoff and White, 1969) (incubated cells with ^{125}I and used autoradiography to

demonstrate iodination). In the same year it was found that patients whose neutrophils lacked MPO may also be immunodeficient (Lehrer et al., 1969). Furthermore, in 1983 it was reported that catalase (breaks down H_2O_2) negative organisms very rarely cause infection in CGD patients (Gallin et al., 1983). It was suggested that these pathogens may be capable of generating their own H_2O_2 enough to catalyse their own MPO mediated halogenation.

In addition various *in vivo* studies have also reported that MPO activity may be important for host defence against both fungi and bacteria, and that killing may be species specific (Aratani et al., 1999; Aratani et al., 2000). More specifically, Aratani and colleagues showed that intratracheal challenge of MPO knock out mice with *C. albicans* increased their susceptibility to pneumonia and death. Approximately 500 times more viable fungi were cultured from the lungs of MPO knock out mice in comparison to wild-type mice, and 18 of the 27 test animals died after 5 days of injection. These authors also investigated HOCl generation indirectly by measuring the chlorination of monochlorodimedon (MCD) to form dichlorodimedon. Their results showed that neutrophils from wild-type mice generated HOCl at a level of 0.47 nmol/min/10^6 cells, where as HOCl generation from MPO deficient mice was undetectable. The authors suggested that the MPO knock out mice were unable to destroy *C. albicans* as they were unable to generate HOCl (Aratani et al., 1999). Aratani and colleagues also investigated the effects of *S. aureus* on MPO knock out mice, and interestingly these mice were able to clear the infection effectively and to similar levels as wild-type mice. Based on these results the group proposed that MPO mediated killing may be species specific and that *S. aureus* may be destroyed by other ROS such as $O_2^{\cdot-}$, which is rather surprising as $O_2^{\cdot-}$ itself is not a particularly reactive species (Babior et al., 1975; Klebanoff, 1974). A similar article was published the following year which reported that MPO knock out mice were susceptible to *C. albicans*, *C, tropicalis*, *T. asahii* and *P. aeruginosa*, but not *C. glabrata*, *S. aureus* and *S. pneumoniae* (Aratani et al., 2000).

1.2.4 The controversy - Do ROS and MPO activity really kill?

More recently Segal and colleagues have argued that previous experiments where ROS and MPO activity were shown to destroy ingested pathogens, were not carried under conditions which truly reflect the conditions of the vacuole. For example the pH of the phagocytic vacuole during the respiratory burst is approximately 7.4-8.0

(Cech and Lehrer, 1984; Reeves et al., 2002; Segal et al., 1981), where as many of the previous experiments were conducted at pH 5-5.5 (Klebanoff, 1967a; Klebanoff, 1968). More importantly, these latter experiments were carried out in the absence of granule proteins, which when ejected onto the ingested pathogen make up approximately 30 % - 40 % of the vacuolar content (Hampton et al., 1998). It has been estimated that these proteins may be present at a concentration as high as 500 mg/ml (Reeves et al., 2002).

With the above vacuolar conditions in mind Reeves and colleagues re-examined the bactericidal effects of $O_2^{\cdot-}$, H_2O_2, HOCL and MPO-induced iodination *in vitro* (Reeves et al., 2002). The results of their study contradict those previously reported, and propose a more important role for granule proteases in microbial destruction. It was found that $O_2^{\cdot-}$ was non-toxic to *S. aureus*, furthermore high concentrations (100 mM) of H_2O_2 were required to reduce the survival of *S. aureus* and *E.coli* by 50 %, an effect, which disappeared in the presence of only 25 mg/ml granule proteins. Similarly it was reported that although 1-5 μM HOCl was bactericidal to *S. aureus* and *E. coli* the effects disappeared in the presence of granular proteins, although the amount of granule proteins used in these experiments was 20-fold less than what is normally found in the phagocytic vacuole. This suggests that under true vacuolar conditions ROS are not capable of destroying pathogens, and may indeed be consumed by granular proteins.

The notion that MPO mediated iodination constitutes an important killing mechanism is also challenged by the work of Segal and colleagues. In their report from 2003 they examined which proteins became iodinated upon phagocytosis of *S. aureus*. Briefly, they used a reaction mixture consisting of neutrophils, ^{125}I and IgG opsonised bacteria which was taken into 10 % TCA to precipitate out iodinated proteins. These were separated on 2D gels and iodinated proteins were detected autoradiographically. These proteins were excised, trypsin digested and identified by MALDI mass spectrometry. The authors reported that rather than bacterial proteins, the majority of the proteins that incorporated ^{125}I belonged to azurophil and specific granules such as lactoferrin and lysozyme, along with various cytoskeletal proteins such as actin (Reeves et al., 2003). These results were supported by an earlier study which used analytical subcellular fractionation of neutrophils that had been stimulated by PMA, to show that a large proportion of ^{131}I was distributed with neutrophil granules (Segal et al., 1983).

Further support for this model is given by the observation that, although MPO deficient individuals were thought to be immunodeficient (Lehrer et al., 1969) and that MPO knock-out mice were susceptible to infection (Aratani et al., 1999; Aratani et al., 2000), in fact 1 in 2000 individuals are MPO deficient but are nevertheless not unduly

prone to infection (Nauseef, 1988). In addition, the theory that catalase negative organisms rarely infect CGD patients because they may be capable of generating their own H_2O_2 enough to catalyse their own MPO mediated halogenation, has also been questioned. Chang and colleagues reported that injecting catalase deficient *A. nidulans* into $p47^{phox}$ CGD mice was as equally virulent as wild-type catalase positive *A. nidulans* (Chang et al., 1998). Similar results were reported by Messina and colleagues who investigated the virulence of catalase positive and negative strains of *S. aureus* in CGD (Messina et al., 2002).

1.2.5 A new proposal - Granule proteases kill pathogens not ROS or MPO activity

Based on the results described above it was proposed by Segal and co-workers that ROS and MPO activity are not sufficient to kill bacteria and fungi, and that in fact granular neutral proteases play a more direct role in microbial destruction. To test this hypothesis gene targeting techniques were used to develop mice in which neutral proteases such as neutrophil elastase (NE) and cathepsin G (CG) were knocked out, and the effects of subjecting these animals to pathogenic organism were examined (Belaaouaj et al., 1998; Reeves et al., 2002; Tkalcevic et al., 2000).

Specifically, Belaaouaj and colleagues reported that intraperitoneal challenge of *K. pneumonia* into $NE^{-/-}$ mice reduced their survival to 50 % by 16 hrs and by 48 hrs all $NE^{-/-}$ mice were dead. In addition significant bacterial burden was observed in the peritoneal cavities, the bloodstream and vital organs (particularly the lungs) of $NE^{-/-}$ mice in comparison to $NE^{+/+}$ mice. Using electron microscopy it was shown that after 2 hrs of injecting *K. pneumonia* the organism was actively being degraded by $NE^{+/+}$ neutrophils. In contrast, the phagosome of $NE^{-/-}$ neutrophils contained intact intracellular bacteria, some of which were actively dividing. Similar experiments using *E. coli* were carried out and showed that NE was also required for destroying this organism (Belaaouaj et al., 1998). Tkalcevic and colleagues reported that although over time wild-type, single $NE^{-/-}$ and single $CG^{-/-}$ mice resisted intravenous challenge with a small dose of *A. fumigatus* (80,000 viable spores), 60% of dual protease knock out mice ($NE^{-/-}CG^{-/-}$) did not survive. Moreover, histopathological studies showed that in comparison to wild-type mice, $NE^{-/-}CG^{-/-}$ mice carried a substantial load of the organism in the kidneys, which was not due to a defect in infiltrating neutrophils to the site of infection. These results suggest that both NE and CG are required to fully protect

against *A. fumigatus*, and that both proteases may act synergistically with other granule proteins to enhance the bactericidal effect. More importantly these authors reported a normal respiratory burst by $NE^{-/-}CG^{-/-}$ neutrophils, as determined using flow cytometry (measured the oxidation of dihydro-rhodamine to rodamine, by product of the respiratory burst) (Tkalcevic et al., 2000).

Reeves and colleagues reported that $CG^{-/-}$ mice were more susceptible to intravenous challenge by *S. aureus* but not *C. albicans*, where as $NE^{-/-}$ mice were more susceptible to infection by *C. albicans* but not *S. aureus*. However, both organisms were significantly virulent in the absence of both proteases, suggesting that both NE and CG are required for full protection against invading pathogens. A mirror image of these results was observed *in vitro* by protease deficient mice neutrophils (Reeves et al., 2002). A cocktail of protease inhibitors and the oxidase inhibitor diphenylene iodonium (DPI) was further used to highlight the importance of neutral proteases for microbial destruction. Addition of either of these components to a suspension of purified human neutrophils and *S. aureus* severely affected microbial destruction, and to similar levels as that observed for CGD cells. More importantly, the authors showed that production of a respiratory burst as determined by measuring cytochrome *c* reduction, and MPO activity as determined through iodination by neutrophils was normal in the protease knock out mice.

Altogether, the results of these mouse knock out studies indicate that neutral proteases play a fundamental role in microbial destruction. However, there is also no doubt that deficiency in NADPH oxidase activity as observed in CGD results in defective microbial killing. This suggests that both factors may be required for effective clearance of infection, and furthermore that they may work in concert; a concept investigated by Reeves and colleagues. Using electron microscopy they followed the impact of NADPH oxidase activity on neutrophil granules. They examined the morphology of phagocytic vacuoles from neutrophils of a normal patient, of an X-linked CGD patient and of a variant X- linked CGD patient (Reeves et al., 2002). Although in the latter two patients NADPH oxidase is defective, X-linked variant CGD patients still exhibit 10-12 % oxidase activity. Electron micrographs showed that > 90 % of neutrophil granules were uniformly dispersed in normal neutrophils. In contrast < 30 % and < 20 % were dispersed in X-linked CGD and variant X-CGD cells; respectively (granules appeared clumped). These results suggest that NADPH oxidase activity may actually influence neutrophil granules by causing them to disperse their contents. With this observation on hand and the facts that not only is a large amount of

$O_2^{\cdot-}$ generated during the respiratory burst (approximately 4mol l^{-1}), and that the 10-12 % (0.5 mol l^{-1}) of $O_2^{\cdot-}$ generated in X-linked variant CGD neutrophils is not sufficient for pathogen destruction, led Segal's group to hypothesise that $O_2^{\cdot-}$ generation within the phagocytic vacuole may influence neutrophil granules, rather than directly killing pathogens or producing the substrate for MPO. In fact, Reeves and colleagues presented evidence to suggest that $O_2^{\cdot-}$ generation influences granules by altering the vacuolar pH and ion concentrations, and propose that these conditions activate neutrophil proteases and it is these proteases, which destroy ingested pathogens (Reeves et al., 2002).

1.2.5.1 Killing is mediated by phagosomal pH and ion concentrations

It is well established that NADPH oxidase is electrogenic as the transfer of electrons across the vacuolar membrane to produce $O_2^{\cdot-}$ causes a charge imbalance (Henderson et al., 1987). This was shown through using the membrane potential indicator oxonol V. The absorbance of oxonol from un-stimulated cytoplasts gave a resting membrane potential of -100 ± 6.8mV, which rapidly increased upon addition of the oxidase activator PMA. Membrane potential depolarisation was connected to oxidase activity as PMA stimulated cytoplasts showed a 120-fold increase in $O_2^{\cdot-}$ production, as determined by reduction of cytochrome *c*. Furthermore both, membrane depolarisation and $O_2^{\cdot-}$ generation in PMA stimulated cytoplasts, were inhibited in the presence of the oxidase inhibitor DPI (Henderson et al., 1987). In order to prevent membrane depolarisation and to maintain NADPH oxidase function, the influx of electrons has to be compensated for i.e. a balance in charge movement has to take place with either a positive charge moving into the vacuole or a negative charge moving out of the vacuole. This charge balance is generally believed to be bought about by the influx of protons into the vacuole, as membrane depolarisation has shown to be enhanced in the presence of Cd^{2+} ions (block H^+ currents) (Henderson et al., 1987). However, $O_2^{\cdot-}$ generation in the vacuole ultimately leads to the production of H_2O_2; a process which consumes protons and increases the vacuolar pH from 5.5-6.0 to 7.8-8.0 despite the release of acid granule proteins. Segal and co-workers argue that if only protons are involved in charge compensation then this would cause a buffering effect (neutral pH) and does not explain the observed rise in vacuolar pH. In support of their argument they have shown that blocking proton channels with Zn^{2+} and Cd^{2+} (proton channel inhibitors) did not block NADPH oxidase activity (Ahluwalia et al., 2004), thus suggesting that ions other than protons may be involved in charge compensation. More

specifically, they presented evidence to suggest that part of the charge is compensated for by K^+ influx. This not only increased the vacuolar pH but to also activated granule proteases for microbial destruction (Ahluwalia et al., 2004; Reeves et al., 2002). These findings are discussed in more detail below.

The involvement of K^+ was shown through various experiments including a quantitative assay where secretion of $^{86}Rb^+$ from vacuoles was measured (Reeves et al., 2002). $^{86}Rb^+$ is a marker commonly used in K^+ transport studies (Rb^+ belongs to the same atomic family as K^+). Reeves and colleagues reported that transport of $^{86}Rb^+$ from stimulated neutrophils was suppressed in the presence of DPI (Reeves et al., 2002), suggesting that NADPH oxidase may in fact require K^+. Furthermore Ahluwalia and colleagues reported that large conductance Ca^{2+} activated K^+ (BK_{Ca}) channels were involved in K^+ flux. These channels were identified by western blotting to be present in the cell membranes of neutrophils and in the membranes of cytoplasmic granules. Blocking of these channels with iberiotoxin or paxilline (selective and potent BK_{Ca} channel inhibitors) not only inhibited the secretion of $^{86}Rb^+$ but also prevented vacuolar alkalinization as well as inhibiting the destruction of *S. aureus*, *S. marcescens* and *C. albicans*. The vacuolar pH was determined from the excitation spectrum of fluoresceine labelled IgG-coated *S. aureus*, which was compared with a calibration curve produced from bacteria in buffers of differing pH values. Moreover, neutrophil iodination and oxidase activity were not affected in the presence of these BK_{Ca} channel inhibitors. Altogether these results suggest that K^+ flux is important for effective microbial destruction, and that ROS and MPO activity are not as directly involved as previously believed. This then raises the question of how K^+ is involved in destroying ingested pathogens.

1.2.5.2 The link between K^+ influx and neutral proteases

The findings by Segal's group that K^+ flux and granular proteases are required for pathogen destruction, led to the proposal that K^+ may be involved in solubilising the anionic sulphated proteoglycan matrix, within which the proteases are tightly bound (Kolset and Gallagher, 1990). Surface plasmon resonance measurements showed that the binding affinities for the interaction between the matrix protein heparin and purified cathepsin G, elastase and MPO are 5.3 nM, 8.9 nM and 20.4 nM; respectively (Reeves et al., 2002). The acidic environment (pH 5.0) within granules keeps these proteases inactive (Styrt and Klempner, 1982), while the influx of K^+ raises the pH and thereby

produces the optimum conditions for these proteases to function at. Furthermore, these authors showed that K^+ is linked with microbial destruction as incubating isolated granules with *S. aureus* and 200-400 mM KCl was bactericidal, and this effect was partially inhibited in the presence of protease inhibitors. In the absence of KCl the granules were not bactericidal. Finally, Reeves and colleagues suggested that H_2O_2 generation may be a mere by-product of the respiratory burst and that the primary role of MPO may be to protect proteases against oxidative damage. They reported that in their preliminary studies cathepsin G was sensitive to oxidation by H_2O_2, and that it was rendered inactive in neutrophils treated with azide, which inhibits MPO (Reeves et al., 2002).

1.2.6 Final conclusions on microbial killing by neutrophils

Based on studies by many groups, including those of Babior and Klebanoff it became generally accepted that ROS and MPO activity were directly involved in pathogen destruction by neutrophils. However, more recently it has been argued by Segal and colleagues that ROS and MPO activity are not sufficient to kill ingested pathogens. Instead a new model has been put forward, in which it was proposed that $O_2^{\cdot-}$ is produced to 'mop-up' free protons and induce K^+ influx, which elevates the vacuolar pH to levels that are optimum for the function of granule proteases. In addition, in this model K^+ influx solubilises the anionic sulphated proteoglycan matrix to release granular proteases and peptides, rendering them active for microbial destruction. In spite of the fundamental differences in these models for the mechanism of pathogen destruction by neutrophils, it is important to keep in mind that there is no doubt at all that NADPH oxidase activity is absolutely essential for the killing of pathogens to take place.

1.2.7 Microbial destruction is defective in chronic granulomatous disease

Chronic granulomatous disease (CGD) is a rare genetic disorder affecting approximately 1:200,000 - 1:250,000 individuals (Winkelstein et al., 2000). It manifests in early childhood and predominantly effects boys. CGD is caused by mutations including missence, nonsense, insertions, deletion and splice site mutations, in the genes

encoding the NADPH oxidase subunits (described in detail in section 1.3). These mutations result in the complete absence or severely reduced levels of the affected protein, either because the gene is completely or partially deleted or the protein is unstable. In turn this results in the inability to produce or produce sufficient amounts of $O_2^{\cdot-}$ to clear infections effectively (Dinauer, 2005; Heyworth et al., 2003; Meischl and Roos, 1998; Segal, 1996). The exact locations of these mutations can be found in a range of extensive databases (Cross et al., 1996a; Cross et al., 1996b; Heyworth et al., 1997; Roos et al., 1996). Mutations in human CGD have allowed researchers to gain invaluable information about the NADPH oxidase subunits, their functional domains and their modes of interaction to form the active NADPH oxidase complex. Mutations in the CYBB gene which encodes for $gp91^{phox}$ (Xp21) gives rise to the X-linked CGD form and is the most common form of the disease, which accounts for approximately 65 % of all cases. Of all the non-X linked autosomal recessive forms of CGD, mutations in the NCF-1 gene (7q11), which encodes for $p47^{phox}$ are the most common which accounts for approximately 25 % of all CGD cases. Mutations in the NCF-2 gene (1q25), which encodes for $p67^{phox}$ and the CYBA (16q24) gene, which encodes $p22^{phox}$ are infrequent, each accounting for approximately 5 % of all cases. CGD associated mutations in the NCF-4 gene which encodes for $p40^{phox}$ (22q13.1) have not been reported as of yet. CGD predisposes patients to recurrent bacterial and fungal infections which can often be life-threatening. These infections are typically characterised by pneumonia, lymphadenitis, abscesses in subcutaneous tissues, bones and vital organs such as lungs and liver. Common infecting pathogens in CGD patients include *C. albicans, S. aureus* and *A. fumigatus* which can cause pneumonia and is the most frequent cause of death in CGD patients. Treatment for CGD patients includes prophylactic antibiotics and interferon-γ (IFN--γ) therapy, and bone marrow transplants and gene therapy potentially offers a future resolution (Dinauer, 2005; Heyworth et al., 2003; Meischl and Roos, 1998; Segal, 1996).

1.3 The NADPH oxidase complex

The NADPH oxidase is a tightly regulated multi-component enzyme composed of six subunits termed the phox proteins (phagocytic oxidase). It is found in an inactive and active state, and in the inactive state the enzyme subunits are kept in different subcellular locations to prevent inappropriate activation and assembly (Figure 5). Two of the enzyme components are integral membrane proteins ($gp91^{phox}$and $p22^{phox}$) and form a heterodimer known as flavocytochrome b_{558}, named after an absorption maximum of the α-band near 558 nm (also known as cytochrome b_{-245} after its midpoint reduction potential of -245V). Flavocytochrome b_{558} is considered as being the catalytic core of the NADPH oxidase as it contains all the components required for the electron transfer reaction to generate superoxide anion ($O_2^{\cdot-}$) The remaining four subunits are located in the cytosol ($p47^{phox}$, $p67^{phox}$, $p40^{phox}$ and the small GTPase Rac). Upon appropriate activation the cytosolic proteins translocate and associate with the membrane-bound cytochrome and Rac (Figure 5C) to form the catalytically active NADPH oxidase complex.

1.3.1 Flavocytochrome b_{558}

The existence of a 'respiratory burst' that is required for microbial killing, and which is defective in patients with CGD has been known for a long time. However, it wasn't until 1978 that Segal and Jones discovered a novel *b*-type cytochrome which is incorporated into neutrophil phagocytic vacuoles was responsible for this activity. The cytochrome was identified when significant changes in the difference spectra of purified human neutrophil homogenates (activated by PMA or IgG opsonised latex particles) were observed, and was confirmed to be a *b*-type cytochrome as dithionite (reduces *b*-type cytochromes) difference spectra gave a similar pattern (Segal and Jones, 1978). Importantly this cytochrome was shown to be absent in certain CGD neutrophil homogenates, thereby indicating that it constitutes the oxidase system that is responsible for the microbicidal activity of neutrophils (Segal and Jones, 1978).

Purification of the cytochrome by detergent extraction of neutrophil membranes and subsequent column chromatography yielded a single protein that migrated at an apparent molecular weight of 68-78 kDa on SDS-PAGE (Harper et al., 1984). This protein is now known as the $gp91^{phox}$ subunit and was the first NADPH oxidase subunit

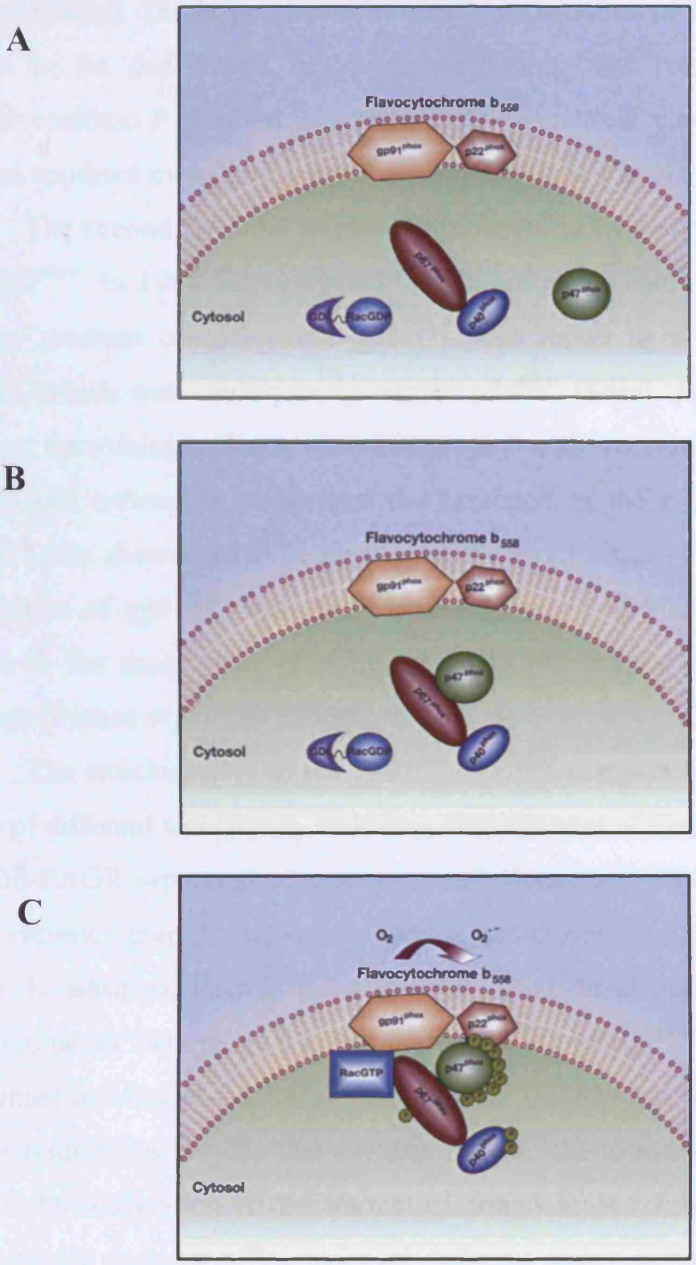

Figure 5: Activation of the NADPH oxidase. A. The resting state of NADPH oxidase where the membrane components ($gp91^{phox}$ and $p22^{phox}$) are separate from the cytosolic components ($p47^{phox}$, $p67^{phox}$, $p40^{phox}$ and Rac). B. At some point after cell stimulation some $p47^{phox}$ binds dimeric $p67^{phox}$-$p40^{phox}$ to form the $p47^{phox}$-$p67^{phox}$-$p40^{phox}$ trimeric complex. C. The active state of NADPH oxidase where the cytosolic components translocate and interact with the membrane integrated flavocytochrome b_{558}, resulting in the formation of the active enzyme complex.

to be identified. The large molecular weight distribution of this protein on SDS gels was shown to be due to its heavy glycosylation, and removal of carbohydrates by endoglycosidase F resulted in a protein that runs as a sharp single band on SDS gels with an apparent molecular weight of 55 kDa (Harper et al., 1985).

The second NADPH oxidase component to be discovered in human neutrophils was $p22^{phox}$. In 1987 Segal reported that throughout chromatographic purification and sucrose gradient centrifugation $gp91^{phox}$ was found tightly associated with a 23 kD protein, which was subsequently named $p22^{phox}$ (Segal, 1987). A similar purification strategy combining column chromatography with sucrose density gradients used by Parkos and colleagues confirmed the presence of the $p22^{phox}$ subunit, which unlike $gp91^{phox}$ was shown not to be glycosylated (Parkos et al., 1987). Further support for an association of $gp91^{phox}$ with $p22^{phox}$ was provided by the fact that both subunits are absent in the neutrophils of X-linked CGD patients, as determined by western blot analysis (Parkos et al., 1987; Segal, 1987).

The stoichiometry of the $gp91^{phox}$-$p22^{phox}$ complex was shown to be 1:1 using a range of different techniques, including densitometry of Coomasie stained protein bands of SDS-PAGE separated cytochrome, and absorbance measurements of each subunit after chromatographic separation under denaturing conditions (Wallach and Segal, 1996). In addition, Huang and colleagues used direct peptide sequencing of purified cytochrome to determine the ratio of $gp91^{phox}$ to $p22^{phox}$. In this work the authors performed automated Edman degradation on the flavocytochrome, which released two amino acids in each cycle that corresponded to the reported sequences of $gp91^{phox}$ and $p22^{phox}$. Quantification of the amount of amino acids released in each cycle (corrected for different recovery efficiencies of different amino acids) clearly pointed towards a 1:1 ratio of $gp91^{phox}$ to $p22^{phox}$ (Huang et al., 1995).

The observation that mutations found in some CGD patients that interfere with the expression of one of the two cytochrome subunits, often lead to the absence of the other (Parkos et al., 1989; Segal, 1987) further supports the notion of a tight association of the two subunits, and importantly suggests that each other's presence may be required for mutual stabilisation or folding. This idea is further supported by the fact that co-expression of both subunits in COS-7 or NIH-3T3 cells (used because they lack endogenous $p22^{phox}$, which otherwise is present in many different cell types) significantly increased the amount of mature $gp91^{phox}$ (Yu et al., 1998). Furthermore, DeLeo and colleagues showed that during biosynthesis of the flavocytochrome the uncomplexed subunits were susceptible to proteasomal degradation (DeLeo et al.,

2000). Nevertheless, it should be noted that $p22^{phox}$ is found in many different cell types, even in the absence of $gp91^{phox}$ and hence that there are clear differences in the stability of these proteins depending on the cell type.

1.3.1.1 $Gp91^{phox}$

The $gp91^{phox}$ subunit (also called the β-subunit) of flavocytochrome b_{558} consists of 570 amino acids. The N-terminal portion of the protein is hydrophobic and predicted to contain six transmembrane helices, where as the C-terminal region is hydrophilic and located in the cytosol (Royer-Pokora et al., 1986) (Figure 6). $Gp91^{phox}$ binds all the cofactors required for the electron transfer reaction process to take place; namely two heme molecules, FAD and NADPH (discussed in more detail below). Electrons are transferred from NADPH via FAD to the two heme groups to reduce O_2 to $O_2^{\cdot-}$ in the vacuole. The two heme molecules are coordinated by histidine residues in the N-terminal membrane spanning region of $gp91^{phox}$, while the binding sites for FAD and NADPH are located in the cytoplasmic region. This region shows some degree of sequence homology with the family of ferredoxin-NADP reductases, which enabled Taylor and colleagues to suggest a model for the three-dimensional structure of this domain, based on the known structure of ferredoxin-NADP reductase (Taylor et al., 1993). Currently this is the only available structural information of this subunit.

It was first suggested in 1977 that the superoxide-generating enzyme of neutrophils was a flavoprotein, as an increase in $O_2^{\cdot-}$ production was observed when FAD was added to a system containing broken cell preparations from zymosan-treated normal neutrophils. The involvement of FAD was further supported by the fact that FAD failed to support $O_2^{\cdot-}$ generation in a system containing particles from zymosan-treated CGD neutrophils (Babior and Kipnes, 1977). In addition, the authors of this study reported that FAD was the preferred cofactor over many others, including flavin mononucleotide (FMN), riboflavin, adenosine 5'-diphosphate (ADP) and adenosine 5'-monophosphate (AMP) (Babior and Kipnes, 1977).

The fact that the cytochrome itself is the FAD binding component has been established independently by three groups in 1992. A combination of sequence analysis, reconstituted NADPH oxidase assays in the absence or presence of FAD, and the measurement of FAD content in the membranes of resting and activated neutrophils clearly showed that the FAD binding site is located within the $gp91^{phox}$ subunit, and that

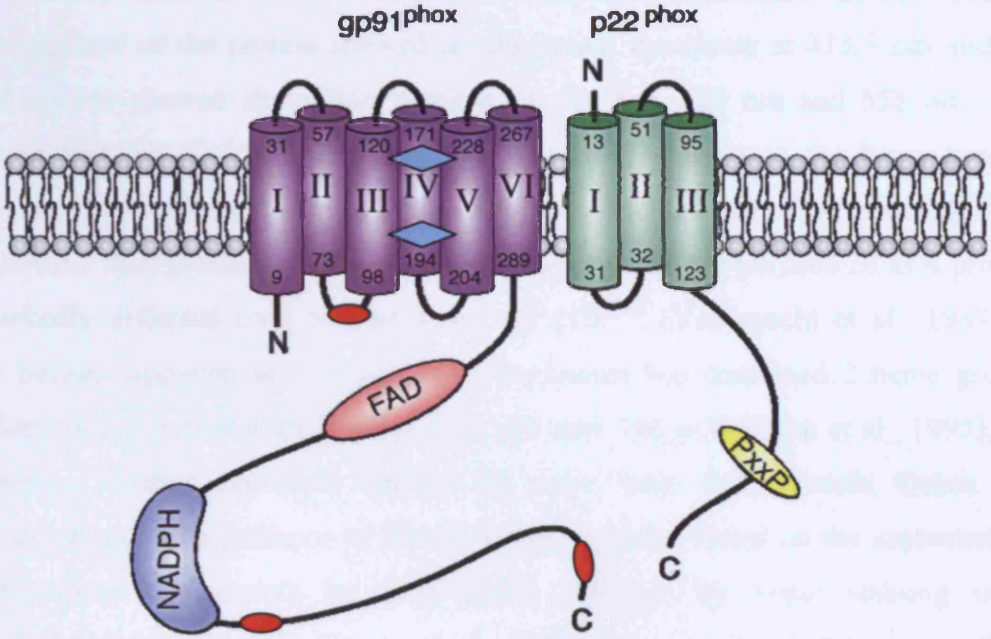

Figure 6: **Flavocytochrome b_{558}.** Model showing the predicted domain structures of $gp91^{phox}$ (purple) and $p22^{phox}$ (green). The FAD and NADPH binding sites in $gp91^{phox}$ are shown in red and blue; respectively. The heme binding sites are shows as blue diamonds. The PXXP motif in the cytoplasmic tail of $p22^{phox}$ that interacts with the tandem SH3 domains of $p47^{phox}$ is shown in yellow. The regions in $gp91^{phox}$ that are believed to interact with $p47^{phox}$ in the active state are shown as red dots (taken and adapted from Groemping and Rittinger, 2005).

FAD is present even before activation of the oxidase (Rotrosen et al., 1992; Segal et al., 1992; Sumimoto et al., 1992). Based on sequence comparisons presented in these studies it was suggested that the $gp91^{phox}$ subunit could also contain the binding site for NADPH. This has been confirmed by photoaffinity labelling of neutrophil membranes with 2-azido-$NADP^+$ (Segal et al., 1992).

The number and location of the heme groups present in the cytochrome has been controversial, and it was initially suggested that the heme-binding component of flavocytochrome b_{558} was $p22^{phox}$. Yamaguchi and colleagues chromatographically purified flavocytochrome b_{558} to yield a 20 kDa subunit as determined by SDS-PAGE. Oxidised spectra of the protein showed an absorption maximum at 413.5 nm and the reduced spectra showed absorption maxima of 426 nm, 529 nm and 558 nm, thus suggesting that the 20 kDa subunit of the flavocytochrome was the heme bearing component. However, their proposal has since been rejected as not only was $gp91^{phox}$ absent in their final product but the amino acid sequence of the purified 20 kDa protein was markedly different from that predicted for $p22^{phox}$ (Yamaguchi et al., 1989). It quickly became apparent that in fact flavocytochrome b_{558} contained 2 heme groups with midpoint redox potentials (Em) of -225 mV and -265 mV (Cross et al., 1995), yet their precise location remained unclear for some time. For example Quinn and colleagues reported the presence of hemes in both subunits based on the separation of the cytochrome components by LDS-PAGE followed by heme staining using tetramethylbenzidine (TMBZ) (Quinn et al., 1992). It was suggested that one of the heme molecules may be shared with $p22^{phox}$, which was supported by the finding that not only does $p22^{phox}$ contain a histidine at position 94 (His94) which aligns exactly the same as the heme coordinating histidine in myoglobin, but that the region surrounding His94 also resembled that of a heme bearing region of mitochondrial cytochrome *c* oxidase (Parkos et al., 1988).

However since these reports, there has been overwhelming evidence to suggest that histidine residues in the N-terminal hydrophobic portion of $gp91^{phox}$ coordinate both hemes. Yu and colleagues conducted studies where they spectrophotometrically examined the membranes of transgenic COS7 cell lines expressing $gp91^{phox}$, $p22^{phox}$ or both. They reported that cell lines expressing $gp91^{phox}$ or both $gp91^{phox}$ and $p22^{phox}$ had a heme spectrum similar to that of human neutrophil flavocytochrome b_{558}. However, this spectrum was absent in cell lines only expressing $p22^{phox}$. In addition, cell lines expressing $gp91^{phox}$ alone exhibited mid-point potentials of -233 mV and -264 mV, supporting the hypothesis that $gp91^{phox}$ is the sole bearer of the two heme groups (Yu et

al., 1998). The heme-coordinating histidine residues have been suggested to be located in predicted helices III and V: 101:209 and 115:222, based on mutational studies by Biberstine-Kinkade and colleagues. These authors reported that mutation of either of the histidine residues to leucine significantly reduced the heme spectrum and $O_2^{\cdot-}$ generation (Biberstine-Kinkade et al., 2001). In addition, missense mutations in any of these histidine residues have been associated with X-linked CGD.

1.3.1.2 $P22^{phox}$

The $p22^{phox}$ subunit (also called the α-subunit) of flavocytochrome b_{558} consists of 195 amino acids. Secondary structure and hydropathy analysis of $p22^{phox}$ predicts the N-terminal, hydrophobic portion of the protein to contain three transmembrane α-helices (Parkos et al., 1988) (Figure 6). The C-terminal cytoplasmic region does not contain any predicted secondary structure and is believed to be highly flexible. The only recognisable motif within this region is a proline-rich (PR) or PxxP motif that is known to be the target sequence for the Src-homology 3 (SH3) domains.

By now it is well established that this PR motif within the cytoplasmic portion of $p22^{phox}$ constitutes the docking site for active $p47^{phox}$. One of the early studies, which provided evidence for this was by Sumimoto and colleagues who used a monoclonal antibody that specifically recognizes p47SH3 to show a direct interaction between $p47^{phox}$ SH3 domains and $p22^{phox}$ (Sumimoto et al., 1994). Similar evidence for a $p22^{phox}$-$p47^{phox}$ interaction was provided by Leto and colleagues using biotinylated $p47^{phox}$ SH3 domains to probe nitrocellulose membranes blotted with $p22^{phox}$ (aa 127-195) (Leto et al., 1994). The importance of this interaction has been highlighted by the mutation of proline 156 to glutamine that has been identified in a $p22^{phox}$ deficient CGD patient (Dinauer et al., 1991). Loss of proline 156 completely abolishes the translocation of the cytosolic component $p47^{phox}$ to the membrane and prevents NADPH oxidase activity (Leto et al., 1994; Leusen et al., 1994a).

1.3.2 Cytosolic components

In the resting state of the NADPH oxidase the subunits $p47^{phox}$ (Segal et al., 1985) $p67^{phox}$ (Leto et al., 1990), $p40^{phox}$ (Wientjes et al., 1993) and the small GTPases Rac (Abo et al., 1991) are located in the cytosol. Their discovery and characterisation has been aided immensely by the development of cell-free assays for reconstitution

studies which was originally developed in 1984 (Bromberg and Pick, 1984; Heyneman and Vercauteren, 1984), and production of specific antibodies against the different subunits. Briefly, cell-free assays involve recovering membrane and cytosolic fractions from resting neutrophils and activating the NADPH oxidase by mixing the subcellular fractions with activators such as protein kinase C (PKC), the bacterial peptide fMLP, the PKC activator phorbol myristate acetate (PMA) or sodium dodecyl sulfate (SDS) which is believed to mimick phosphorylation by providing negative charges (Abo et al., 1994; Bromberg and Pick, 1984; Heyneman and Vercauteren, 1984; Park et al., 1992). In contrast, whole cell assays involves the activation of intact cells followed by recovering membrane and cytosolic fractions, and subsequent detection of NADPH oxidase components by immunoblot assays (Abo et al., 1994; Heyworth et al., 1991; Nauseef et al., 1991).

Many researchers believe that during the resting state of the NADPH oxidase some cytosolic $p47^{phox}$ exists in complex with $p67^{phox}$ and $p40^{phox}$, as a tight hetero-trimer of approximately 240-300 kDa. Evidence for this has been provided using chromatographic purification and immunoprecipitation of resting neutrophil cytosols followed by immunoblot assays (Park et al., 1992; Someya et al., 1993; Wientjes et al., 1993). Lapouge and colleagues further employed analytical ultracentrifugation, dynamic light scattering and isothermal titration calorimetry to show that the large apparent molecular weight of the $p47^{phox}$-$p67^{phox}$-$p40^{phox}$ complex detected by gel filtration is due to its extended non-globular structure, rather than the presence of multiple copies of the components as previously believed (Lapouge et al., 2002).

However, more recently this model has been challenged by Brown and colleagues, who developed a new assay for studying NADPH oxidase activation, in which they permeabilised resting neutrophil membranes with Streptolysin-O to allow the cytosolic contents to gently leak out into the surroundings, whilst maintaining the intracellular structure as verified by electron microscopy (Brown et al., 2003). As determined by gel filtration chromatography and immunoblot assays, under these conditions it was found that only $p40^{phox}$-$p67^{phox}$ co-eluted and that $p47^{phox}$ eluted separately. Moreover immuno-depletion of $p47^{phox}$ from resting cytosols did not lead to depletion of $p67^{phox}$ or $p40^{phox}$, thus suggesting that $p47^{phox}$ associates at a later stage to form the hetero-trimeric complex, which translocates to the membrane (Brown et al., 2003). The authors of this study argue that the experimental conditions used by previous researchers, in which cells were ruptured to separate membranes from cytosols, were physically harsh and may have accidentally activated/forced the formation of the

trimeric complex. They suggest that their approach is less manipulative and that the results obtained using this novel assay are a true representation of the neutrophil resting state. In this new model $p47^{phox}$ would exist separately from the $p67^{phox}$-$p40^{phox}$ complex in the resting state, and formation of the trimeric complex would in fact constitute the first step along the activation pathway.

Not enough data are currently available to fully understand the conflicting observations made, and to decide what truly constitutes the resting state of the NADPH oxidase. Further studies are now required to gain a better insight into this aspect of the activation process. However, it is clear that neutrophil stimulation causes a trimeric complex consisting of $p47^{phox}$-$p67^{phox}$-$p40^{phox}$ to translocate to the membrane and associate with the flavocytochrome to form the active NADPH oxidase enzyme. It is also important to note that there is an excess of free cytosolic $p47^{phox}$, however the physiological significant of this is not understood at present.

1.3.2.1 $P47^{phox}$

$P47^{phox}$ consists of 390 amino acids and has a molecular weight of approximately 47 kDa. It possesses two different types of protein interaction domains (interaction domains are described in more detail in section 1.4): two adjacent SH3 domains and a phox (PX) homology domain. In addition it contains a proline-rich region (PR) and an auto-inhibitory polybasic region (rich in arginine, lysine and serine residues) (Figure 7). $P47^{phox}$ was initially identified by Segal and co-workers from autosomal recessive CGD neutrophils, as a phosphoprotein in which enhanced phosphorylation was absent. This was determined by measuring the rate of ^{32}P-incorporation in PMA activated whole cells (Segal et al., 1985). The Babior group further highlighted a possible link between $p47^{phox}$ phosphorylation and the respiratory burst. They reported that when normal neutrophils were incubated with ^{32}P and activated by either PMA, fMLP or arachidonic acid, that $p47^{phox}$ was able to take up the label. However, this uptake was not observed when $p47^{phox}$ deficient CGD neutrophils were used, thus suggesting that phosphate uptake by $p47^{phox}$ may be involved in NADPH oxidase activation (Hayakawa et al., 1986). Various groups further verified the importance of $p47^{phox}$ in NADPH oxidase activity in the late 1980's. For example Nunoi and colleagues showed that when $p47^{phox}$ purified form normal neutrophils was added to cell-free assays containing $p47^{phox}$ deficient CGD neutrophils, $O_2^{\cdot-}$ generation was restored (Nunoi et al., 1988). In support of this Lomax and colleagues used recombinant

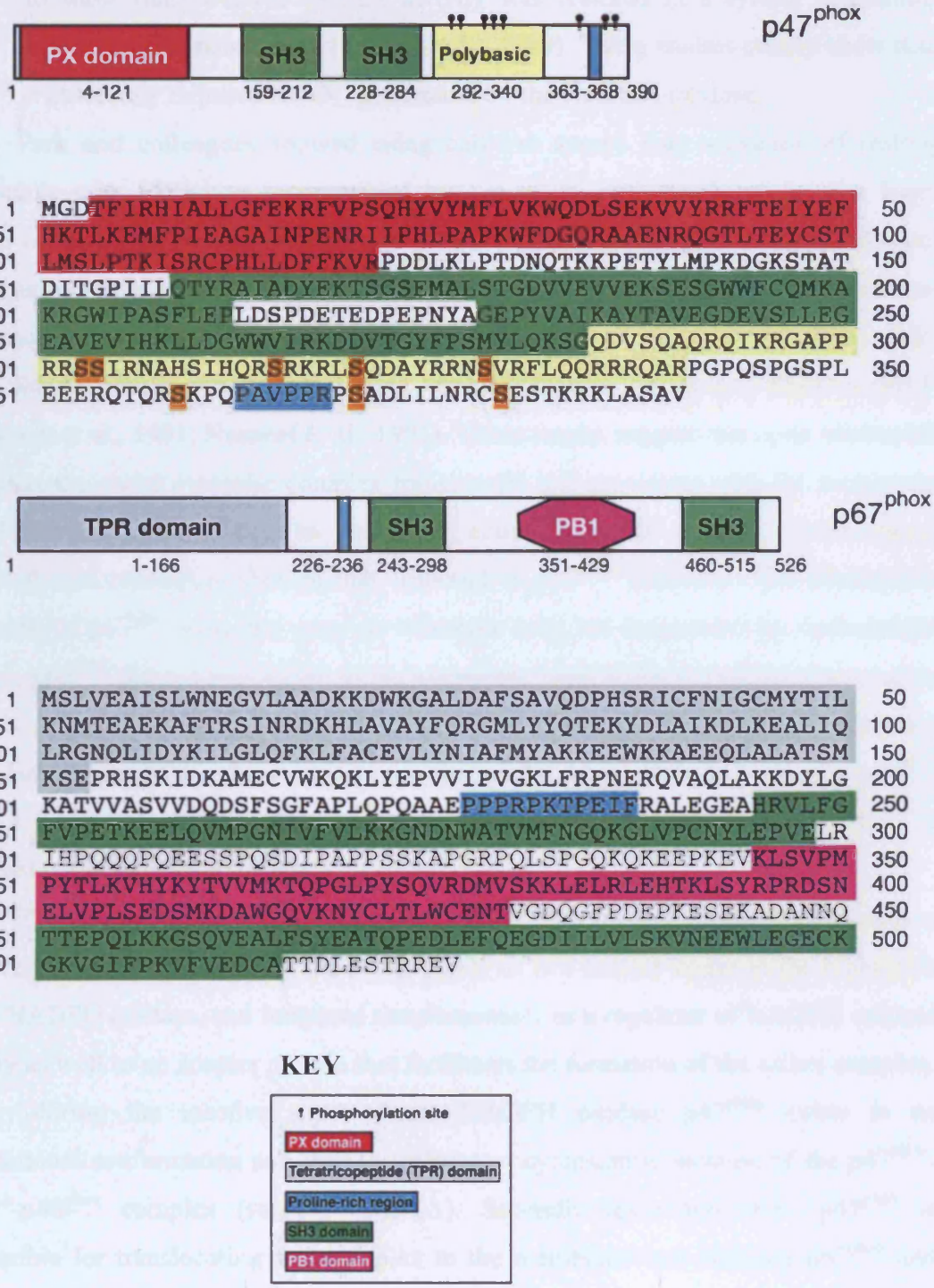

Figure 7: Domain arrangements and amino acid sequences of the cytosolic NADPH oxidase proteins p47^{phox} and p67^{phox}. The domain arrangement for p47^{phox} and p67^{phox} are shown with the corresponding amino acid sequences. P47^{phox} phosphorylation sites (serine residues) are highlighted in orange in the amino acid sequence, and shown as sticks in the domain arrangement. Boundaries of the individual domains were obtained from the Pfam database (Bateman et al., 2004) and the Prosite database (Hulo et al., 2006).

$p47^{phox}$ to show that NADPH oxidase activity was restored in a system containing $p47^{phox}$ deficient CGD neutrophils (Lomax et al., 1989). These studies clearly show that $p47^{phox}$ is absolutely required for $O_2^{\cdot-}$ generation by the NADPH oxidase.

Park and colleagues showed using cell-free assays that activation of resting neutrophils with SDS was accompanied by generation and translocation of a large protein complex comprising of $p47^{phox}$ and $p67^{phox}$, from the cytosol to the membrane. This translocation however was not observed if membranes lacked flavocytochrome b_{558}, as observed using neutrophil membranes from X-linked CGD patients (Park et al., 1992). Similar results were reported using whole cell assays activated by PMA or fMLP (Heyworth et al., 1991; Nauseef et al., 1991). These results suggest that upon neutrophil activation the entire cytosolic complex translocates and associates with the membrane bound flavocytochrome b_{558} to form the active NADPH oxidase. Furthermore, Heyworth and colleagues showed that, although in $p47^{phox}$ deficient CGD neutrophils the levels of $p67^{phox}$ were the same as wild-type cells (as determined by immunoblot assays), $p67^{phox}$ did not translocate to the membrane upon PMA activation. However in $p67^{phox}$ deficient CGD neutrophils, $p47^{phox}$ was detected in membrane fractions (Heyworth et al., 1991), clearly suggesting that of the three cytosolic proteins ($p40^{phox}$ had not been discovered at the time) that comprise the trimeric complex, $p47^{phox}$ is responsible for mediating membrane translocation.

Taken together the results from numerous studies by many different groups it is now well established that $p47^{phox}$ is a key player at two crucial stages in the regulation of the NADPH oxidase, and functions simultaneously as a regulator of NADPH oxidase activity as well as an adapter protein that facilitates the formation of the active complex. Firstly, during the inactive state of the NADPH oxidase $p47^{phox}$ exists in an autoinhibited conformation and thereby enforces a cytoplasmic location of the $p47^{phox}$-$p67^{phox}$-$p40^{phox}$ complex (section 1.3.2.1.1). Secondly upon activation, $p47^{phox}$ is responsible for translocating this complex to the membrane and bringing $p67^{phox}$ and $p40^{phox}$ into close proximity to the flavocytochrome and Rac. Membrane translocation is achieved by the specific recognition of the cytosolic portion of $p22^{phox}$ by $p47^{phox}$, as well as the interaction between the $p47^{phox}$ PX domain and membrane lipids. Additional interactions with the cytoplasmic region of $gp91^{phox}$, as described in more detail below, may further contribute to the stabilisation of the active enzyme complex.

1.3.2.1.1 The inactive state of $p47^{phox}$

The first insight into the mechanistic basis of the regulation of NADPH oxidase activity by $p47^{phox}$, came in 1994 when Sumimoto and co-workers showed that activation of the NADPH oxidase involved the interaction between the SH3 domains located in the central region of $p47^{phox}$ and $p22^{phox}$. Importantly, in this work the authors showed that the SH3 domains appear to be masked in the resting state and that activation *in vitro* by agents such as arachidonic acid or SDS relieves these autoinhibitory interactions (Sumimoto et al., 1994), thereby paving the way for the notion that NADPH oxidase activity is regulated by reversible intra- and intermolecular protein-protein interactions.

Regulation of protein function through intramolecular, auto-inhibitory interactions is a common mechanism that is found in many different systems. For example the Src family of non-receptor protein-tyrosine kinases (including Src, Lck, Hck, Fyn, Blk, Lyn, Fgr, Yes and Yrk) (Hofmann et al., 2005) contain regulatory SH3 and SH2 domains, a kinase domain, and a conserved tyrosine residue in the C-terminal tail of the protein. In the inactive state, kinase activity is inhibited due to an intramolecular interaction between the SH2 domain and the conserved phosphotyrosine in the C-terminal tail. In addition, the SH3 domain interacts with the SH2 domain-kinase linker region and thereby contributes to the inhibition of kinase activity (Sicheri et al., 1997; Williams et al., 1997; Xu et al., 1997). Similarly in the resting state of the NADPH oxidase enzyme, activity is prevented due to an auto-inhibited conformation of $p47^{phox}$.

The fact that SH3 domains can bind PR sequences and that $p47^{phox}$ itself contains a PR stretch in the C-terminal region, led to the suggestion that that during the inactive state of $p47^{phox}$ the SH3 domains may be masked by the C-terminal PR region of $p47^{phox}$ in an intramolecular fashion (Sumimoto et al., 1994). The model in which intramolecular interactions within $p47^{phox}$ prevent binding to $p22^{phox}$ was supported by a number of studies including that by Hata and colleagues, who showed through *in vitro* GST pull-down assays that full-length wild-type GST-$p47^{phox}$ could not bind its membrane target $p22^{phox}$. However, truncated $p47^{phox}$ where the C-terminal region was absent bound to $p22^{phox}$ as strongly as the isolated $p47^{phox}$ SH3 domains ($p47SH3_2$), as determined by western blot analysis. These results were in good agreement with *in vivo* binding assays using the yeast-2-hybrid system (Hata et al., 1998). The study also suggested that the region in $p47^{phox}$ recognised by the SH3 domains does not involve the

PR region, which instead mediates the interaction with $p67^{phox}$. Similar results were reported by Ago and colleagues using both *in vivo* (yeast-two hybrid assay) and *in vitro* (pull-down assays using purified proteins) methods. The authors of this study showed that while full-length wild-type $p47^{phox}$ was unable to bind $p22^{phox}$, full-length mutant $p47^{phox}$ carrying either the P299Q/P300Q or R301E/R302E mutations (located in the polybasic region) was able to bind $p22^{phox}$. This observation further supports the model that an intramolecular interaction between the SH3 domains of $p47^{phox}$ and the region C-terminal to these domains prevents binding to $p22^{phox}$, and that the binding site for $p22^{phox}$ only becomes accessible after this intramolecular interaction is disrupted (Ago et al., 1999).

More recently this model has been verified by crystal and solution structures of inactive $p47^{phox}$ which clearly show that the ligand binding sites of the tandem SH3 domains are masked by an intramolecular interaction with the polybasic region (Groemping et al., 2003; Yuzawa et al., 2004a; Yuzawa et al., 2004b) (Figure 8). The crystal structure of the auto-inhibited core of $p47^{phox}$ (aa 156-340) shows that the two SH3 domains cooperate and that their conserved ligand binding sites are juxtaposed in such a fashion that they form a novel, single ligand binding site, a conformation now called the superSH3 domain (Groemping et al., 2003) (superSH3 domains are described in more detail in section 1.6). The polybasic region is bound to this novel ligand binding site via the non-consensus sequence $_{296}$RGAPPRRSS$_{304}$ (Figure 8). The core $_{297}$GAPPR$_{301}$ region adopts a PPII conformation (section 1.4.1), and makes contacts with both the $SH3_A$ and $SH3_B$ domains. In addition, extensive contacts are also made by the remainder of the polybasic region, which interacts with both SH3 domains and the linker connecting the two domains. To investigate the importance of these additional contacts Groemping and colleagues carried out quantitative binding studies using isothermal titration calorimetry (ITC). They showed that a peptide with the sequence $_{296}$RGAPPRRSS$_{304}$ bound to the tandem SH3 domains, but not the individual SH3 domains, with an affinity of 29 μM. However, when the peptide was extended to include an additional 26 residues (296-330), the affinity for the tandem SH3 domains was increased to 1.5 μM (Groemping et al., 2003). These results suggest that additional contacts outside the core binding region significantly contribute to the maintenance of the auto-inhibited state. Furthermore, these studies support the notion that the region containing amino acids 156-340 is sufficient to maintain the auto-inhibited state. This region will be referred to as the "auto-inhibited core".

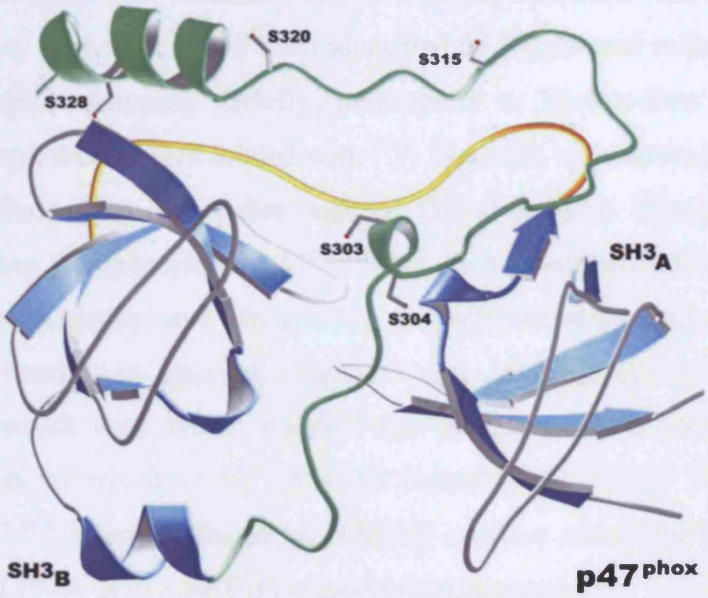

Figure 8: Structure of $p47^{phox}$ in the auto-inhibited state. The tandem SH3 domains (blue) are masked by an intramolecular interaction with the polybasic region (green). Phosphorylation sites in the polybasic region are shown as sticks (S303, 304, 315, 320 and 328). The linker connecting $SH3_A$ and $SH3_B$ is shown in yellow. PDB identifier 1NG2 (Groemping et al., 2003). The figure was prepared using the program Molscript.

1.3.2.1.2 $P47^{phox}$ phosphorylation relives the auto-inhibited conformation

The phosphorylation of $p47^{phox}$ plays a key role in the activation process of the NADPH oxidase, and was first linked with NADPH oxidase activity when it was shown that that phosphorylation of this protein was abnormal in $p47^{phox}$ deficient CGD patients (Hayakawa et al., 1986; Segal et al., 1985). $P47^{phox}$ is the most extensively phosphorylated subunit of the NADPH oxidase and so far eleven serine residues have been shown to become phosphorylated. Interestingly, they are all located in the region C-terminal to the tandem SH3 domains (S303, 304, 310, 315, 320, 328, 345, 348, 359, 370 and 379). Many of the sites have been identified by Babior and collaborators using tryptic phosphopeptide mapping. Briefly, neutrophils or Epstein-Barr virus (EBV)-transformed B lymphoblasts were loaded with ^{32}P. The cells were activated and $p47^{phox}$ was immunopurified using antibodies against the C-terminal portion of $p47^{phox}$. Fractions containing phosphorylated $p47^{phox}$ were then characterised by SDS-PAGE followed by autoradiography, and identified as a single radioactive band migrating at ~47 kDa. The band was excised, digested and phosphopeptides detected by autoradiography, which were HPLC purified and phosphorylation sites identified by Edman degradation (el Benna et al., 1994; El Benna et al., 1996). To examine the importance of $p47^{phox}$ phosphorylation in NADPH oxidase activation Babior's group subsequently used PMA activated EBV-transformed lymphoblasts deficient in $p47^{phox}$ which were transfected with different $p47^{phox}$ serine to alanine mutants,. These studies showed that a mutant protein where all eleven serine residues between S303 and S379 were substituted for alanine was i) not phosphorylated and ii) almost completely failed to support $O_2^{\cdot-}$ generation (Faust et al., 1995). These results clearly suggest that $p47^{phox}$ phosphorylation is essential for normal NADPH oxidase activation.

Several approaches were used to identify the kinases responsible for phosphorylation of $p47^{phox}$. For example El-Benna and colleagues used immunoprecipitated $p47^{phox}$ from resting neutrophils, and incubated it with [γ-^{32}P]ATP and either protein kinase C (PKC), protein kinase A (PKA) or mitogen activated protein kinase (MAP). They then employed tryptic phosphopeptide mapping to identify which $p47^{phox}$ phosphorylation sites were phosphorylated by which kinase. Peptide mapping revealed that PKA only phosphorylated Ser320 and Ser328 and/or the Ser359/370 peptides, and MAP kinase only phosphorylated the Ser345/348 peptide. However, PKC phosphorylated all the $p47^{phox}$ peptides other than that corresponding to Ser345/348, thus suggesting that PKC may be a key kinase for phosphorylation of $p47^{phox}$ (El Benna

et al., 1996). There is now a great deal of evidence supporting a positive role for PKC in NADPH oxidase activation; for example Nauseef and colleagues showed that staurosporine which is a potent PKC inhibitor prevented i) PMA activated $O_2^{\cdot-}$ generation ii) $p47^{phox}$ phosphorylation as determined by autoradiography and iii) $p47^{phox}$ membrane translocation as determined by immunoblot assays (Nauseef et al., 1991). Altogether this suggests that $p47^{phox}$ phosphorylation by PKC is associated with membrane translocation of $p47^{phox}$, and the assembly of active NADPH oxidase complex.

The contribution of individual $p47^{phox}$ serine residues to NADPH oxidase activation has been studied extensively, and many of these studies have made use of phosphorylation mimics, where serine residues have been substituted with either aspartate or glutamate residues. These amino acids are the closest in conformation to a phosphoserine (Figure 9). Based on a number of studies it appears as phosphorylation of only eight $p47^{phox}$ serine residues is sufficient for NADPH oxidase activation, as described in more detail below. These include serine residues 303, 304, 315, 320, 328, which are located in the polybasic region and form part of the auto-inhibitory region. Further phosphorylation sites required for activation includes serine 359, which is located N-terminal and serine residues 370 and 379, which are located C-terminal to the PR region, a segment that otherwise mediates the interaction with $p67^{phox}$. Ago and colleagues used the yeast two-hybrid system to show that the simultaneous substitution of serine residues 303, 304 and 328 by either aspartate or glutamate was sufficient to disrupt autoinhibitory, intramolecular interactions and allow binding to $p22^{phox}$. Furthermore, the authors of this study showed that these mutations supported $O_2^{\cdot-}$ generation in cell-free systems without the need of activators such as arachidonic acid or SDS (Ago et al., 1999), strongly indicating that these residues play a key role in NADPH oxidase activation. This suggestion is further supported by the observation that the substitution of all serine residues known to become phosphorylated (S303, 304, 310, 315, 320, 328, 345, 348, 359, 370 and 379) by either aspartate or glutamate except either one of S303, S304 or S328 produced mutant proteins that failed to interact with $p22^{phox}$, thus further highlighting the importance of phosphorylation of $p47^{phox}$ serine residues 303, S304 and S328 for $p22^{phox}$ binding and NADPH oxidase activation (Ago et al., 1999).

Additional support for the importance of these serine residues was provided by Groemping and colleagues who quantified the contribution of individual residues to the

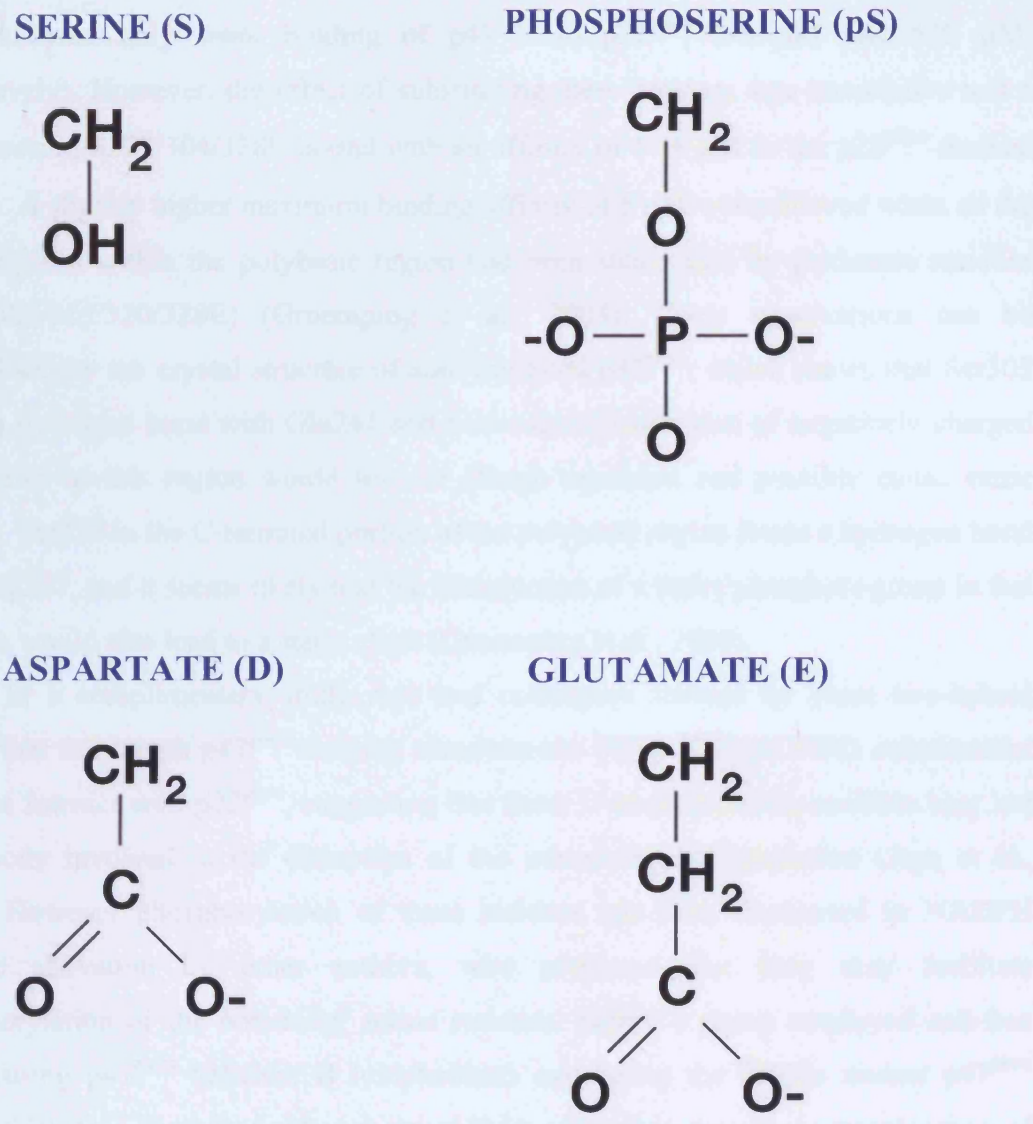

Figure 9: **Side-chain structures of phosphorylation mimics.** The side-chains of the amino acids serine (S), phosphoserine (pS), aspartate (D) and glutamate (E). Glutamate is closest in conformation to phosphoserine.

activation process by fluorescence spectroscopy using a fluoresceine-labelled $p22^{phox}$ peptide and $p47^{phox}$ recombinant proteins (Groemping et al., 2003). They showed that the double substitution of S303 and S304 to glutamate or the single substitution of S328 alone allowed only weak binding of $p47^{phox}$ to $p22^{phox}$ (93 μM and 590 μM, respectively). However, the effect of substituting these residues was cumulative and a triple mutant, S303/304/328E bound with an affinity of 17.8 μM to the $p22^{phox}$-derived peptide. A slightly higher maximum binding affinity of 8 μM was achieved when all the serine resides within the polybasic region had been substituted by glutamate residues (S303/304/315/320/328E) (Groemping et al., 2003). These observations can be rationalised by the crystal structure of auto-inhibited $p47^{phox}$, which shows that Ser303 forms a hydrogen bond with Glu241 and hence that introduction of negatively charged phosphates in this region would lead to charge repulsion and possibly cause steric clashes. Ser328 in the C-terminal portion of the polybasic region forms a hydrogen bond with Arg267, and it seems likely that the introduction of a bulky phosphate group in this position would also lead to a steric clash (Groemping et al., 2003).

In a complimentary study Ago and colleagues showed by yeast two-hybrid assays that full-length $p47^{phox}$ carrying simultaneous S359, 370 and 379D substitutions failed to interact with $p22^{phox}$, suggesting that these C-terminal serine residues may not be directly involved in the disruption of the intramolecular interaction (Ago et al., 1999). However phosphorylation of these residues has been implicated in NADPH oxidase activation by other authors, who proposed that they may facilitate phosphorylation of the remaining serine residues. Babior's group employed cell-free assays using $p47^{phox}$ deficient B lymphoblasts expressing the double mutant $p47^{phox}$ S303A/S304A to show that although upon PMA activation, membrane translocation of the mutant was not affected (as determined by immunoblot assays) it nevertheless almost completely failed to support $O_2^{\cdot-}$ generation. Enzyme activity was restored when the alanines were replaced with glutamates, thus suggesting that phosphorylation of S303 and S304 is essential for NADPH oxidase activation but not for translocation (Inanami et al., 1998). However, in a similar assay $p47^{phox}$ S359A/S370A or S359K/S370K mutants caused a dramatic reduction in $O_2^{\cdot-}$ generation and prevented phosphorylation of other serine residues, as well as prevented membrane translocation. Although oxidase activity was still reduced when these mutations were replaced by aspartate or glutamate residues (S359D/S370D or S359E/S370E), these mutant proteins translocated to the membrane in a normal manner and phosphorylation of other serine residues was restored (Johnson et al., 1998). Based on these results the Babior group

proposed that phosphorylation of S359 and/or S370 takes place first, which is then followed by phosphorylation of S379 and then S303 and/or S304. S379 is believed to play a central role in $p47^{phox}$ activation in this model as Faust and colleagues showed that in comparison to other $p47^{phox}$ serine residues, mutation of S379 to alanine alone resulted in the most significant loss in $p47^{phox}$ translocation and consequently $O_2^{\cdot-}$ generation (Faust et al., 1995). However, this model is contradictory to other data which clearly show that phosphorylation of serine residues 303, 304 and 328 are sufficient for membrane translocation of the trimeric complex and $O_2^{\cdot-}$ production (Ago et al., 1999). Further studies are now required to fully understand the biological significance of phosphorylation of serine residues 359, 370 and 379, and to establish if phosphorylation of $p47^{phox}$ occurs in a sequential manner that requires phosphorylation of a particular serine residue to allow further phosphorylation events.

1.3.2.1.3 $P47^{phox}$ tandem SH3 domains bind the cytoplasmic region of $p22^{phox}$

The studies described above clearly show that $p47^{phox}$ activation induces conformational changes within the protein, which disrupt an intramolecular interaction and expose the SH3 domains allowing them to bind to $p22^{phox}$. While the importance of a $p47^{phox}$-$p22^{phox}$ interaction has been generally accepted there were conflicting data concerning the requirement of one or both SH3 domains of $p47^{phox}$. These were mostly due to the fact that different techniques had been used to investigate this interaction (for example immunoblot, pull-down or yeast two-hybrid assays), which may have underestimated the contribution of both domains to complex formation (de Mendez et al., 1997; Sumimoto et al., 1996). However, the simultaneous requirement for both SH3 domains of $p47^{phox}$ to form a tight complex with $p22^{phox}$ has since been confirmed by the structure of the tandem SH3 domains of $p47^{phox}$ bound to a peptide derived from $p22^{phox}$ (which is thought to mimick the active state of $p47^{phox}$). This structure shows that the tandem SH3 domains adopt a superSH3 domain conformation as previously observed in the autoinhibited protein, and interact with the consensus PXXP motif ($_{154}$NPPPRP$_{159}$) located in the cytoplasmic tail of $p22^{phox}$ (Figure 10) (Groemping et al., 2003). Although $SH3_A$ is the dominant component in the interaction with $p22^{phox}$, the cooperation of both, $SH3_A$ and $SH3_B$ is required to achieve tight complex formation with $p22^{phox}$, as highlighted by ITC experiments that show that whilst isolated $SH3_A$ is able to bind to $p22^{phox}$ on its own with an affinity of 3.4 μM, the strength of this interaction

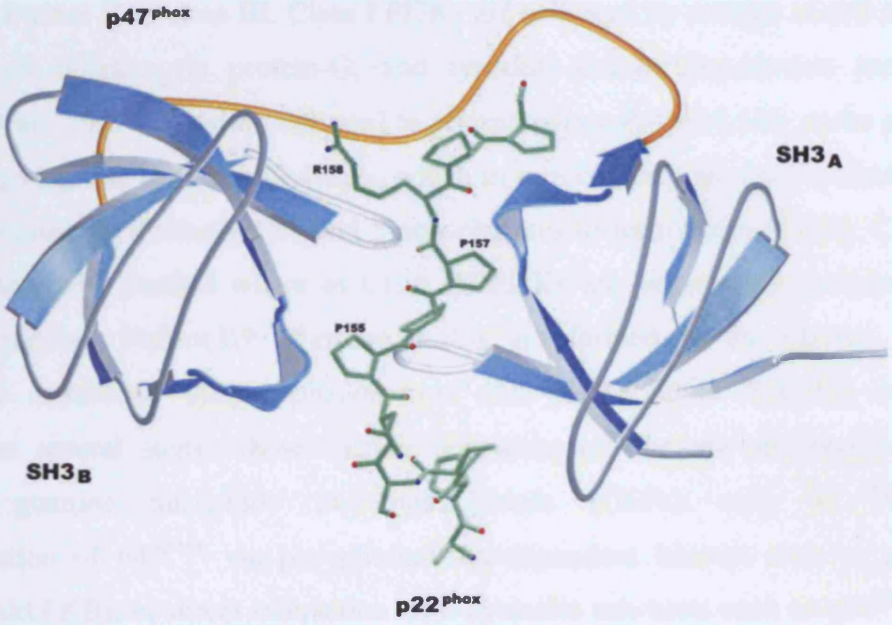

Figure 10: Structure of an active form of $p47^{phox}$ in complex with a $p22^{phox}$-derived peptide. The tandem SH3 domains are shown in blue, and the linker connecting $SH3_A$ and $SH3_B$ in yellow. The $p22^{phox}$ peptide is shown in green stick format, and key residues of the PXXP motif are highlighted (R158, P157 and P155). PDB identifier 1OV3 (Groemping et al., 2003). The figure was prepared using the program Molscript.

is greatly increased to 0.19 μM by the presence of $SH3_B$ (Groemping et al., 2003). Furthermore this structure also provides a molecular basis for the observation that substitution of proline 156 in $p22^{phox}$ by glutamine causes CGD, by highlighting the extensive contacts made between this residue and $p47^{phox}$.

1.3.2.1.4 $P47^{phox}$ PX domain binds PtdIns(3,4)P_2

Phosphoinositide 3-kinases (PI3K) are a family of enzymes which belong to either class I, class II or class III. Class I PI3Ks are activated by a range of cell surface receptors that operate via protein-G, and tyrosine kinase transduction pathways (Hawkins et al., 2007). They are believed to phosphorylate PtdIns(4,5)P_2 in the plasma membrane giving rise to PtdIns(3,4,5)P_3, which in turn can be dephosphorylated by 3-proteases to generate PtdIns(4,5)P_2 and 5-phosphatases to form PtdIns(3,4)P_2. Class II PI3Ks are less well studied where as Class III PI3Ks are believed to phosphorylate PtdIns to generate PtdIns(3)P. Various PtdIns are formed in the plasma and/or phagosomal membrane during phagocytosis and can regulate NADPH oxidase activation at several steps. These include activation of Rac via phosphoinositide-dependent guanine nucleotide exchange factors (GEFs) such as P-Rex1, phosphorylation of $p47^{phox}$ via phosphoinositide-dependent kinases such as protein kinase B (Akt/PKB), or direct interaction with cytosolic sub-units such as $p47^{phox}$ and $p40^{phox}$, as described in more detail below (reviewed by Hawkins, 2007).

The products of PI3Ks are well established signalling molecules which interact with a range of protein interaction domains including the PX domain (for details see section 1.4.4). The N-terminal regions of $p47^{phox}$ and $p40^{phox}$ both contain a PX domain and binding of these domains to PtdIns contributes to subcellular localisation and membrane association. The lipid specificity of PX domains and specifically of the PX domain within $p47^{phox}$ was established by Kanai and colleagues, who carried out protein-lipid binding assays using so-called PIP-arrays, in which various phosphatidylinositols were spotted onto nitrocellulose membranes. These were incubated with either $p47^{phox}$ or $p40^{phox}$ PX domain GST-fusion proteins and binding was detected using anti-GST antibodies (Kanai et al., 2001). The authors of this study showed that the $p47^{phox}$ PX domain bound strongly to PtdIns(3,4)P_2 but weakly to various other PtdIns including PtdIns (3,5)P_2, PtdIns(3)P and PtdIns(3,4,5)P_3. In contrast the $p40^{phox}$ PX domain specifically only bound to PtdIns(3)P. This suggests that the $p47^{phox}$ PX domain has a strong preference for PtdIns (3,4)P_2, where as the $p40^{phox}$

PX domains has a preference for PtdIns(3)P. This observation was verified by a number of other *in vitro* assays including ultracentrifugation assays for lipid-vesicle binding (see Materials and Methods). Furthermore this study showed that mutation of R42Q in the PX domain of $p47^{phox}$, which is found in some CGD patients completely eliminated binding to PtdIns $(3,4)P_2$, thus further highlighting the importance of lipid binding for full NADPH oxidase activity (Kanai et al., 2001).

Karathanassis and colleagues furthered our understanding of the lipid binding activity of the $p47^{phox}$ PX domain, by carrying out more quantitative binding studies using surface plasmon resonance (SPR) with lipid vesicles coupled to sensor chips (Karathanassis et al., 2002). They showed that in the absence of PtdIns$(3,4)P_2$, purified recombinant $p47^{phox}$ PX domain had a low affinity (>20 μM) for vesicles only containing phosphatidylcholine (PC) or phosphatidylethanolamine (PE). However when PtdIns$(3,4)P_2$ was included the affinity dramatically increased to 38 nM. Furthermore, mutations in the PtdIns$(3,4)P_2$ binding pocket such as R43Q and R90A decreased the affinity by 245-fold and 84-fold; respectively (Karathanassis et al., 2002). These results clearly show that the $p47^{phox}$ PX domain binds with high affinity to PtdIns$(3,4)P_2$. Interestingly, the crystal structure of the $p47^{phox}$ PX domain shows that it contains a second, smaller lipid binding pocket which might possibly accommodate small anionic lipids (Figure 17). This is supported by the observation that in the presence of phosphatidic acid (PA) the affinity for PtdIns$(3,4)P_2$ in increased 63-fold, while the presence of phosphatidylserine (PS) increased the affinity 25-fold. These results indicate that simultaneous binding in the presence of an anionic phospholipid, preferentially PA, may synergistically increases membrane affinity (Karathanassis et al., 2002).

1.3.2.1.5 $P47^{phox}$ phosphorylation relieves the PX domain for PtdIns$(3,4)P_2$ binding

During the resting state of the NADPH oxidase, binding of the $p47^{phox}$ PX domain to PtdIns appears to be masked (in the context of the full-length protein). Using SPR Karathanssis and colleagues showed that the binding affinity for PtdIns$(3,4)P_2$ was 34-fold weaker (1.3 μM) than that for the isolated PX domain (38 nM), suggesting that in the resting state of the enzyme the PX domain is not fully accessible (Karathanassis et al., 2002). Ago and colleagues similarly showed using liposome binding assays (for details see Material and Methods) that full-length recombinant GST-$p47^{phox}$ was unable to bind liposomes containing PtdIns$(3,4)P_2$, where as isolated GST-$p47^{phox}$ PX domain

bound effectively (Ago et al., 2003). A subset of PX domains contain a consensus PxxP motif, which is typically known to bind SH3 domains, leading to the suggestion that intramolecular PxxP-SH3 domain interactions in $p47^{phox}$ may be responsible for inhibition of lipid binding. This model originated from a study by Hiroaki and colleagues who showed through NMR chemical shift perturbation assays, that the $p47^{phox}$ PX domain was able to bind the $p47^{phox}$ $SH3_B$ domain with an affinity of around 50 μM (Hiroaki et al., 2001). However, the crystal structure solved by Groemping and colleagues has since shown that during the resting state, the polybasic region already occupies the binding surfaces of the tandem SH3 domains, which are thus not available to interact with the PX domain (Groemping et al., 2003).

Interestingly though, certain mutations in $p47^{phox}$ that interfere with auto-inhibition and lead to NADPH oxidase activation have been shown to restore lipid binding. For example Karathanssis and colleagues used SPR to show that mutation of the conserved $SH3_B$ residue W263 (W263R) in full-length protein increased the affinity for lipid vesicles by 560-fold, in comparison to full-length wild-type $p47^{phox}$. Similar observations were made using *in vitro* liposome binding assays (Ago et al., 2003). Importantly, it has emerged that phosphorylation of the same serine residues that induce activation of $p47^{phox}$ exposes the PX domain and thereby allows interaction with PtdIns. For example, Ago and colleagues used the whole-cell system where they transfected either wild-type full-length $p47^{phox}$ or a full-length mutant carrying the S303/304/328A substitution into K562 cells (leukemic cell line transduced with $gp91^{phox}$ and $p67^{phox}$) (Ago et al., 2003). They showed that when these cells were stimulated with PMA the triple mutant did not translocate to membranes as determined by immunoblot assays, and failed to support $O_2^{\cdot-}$ generation. However wild-type $p47^{phox}$ supported both, thus indicating that phosphorylation of S303, 304 and 328 is required to induce a conformational change in $p47^{phox}$, which renders the PX domain free for PtdIns binding. This was further supported by the observation that full-length GST-$p47^{phox}$, which was phosphorylated *in vitro* by PKCβII bound to PtdIns liposomes, however full-length GST- $p47^{phox}$ S303/304/328A did not. More importantly, the $p47^{phox}$ phosphorylation mimic carrying S303/304/328D substitutions was capable of binding PtdIns liposomes without treatment with PKC (Ago et al., 2003). Similarly Karathanassis and colleagues showed through SPR analysis that a quintuple full-length $p47^{phox}$ phosphorylation mimic carrying S303, 304, 328, 359 and 370E substitutions, bound to PtdIns(3,4)P_2 lipid vesicles with an affinity 100-fold greater than wild-type $p47^{phox}$ (Karathanassis et al., 2002).

Although it is not clear how phosphorylation of the C-terminal serine residues 359 and 370 may contribute to the exposure of the PX domain, it is well accepted that phosphorylation of the serine residues located within the auto-inhibited segment (S303, 304 and 328) plays a key role. Overall, the studies carried out so far leave no doubt that the $p47^{phox}$ PX domain is masked in the full-length protein. Nevertheless the exact binding target of the PX domain is unknown, and will most likely involve the complete auto-inhibitory core rather than solely the $SH3_B$ domain of $p47^{phox}$ as initially suggested.

1.3.2.1.6 Active $p47^{phox}$ may interact directly with $gp91^{phox}$

In addition to the interaction between $p47^{phox}$ and $p22^{phox}$ it has been proposed that active $p47^{phox}$ may also directly interact with $gp91^{phox}$ at potentially three different sites (Figure 6). One of these was identified by Leusen and colleagues using neutrophils from an X-linked CGD patient carrying the $gp91^{phox}$ N500G mutation. Using PMA activated cell-free assays they reported that neutrophils from this patient failed to support $O_2^{\cdot-}$ generation and that membrane association of $p47^{phox}$ was strongly reduced (determined by immunoblot assays) (Leusen et al., 1994b). Moreover this failure was corrected when membranes were replaced with those from normal neutrophils, suggesting that $p47^{phox}$ directly interacts with $gp91^{phox}$ at position 500 in the extreme C-terminal region. This proposal was further confirmed by the observation that pre-incubation of normal neutrophil membranes in cell-free assays with a synthetic wild-type peptide spanning $gp91^{phox}$ at amino acids 491-504 interfered with both, $p47^{phox}$ membrane translocation and $O_2^{\cdot-}$ generation. However, a mutant peptide carrying the N500G substitution was 10-fold less potent than the wild-type peptide (Leusen et al., 1994b). DeLeto and colleagues used random-sequence peptide phage display library analysis of recombinant $p47^{phox}$, to further identify potential sites of interaction between $p47^{phox}$ and flavocytochrome b_{558}. They mapped two additional sites encompassing amino acids 450-457 (close to the NADPH binding site) and amino acids 86-93 (in the first cytosolic loop of $gp91^{phox}$) and reported that synthetic peptides to these regions also inhibited $O_2^{\cdot-}$ generation (DeLeo et al., 1995). Furthermore, peptide walking experiments have been used to map possible regions in $p47^{phox}$ that may bind $gp91^{phox}$. Briefly, overlapping peptides spanning $p47^{phox}$ were added to a cell free system and their ability to inhibit NADPH oxidase activity determined. Results of such studies identified the region spanning residues 301-339 in $p47^{phox}$ as a possible $gp91^{phox}$ binding site (Morozov et al., 1998).

These proposed multiple interactions between $p47^{phox}$ and $gp91^{phox}$ may take place to correctly position $p67^{phox}$ for interaction with $gp91^{phox}$, or may induce conformational changes in flavocytochrome b_{558}. However the molecular details of such an interaction are unknown.

1.3.2.2 $P67^{phox}$

$P67^{phox}$ consists of 526 amino acids and has a molecular weight of approximately 60 kDa. It contains three different types of protein interaction domains: a tetratricopeptide repeat (TPR) domain, consisting of four repeats, two SH3 domains and a PB1 domain. In addition it contains a PR region (Figure 7). $P67^{phox}$ was initially identified through immunoblot assays as a protein missing in neutrophils from patients with a form of autosomal recessive CGD (Volpp et al., 1988). Its importance for NADPH oxidase activity was highlighted by Leto and colleagues using cell-free assays, where the authors showed that purified recombinant $p67^{phox}$ was able to partially restore NADPH oxidase activity in $p67^{phox}$ deficient CGD neutrophils (Leto et al., 1990). In the resting state of the oxidase $p67^{phox}$ interacts simultaneously with $p40^{phox}$ and $p47^{phox}$ (for detailed descriptions refer to section 1.3.2) and acts as a bridge that connects these two proteins (section 1.5). After activation and translocation to the membrane $p67^{phox}$ interacts with the membrane bound flavocytochrome b_{558}, and with Rac. The possible functional significance of these interactions are discussed in detail below.

1.3.2.2.1 $P67^{phox}$ is absolutely required for NADPH oxidase activity

Heyworth and colleagues showed that $p67^{phox}$ failed to migrate to the membrane in $p47^{phox}$ deficient CGD neutrophils stimulated with PMA, thus suggesting that membrane translocation of $p67^{phox}$ is dependent on the presence of $p47^{phox}$ (Heyworth et al., 1991). However, using cell-free assays Freeman and Lambeth showed that as long as $p67^{phox}$ and Rac were present at high concentration, $p47^{phox}$ was not essential for generating large amounts of $O_2^{\cdot-}$ Nevertheless, if either $p67^{phox}$ or Rac were omitted from the system then no NADPH oxidase activity was observed, even in the presence of high concentrations of $p47^{phox}$ (Freeman and Lambeth, 1996). This highlights the importance of $p67^{phox}$ in NADPH oxidase activity, and suggests that although $p47^{phox}$ plays an important role as an adaptor protein it is $p67^{phox}$ and Rac, which are essential for $O_2^{\cdot-}$ generation. These authors go on to suggest that $p67^{phox}$ and/or Rac may be

directly involved in regulating NADPH oxidase activity (Freeman and Lambeth, 1996) as discussed in more detail in section 1.3.2.4.5.

Molecular details of the involvement of $p67^{phox}$ in regulating NADPH oxidase activity were beginning to emerge in 1998 when Han and colleagues reported that truncated $p67^{phox}$ (1-198) failed to support $O_2^{\cdot-}$ generation in cell-free systems. Shorter truncations (1-235, 1-221, 1-216 and 1-210) generated $O_2^{\cdot-}$ similar to wild-type $p67^{phox}$, however any $p67^{phox}$ construct shorter than 210 amino acids failed to support enzyme activity. Based on these results the authors proposed that $p67^{phox}$ contained an 'activation domain' in the region spanning residues 199-210. They further defined the activation domain by making single amino acid mutations (converted to alanine or leucine), and examining the effects these mutations had on $O_2^{\cdot-}$ generation. They showed that the mutations significantly reduced the ability of $p67^{phox}$ to support NADPH oxidase activity, and based on these results the authors proposed that the $p67^{phox}$ activation domain may directly interact with flavocytochrome b_{558} to regulate enzyme activity. In addition the authors reported that mutations in the activation domain did not affect binding of $p67^{phox}$ to Rac, as determined by fluorescence spectroscopy. Based on these results and the fact that Rac is absolutely essential for NADPH oxidase activity, the authors proposed that the role of Rac in the NADPH oxidase system may be to correctly orientate $p67^{phox}$ so that the activation domain is juxtaposed with $gp91^{phox}$ for the electron transport reaction to take place (Han et al., 1998).

Using cell-free assays Nisimoto and colleagues measured the reduction of FAD by NADPH fluorophotometrically (Nisimoto et al., 1999). The authors of this study showed that adding NADPH to the system gradually reduced FAD over the course of the measurement, which corresponded to the observed increase in $O_2^{\cdot-}$ generation. However, when $p67^{phox}$ was omitted from the system the flavin was almost completely oxidised and $O_2^{\cdot-}$ was not generated. Such a complete loss was not observed when $p47^{phox}$ was omitted from the system, thus suggesting that $p67^{phox}$ is crucial for the reduction of FAD and hence NADPH oxidase activity. They further reported that truncated $p67^{phox}$ (1-198) where the activation domain was absent, resulted in a very low level of FAD reduction and failed to support detectable levels of $O_2^{\cdot-}$ production. Similar results were observed with $p67^{phox}$ activation domain mutants (V204A and V205A), thus suggesting that the activation domain of $p67^{phox}$ may be involved in regulating the reduction of FAD by NADPH (Nisimoto et al., 1999). The results of this study were further supported by a similar article published a year later (Han and Lee, 2000).

Ultimately a direct interaction between $p67^{phox}$ and the $gp91^{phox}$ subunit of the membrane flavocytochrome was shown by Dang and colleagues using three different approaches (Dang et al., 2001). An overlay assay was used in the first approach where neutrophil specific granules (source of flavocytochrome b_{558}) from a normal patient and from a $gp91^{phox}$ CGD patient were resolved and transferred to a nitrocellulose membrane. The membranes were incubated with phosphorylated $p67^{phox}$ (^{32}P) and analysed by autoradiography. Their results showed that $p67^{phox}$ recognised a band running at ~91 kDa in normal neutrophils, but was not recognised in $gp91^{phox}$ deficient neutrophils. They confirmed that this 91 kDa band was indeed $gp91^{phox}$ through immunoblot assays using antibodies against $gp91^{phox}$. The second approach used dot-blot assays where binding of $p67^{phox}$ to purified flavocytochrome b_{558} was detected using antibodies against $p67^{phox}$. Their third approach used affinity precipitation where GST-$p67^{phox}$ was incubated with flavocytochrome b_{558}, to which glutathione-sepharose 4B beads were added. The beads were pelleted and immunoblot assays were carried out to show binding between $p67^{phox}$ and $gp91^{phox}$ using antibodies against the latter. Altogether their result concluded that indeed $p67^{phox}$ does interact directly with $gp91^{phox}$, and such a direct interaction could explain the observation that $p67^{phox}$ is absolutely required for enzyme activity. These authors also provided evidence for the importance of Rac in the NADPH oxidase system. They showed through affinity precipitation assays and scanning densitometry, that binding of $p67^{phox}$ to $gp91^{phox}$ was enhanced in the presence of Rac1, thereby suggesting that the role of Rac1 is to promote the interaction between $p67^{phox}$ and flavocytochrome b_{558} (Dang et al., 2001).

In addition it has been suggested that $p67^{phox}$ may also contain a binding site for NADPH. Smith and colleagues showed that treating neutrophil cytosol with a 2', 3'-dialdehyde derivative of NADPH, inactivated $O_2^{\cdot-}$ generation which was reversed upon addition of NADPH (but not NADP, NAD or GTP). Chromatographic purification of the cytosol yielded fractions containing the dialydehyde sensitive component, as determined by its ability to restore the loss in NADPH oxidase activity. This component was identified by immunoblot assays to be $p67^{phox}$, suggesting that $p67^{phox}$ may be the NADPH dialydehyde sensitive component (Smith et al., 1996). In further support of this proposal the authors showed that adding purified recombinant $p67^{phox}$ to NADPH dialydehyde treated cytosol was capable of restoring NADPH oxidase activity. In addition affinity labelling studies using radioactive NADPH dialydehyde showed that only $p67^{phox}$ was labelled, and this labelling was reduced by NADPH. Although it is generally accepted that $gp91^{phox}$ contains all the catalytic machinery necessary for

oxygen reduction, based on these data Smith and colleagues proposed that NADPH oxidase may contain two separate catalytic NADPH binding sites; one in $gp91^{phox}$ and the other in $p67^{phox}$. They speculate that upon translocation of $p67^{phox}$ to the membrane, the two NADPH binding sites may cooperate to form a single NADPH catalytic unit. Dang and colleagues provided further evidence for this model. The authors of this study made the following truncated forms of $p67^{phox}$: $p67^{phox}$ (1-243), $p67^{phox}$ (1-210), $p67^{phox}$ (1-199) and $p67^{phox}$ (244-526). Using fluorescence spectroscopy they showed that the fragments of $p67^{phox}$ that contained the N-terminal portion of the protein bound NADPH whereas the C-terminal fragment did not, thus suggesting that the N-terminal portion of $p67^{phox}$ may contain the NADPH binding site (Dang et al., 1999). Furthermore the authors showed that $p67^{phox}$ (1-119), which contains the TPR domain, bound to NADPH with a K_d of 6.4 μm which was similar to that of full-length $p67^{phox}$ (7.2 μm). Based on these results Dang and colleagues proposed that $p67^{phox}$ may bind NADPH via its TPR domain (Dang et al., 1999). However, such an interaction could not be reproduced by other groups (unpublished data) and further work is required to gain a better understanding about this possible $p67^{phox}$-NADPH interaction.

1.3.2.3 $P40^{phox}$

$P40^{phox}$ consists of 339 amino acids and has a molecular weight of approximately 39 kDa. $P40^{phox}$ was the last NADPH oxidase subunit to be discovered and was identified via its co-purification with $p67^{phox}$ (Someya et al., 1993; Wientjes et al., 1993), $P40^{phox}$ contains three different types of protein interaction domains; a PX domain, a SH3 domain and a PB1 domain (Figure 11). $P40^{phox}$ is tightly associated with $p67^{phox}$ and its presence in the cytosol of patients with $p67^{phox}$ deficient CGD is markedly reduced, leading to the suggestion that the interaction between $p67^{phox}$ and $p40^{phox}$ may have a stabilising effect on the individual proteins. In contrast, there are no reports of a reduction in $p40^{phox}$ levels in patients lacking $p47^{phox}$ (Wientjes et al., 1993).

To date there are no reported cases of $p40^{phox}$ linked CGD, and the exact role of $p40^{phox}$ is controversial as it has been seen to both inhibit and stimulate NADPH oxidase activity. For example, Sathyamoorthy and colleagues showed that when $p40^{phox}$ was added to neutrophil membranes plus $p47^{phox}$, $p67^{phox}$ and Rac, $O_2^{\cdot-}$ generation was inhibited by 35 %. Furthermore, the isolated SH3 domain of $p40^{phox}$ had an even greater effect by reducing NADPH oxidase activity by 60 %, thus suggesting that $p40^{phox}$ may

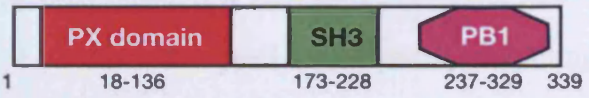

p40^{phox}

```
1   MAVAQQLRAESDFEQLPDDVAISANIADIEEKRGFTSHFVFVIEVKTKGG  50
51  SKYLIYRRYRQFHALQSKLEERFGPDSKSSALACTLPTLPAKVYVGVKQE 100
101 IAEMRIPALNAYMKSLLSLPVWVLMDEDVRIFFYQSPYDSEQVPQALRRL 150
151 RPRTRKVKSVSPQGNSVDRMAAPRAEALFDFTGNSKLELNFKAGDVIFLL 200
201 SRINKDWLEGTVRGATGIFPLSFVKILKDFPEEDDPTNWLRCYYYEDTIS 250
251 TIKDIAVEEDLSSTPLLKDLLELTRREFQREDIALNYRDAEGDLVRLLSD 300
301 EDVALMVRQARGLPSQKRLFPWKLHITQKDNYRVYNTMP
```

KEY:

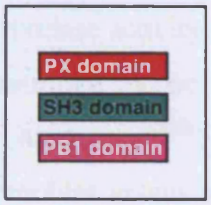

Figure 11: Domain arrangement and amino acid sequence of the cytosolic NADPH oxidase protein p40^{phox}. Boundaries of the individual domains were obtained from the Pfam database (Bateman et al., 2004) and the Prosite database (Hulo et al., 2006).

down-regulate NADPH oxidase activity. Based on these observation and yeast-two hybrid screens that showed an interaction between the $p40^{phox}$ SH3 domain and the C-terminal PR region of $p47^{phox}$ (Fuchs et al., 1996), Sathyamoorthy and colleagues proposed that $p40^{phox}$ may compete with $p67^{phox}$ for binding to $p47^{phox}$ and thereby down-regulate NADPH oxidase activity (Sathyamoorthy et al., 1997). Further support for a potential interaction between $p40^{phox}$ and $p47^{phox}$, and hence for this model comes from gel filtration and small angle neutron scattering experiments (Grizot et al., 2001), and the affinity-bead method using recombinant proteins coupled to Hitrap columns (Wientjes et al., 1996). However $p40^{phox}$ only binds weakly to $p47^{phox}$ with an affinity in the range of 5 μM, as estimated based on small angle neutron scattering studies (Grizot et al., 2001) and analytical ultracentrifugation (Lapouge et al., 2002). While the interaction between the C-terminal PR region of $p47^{phox}$ and the C-terminal SH3 domain of $p67^{phox}$ occurs with a high affinity, between 20-40 nM as determined by ITC and surface plasmon resonance (Lapouge et al., 2002; Wientjes et al., 1996), thus making a direct competition unlikely.

At the same time there is overwhelming evidence to suggest that $p40^{phox}$ may be a positive regulator of NADPH oxidase activity. For example Tsunawaki and colleagues reported that mixing resting neutrophil cytosol with antibodies against the C-terminal region of the $p40^{phox}$ (which binds $p67^{phox}$) prevented co-immunoprecipitation of $p67^{phox}$, as determined by immunoblot assays and importantly reduced $O_2^{\cdot-}$ generation by up to 55 % (Tsunawaki et al., 1996). Kuribayashi and colleagues used K562 cells (which express functional flavocytochrome b_{558}, $p47^{phox}$ and $p67^{phox}$) and tested the reaction of these cells upon stimulation with PMA in the presence or absence of co-transfected $p40^{phox}$. These experiments showed that in cells that did not express $p40^{phox}$, $p47^{phox}$ and $p67^{phox}$ were able to translocate to the membrane in a time-depended manner, as determined by immunoblot assays. However, the presence of $p40^{phox}$ not only increased membrane translocation 2-3 fold but also $O_2^{\cdot-}$ generation. Thus suggesting that binding of $p40^{phox}$ to PtdIns(3)P may aid the recruitment of $p67^{phox}$, which does not contain a PX domain to the membrane flavocytochrome. Furthermore, the authors of this study reported that this enhancement was dependent on the interaction between $p40^{phox}$ and $p67^{phox}$, as cells expressing $p40^{phox}$ with the mutation D289A (residue important in the interaction between $p40^{phox}$ and $p67^{phox}$) was not capable of enhancing $O_2^{\cdot-}$ generation (Kuribayashi et al., 2002). Finally, Ellson and colleagues used $p40^{phox}$ mouse knock-out models to show that neutrophils from these mice produced 69-84 % less $O_2^{\cdot-}$ than wild-type mice. These $p40^{phox}$ deficient mice also

presented severe deficiency in destroying *S. aureus* both *in vitro* and *in vivo*, thus suggesting that $p40^{phox}$ is essential for pathogen destruction (Ellson et al., 2006).

1.3.2.3.1 $P40^{phox}$ PX domain binds PtdIns(3)P

The PX domain of $p40^{phox}$ shows a very strong preference for binding phosphatidylinositol 3-phosphate (PtdIns(3)P), as determined using a variety of methods including protein-lipid overlay and liposome binding assays (Ago et al., 2001; Kanai et al., 2001) as well SPR (Ellson et al., 2001). The molecular basis of this specificity could be explained by the crystal structure of the isolated PX domain bound to PtdIns(3)P (Bravo et al., 2001), and more recently the structure of full-length $p40^{phox}$ bound to PtdIns(3)P (Honbou et al., 2007) (for further details see section 1.4.4). PtdIns(3)P which is a product of PI3K signalling pathways becomes abundantly available in the phagosomal membrane during phagocytosis, and thus may act as a signalling molecule to direct the NADPH oxidase complex by binding to $p40^{phox}$ (Ellson et al., 2001). The functional integrity of the PX domain seems crucial for the positive regulatory role of $p40^{phox}$, as transgenic mice with a mutation in the PX domain (R58A) are severely impaired in their ability to kill *S. aureus*, and neutrophils derived from these mice show a reduced production of $O_2^{\cdot -}$ upon stimulation (Ellson et al., 2006), thus further supporting a positive regulatory role of $p40^{phox}$.

All in all there are now an increasing number of reports that support a positive role for $p40^{phox}$ in NADPH oxidase regulation. However the molecular basis of such a positive regulatory role is still not understood and further studies are required to fully bring to light the precise role of this subunit

1.3.2.4 Rac

Rac belongs to the Rho family of small GTPases, which are approximately 20 kDa in size and constitute a subfamily of the Ras superfamily of small GTPases. Two closely related Rac isoforms exist; Rac1 and Rac2, which primarily differ in their C-terminal region which is more basic in Rac1 than Rac2. Rac1 is ubiquitously expressed whereas Rac2 is only expressed in hematopoietic cells. Like all small GTPases Rac1 and Rac2 carry a lipid modification in their C-terminus; a geranylgeranyl group which anchors these proteins to the membrane.

Members of the Rho family of small GTPases play important roles in the regulation of a large wide variety of cellular processes including cell growth and differentiation, cytoskeletal organisation, lipid vesicle transport and $O_2^{\cdot -}$ generation. They act as molecular switches only relaying signals when in their active form (Figure 12). Specifically, Rac alternates between an inactive GDP-bound state and an active GTP-bound state. Binding of an extracellular ligand to a specific cell surface receptor causes Rac-specific guanine-nucleotide exchange factors (GEFs) such as the PIP3-dependent Rac exchanger (P-Rex1) to catalyse the dissociation of GDP from Rac, thereby allowing GTP, which exists in much higher concentration within the cell, to bind. This GTP-bound Rac recognises and binds specific downstream proteins (Figure 12) and thereby induces a specific cellular response, either through inducing a conformational change in the effector protein, a change in its subcellular localisation or by inducing the assembly of large, multi-protein complexes as observed in NADPH oxidase. The signal is terminated by GTPase activating proteins (GAPs), which bind activated GTPases and increase the rate of GTP hydrolysis by several orders of magnitude, switching it from the GTP-bound form to the inactive GDP-bound (Takai et al., 2001). In addition, Rho family proteins associate with guanine-nucleotide dissociation inhibitors (GDIs) while in their GDP bound form. GDIs contain a hydrophobic pocket that is able to accommodate the geranylgeranyl group, and thereby extract the GTPase from the membrane and keep it cytosolic in its inactive state (Hoffman et al., 2000; Scheffzek et al., 2000).

Like all small GTPases, Rac contains the so-called switch I region (aa 30-40) and switch II region (aa 60-67) in its N-terminal portion. These regions are the only part of the molecule that change their conformation upon switching between the inactive and active form, and are those regions that are recognised by downstream effectors as well as regulatory proteins. In addition, Rac contains a so-called insert region, also called insertion helix, which is specific to Rho-family GTPases, but whose function is not really understood at present (see below).

1.3.2.4.1 Rac is involved in activating the NADPH oxidase

Several groups first suggested the involvement of a small GTPase in the regulation of the NADPH oxidase in the late 1980's. For example a study by Ishida and colleagues showed that SDS activated cell-free systems containing membrane bound

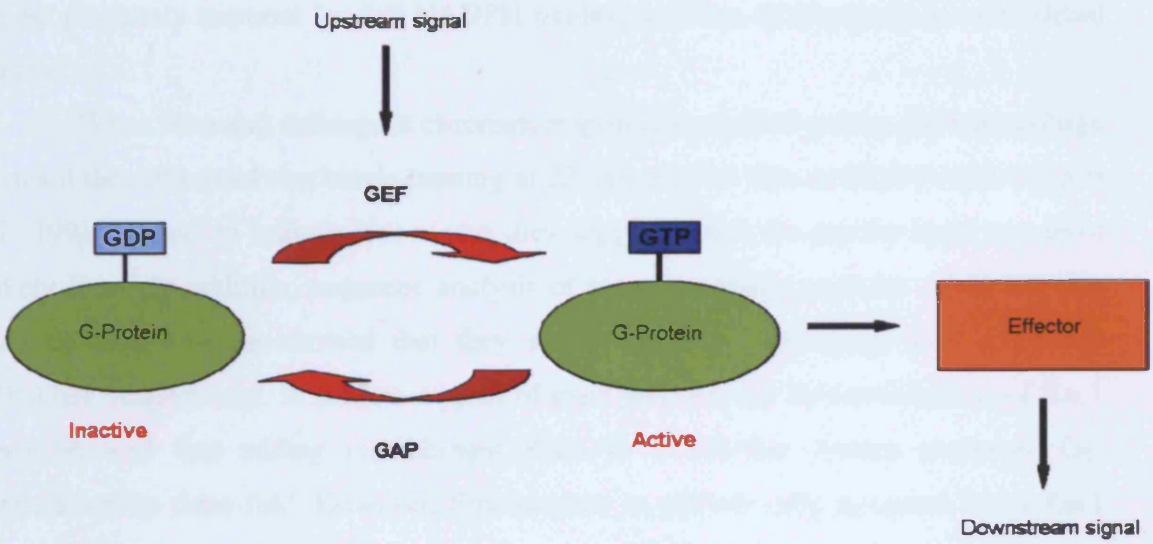

Figure 12: Regulation of small G-protein activity. Illustration shows that small GTPases act as molecular switches, alternating between an inactive GDP-bound state and an active GTP-bound state. Binding of guanine-nucleotide exchange factors (GEFs) catalyse the conversion from GDP to active GTP bound forms. The GTP-bound form recognises and binds specific effector proteins to induce downstream signals. The signal is terminated by GTPase activating proteins (GAPs) by binding and converting the active GTP bound form to the inactive GDP form (taken and adapted from Takai et al., 2001).

flavocytochrome b_{558}, and cytosolic $p47^{phox}$ and $p67^{phox}$ were not sufficient to support NADPH oxidase activity. However when GTP or GTP-γS (a non-hydrolysable GTP analogue) were added, $O_2^{\cdot-}$ generation was increased several fold. This effect was decreased when GDP was added, thereby suggesting that a guanine nucleotide regulatory protein may be involved in regulating NADPH oxidase activity (Ishida et al., 1989). This protein was subsequently identified to be Rac1 or Rac2, which were shown to be absolutely required for full NADPH oxidase activity, as discussed in more detail below.

When Abo and colleagues chromatographically purified guinea pig macrophage cytosol they observed two bands running at 22 kDa and 26 kDa on SDS-PAGE (Abo et al., 1991). Based on immunoblot assays they suggested that the smaller band was most likely Rac1. In addition, sequence analysis of trypsin digested peptides of the 22 kDa and 26 kDa proteins showed that they shared sequence homology with Rac1 and RhoGDI, respectively. In further support of their proposal for the involvement of Rac1 they showed that adding recombinant Rac1 to a cell-free system increased $O_2^{\cdot-}$ generation by three-fold. However, this increase in activity only occurred when Rac1 was pre-incubated with GTP-γ-S but not with GDP-βS. This suggested that not only was Rac essential for NADPH oxidase activity, but that it was kept inactive when bound to RhoGDI, and only became active when in a GTP-bound form (Abo et al., 1991). Similar experiments were carried out by Knaus and colleagues, however in that study cytosol from human neutrophils was used, and sequence analysis subsequently identified the small GTPase involved to be Rac2 (Knaus et al., 1991).

Since then there have been numerous *in vitro* and *in vivo* studies to show that Rac is absolutely required for $O_2^{\cdot-}$ generation. For example Freeman and Lambeth showed through cell-free assays that when Rac was omitted from the assay, $O_2^{\cdot-}$ generation could not be detected (Freeman and Lambeth, 1996). Furthermore, Roberts and colleagues showed a significant reduction in the amount of $O_2^{\cdot-}$ generation from bone marrow-derived neutrophils from Rac2 deficient mice. These Rac2 deficient mice also showed increased mortality upon challenge with *A. fumigatus* (Roberts et al., 1999), suggesting that Rac is essential for normal NADPH oxidase activity.

1.3.2.4.2 Rac2 is the predominant isoform in human neutrophils

Heyworth and colleagues reported that both, recombinant Rac1 and Rac2, were capable of supporting $O_2^{\cdot-}$ generation to comparable levels in human neutrophil cell-free

systems, where the cytosol was replaced by recombinant $p47^{phox}$ and $p67^{phox}$ and supplemented with GTP-γS or GTP (Heyworth et al., 1993). This result is not surprising as both isoforms share 92 % sequence homology (Didsbury et al., 1989). However, it has been shown by various groups that the predominant Rac isoform involved in activating the NADPH oxidase in human neutrophils is in fact Rac2. For example a study by Knaus and colleagues showed that an antibody against the C-terminus of Rac2 significantly inhibited $O_2^{\cdot-}$ production in neutrophil cell-free systems, while an antibody against the C-terminus of Rac1 had a much lower inhibitory effect (Knaus et al., 1991). In support of these findings, Abo and colleagues chromatographically purified the cytosol of resting neutrophils and immunoblot assays using antibodies against Rac1 and Rac2 showed that the cytosol predominantly contained Rac2 (Abo et al., 1994). Furthermore, Heyworth and colleagues quantitated the relative amounts of Rac by using highly purified neutrophil Rac2 as a standard, alongside neutrophil cytosol which was diluted so that the final concentration was within the linear range of the standard curve. This was followed by immunoblotting to show that > 96 % of Rac present in neutrophils was indeed Rac2 (Heyworth et al., 1994).

The physiological importance of Rac2 in NADPH oxidase activity has been highlighted by the discovery of a case of CGD where Asp57 located N-terminal to the switch II region was substituted for Asn ($Rac2^{D57N}$). Neutrophils from this patient could not support $O_2^{\cdot-}$ generation *in vitro* (Ambruso et al., 2000). The equivalent mutation in Ras (D57N) has previously been shown to act in a dominant negative manner where it preferentially bound GDP and formed a stable complex with GEFs thereby interfering with activation of Ras (Jung et al., 1994). Ambruso and colleagues showed that $Rac2^{D57N}$ had a similar effect as recombinant $Rac2^{D57N}$ could bind [^{3}H]GDP but was unable to bind [^{35}S]GTP[γS]. Furthermore, recombinant $Rac2^{D57N}$ was unable to support $O_2^{\cdot-}$ generation in a cell-free system, suggesting that $Rac2^{D57N}$ does indeed act in a dominant negative manner thereby preventing NADPH oxidase activation.

1.3.2.4.3 Membrane translocation of Rac

Initially it was believed that Rac would translocate together with $p47^{phox}$ and $p67^{phox}$ to the membrane. This idea was based on data from cell-free assays in which activation was induced with SDS, and membrane translocation, followed by the preparation of membrane and cytosol fractions and their subsequent analysis by western blotting (Abo et al., 1994). In a parallel study Heyworth and colleagues carried out cell-

free and whole cell assays using CGD neutrophils lacking $p47^{phox}$ or $p67^{phox}$, to determine if Rac2 translocation was dependent on these cytosolic proteins. Their results showed that even in the absence of $p47^{phox}$ or $p67^{phox}$, Rac2 was still able to translocate and associate with the membrane in a normal manner, thus suggesting that Rac2 must translocate to the membrane in an independent fashion (Heyworth et al., 1994). A similar study using $p47^{phox}$ and $p67^{phox}$ deficient CGD neutrophils was conducted by Dusi and colleagues, who also reported that Rac2 translocated to the membrane independent of either these subunits (Dusi et al., 1996). Since then there has been overwhelming evidence to show that Rac indeed translocates to the membrane independently.

1.3.2.4.4 The interaction between Rac and $p67^{phox}$ is crucial for NADPH oxidase activity

In order to identify the functional target protein for Rac in the NADPH oxidase system, Diekman and colleague's purified recombinant GST-tagged $p67^{phox}$ and $p47^{phox}$ and carried out *in vitro* binding assays using Rac1, which was bound to radioactively labelled GTP or GDP. These assays showed that Rac only bound to $p67^{phox}$ but not $p47^{phox}$, suggesting that $p67^{phox}$ is the functional target for Rac. Importantly, this interaction only took place when Rac was in its active GTP-bound form, suggesting that $p67^{phox}$ is a bona fide downstream effector of Rac (Diekmann et al., 1994). The authors of this study further attempted to define the binding region for Rac within $p67^{phox}$, and using different $p67^{phox}$ truncations in pull-down assays were able to show that Rac binds the N-terminal region of $p67^{phox}$ between residues 1-199. Simultaneously, the authors showed that Rac binds $p67^{phox}$ via its effector region, as three effector region mutants (aa 35, 38 and 40 substituted with alanine or lysine) were unable to support $O_2^{\cdot-}$ generation and no loner bound $p67^{phox}$ (Diekmann et al., 1994).

Since then there have been numerous reports, which confirm the proposal that Rac supports NADPH oxidase activity by binding the N-terminal region of $p67^{phox}$; a region which is comprised of four tetratricopeptide repeats (TPR). An interesting study was carried out by Koga and colleagues who introduced mutations into the TPR motif of $p67^{phox}$ which were expected to disrupt the packing of the TPR helices. Specifically, they substituted small conserved amino acids with bulky Gln residues and deleted a conserved residue at position 22 in the TPR motifs, resulting in incorrect packing between adjacent TPRs (similar mutations in the $p67^{phox}$ TRP motif have been reported

in CGD patients). The effects of these mutations on Rac2-$p67^{phox}$ binding was examined using the yeast two-hybrid system and overlay assays with GST-fusion recombinant proteins (Koga et al., 1999). The authors of this study reported that mutations in the first three repeats resulted in defective $p67^{phox}$-Rac binding and abolished $O_2^{\cdot-}$ generation under cell-free conditions, suggesting that only the first three TPRs of $p67^{phox}$ are involved in Rac binding. However, although mutations in the last TPR did not affect $p67^{phox}$-Rac binding, they showed little or no support for NADPH oxidase activity. This suggests that the fourth TPR may contribute to enzyme activation possibly by interacting with other components such as flavocytochrome b_{558}. Together the authors of this study proposed that the TPRs of $p67^{phox}$ are packed in a manner as to provide the binding site for Rac2, which plays a crucial role in NADPH oxidase activation (Koga et al., 1999). Additional support for the importance of the Rac-$p67^{phox}$ interaction for NADPH oxidase activity comes from the observation that point mutations within switch I of both Rac1 and Rac2 significantly reduce $O_2^{\cdot-}$ generation (Freeman et al., 1994; Xu et al., 1994).

The importance of the TPR domain in $p67^{phox}$ for complex formation with Rac has been confirmed by the crystal structure of this domain in complex with Rac-GTP (Lapouge et al., 2000) (Figure 15). The structure revealed that the switch I region of Rac-GTP plays an important role in complex formation and further explained the molecular basis for the specificity of this interaction. In addition, the authors of this study used isothermal titration calorimetry (ITC) to quantify the interaction between Rac1/2 and $p67^{phox}$ and investigate if the remainder of $p67^{phox}$ may contribute to complex formation. No significant differences were found between Rac1 and Rac2 or between full-length $p67^{phox}$ and the isolated TPR domain. Thus clearly showing that the C-terminal portion of $p67^{phox}$ neither contributes nor is affected by complex formation, and that any differences detected *in vivo* between Rac1 and Rac2 may be due to differences in their affinity for $p67^{phox}$.

1.3.2.4.5 Models for Rac function in NADPH oxidase regulation

Members of the Rho-family of GTPases have the interesting property that they contain an insertion of 12 amino acids at position 123-135, which has been called the insertion helix. Although many groups have studied the role of this insertion helix its function is still controversial. In fact, the role of Rac in NADPH oxidase activity has for a long time believed to be the most convincing case for a functional role of this

insertion. The crystal structure of the p67TPR-Rac.GTP complex (Lapouge et al., 2000) (Figure 15) has shown that the insertion helix is distant from the p67TPR/Rac interface and not required for complex formation, however, the insertion is exposed and hence available for other interactions, for example with the cytochrome. So far mutational studies have produced conflicting results concerning the involvement of the insertion helix in $O_2^{\cdot-}$ production, as discussed in more detail in the models that follow. Furthermore, there is still controversy about the precise role of Rac in the regulation of NADPH oxidase activity, whether it acts primarily as an adaptor or is an active participant in the catalytic process. These models are described as follows.

The model proposed by Lambeth and colleagues suggests $p67^{phox}$ is the main driving force for the electron transport reaction, and that Rac functions solely as an adaptor protein. They propose that once Rac becomes activated it is recruited to the membrane where it binds $p67^{phox}$ via the switch I region and may bind flavocytochrome b_{558} via the insert-region. They believe that these interactions take place to orientate the $p67^{phox}$ activation domain in such a manner that it is aligned perfectly for contact with flavocytochrome b_{558}, to regulate the electron transfer reaction (Lambeth, 2000). In this model it is believed that a possible interaction between the Rac insertion helix and the flavocytochrome does not directly regulate the electron transport reaction. This is based on the observation that mutation of single amino acids or deletion of the insert region of Rac1 reduced the affinity of Rac for the oxidase by 13-25 fold, as determined by the EC_{50} value (effective concentration at 50 % of V_{max}), but did not effect the maximal rate (V_{max}) of $O_2^{\cdot-}$ generation (Freeman et al., 1996).

Edgar Pick's group on the other hand have proposed a number of models, some of which contradict one another (most likely because they are based on data gained using different experimental approaches). Originally the group used peptide walking experiments under cell free conditions to show that the Rac insertion helix is important for $O_2^{\cdot-}$ generation (Joseph and Pick, 1995). However, later they proposed a model similar to that by Lambeth where $p67^{phox}$ regulates the electron transport reaction, and Rac functions primarily as an adaptor protein. In contrast to Lambeth's model the Pick group propose that Rac does not directly interact with flavocytochrome b_{558}, and that the Rac insertion helix is not important for NADPH oxidase activity. The former part of this model was based on the observation that in cell-free assays prenylated Rac was able to bind phospholipid vesicles in both the presence and absence of flavocytochrome b_{558} (Gorzalczany et al., 2000) whereas non-prenylated Rac could not. Thus indicating that the lipid tail is required for membrane association, but more importantly that Rac does

not depend on the flavocytochrome for this interaction. These experiments involved incubating prenylated or non-prenylated Rac.mant-GTP (a fluorescent GTP analogue) with recombinant $p67^{phox}$ and $p47^{phox}$, along with either membrane vesicles containing membrane bound flavocytochrome b_{558} or phosphatidylcholine vesicles. The samples were purified by gel filtration and the presence of free Rac and membrane associated Rac was measured spectrofluorometrically. The latter part of this model was based in the observation that a recombinant chimeric protein comprising $p67^{phox}$(1-212) fused to Rac1 but which was lacking the insertion helix, fully supported $O_2^{\cdot-}$ generation in cell-free systems (Alloul et al., 2001), thus suggesting that the insertion helix is not required for NADPH oxidase activity.

More recently the same group proposed another model for the involvement of Rac in the regulation of NADPH oxidase activity. In this model Pick and colleagues propose that a) Rac tethers $p67^{phox}$ to the membrane whereby it orientates $p67^{phox}$ with respect to flavocytochrome b_{558} and b) Rac induces conformational changes within $p67^{phox}$ thereby activating it (Sarfstein et al., 2004). The former part of the model is based on the observation that mutating six basic residues in the Rac C-terminus (residues important for membrane association) of a chimera comprising $p67^{phox}$ (aa 1-212) fused to full-length Rac1, failed to support $O_2^{\cdot-}$ generation in a cell free assay. The latter part of the model is based on the observation that mutating key residues that are involved in the $p67^{phox}$ Rac1 interaction such as R102E (in $p67^{phox}$-TPR domain), A27K and G30S (Rac1-swith I region) resulted in a severe loss in NADPH oxidase activity. The authors suggested that the intrachimeric bonds between $p67^{phox}$ and Rac may be important for inducing conformational changes within $p67^{phox}$ (possibly within the activation domain). In support of this theory they showed that enzyme activity was resorted when exogenous Rac1 (Rac1-GTPγS) was added to the system, but not when exogenous $p67^{phox}$ was added. Altogether, based on the above findings Pick and colleagues propose that Rac plays a dual role where it tethers $p67^{phox}$ to the membrane and induces conformational changes within $p67^{phox}$, possibly to increase the affinity of $p67^{phox}$ for $gp91^{phox}$ or to activate electron flow through $gp91^{phox}$ (Sarfstein et al., 2004).

In contrast to the two previous models, Deibold and Bokoch propose that Rac plays a direct regulatory role and is important for the two-step electron transfer reaction, from NADPH to FAD (1^{st} step) and from FAD to heme (2^{nd} step) and then onto molecular oxygen (Diebold and Bokoch, 2001). Their proposal is based on experiments using a cell-free assay, which contained recombinant $p67^{phox}$ and $p47^{phox}$, flavocytochrome b_{558} purified from human neutrophils and prenylated Rac2. They

measured electron transfer in the 1st step by monitoring reduction of iodonitrotetrazolium violet (INT); an artificial two-electron acceptor, and in the 2nd step by monitoring cytochrome *c* reduction. The authors of this study generated Rac2 and $p67^{phox}$ mutants which were unable to interact with one another and found that both, a $p67^{phox}$ mutant (Δ178-184) and Rac2 switch I region mutants were able to support INT reduction (1st step) to similar levels as wild-type $p67^{phox}$, but support for cytochrome *c* reduction (2nd step) was significantly reduced. Thus suggesting that i) interaction between $p67^{phox}$ and Rac2 was not required for the 1st step, ii) Rac and $p67^{phox}$ independently regulate electron transfer from NADPH to FAD and iii) that $p67^{phox}$ and Rac2 have to interact for subsequent electron transfer in the 2nd step. Based on these results Deibold and Bokoch propose that Rac2 may play a regulatory role in the electron transfer reaction of the NADPH oxidase. Importantly, these authors were able to show that the fluorescence intensity of wild-type fluorescently labelled (mant-GppNHp) Rac2 increased in the presence of flavocytochrome b_{558}, thus suggesting a direct interaction between the two components. This interaction was not observed when Rac2 insert deletion mutants were used, suggesting that Rac2 may regulate the electron transfer reaction by binding the cytochrome via the insertion helix (Diebold and Bokoch, 2001).

1.4 Protein interaction domains

Regulatory proteins are often constructed in a block-like manner, in which multiple protein interaction domains are connected by linkers of varying length and flexibility (Pawson, 1995; Pawson and Nash, 2003). Protein interaction modules are independently folding units of 35-150 amino acids that can be separated into domain families based on sequence homology. Individual protein interaction domains normally exhibit clearly defined ligand binding properties and can mediate the formation of protein-protein, protein-nucleic acid and protein-lipid complexes. Very often these domains are crucial for the formation of multi-protein complexes that drive and regulate signalling processes. Typical protein-protein interaction modules include the Src-homology 3 (SH3) domain, which recognizes proline-rich regions and the Src-homology 2 (SH2) domain, which binds phosphotyrosine-containing sequences. Examples of lipid binding modules include the phox homology (PX) domain and the pleckstrin domain (PH), both of which bind membrane lipids (phosphoinositides) with varying specificities.

In order to understand the molecular mechanism of NADPH oxidase regulation, it is important to understand the interactions that take place between the various protein components during activation and assembly. $P47^{phox}$, $p67^{phox}$ and $p40^{phox}$ are multi-domain proteins, each containing several protein-protein and protein-lipid interaction modules as shown in Figures 7 and 11. The properties of protein interaction domains that are present in $p47^{phox}$, $p67^{phox}$ and $p40^{phox}$ are described in sections 1.4.1 to 1.4.4.

1.4.1 SH3 domain

SH3 domains were first recognised as non-catalytic homology regions of approximately 60 amino acids, in protein kinases related to Src (Mayer et al., 1988). SH3 domains mediate the formation of protein-protein interactions, and are known to be involved in a range of biological processes from enzyme regulation via intramolecular interactions, to mediating the assembly of multi-protein complexes (Mayer, 2001). Extensive structural studies (X-ray crystallography and NMR spectroscopy) have shown that all SH3 domains possess the same basic topology (Lim and Richards, 1994; Noble et al., 1993; Terasawa et al., 1994; Yu et al., 1992). They contain five or six anti-parallel β-strands packed at approximately right angles into two sheets with three characteristic

interconnecting loops: the RT (Arg-Thr) loop, the N-Src loop (neuronal Src) and the distal loop (Figure 13A). The N-Src and RT loops form part of the ligand binding surface. The distal loop is located on the opposite face and may interact with other regions of the binding partner (Dalgarno et al., 1997). The first β-sheet is formed by β-stands A and E and the first half of β-strand B. The second β-sheet is formed by the second half of β-strand B and β-strands C and D. The RT loop separates β-strands A and B, the N-Src loop separates β-strands B and C, and the distal loop separates β-strands C and A. A 3_{10} helical conformation (4-5 amino acids) is generally observed between β-strands D and E, and a type II β-turn can be seen N-terminal to β-stand B. This overall fold brings the most conserved residues of the SH3 domain close together to form a patch of aromatic residues on the surface of the domain for ligand binding (Larson and Davidson, 2000). SH3 domain alignments show that there are several conserved positions that are important for ligand binding (positions *8(Y), 10(Y), 35(G), 36(W), 51(P), 53(N) and 54(Y), numbering according to the consensus sequence*), of which positions 36(W) and 51(P) are fully conserved among all SH3 domains (Figure 13B). SH3 domains also contain a hydrophobic core which is crucial for maintaining protein stability (Dill, 1990). The core is made up of several conserved hydrophobic residues (Bashford et al., 1987; Chothia et al., 1998) (*positions 4(V), 10(Y), 18(L), 20(F), 26(I), 28(V), 37(W), 50(F) and 55(V)*) (Larson and Davidson, 2000).

SH3 domains have a flat hydrophobic ligand-binding surface, consisting of three shallow grooves (Mayer, 2001). The hydrophobic surface of SH3 domains typically binds to proline rich sequences, preferentially recognising PXXP as the core-binding motif (P being a proline and X being any amino acid, although aliphatic residues are preferred) (Feller et al., 1994; Mayer and Eck, 1995; Ren et al., 1993). The specificity and affinity of SH3 domains for their target ligands are generally low, with affinities ranging from 5 μM to 100 μM (Chen et al., 1993). However, this can be increased by additional contacts made outside of the core binding motif, for example by residues in the RT and N-Src loops (Feng et al., 1995).

Proline-rich (PR) motifs contain seven to ten amino acids, and often adopt a left handed polyproline-II helix (PPII) conformation. In this conformation the helix has three residues per turn, meaning that it is triangular in cross section. As a consequence, the core proline residues are on the same face of the helix, separated by two amino acids (PXXP). This PXXP motif lies along the binding site of the SH3 domain, and adheres to the three hydrophobic pockets within the binding surface of SH3 domains

A

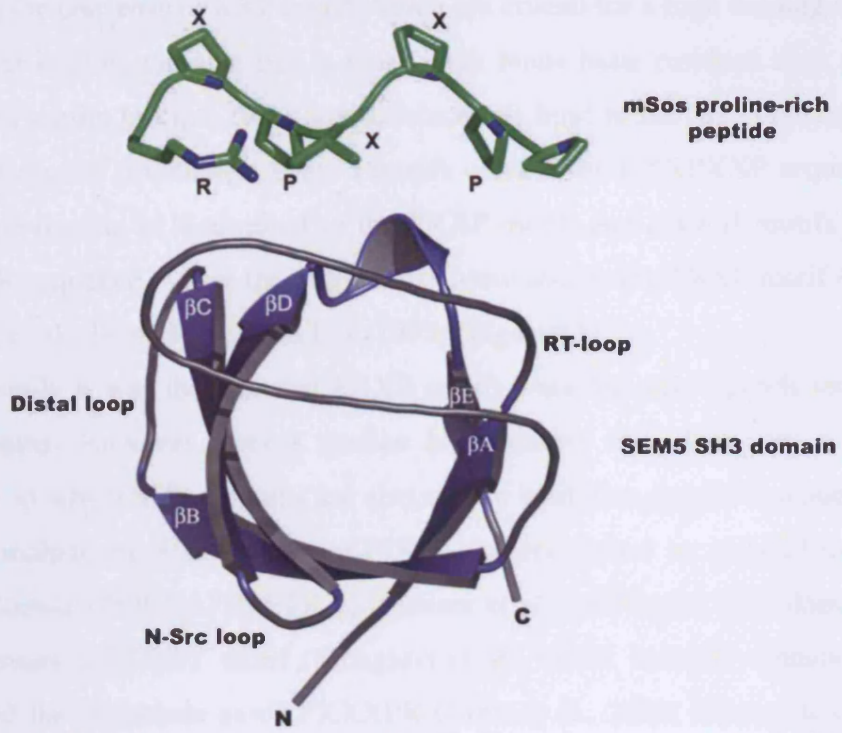

B

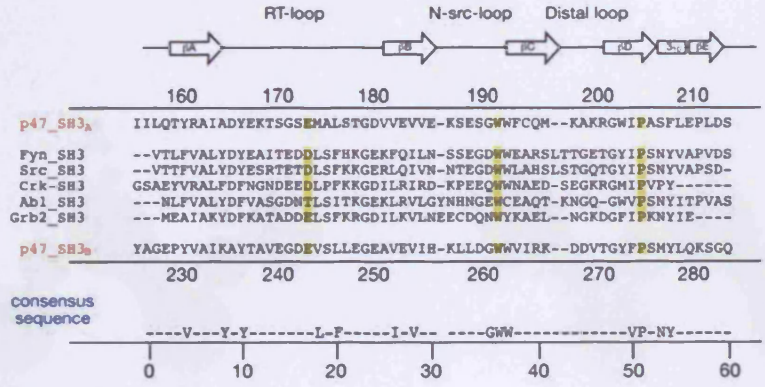

Figure 13: **The structure of a typical SH3 domain and sequence alignment.** A. The SH3 domain (blue) from the sex muscle abnormal protein 5 (SEM5), in complex with a proline-rich peptide (type II) from mSos (green). The positions of PXXPXR are indicated. The SH3 domain characteristic loops are shown in grey and the β-stands are labelled βA-E. PDB identifier 1SEM (Lim et al., 1994). B. A sequence alignment of different SH3 domains. Conserved residues that are involved in ligand binding are highlighted in yellow (taken and adapted from Groemping et al., 2003). The consensus sequence as defined by Larson and Davidson, 2000 is shown below the alignment. All structural pictures were generated in PyMOL (http://www.pymol.org) unless otherwise stated.

(Mayer, 2001). Two of the binding pockets can accommodate the two conserved prolines in the consensus PXXP motif, which are crucial for a high binding affinity. The third pocket is more variable but in most cases binds basic residues such as arginine. Proline rich motifs fall into two classes, which can bind to the SH3 domain either in a forward or reverse orientation. Class I motifs contain the RXXPXXP sequence, where the arginine residue is N-terminal to the PXXP motif, and class II motifs contain the XPXXPXR sequence, where the arginine is C-terminal to the PXXP motif (Feng et al., 1994; Lim et al., 1994; Mayer and Eck, 1995) (Figure 14).

Initially it was thought that PXXP motifs were the only ligands recognised by SH3 domains. However, recent studies have shown that there are a number of exceptions in which SH3 domains are also able to bind non-canonical sequences. Such examples include the SH3 domain of PIX, which recognises an unusual motif in p21-activated kinase (PPPVIAPRPETKA) (Manser et al., 1998), the SH3 domain of Eps8 that recognises a PXXDY motif (Mongiovi et al., 1999), the SH3 domains of CIN85 which bind the consensus motif PXXXPR (Jozic et al., 2005; Kowanetz et al., 2003) and many others.

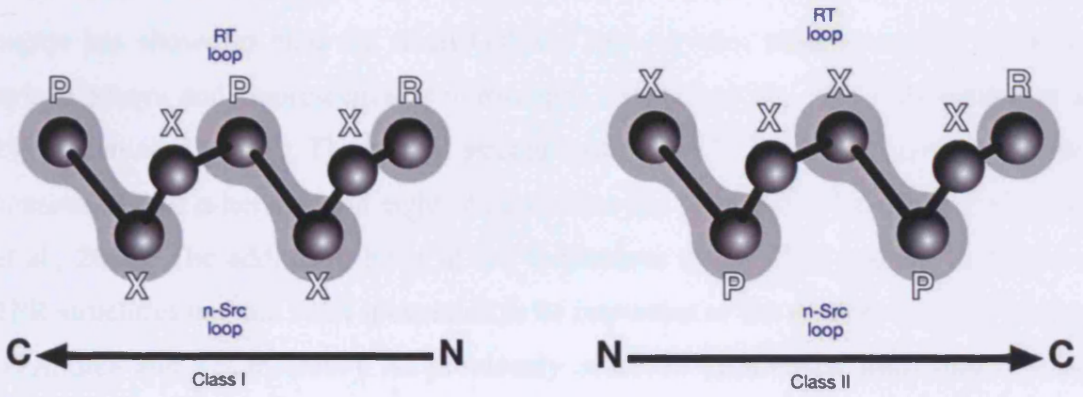

Figure 14: Models of class I and II proline-rich ligands. The ligands are shown schematically where 'P' and 'R' indicate conserved proline and arginine residues; respectively. 'X' indicates any amino acid (taken and adapted from Mayer, 2001).

1.4.2 Tetratricopeptide repeat (TPR) domain

Tetratricopeptide repeats (TPR) are degenerate 34 amino acid sequences that are normally found in tandem arrays of 3-16 motifs. TPR domains were first identified in 1990 in the *S.cerevisiae* protein CDC23 (Hirano et al., 1990) and the *S.pombe* protein $nuc2^{+}$ (Sikorski et al., 1990), both of which are involved in mitosis. TPR domains are often found in proteins that form scaffolds for the assembly of multi-protein complexes to facilitate protein-protein interactions (Das et al., 1998). The first structure solved of a TPR domain was that of protein phosphatase 5, which showed that each repeat folds into two anti-parallel helices that are arranged in a regular fashion next to one another (Das et al., 1998). This regular arrangement of α-helices leads to the formation of a groove, which was suggested to constitute the ligand binding site. The suggestion was supported by the structure of a complex between the TPR domain of the adaptor protein HOP and a peptide derived from its ligand Hsp90 (Figure 15A) (Scheufler et al., 2000). However, since these studies it has emerged that TPR domains are in fact extremely versatile, and can bind their ligands via different binding surfaces. One such example is the $p67^{phox}$ TPR domain, where ligand binding occurs outside of the groove (Lapouge et al., 2000).

$P67^{phox}$ contains four TPR motifs in the N-terminal 200 amino acids, and this region has shown to bind the small GTPase Rac *(in vitro* binding assays, yeast two-hybrid assays and fluorescence spectroscopy) (Ahmed et al., 1998; Diekmann et al., 1994; Han et al., 1998). The crystal structure of the $p67^{phox}$ TPR domain shows that it consists of nine α-helices, and eight of these form the TPR motif (Figure 15B) (Lapouge et al., 2000). The additional helix at the C-terminus (helix C) is present in almost all TPR structures and has been speculated to be important in the stability of these domains (D'Andrea and Regan, 2003). As previously observed each repeat folds into two anti-parallel α-helices (helix A and B). A twenty amino acid insertion between the third and fourth repeats of $p67^{phox}$ folds into two short anti-parallel β-strands and a 3_{10} helical turn, which is known as the β-hairpin insertion. The β-hairpin insertion together with the loops connecting the TPR segments (TR1 with TRP2, and TPR2 with TPR3) form the binding surface for the small GTPase Rac.

A

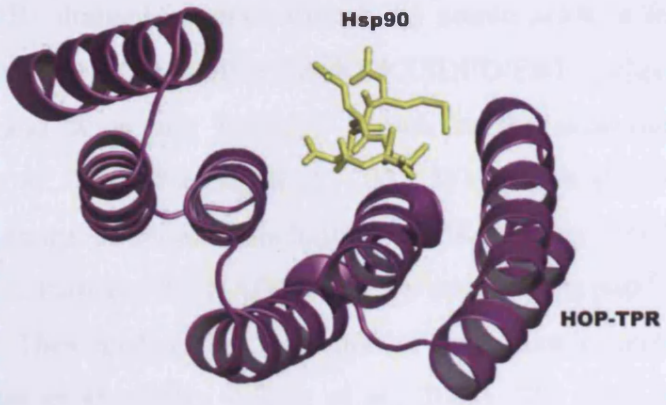

B

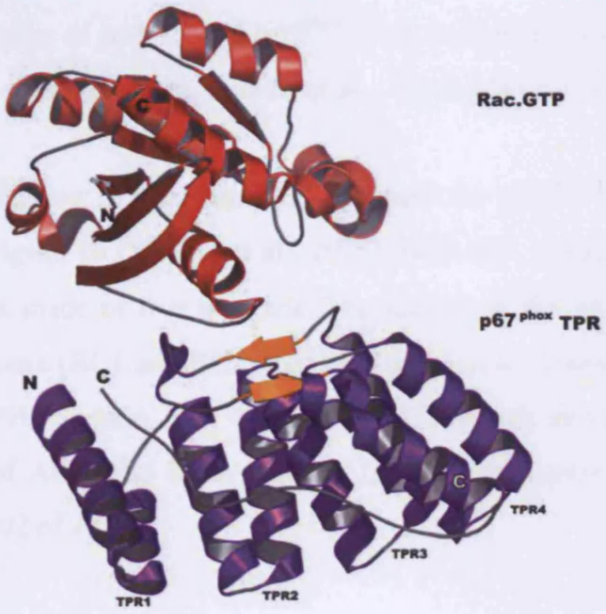

Figure 15: The structure of HOP and p67^{phox} TPR domains in complex with their ligands. A. The HOP TPR domain is shown in purple, and the Hsp90 peptide in yellow sticks. PDB identifier 1ELR (Scheufler et al., 2000). B. The p67^{phox} TPR domain is shown in purple in complex with Rac.GTP (red). The β-hairpin insertion which is crucial for complex formation is highlighted in orange, and the TPR repeats are labeled 1-4. The additional helix at the C-terminus is highlighted in white text as 'C'. PDB identifier 1E96 (Lapouge et al., 2000).

1.4.3 PB1 domain

The PB1 domain is approximately 85 amino acids in length and contains the consensus sequence ✱XYXDEDGDX✱X✱XSDED/E✱X (where ✱ is a hydrophobic amino acid and X is any residue), known as the octicosapeptide repeat (OPR) (Nakamura et al., 1998; Ponting et al., 2002; Wientjes et al., 1993). PB1 domains are present in a range of proteins including MAPK kinases (MEK5 or MAPKK5), the adaptor protein Par6 and the NADPH oxidase components $p40^{phox}$ and $p67^{phox}$ (Ponting et al., 2002). They mediate the formation of homodimeric and heterodimeric protein complexes (Ito et al., 2001; Wilson et al., 2003). The PB1 domain of $p40^{phox}$ was originally called the PC motif due to its presence in phagocytic oxidase and cdc24. However recently, after sequence analysis it was suggested that in fact PC motifs and octicosapeptide repeats should be classified as a single family known as the PB1 domain. The PB1 domains of $p40^{phox}$ and $p67^{phox}$ bind each other with high affinity (4 nM-10 nM) (Lapouge et al., 2002; Nakamura et al., 1998; Ponting et al., 2002; Wilson et al., 2003).

The crystal structure of the complex between the $p40^{phox}$ and $p67^{phox}$ PB1 domains is shown in Figure 16 (Wilson et al., 2003). Both PB1 domains consist of two α-helices and a β-sheet made of five β-stands. The surface of the $p67^{phox}$ PB1 domain contains two basic clusters (BC1 and BC2) that bind two acidic clusters (AC1 and AC2) present in the $p40^{phox}$ PB1 domain. BC1 contains Lys355, which interacts with Asp289, Glu291 and Asp293 of AC1, and BC2 contains Lys382 and Lys365 which interacts with Glu301 and Asp302 of AC2.

1.4.4 PX domain

The phox homology (PX) domain is approximately 125 amino acids in length and is found in a variety of proteins including membrane trafficking proteins such as Vam7p and the yeast protein Bem1p. It was first discovered in the $p40^{phox}$ and $p47^{phox}$ cytosolic proteins of the NADPH oxidase (Ponting, 1996). Originally it was thought that PX domains may bind to SH3 domains due to the presence of a proline-rich region in many PX domains. Indeed, an NMR study by Hiroaki and colleagues showed that the $p47^{phox}$ PX domain could interact with the isolated $p47^{phox}$ C-terminal SH3 domain with an affinity of ~ 50 μM (Hiroaki et al., 2001). However, more recent studies have shown

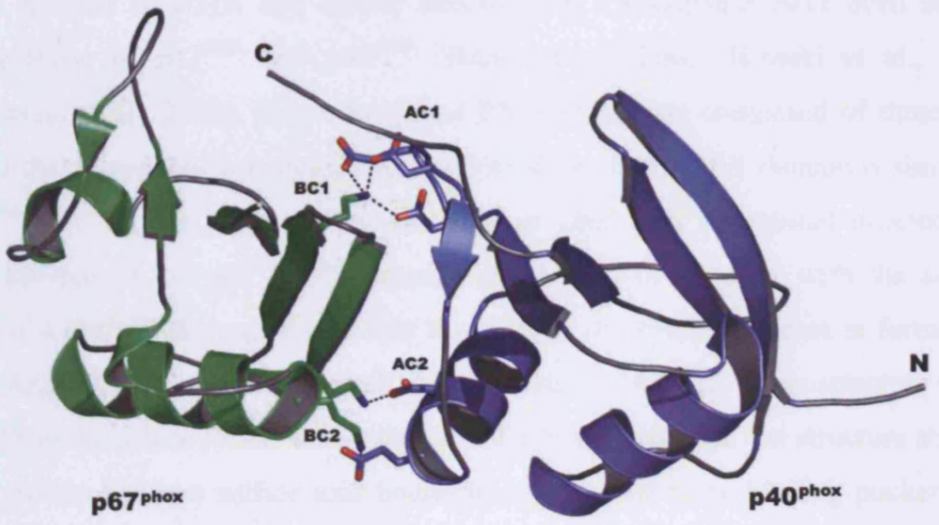

Figure 16: The structure of the p40^{phox} and p67^{phox} PB1 domains. The complex between the PB1 domain of p40^{phox} (blue) and p67^{phox} (green). Key residues from the basic clusters (BC1 and BC2)-p67^{phox}, and acidic clusters (AC1 and AC2)-p40^{phox}, which are involved in complex formation are represented as sticks. PDB identifier 1OEY (Wilson et al., 2003).

that PX domains belong to the family of lipid binding modules along with PH (Pleckstrin homology) and FYVE (Fab1, YOTB/ZK632.12, Vac1 and EEA1) domains, and that they interact specifically with phosphoinositides (Corvera et al., 1999; Fruman et al., 1999; Prehoda and Lim, 2001; Simonsen and Stenmark, 2001; Wishart et al., 2001). These protein-lipid interactions are important in recruiting proteins to specific cell membranes.

A number of NMR and crystal structures of PX domains have been solved, including those of $p47^{phox}$ and $p40^{phox}$ (Bravo et al., 2001; Hiroaki et al., 2001; Karathanassis et al., 2002). They reveal that PX domains are composed of three anti-parallel β-sheets and four α-helices. The structure of the $p40^{phox}$ PX domain is similar to the $p47^{phox}$ PX domain, with the exception of an additional N-terminal α-helix. The crystal structure of the $p40^{phox}$ PX domain was solved in complex with the soluble ligand di-C4-PtdIns(3)P, and shows that the wall of the binding pocket is formed by Arg105, Arg85 and Tyr59 (Bravo et al., 2001) (Figure 17A). The X-ray structure of the $p47^{phox}$ PX domain was solved in the absence of a lipid. However, the structure showed that the protein had two sulfate ions bound in two distinct basic binding pockets (the sulfate ions are believed to mimic phosphate groups). The first binding pocket is larger than the second, and is assumed to be the phosphoinositide binding site. This binding pocket is formed by Arg43 which makes hydrogen bonds with the sulphate, and through van der Waals interactions with Arg90 (Figure 17B) (Karathanassis et al., 2002). Mutation of R43Q has been found in CGD patients and leads to loss of $p47^{phox}$ expression and stability, demonstrating that the $p47^{phox}$ PX domain plays a key role in protein integrity (Heyworth and Cross, 2002). The second, shallower basic pocket, which has not been seen in any other PX domain structure, has been suggested to bind anionic phospholipids such as phosphatidic acid (PA) or phosphatidylserine (PS). The walls of the pocket are formed by the side chains of Arg70, Lys55 and His51, which gives the pocket its basic character. Both the $p40^{phox}$ and $p47^{phox}$ PX domains have exposed hydrophobic residues in the vicinity of the lipid binding pockets, which could penetrate into the membrane and thereby synergistically increase membrane affinity (Karathanassis et al., 2002).

A

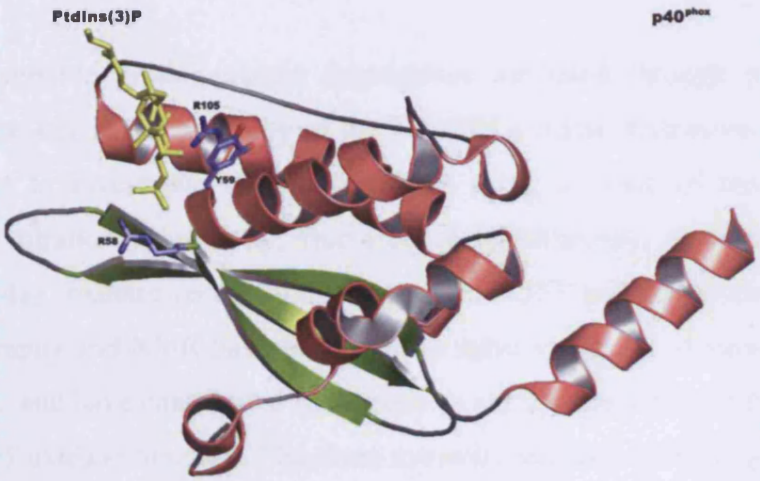

B

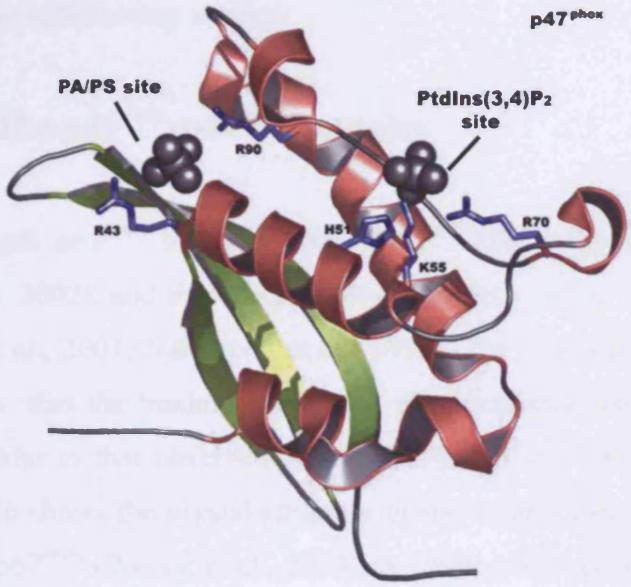

Figure 17: The structures of the p40^{phox} and p47^{phox} PX domains. A. The p40^{phox} PX domain in complex with di-C4-PtdIns(3)P (yellow sticks). The positions of residues forming important contacts with the phosphoinositide are shown as blue sticks. PDB identifier 1H6H (Bravo et al., 2001). B. The p47^{phox} PX domain bound to two sulfates ions (sulfates shown in CPK representation). The position of residues involved in forming the phosphoinositide and anion binding pockets are shows as blue sticks. PDB identifier 1O7K (Karathanassis et al., 2002). In both figures the β-sheets are shown in green and α-helices in pink.

1.5 Protein interactions in the resting state of the NADPH oxidase

Reversible protein-protein interactions mediated through protein interaction domains are key in the assembly of the NADPH oxidase. Extensive studies have been carried out to investigate these interactions using a range of techniques including isothermal titration calorimetry, fluorescence spectroscopy, yeast-two hybrid assays, phage display, oxidase reconstitution assays and GST pull-down assays. Furthermore, crystallography and NMR have been used to solve structures of various fragments and complexes, and have contributed immensely to our understanding of the molecular basis of NADPH oxidase function. The three cytosolic subunits $p40^{phox}$, $p47^{phox}$ and $p67^{phox}$ are able to form a tight heterotrimeric complex (Figure 18) (for details concerning the formation of this complex refer to section 1.3.2). The molecular details of this complex are described in the following section.

1.5.1 The $p67^{phox}$-$p40^{phox}$ complex

Full-length $p67^{phox}$ interacts with $p40^{phox}$ with a binding affinity of 10 nM (Lapouge et al., 2002), and this binding event is solely driven by their respective PB1 domains (Ito et al., 2001; Nakamura et al., 1998). This finding has been confirmed by the observation that the binding affinity of the interaction between the isolated PB1 domains is similar to that observed for the full-length protein (4 nM) (Wilson et al., 2003). Figure 16 shows the crystal structure of the complex between the PB1 domains of $p40^{phox}$ and $p67^{phox}$ (Wilson et al., 2003). A single point mutation in the $p40^{phox}$ PB1 domain, D289A, disrupts the interaction with $p67^{phox}$ and thereby prevents membrane translocation of $p40^{phox}$ and $O_2^{\cdot-}$ generation (Kuribayashi et al., 2002). However despite our current understanding of the molecular details of the $p40^{phox}$-$p67^{phox}$ interaction, the exact biological significance of complex formation is not clear at present.

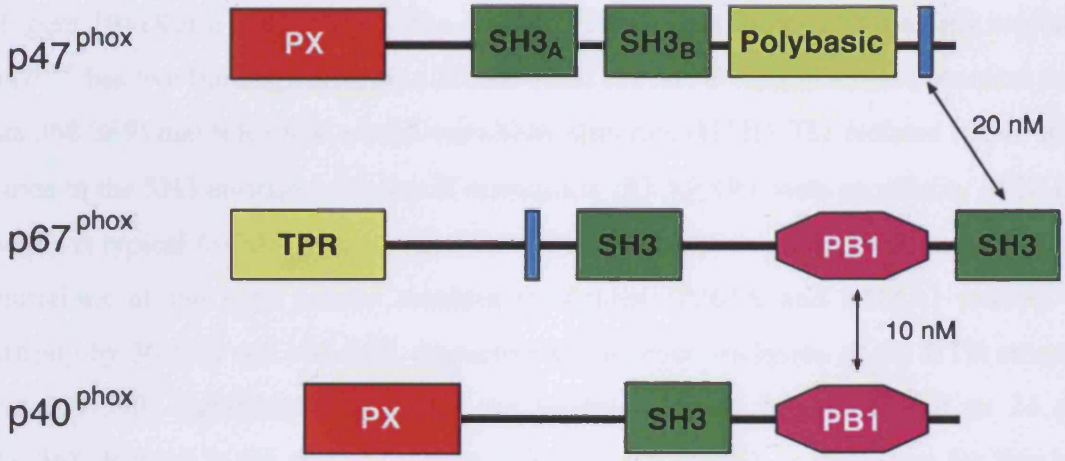

Figure 18: Model for the p47^{phox}-p67^{phox}-p40^{phox} complex in the resting state of NADPH oxidase. The p47^{phox} C-terminal proline-rich region (shown in blue) interacts with p67^{phox}(SH3)$_B$ with a binding affinity of 20 nM. P67^{phox} interacts with p40^{phox} via their PB1 domains with a binding affinity of 10 nM (taken and adapted from Lapouge et al., 2002).

1.5.2 The $p47^{phox}$-$p67^{phox}$ complex

The interaction between $p47^{phox}$ and $p67^{phox}$ is mediated by the PR region located in the C-terminus of $p47^{phox}$ and the C-terminal SH3 domain of $p67^{phox}$ ($p67^{phox}(SH3)_B$), which bind each other with a binding affinity of 20 nM (Finan et al., 1994; Lapouge et al., 2002; Leto et al., 1994). The structure of a complex between $p67^{phox}(SH3)_B$ and this PR region (aa 359-390) has been solved by NMR spectroscopy (Figure 19) (Kami et al., 2002). The structure shows that the $p67^{phox}$-binding region of $p47^{phox}$ has two binding surfaces: a PXXP motif (aa 360-370) and a non-canonical motif (aa 368-389) that folds into a helix-turn-helix structure (HTH). The isolated PXXP motif binds to the SH3 domain in a class II orientation (PXXPXR), with an affinity of 20 μM, which is typical for SH3 domain mediated interactions. Disruption of this interaction via mutations of the core proline residues to alanine (P363A and P366A) reduces the affinity by 30-fold and 100-fold, respectively. However, inclusion of the HTH structure (aa 359-390) significantly enhances the binding affinity by ~1000-fold to 24 nM. Arg368, located in the class II consensus motif (PXXPXR), is important for this high affinity interaction, as mutation of this residue to alanine reduces the affinity 625-fold. In addition, Ile374 (in helix α1) and Thr382 (in helix α2) in the HTH structure are also important for complex formation. Substitution of either of these residues to alanine reduces the affinity to 3.0 μM and 1.1 μM, respectively.

Interestingly, three phosphorylation sites (serine residues 359, 370 and 379) are located in the C-terminal region of $p47^{phox}$, adjacent to the PR sequence motif. However, the precise function of these phosphorylation sites is not yet known (for a more detailed discussion see section 1.3.2.1.2). In addition to the interaction with $p67^{phox}$, the C-terminal PR region of $p47^{phox}$ has also been suggested to be the target of the SH3 domain of $p40^{phox}$, which may compete with $p67^{phox}$ for binding to this region. However the binding affinity of this interaction is significantly weaker than the $p47^{phox}$-$p67^{phox}$ interaction, making a direct competition unlikely.

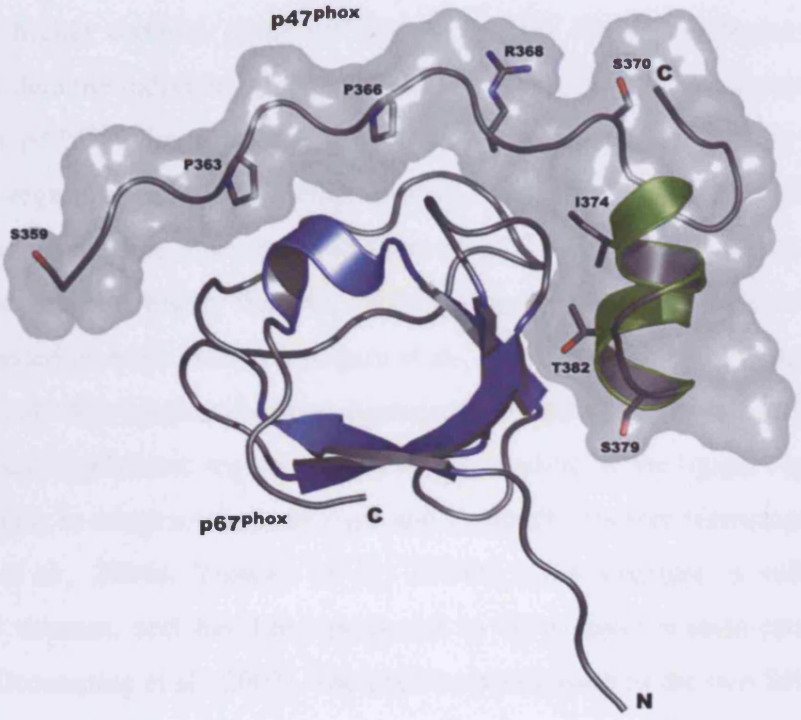

Figure 19: C-terminal SH3 domain of p67^{phox} in complex with the C-terminal region of p47^{phox}. The $SH3_B$ domain of p67^{phox} is shown in blue. The C-terminal peptide of p47^{phox} is shown as a surface representation (grey) with underlying ribbons shown in green. Important residues involved in complex formation are shown as sticks (Arg368, Ile374 and Thr382), along with key phosphorylation sites (Ser359, Ser370 and Ser379). Pro363 and Pro366 of the PXXP motif are also indicated. PDB identifier 1K4U (Kami et al., 2002).

1.6 The superSH3 domain as a novel protein-protein interaction module

Adjacent protein interaction modules can work in coordination with one another to increase the affinity and specificity for bivalent targets as seen for example with a number of SH2 domain containing proteins (Ottinger et al., 1998). Alternatively, they can form higher ordered structures that may have slightly different ligand binding properties than the individual domains (Fedoroff et al., 2004). An example of the former is seen in $p47^{phox}$ where the tandem SH3 domains work together to bind either the polybasic region or $p22^{phox}$ (Groemping et al., 2003; Yuzawa et al., 2004a; Yuzawa et al., 2004b). In the free, uncomplexed form of $p47^{phox}$, the linker region connecting the two SH3 domains is highly flexible, allowing the two domains to move freely resulting in an extended globular structure (Ogura et al., 2005). However, upon ligand binding the two adjacent SH3 domains become juxtaposed in both the active ($p22^{phox}$-bound) and auto-inhibited (polybasic region-bound) states. Binding of the ligand causes the tandem SH3 domains to adopt a relatively rigid and compact structure (Groemping et al., 2003; Yuzawa et al., 2004a; Yuzawa et al., 2004b). This structure is referred to as the superSH3 domain, and has been proposed to be a novel protein-protein interaction module (Groemping et al., 2003). The relative positioning of the two SH3 domains with respect to one another within the superSH3 domain is important to form a single binding surface of high affinity. The formation of this conformation appears to be dependent on two structural features: the covalent linker, which connects the two SH3 domains, and a conserved 'GWW' motif located in the n-Src loops, a region where the two SH3 domains make contact.

1.6.1 The linker

Other than physically connecting interaction domains together, linkers can be important in facilitating protein function. For example, using site-directed deletion mutagenesis Govindaraj and Pouolos showed that the length of the linker connecting the heam and FAD binding sites of cytochrome P450BM-3, was important in controlling the electron transfer reaction of this enzyme (Govindaraj and Poulos, 1995). Hegvold and Gabrielsen showed that increasing the flexibility of the linker (through proline to glycine substitutions) connecting the R2 and R3 repeats in the DNA binding domain of

c-Myb protein, affected DNA binding (Hegvold and Gabrielsen, 1996). Linkers have also shown to play an important role in proteins where the activity is regulated by auto-inhibitory interactions. For example increasing the flexibility of the SH2-SH3 linker (proline to glycine substitution) in Src kinase relieves auto-inhibition and induces kinase activation (Young et al., 2001).

Similarly, the activity of the NADPH oxidase is prevented by an intramolecular interaction between the tandem SH3 domains of $p47^{phox}$ and the polybasic region. The linker connecting the two SH3 domains may be important for the formation of the 'auto-inhibited core', as the crystal structure of the auto-inhibited $p47^{phox}$ shows that the linker region is well ordered and makes a number of contacts with the remainder of the protein (Groemping et al., 2003; Yuzawa et al., 2004a; Yuzawa et al., 2004b). Importantly, the linker is absolutely essential for the formation of the superSH3 domain, as no interaction between the individual SH3 domains is observed in free solution (Groemping et al., 2003). However, at present it is not clear how factors such as linker length, composition and flexibility contribute to the formation and stabilisation of the superSH3 domain.

The $p47^{phox}$ linker makes contacts with the polybasic region at many points along its length, as well with the two SH3 domains. The N-terminal region of the linker makes contacts with $SH3_A$, where as the C-terminal region contacts $SH3_B$. Key residues of the linker involved in these interactions include E218, E220 and D221. E218 makes hydrogen bonds with $Lys188_A$ and $Tyr161_A$. E220 makes hydrogen bonds with $Gln159_A$ and $Lys188_A$. D221 makes a single hydrogen bond with $Leu260_B$ (Figure 20). Interestingly, during the active state the linker does not directly contact $p22^{phox}$, and only residues E220 and D221 form hydrogen bonds with the SH3 domains (E220 makes a hydrogen bond with $Try161_A$, and D221 makes a hydrogen bond with Leu260).

The $p47^{phox}$ linker is composed of fifteen amino acids ($_{213}$LDSPDETEDPEPNYA_{227}), and this specific length may be important in maintaining the correct distance and orientation between $SH3_A$ and $SH3_B$. In addition, the linker of $p47^{phox}$ contains three proline residues at positions 216, 222 and 224. The side-chain ring of a proline is covalently attached to its backbone nitrogen atom, making it a rigid structure that strongly influences the conformation of proline containing sequences. Therefore, linker rigidity imposed by these proline residues may also contribute to the stabilisation of the superSH3 domain. However, so far no systematic studies have been carried out to investigate the importance of $p47^{phox}$ linker specifics (length, composition

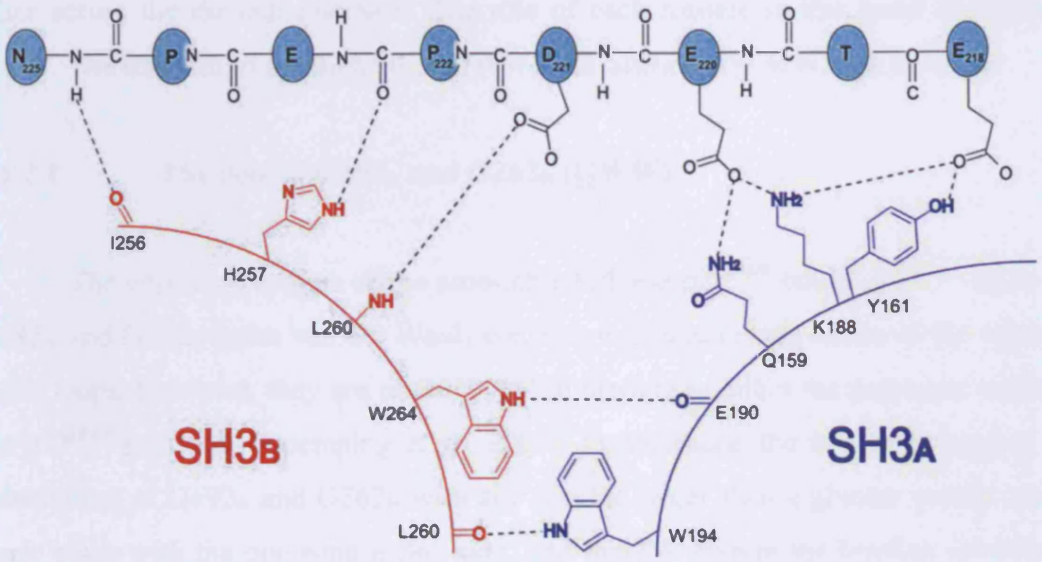

Figure 20: P47^{phox} linker interactions with the tandem SH3 domains in the auto-inhibited state. Schematic representation showing the hydrogen bond interactions between E218, E220 and D221 and the tandem SH3 domains. All others are backbone interactions. $W194_A$ and $W264_B$ make hydrogen bonds across the domain interface. PDB identifier 1NG2 (Groemping et al., 2003). The figure was prepared using the program ISIS draw.

and flexibility) for the formation and stabilisation of the superSH3 domains in the active and auto-inhibited states.

1.6.2 The GWW motif

The second feature that appears to be crucial for the formation of the superSH3 domain is the presence of a 'GWW' motif in either SH3 domain. This motif is located in the n-Src loops, the region where the two domains come closest and contact each other across the domain interface. The role of each residue in this motif is discussed below. The location of the motif is $_{192}$GWW$_{194}$ in SH3$_A$ and $_{262}$GWW$_{264}$ in SH3$_B$.

1.6.2.1 The role of G192$_A$ and G262$_B$ (GWW)

The crystal structures of the auto-inhibited and p22^{phox}-bound p47^{phox} show that G192$_A$ and G262$_B$ make van der Waals contacts with main chain atoms of the opposing n-Src loops. However, they are not involved in binding to either the polybasic region or the p22^{phox} peptides (Groemping et al., 2003). Furthermore, the structures suggest that substitution of G192$_A$ and G262$_B$ with any residue larger than a glycine would cause a steric clash with the opposing n-Src loop, and thereby disrupt the binding interface of the superSH3 domain (Figure 21). In order to investigate this hypothesis, Groemping and colleagues made glycine to serine mutants (G192S$_A$ and G262S$_B$), and performed binding measurements using ITC (Groemping et al., 2003). These studies showed that mutation of either glycine resulted in proteins that were less soluble than the wild-type protein, and that the double mutant was completely insoluble, suggesting that G192$_A$ and G262$_B$ are critical for correct protein folding. Furthermore, binding studies using the individual mutant proteins showed a dramatic reduction in the affinity for the polybasic region and p22^{phox}-derived peptides, clearly indicating that the formation of the superSH3 domain is compromised. This observation is further emphasised by a form of CGD, in which patients carry glycine to serine mutations in exactly these positions (Noack et al., 2001). Based on these observations, it was suggested that the role of G192$_A$ and G262$_B$ is to allow the correct orientation of the SH3 domains with respect to each other, and to enhance the structural integrity of the protein.

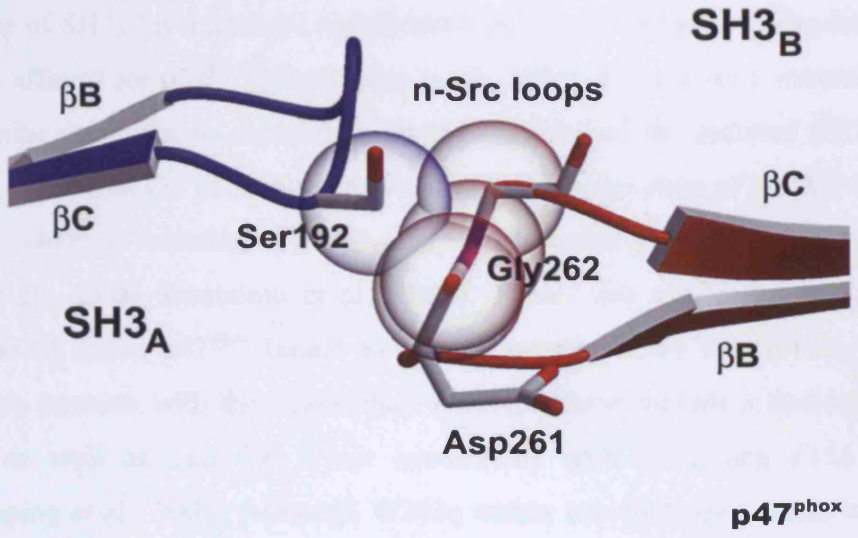

Figure 21: $G192_A$ and $G262_B$ in the superSH3 domain. The n-Src loops at the interface between $SH3_A$ and $SH3_B$. The modelled mutation of $G192S_A$ results in steric clashes with main chain atoms from the n-Src loop of $SH3_B$. The blue sphere represents the van der Waals surface of Cβ of S192, and the red spheres those of main chain Cβs in the n-Src loop of $SH3_B$. Illustration courtesy of Groemping et al., 2003.

1.6.2.2 The role of $W193_A$ and $W263_B$ (GWW)

The positions corresponding to $W193_A$ and $W263_B$ are fully conserved among SH3 domains and are crucial for ligand binding (position 36(W)-Figure 13) (Larson and Davidson, 2000). Many studies have shown that $W193_A$ plays a more important role in NADPH oxidase activity than $W263_B$. The importance of $W193_A$ can be rationalised by the fact that the interaction between $p47^{phox}$ and $p22^{phox}$ is dominated by $SH3_A$. In fact, immunoblott assays (Sumimoto et al., 1996), *in vitro* binding assays (de Mendez et al., 1997) and quantitative binding studies (Groemping et al., 2003) have shown that isolated $SH3_A$ is able to bind to $p22^{phox}$ but isolated $SH3_B$ cannot. However, the presence of $SH3_B$ (as a tandem) significantly increases binding (de Mendez et al., 1997) and the affinity for $p22^{phox}$ (Groemping et al., 2003). Furthermore, mutation of $W193_A$ to arginine is shown to completely abolish binding of the isolated $SH3_A$ domain to $p22^{phox}$, as well as $O_2^{\cdot-}$ production and membrane translocation of the full-length mutant protein, where as mutation of $W263_B$ only has a partial effect (de Mendez et al., 1997; Hata et al., 1998; Sumimoto et al., 1996). These data are further supported by the structure of active $p47^{phox}$ bound to $p22^{phox}$, which shows that $W193_A$ makes more extensive contacts with the ligand than $W263_B$. These include a hydrogen bond with N154, as well as van der Waals interactions with P152 and P156 (Figure 22) (Groemping et al., 2003). Although $W263_B$ makes two hydrogen bonds with P156 and P157, it is not found within a similar hydrophobic environment as its counterpart $W193_A$.

Unlike $p22^{phox}$ which can bind isolated $SH3_A$, the polybasic region requires the presence of both SH3 domains for complex formation (Groemping et al., 2003). However, the precise role of $W193_A$ and $W263_B$ in the auto-inhibited state is unclear at present. The structure of auto-inhibited $p47^{phox}$ shows that $W193_A$ makes extensive contacts with the core binding motif of the polybasic region. Specifically, it makes a hydrogen bond with G297 plus van der Waals and hydrophobic interactions with P299 and R296. $W263_B$ on the other hand only forms one hydrogen bond with P299 and stacks against R301 (Groemping et al., 2003; Yuzawa et al., 2004a; Yuzawa et al., 2004b). These biochemical and structural data suggest that although $SH3_A$ and $SH3_B$ are required for the formation of a high affinity ligand binding site, $W193_A$ may make a bigger contribution.

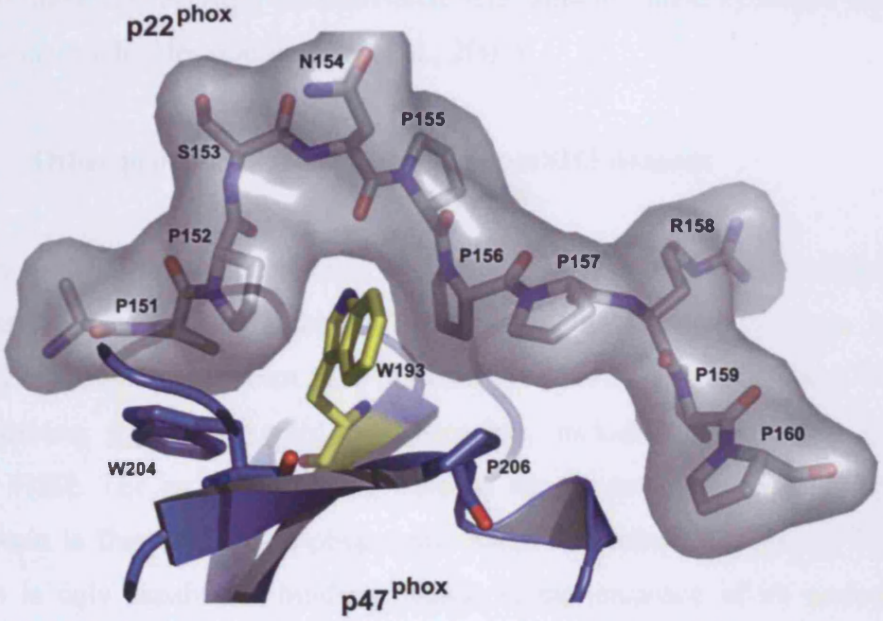

Figure 22: The binding pocket formed by $p22^{phox}$ for $W193_A$. The binding pocket is formed by P152, N154 and P156 of the core peptide binding region of $p22^{phox}$ (grey sticks). $W193_A$ is shown in yellow which fits into the binding pocket. PDB identifier 1OV3 (Groemping et al., 2003).

1.6.2.3 The role of $W194_A$ and $W264_B$ (GWW)

$W194_A$ and $W264_B$ are not involved in direct contacts with ligands. Instead they are located at the SH3 domain interface, making contacts across the interface and contribute to the stabilisation of the superSH3 domain conformation (Figure 20). The crystal structure of auto-inhibited $p47^{phox}$ shows that $W194_A$ makes a hydrogen bond with $L260_B$, and $W264_B$ with $E190_A$ (Groemping et al., 2003; Yuzawa et al., 2004a; Yuzawa et al., 2004b). In the $p22^{phox}$-bound state similar interactions are made, but due to slight rearrangements between the individual SH3 domains, these hydrogen bonds are bridged via water molecules (Groemping et al., 2003).

1.6.2.4 Other proteins that may form a superSH3 domain

Many proteins involved in signal transduction processes contain multiple SH3 domains that are connected by linkers of varying length. A subset of these proteins contains a GWW motif in adjacent SH3 domains (see SH3 family alignment from the SMART database, http://smart.embl-heidelberg.de/), including the adaptor proteins CIN85 and FISH. The most convincing case so far for another superSH3 domain-forming protein is that of the non-phagocytic NADPH oxidase homologue NOXO1. This protein is only capable of binding ligands in the presence of its tandem SH3 domains (Dutta and Rittinger, unpublished data). In addition, there are also biochemical data available for CIN85 as well as FISH that strongly suggest that a subset of the SH3 domains present in these proteins cooperate for ligand binding (Abram et al., 2003; Kowanetz et al., 2003). Further studies are now required to determine whether the superSH3 domain may indeed be a novel signal transduction module.

1.7 Aims of the project

The activity of the NADPH oxidase is regulated by a complex set of protein-protein and protein-lipid interactions. A central player in the activation and assembly of this enzyme is $p47^{phox}$, whose activity is regulated by protein-protein and protein-lipid interactions. The aim of this project is to investigate the conformational changes or changes in protein-protein and protein-lipid interactions that take place in $p47^{phox}$ during the activation and assembly process.

Most studies have focused on the effects of phosphorylation of serine residues located within the polybasic region of $p47^{phox}$ (S303, 304, 315, 320 and 328), on NADPH oxidase activation. It is not clear whether the C-terminal serine residues (S359, 370 and 379) contribute to this activation process. Here, experiments are described investigating whether phosphorylation of the C-terminal serine residues act synergistically with phosphorylation of the polybasic region, to promote the interaction with $p22^{phox}$, as well as the effects on binding to $p67^{phox}$. In addition, the effect of $p47^{phox}$ C-terminal phosphorylation on lipid binding will be explored (chapter 3).

The superSH3 domain has been proposed to be a novel protein-protein interaction module, and key to its formation is believed to be the covalent linker between the two SH3 domains, and a 'GWW' motif located in the respective n-Src loops of either SH3 domain. The aim of this study is to investigate the structural requirements with respect to these two features, for the formation of the superSH3 domain in the active ($p22^{phox}$-bound) and auto-inhibited (polybasic region-bound) states of $p47^{phox}$ (chapter 4). This may enable us to determine which other proteins may behave in a similar fashion.

CHAPTER TWO

2.0 Materials and Methods

All standard chemicals used in this work were obtained from Sigma, BDH and Bio-Rad, and were of the highest purity commercially available. Details of other reagents, cell lines, media, buffer compositions and gel compositions can be found in the Appendix. Restriction enzymes were purchased from New England Biolabs, oligonucleotides from Oswel and DNA purification kits from Qiagen. PtdIns(3,4)P_2 was purchased from CellSignals and all other lipids from Sigma. PIP beads were purchased from Echelon Biosciences. All structural pictures were generated in PyMOL (http://www.pymol.org) unless otherwise stated.

2.1 General molecular biology procedures

2.1.1 Plasmid vectors and constructs

Recombinant proteins were expressed in the Glutathione S-transferase (GST) fusion vectors pGEX-6-P1 ($p47^{phox}$) (refer to Table 6) and pGEX-4-T1 ($p67^{phox}$) (refer to Table 7). Figure 23 shows a map of the GST fusion vectors with the reading frames and main features. Expression of GST fusion proteins is under the control of the tac promoter, which is induced by isopropyl β-D thiogalactoside (IPTG), a lactose analogue. The lacIq gene, also present in pGEX vectors functions as a repressor, and binds to the operator region of the tac promoter to prevent basal expression until IPTG induction. Hence, the lacIq gene maintains a relatively tight control over the expression of insert.

2.1.2 Transformation of competent cells

50 µl of competent *E. coli* cells (NovaBlue or BL21(DE3)) were thawed on ice. 100 ng of plasmid DNA was pipetted into the cells, gently mixed and incubated for 30 mins on ice. The cells were subjected to heat shock at 42 °C for 1 min before returning to ice for a further 2 min. 300 µl of LB media (see Appendix: A2) (excluding ampicillin) was added to the sample, which was gently mixed and incubated at 37 °C for 1 hr. 20-200 µl of the sample were spread onto an LB agar plate containing 100 µg/ml ampicillin and incubated overnight at 37 °C.

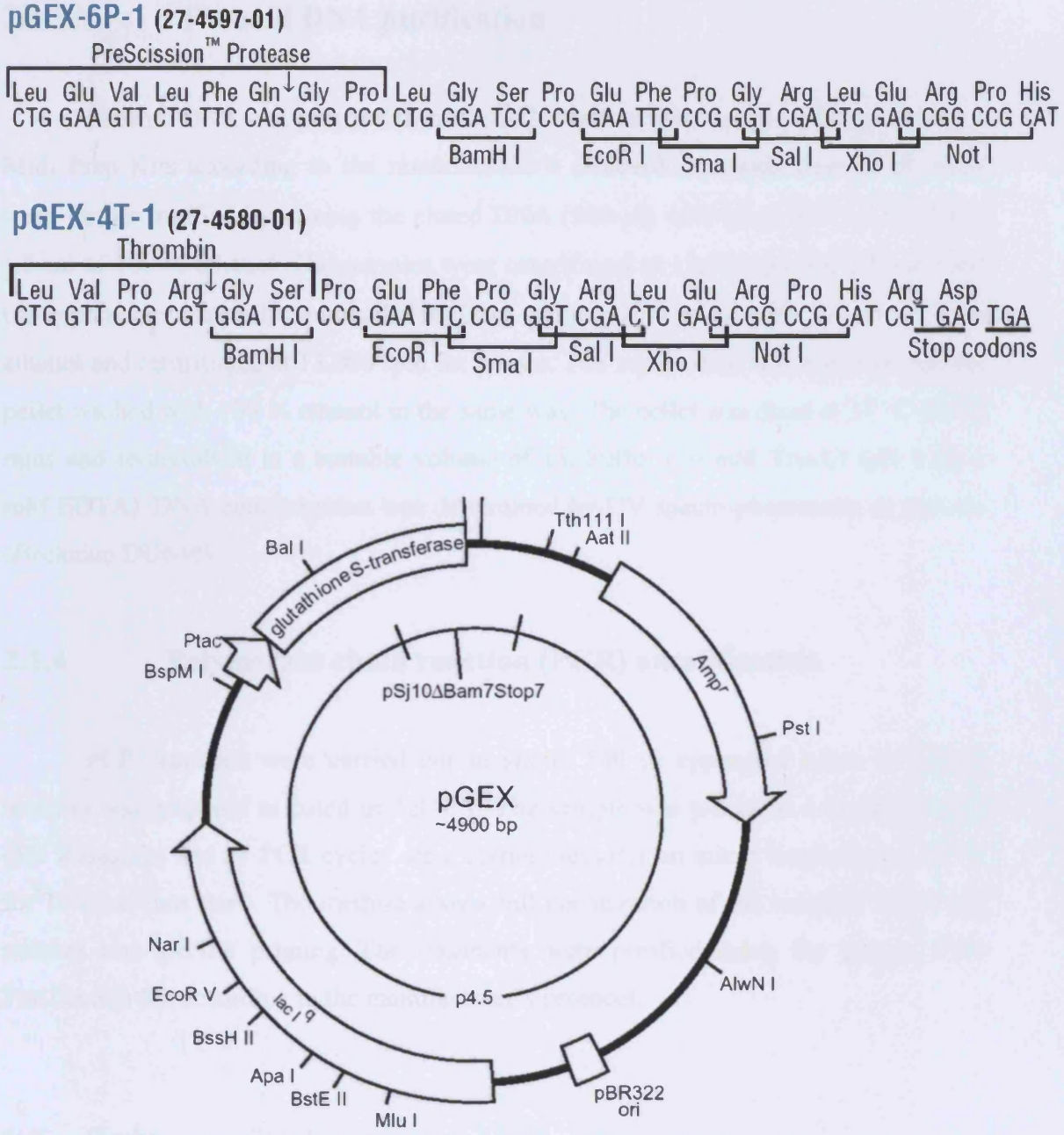

Figure 23: **Map of the Glutathione S-transferase fusion vectors**. The reading frames and main features of the pGEX vector are indicated.

2.1.3 Plasmid DNA purification

Plasmid DNA was purified from *E.coli* NovaBlue cells using the Qiagen Mini or Midi Prep Kits according to the manufacturer's protocol. Plasmids from Midi preps were further purified by mixing the eluted DNA (500 µl) with 20 µl of 5 M NaCl and 1.3 ml of 100 % ethanol. The samples were centrifuged at 13,000 rpm for 20 mins and the supernatant carefully removed. The DNA pellet was washed with 500 µl of 70 % ethanol and centrifuged at 13,000 rpm for 5 mins. The supernatant was removed and the pellet washed with 100 % ethanol in the same way. The pellet was dried at 37 °C for 10 mins and re-dissolved in a suitable volume of TE buffer (10 mM Tris.Cl (pH 8.0), 1 mM EDTA). DNA concentration was determined by UV spectrophotometry at 260 nm (Beckman DU640).

2.1.4 Polymerase chain reaction (PCR) amplification

PCR reactions were carried out in sterile 500 µl eppendorf tubes. A typical reaction was prepared as listed in Table 1. The sample was placed in a thermal cycler (MJ Research) and 25 PCR cycles were carried out after an initial incubation at 94 °C for 10 mins (hot start). The method allows full denaturation of the template DNA and reduces non-specific priming. The fragments were purified using the Qiagen PCR Purification Kit according to the manufacturer's protocol.

94 °C	10 mins	(Initial incubation)
<u>Per cycle</u>		
94 °C	2 mins	(DNA denaturation)
55 °C	2 mins	(Primer annealing)
72 °C	2 mins	(Primer extension)
<u>After 25 cycles</u>		
72 °C	10 mins	(Final extension)

Table 1: **Typical reagent mixture for a PCR reaction.**

Reagent	Volume (µl)
10 X PCR buffer (1.2 M Tris-HCl (pH 8.0), 100 mM KCl, 60 mM $(NH4)_2S0_4$, 1 % Triton X-100, 0.01 % BSA)	5
$MgCl_2$ (25 mM)	2
dNTP mixture (8 mM total, 2 mM each)	5
Template DNA (0.5-1 µg total)	1
Oligo 1 (20 µM)	1
Oligo 2 (20 µM)	1
Kod polymerase (2.5 U/µl)	1
dH_20	34
TOTAL	50

2.1.5 Agarose gel electrophoresis

DNA was analysed using a 1 % agarose gel containing 0.1 µg/ml ethidium bromide (see Appendix: A3). 2-5 µl of sample was mixed with 3 µl 6X loading buffer (see Appendix: A3) and subjected to electrophoresis in 1x TAE buffer at 80 V for 30-40 mins, and visualized on an UV-transilluminator (BDH).

2.1.6 Restriction enzyme digests

DNA fragments and vectors were digested using appropriate restriction enzymes (see Tables 6 and 7) at 37 °C for 3 hrs. A typical reaction mixture is shown in Table 2. The digested DNA was subjected to electrophoresis on a 1 % agarose gel as described in section 2.1.5. The required bands were excised from the gel using a sterile scalpel blade and purified using the Qiagen Gel Extraction Kit, according to the manufacture's protocol.

2.1.7 Ligation reaction

A 1:1, 1:3 or 3:1 molar ratio of vector:insert DNA is recommended for successful cloning of fragment DNA into a plasmid vector (Sambrook et al., 1989). The

following example uses a 1:1 vector:insert ratio, where typically the ligation reaction uses 100-200 ng of vector. The conversion of mole ratios to mass ratios for a 3 kb plasmid, and 0.5 kb insert can be calculated by the following equation (Promega).

$$\frac{\text{ng vector} \times \text{kb size of insert}}{\text{kb size of vector}} \times \frac{\text{molar ratio of insert}}{\text{vector}} = \text{ng of insert} \qquad [3]$$

Ligation reactions were carried out at 16 °C overnight. A typical ligation reaction is shown in Table 3. Ligated samples were transformed into NovaBlue competent cells as described in section 2.1.2.

Table 2: **Typical reaction mixture for a restriction enzyme digest.**

Reagent	**Volume (µl)**
DNA (50-100 ng)	5
10 X reaction buffer (6 mM Tris-HCl (pH 6), 6 mM $MgCl_2$, 150 mM NaCl, 1 mM DTT) *(appropriate to restriction enzyme used, refer to manufacturers instructions)*	2
Restriction enzyme 1 (10 U/µl)	1
Restriction enzyme 2 (10 U/µl)	1
BSA (1 mg/ml)	2
dH_20	9
TOTAL	20

Table 3: **Typical reaction mixture for a ligation.**

Reagent	**Volume (µl)**
Vector (µg)	X
Insert (µg)	Y
T4 DNA 10 X ligase buffer (300 mM Tris/HCl (pH 7.8), 100 mM $MgCl_2$, 100 mM DTT and 5 mM ATP)	2
T4 DNA ligase (3 U/µl)	1
dH_20	Z
TOTAL	20

2.1.8 Site-directed mutagenesis

Mutations were introduced into $p47^{phox}$ using the Quik-Change Site-Directed Mutagenesis Kit (Stratagene, UK). This method is used to make point mutations and delete or insert single or multiple nucleotides. The basic procedure is summarised in Figure 24. The plasmid containing the gene for the target site mutation ($p47^{phox}$Wild-type) is denatured. Two complementary oligonucleotide primers with the desired mutation are annealed to the plasmid. *Pfu* DNA polymerase (Stratagene) was used to extend the mutagenic primers, resulting in nicked circular strands. The methylated non-mutated parental DNA template is then digested using *Dpn*I, and the nicked dsDNA is transformed into NovaBlue competent cells where the nicks in the mutated plasmid are repaired. The primers containing the desired mutation were designed to be between 25-45 bases in length and chosen such that the annealing temperature (T_m) of the primers is 10 °C above the extension temperature (T_m = 81.5 + 0.41 (% GC) – 675 / N - % mismatch, (N = primer length, b.p)).

The mutagenesis PCR reaction was prepared as shown in Table 4. 12-14 PCR cycles were carried out after an initial denaturation at 95 °C for 30 sec (12 cycles for 1 point mutation, 14 cycles for 2-3 point mutations), using the following program:

95 °C	30 secs	(Initial denaturation)
<u>12-14 cycle</u>		
95 °C	30 secs	(DNA denaturation)
55 °C	1 min	(Primer annealing)
68 °C	1 min/kb of plasmid length	(Primer extension)
<u>After 12 cycles</u>		
10 °C	10 mins	(Cooling)

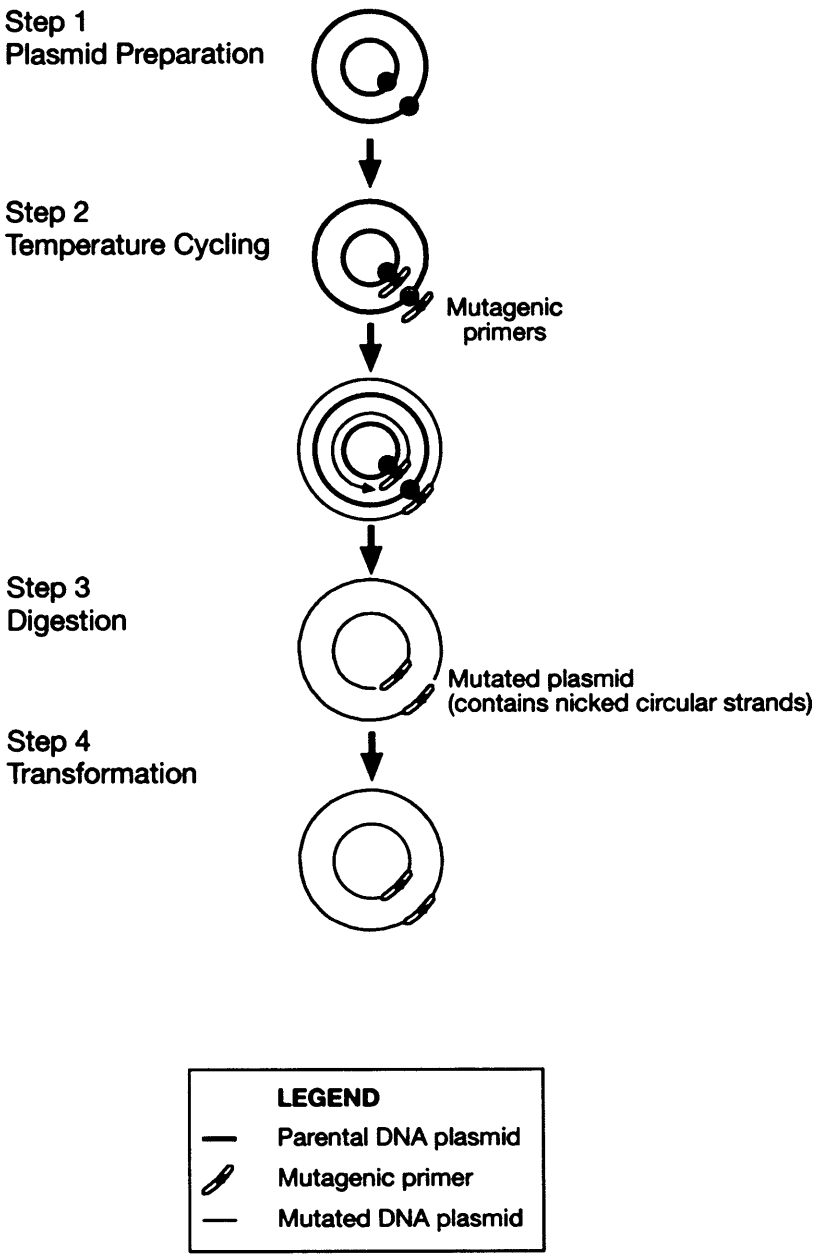

Figure 24: **Overview of the Quik-Change Site-Directed Mutagenesis method**. Taken and adapted from the Quik-Change Site-Directed Mutagenesis Kit Instruction manual, 1996.

Table 4: Composition of a typical mutagenesis reaction.

Reagent	Volume (µl)
10 X *Pfu* reaction buffer (100 mM KCl, 60 mM $(NH4)_2S0_4$, 200 mM Tris- HCl (pH 8.0), 20 mM $MgCl_2$, 1 % Triton X-100)	5
Oligo 1 (125 ng/µl final concentration)	1
Oligo 2 (125 ng/µl final concentration)	1
$p47^{phox}$Wild-type DNA (50 ng/µl final concentration)	1
10 mM dNTP mix (2.5 mM each NTP)	1
Pfu DNA polymerase [2.5 U/µl]	1
dH_20	40
TOTAL	50

The amplified PCR sample was treated with 0.8 µl *Dpn*I endonuclease (10 U/µl), and incubated at 37 °C for 1 hr. The DNA was transformed into NovaBlue competent cells. Midi preps of four colonies were carried out using the Qiagen Midi Prep Kit according to the manufacturer's protocol. All mutations were confirmed by DNA sequencing performed by IC Consultants, Imperial College, London.

2.2 Generation of specific plasmids

All plasmids employed in this study are listed in Tables 6 and 7. The cloning of plasmid pGEX-p47^{phox}S8E is described in detail below in section 2.2.1. The plasmid containing the PH domain of the TAPP1 protein was kindly donated by Dr. Maria Deak (Thomas et al., 2001), and details about the plasmid can be found beneath Table 7.

2.2.1 Cloning of p47^{phox} S303, 304, 315, 320, 328, 359, 370 and 379E (pGEX-p47^{phox}S8E)

P47^{phox} contains eleven phosphorylation sites of which eight have been shown to be required for NADPH oxidase activation. Five of these serine residues; S303, 304, 315, 320, 328 are located within the polybasic region, and the remaining three serine residues; 359, 370, 379 are located in the C-terminal portion of the protein. At the start of this project two full-length plasmids had already been constructed, in which phosphorylation had been mimicked by substitution of serine residues to glutamate (in pGEX-6-P1) (Table 6). The plasmids were pGEX-p47^{phox}S5E (polybasic region mutant) and pGEX-p47^{phox}S3E (C-terminal region mutant) (Table 6). These were used to generate a construct, which combined all eight serine to glutamate mutations in a single plasmid (pGEX-p47^{phox}S8E) (Table 6) (Figure 25a). Briefly, restriction enzyme digests of pGEX-p47^{phox}S5E and pGEX-p47^{phox}S3E plasmids were carried out using the *Sma*I restriction enzyme, and the fragments separated on a 1 % agarose gel. The desired fragments were excised and purified using the Qiagen Gel Purification Kit according to the manufacturer's protocol. As *Sma*I digests result in blunt ended DNA fragments, self-ligation of the pGEX-p47^{phox}S5E in pGEX-6-P1 vector had to be prevented by de-phosphorylation (using phosphatase alkaline shrimp enzyme) (Table 5). The two digested products were mixed and incubated at 37 °C for 30 min and the reaction was terminated by incubating at 65 °C for 15 min and then placed on ice. The de-phosphorylated DNA plasmid was purified using the Qiagen PCR Purification Kit according to the manufacturer's protocol. The vector and insert were ligated (section 2.1.7) and transformed into NovaBlue competent cells (section 2.1.2). Plasmids from six clones were purified using the Qiagen Midi Prep Kit according to the manufacturer's protocol. In order to verify the correct insertion and orientation of the 6 plasmids,

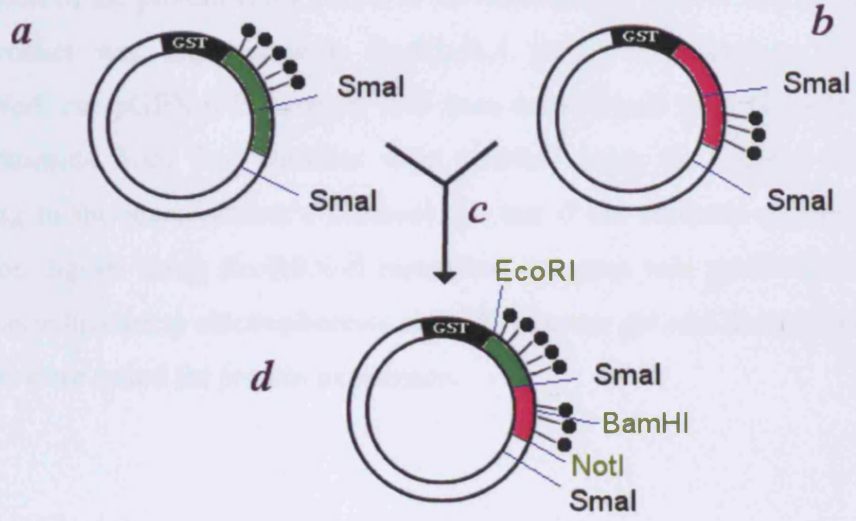

Figure 25a: Schematic outline of the construction of pGEX-p47^{phox}S8E. The pGEX-p47^{phox}S5E plasmid is shown in green (a) and pGEX-p47^{phox}S3E plasmid shown in pink (b). Incubation of 'a' and 'b' with the SmaI restriction enzyme (c) gives two products i) the vector backbone plus N-terminal p47^{phox} (base pairs 1-1020) and ii) a smaller fragment containing the C-terminal region of p47^{phox} (base pairs 1021-1170). The vector backbone plus p47^{phox} from 'a', was ligated with the smaller fragment from 'b', to produce a single plasmid containing all eight phosphorylation sites (pGEX-p47^{phox}S8E) (d). Dark circles indicate phosphorylation sites.

restriction enzyme digests were carried out using the *Not*I and *Bam*HI restriction enzymes. If the insert is in the correct way around then a band of 559 b.p. should be excised upon digestion with *Not*I/*Bam*HI, and if it is inserted the wrong way around then a band of 427 b.p. should be observed. The digested samples were separated on a 1 % agarose gel and those samples showing the correct insertion were sent for DNA sequencing (IC Consultants, Imperial College, London).

Unfortunately, the protein produced from this plasmid was a mixture of full-length protein and a C-terminally deleted variant (possibly caused by the presence of *E.coli* proteases in the culture medium (see section 3.1.2.2). Therefore, PCR was used to engineer a hexahistidine tag (His_6) at the C-terminus of the $p47^{phox}$ construct to aid purification of the protein using Ni-NTA chromatography (Table A5) (Figure 25b). The PCR product was digested with *Eco*RI/*Not*I restriction enzymes, ligated into an *Eco*RI/*Not*I cut pGEX-6-P1 vector, and then transformed into NovaBlue competent cells. Plasmids from five colonies were purified using the Qiagen Midi Prep Kit according to the manufacturer's protocol. To test if the colonies contained the insert, restriction digests using *Eco*RI/*Not*I restriction enzymes was performed. The digested DNA was subjected to electrophoresis on a 1% agarose gel and those clones containing the insert were tested for protein expression.

Table 5: **Composition of a typical de-phosphorylation reaction.**

Reagent	**Volume (µl)**
Phosphatase alkaline shrimp enzyme (0.2 units)	0.5
DNA (1.0 pmol)	30
10 X SAP buffer (200 mM Tris-HCl (pH 8.0), 100 mM $MgCl_2$)	5
dH_20	14.5
TOTAL	50

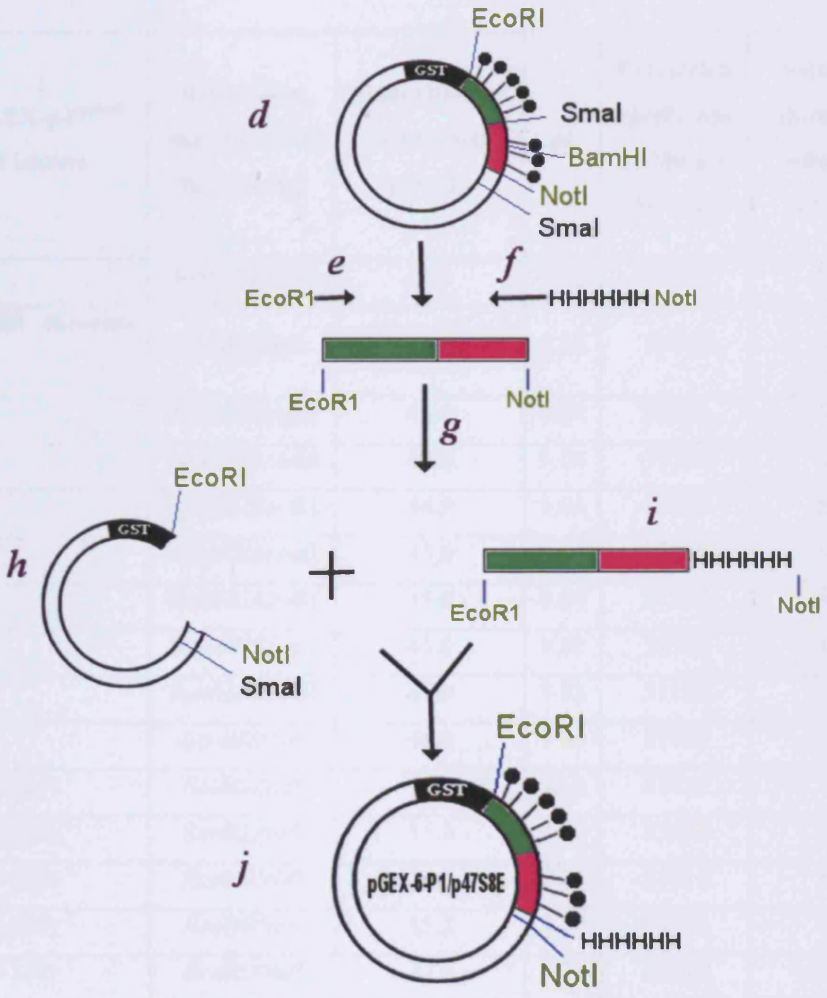

Figure 25b: **Schematic outline of the construction of pGEX-p47^{phox}S8E-His$_6$.** Sense (e) and antisense (f) primers were used to engineer a hexahistidine tag (His$_6$), onto the C-terminus of pGEX-p47^{phox}S8E (g), to generate the His$_6$ fusion construct (i). The pGEX-6-P1 vector (h) as well as the His$_6$ fusion construct were digested with *Eco*RI/*Not*I restriction enzymes, and ligated to produce the pGEX-p47^{phox}S8E-His$_6$ plasmid (j). For purposes of simplicity the pGEX-p47^{phox}S8E-His$_6$ plasmid is hereafter referred to as the pGEX-p47^{phox}S8E plasmid. Dark circles indicate phosphorylation sites.

Table 6: Cloning and protein expression details of $p47^{phox}$ proteins. The molecular weights, isoelectric points (pI), extinction coefficients, protein yields, solubility and restriction enzymes used for the cloning of $p47^{phox}$ proteins. All clones were constructed using the pGEX-6-P1 vector. Indicated values are following 3C precision protease removal of the GST tag. '1' denotes plasmids that were kindly provided by Dr. Karine Lapouge, NIMR, London, and '2' denotes those prepared *de novo*. All proteins are full-length proteins unless an amino acid range is stated in orange.

Cloned pGEX-$p47^{phox}$ plasmid inserts	Restriction enzymes used for cloning	Mass (kDa) of expressed protein	pI	Extinction coefficient at 280 nm ($M^{-1}cm^{-1}$)	Soluble (S)/non-soluble (NS)	Yield per 1 litre culture (mg)
Wild-type [1]	*Bam*HI/*Eco*RI	44.9	9.12	57750	S	8
Tandem SH3 domains (156-285) [1]	*Eco*RI/*Not*I	15.3	4.28	37410	S	5
S359E [1]	*Bam*HI/*Eco*RI	45.0	9.04	57750	S	5
S370E [1]	*Bam*HI/*Eco*RI	45.0	9.04	57750	S	6
S379D [1]	*Bam*HI/*Eco*RI	44.9	9.04	57750	S	5
S359/370E [1]	*Bam*HI/*Eco*RI	45.0	8.93	57750	S	5
S379E [2]	*Bam*HI/*Eco*RI	45.0	9.04	57750	S	5
S3E [1]	*Bam*HI/*Eco*RI	45.0	8.82	57750	S	6
S5E [1]	*Bam*HI/*Eco*RI	45.0	8.82	57750	S	6
S8E [2]	*Eco*RI/*Not*I	46.6	7.01	57750	S	0.8
E218A (156-285) [2]	*Eco*RI/*Not*I	15.3	4.31	37410	S	4
E220A (156-285) [2]	*Eco*RI/*Not*I	15.3	4.31	37410	S	4
D221A (156-285) [2]	*Eco*RI/*Not*I	15.3	4.31	37410	S	4
D/E3A (156-285) [2]	*Eco*RI/*Not*I	15.2	4.40	37410	S	9
D/E3A (156-340) [2]	*Eco*RI/*Not*I	21.6	9.35	38690	NS	0
$W193R_A$ (156-285) [2]	*Eco*RI/*Not*I	15.3	4.35	31720	S	1.2
$W194R_A$ (156-285) [2]	*Eco*RI/*Not*I	15.3	4.35	31720	NS	0
$W194A_A$ (156-285) [2]	*Eco*RI/*Not*I	15.3	4.35	31720	S	0.5
$W263R_B$ (156-285) [2]	*Eco*RI/*Not*I	15.3	4.35	31720	S	3.5
$W264R_B$ (156-285) [2]	*Eco*RI/*Not*I	15.3	4.35	31720	NS	0
$W264A_B$ (156-285) [2]	*Eco*RI/*Not*I	15.3	4.35	31720	S	0.4
$A1^-$ (156-285) [2]	*Eco*RI/*Not*I	15.3	4.28	37410	S	2.3
$A1^+$ (156-285) [2]	*Eco*RI/*Not*I	15.5	4.28	37410	S	1.3
$A2^+$ (156-285) [2]	*Eco*RI/*Not*I	15.5	4.28	37410	S	2.3
3PA (156-285) [2]	*Eco*RI/*Not*I	15.3	4.28	37410	S	2.7
3PA (156-340) [2]	*Eco*RI/*Not*I	21.9	8.0	38690	NS	0

Table 7: Cloning and protein expression details of p67^{phox} proteins. The molecular weights, isoelectric points (pI), extinction coefficients, protein yields, solubility and restriction enzymes used for the cloning of p67^{phox} proteins. All clones were constructed using the pGEX-4-T1 vector Indicated values are following thrombin removal of the GST tag. '1' denotes plasmids that were kindly provided by Dr. Karine Lapouge, NIMR, London. All proteins are full-length proteins unless an amino acid range is stated in orange.

Cloned pGEX-p67^{phox} plasmid inserts	Restriction enzymes used for cloning	Mass (kDa) of expressed protein	pI	Extinction coefficient at 280 nm ($M^{-1}cm^{-1}$)	Soluble (S)/non-soluble (NS)	Yield per 1 litre culture (mg)
Wild-type [1]	*Bam*HI/*Xho*I	59.7	5.88	68560	S	2
$(SH3)_B$ (243-297) [1]	*Bam*HI/*Xho*I	8.8	4.32	6970	S	11

Details about the PH domain:

The plasmid containing the PH domain of TAPP (tandem PH domain containing protein) 1 was provided by Dr. Maria Deak, University of Dundee, Scotland (Thomas et al., 2001). It is cloned into the pGEX-4-T1 vector using the restriction enzymes *Bam*HI/*Bam*HI. The over-expressed protein was purified as a GST-fusion protein without further removal of the GST-tag (section 2.2.3).

2.3 Protein purification

All plasmids were transformed into *E.coli* BL21(DE3) competent cells for recombinant protein expression (see Appendix: A2 for genotype). The proteins were purified by the general methods described below. The composition of the buffers used for purification can be found in Appendix: A4. The characteristics of each protein purified are listed in Tables 6, 7 and 9

2.3.1 Growth and induction of cells

After transformation into *E.coli* BL21(DE3) cells single colonies were picked, streaked onto a fresh LB agar plate and incubated overnight at 37 °C to produce a 'lawn' of cells (1 plate per 750 ml flask of culture). The next morning the cells from each plate were resuspended in 5 ml of terrific broth (TB) and pooled. 5 ml of this starter culture mix was then used to inoculate 750 ml of TB containing 100 μg/ml ampicillin (2 litre flask). The cells were grown to mid log phase (abs at 600 nm = 0.6-0.8) at 37 °C with shaking at 260 rpm. 1 mM IPTG was added to induce recombinant protein expression, and the temperature lowered to 30 °C. After 3 hrs of induction, the cells were harvested by centrifugation at 4000 rpm at 4 °C for 15 min in a Beckman J6 centrifuge. The cell pellets were stored at -20 °C until required. Expression levels were quantified using SDS-PAGE. Typically cells from a 6 litre culture were used per purification preparation, but those proteins to remain as GST-fusions were expressed and purified on a smaller scale (1 litre of cell culture).

2.3.2 Preparation of bacterial lysates

The cell pellet was thawed on ice and re-suspended in approximately 250 ml of buffer A (buffer volume dependent on cell mass, 7 ml/g of cells). The resuspended cells were sonicated on ice using a Branson Sonifier 450 (40 % output, 30 sec pulse plus 1 min rest, x6) with stirring between pulses to ensure complete lysis. The lysate was centrifuged at 18,000 rpm at 4 °C for 45 min using a Beckman J25 centrifuge and the supernatant collected. The first step of protein purifications procedures was an affinity chromatography step using glutathione sepharose 4B resin.

2.3.3 Glutathione sepharose affinity purification and cleavage of fusion proteins

Typically a column was prepared using 10 ml of the glutathione sepharose 4B resin (GE Healthcare) per protein preparation (typically for 4.5 - 6 litres of cell culture). The column was first washed with ten bed volumes of MilliQ water to remove the 20 % ethanol storage solution, and then equilibrated with 10 bed volumes of buffer A. The supernatant collected from the bacterial lysates was applied to the column using a P1 pump (GE Healthcare) at 1 ml/min. The column was then washed at 1 ml/min with 10 bed volumes of buffer B, followed with 10 bed volumes of buffer C.

All $p47^{phox}$ proteins were expressed in pGEX-6-P1 resulting in GST-fusion proteins with a recognition site for 3C PreScission Protease (3C) (GE Healthcare). The GST-tag was removed by incubating the glutathione sepharose 4B resin in 30-50 ml of buffer C containing 1 ml of 3C protease (0.5 mg/ml) at 4 °C overnight. The protease recognises the amino acid sequence **Leu-Glu-Val-Leu-Phe-Gln-Gly-Pro** and cleaves between the Gln and Gly residues (Figure 23). The amount of cleaved protein was determined spectrophotometrically (Table 6). For the purification of $p47^{phox}$S8E, DTT and EDTA in buffer C were substituted with 5 mM β-mercaptoethanol, as it was later to be applied to a Ni-NTA resin for a second step of purification. EDTA would chelate the nickel on the Ni-NTA, whilst DTT can reduce Ni^{2+} ions at high concentrations thus rendering the resin ineffective.

All $p67^{phox}$ proteins were expressed in pGEX-4-T1 resulting in GST-fusion proteins with a recognition site for human α-thrombin (Cambridge Biosciences). The GST-tag was removed by circulating 20 ml of buffer C containing 5 µl (7 mg/ml stock) of α-thrombin at 4 °C overnight. Thrombin recognises the amino acid sequence **Leu-Val-Pro-Arg-Gly-Ser** and cleaves the sequence between the Arg and Gly residues (Figure 23). The amount of cleaved protein was determined spectrophotometrically (Table 7). Depending on the purity of the cleaved proteins, they were further purified by ion-exchange, affinity chromatography or gel filtration (Table 8). Any proteins not mentioned in Table 8 that have been used, were kindly provided by Dr. Karine Lapouge, NIMR, London.

Those proteins required as GST-fusions were purified using 1 ml slurry of glutathione sepharose 4B resin. The resin was washed and equilibrated as described above. Lysates were prepared as described above and the supernatant was incubated

with the resin for 2 hr at 4 °C, washed with 10 ml of buffer B and incubated with 3 ml of buffer C containing 15 mM reduced glutathione, for 2 hrs at 4 °C. The amount of eluted GST-fusion protein was determined spectrophotometrically (Table 9).

Table 8: **Second stage of phox protein purification**. The table shows the different types of chromatography used to purify the proteins at the second stage. The proteins were full-length unless an amino acid range is stated in orange.

Protein	Chromatography column used	pH of Tris/HCl used
$p47^{phox}$ Wild-type	Source S	8.0
$p47^{phox}$ Tandem SH3 domains (156-285)	Gel filtration	7.0
$p47^{phox}$ S359E	Source S	8.0
$p47^{phox}$ S370E	Source S	8.0
$p47^{phox}$ S379E	Source S	8.0
$p47^{phox}$ S3E (S359, 370 and 379E)	Source S	7.5
$p47^{phox}$ S5E (S303, 304, 315, 320 and 328E)	Source S	7.5
$p47^{phox}$ S8E (S303, 304, 315, 320, 328, 359, 370 and 379E)	Ni-NTA	7.7
$p47^{phox}$ E218A (156-285)	Gel filtration	7.5
$p47^{phox}$ E220A (156-285)	Gel filtration	7.5
$p47^{phox}$ D221A (156-285)	Gel filtration	7.5
$p47^{phox}$ D/E3A (E218, E220, D221) (156-285)	Gel filtration	7.5
$p47^{phox}$ $A1^{-}$ (156-285)	Gel filtration	7.5
$p47^{phox}$ $A1^{+}$ (156-285)	Gel filtration	7.5
$p47^{phox}$ $A2^{+}$(156-285)	Gel filtration	7.5
$p47^{phox}$ 3PA (156-285)	Gel filtration	7.5
$p47^{phox}$ $W193R_A$ (156-285)	Gel filtration	7.5
$p47^{phox}$ $W194A_A$ (156-285)	Gel filtration	7.5
$p47^{phox}$ $W263R_B$ (156-285)	Gel filtration	7.5
$p47^{phox}$ $W264A_B$ (156-285)	Gel filtration	7.5
$p67^{phox}$ Wild-type	Source Q	7.5
$p67^{phox}$ $(SH3)_B$ (243-297)	Gel filtration	7.5

Table 9: Protein expression details of GST-fusions. The molecular weights, isoelectric points (pI), extinction coefficients, solubility and protein yields of GST-fusions. Indicated values are following 15 mM reduced glutathione elution. The proteins were full-length unless an amino acid range is stated in orange.

GST-fusion protein	Mass (kDa) of expressed protein	pI	Extinction coefficient at 280 nm ($M^{-1}cm^{-1}$)	Soluble (S)/non-soluble (NS)	Yields per 1 litre culture (mg)
$p47^{phox}$ Wild-type [1]	70.443	8.49	98430	S	23
$p47^{phox}$ S3E [1]	70.569	7.98	98430	S	18
$p47^{phox}$ S5E [1]	70.653	7.22	98430	S	17
$p47^{phox}$ S8E [3]	72.164	6.60	98430	S	11
$p47^{phox}$ PX domain[1] **(4-122)**	41.479	6.84	61310	S	11
TAPP1-PH domain [2] **(7-112)**	46.717	6.55	57180	S	10

2.3.4 Ni-NTA affinity purification

P47^{phox}S8E contains a C-terminal hexahistidine tag (His_6) and was therefore further purified using Ni-chelating chromatography, to capture the full-length protein. His_6-tagged proteins bind with high affinity to Ni^{2+} ions immobilized on the nitrilotriacetic acid (NTA) group of the matrix. P47^{phox}S8E was eluted from the column using imidazole, which competes with the His_6-tag for binding to the matrix (the imidazole ring is part of the histidine structure (Figure 26). In addition, 10-20 mM imidazole was included in the buffers to reduce non-specific low affinity background binding.

The Ni-NTA resin was packed to final bed volume of 10 ml. The resin was washed with 10 bed volumes of sterile water to remove the storage solution and then equilibrated with 10 bed volumes of buffer D. The buffer was applied at a flow rate of 1 ml/min using FPLC (GE Healthcare). The protein eluted from the glutathione sepharose 4B resin was applied at 1 ml/min, and was washed with 10 bed volumes of buffer D until a stable baseline (A_{280}) was obtained. The protein was eluted by running a linear gradient from 20 mM to 1 M imidazole (using buffers D and E). 1 ml fractions were collected and analysed by SDS-PAGE, and those containing pure protein were pooled and dialysed overnight at 4 °C into buffer C to remove the imidazole and β-mercaptoethanol.

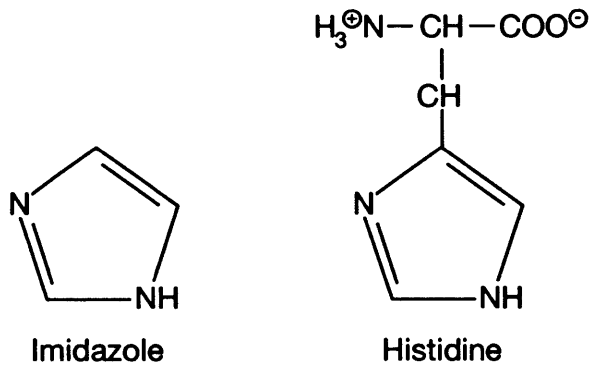

Figure 26: The chemical structures of histidine and imidazole. The imidazole ring is part of the histidine structure. Taken and adapted from the Qiagen handbook for high-level expression and purification of 6XHis-tagged proteins, 2001.

2.3.5 Ion exchange chromatography

For ion exchange chromatography, 50 ml Source S (cation exchanger) and Source Q (anion exchanger) columns were used (GE Healthcare). The columns were equilibrated with buffer F and the protein was applied at a flow rate of 2 ml/min using an FPLC. The column was washed with buffer F until a stable baseline (A_{280}) was observed, and a linear gradient of 50 mM-500 mM NaCl (using buffers F and G) was used to elute the protein. 1 ml fractions were collected and analysed by SDS-PAGE.

2.3.6 Gel filtration chromatography

Gel filtration was carried out on a HiLoad 26/60 Superdex 75 column (GE Healthcare). The column was washed and equilibrated with three column volumes of buffer H using an AKTA prime FPLC system (GE Healthcare). Prior to loading, the protein eluted from the glutathione sepharose 4B resin was concentrated to approximately 4 ml, using a suitable molecular weight cut off (MWCO) Centricon centrifugal concentrator (Millipore). The protein was eluted at 2 ml/min, and the collected 2ml fractions were analysed by SDS-PAGE.

2.3.7 Storage of purified proteins

All the purified proteins were concentrated using a suitable MWCO Centricon centrifugal concentrator (Millipore) to concentrations between 500 μM to 1 mM. Proteins were aliquoted into 100 μl volumes, flash frozen in liquid nitrogen and stored at -80 °C.

2.4 Protein analysis

2.4.1 Determination of protein concentration and sample quality

Protein concentration was determined spectrophotometrically using a Beckman DU640 spectrophotometer at room temperature. The absorbance of the protein solution was scanned from 240-350 nm and the concentration calculated using the extinction coefficients at 280 nm. The extinction coefficients are calculated based on the aromatic residue content of each protein (1280 M -1cm -1 (Tyr), and 5690 M -1cm -1 (Trp)) (see Tables 6, 7 and 9). All purified proteins were verified by electrospray mass spectrometry (Steve Howell, NIMR, London).

2.4.2 SDS-PAGE

All proteins with molecular weights of 15 kDa or less were analysed using NuPAGE Bis-Tris pre-cast gels (gradient 4 – 12 %) (Novex). All other proteins were analysed using 12 % SDS gels (see Appendix: A3). The samples were incubated at 100 °C for 5 min with 4 X sample buffer (see Appendix: A3), and subjected to electrophoresis alongside suitable size standards at 35 mA constant current for 40 min (for 12 % SDS gels), or 200 V constant current for 1 hr (for NuPAGE pre-cast gels). Gels were stained using SimplyBlue SafeStain according to the manufacturer's protocol.

2.4.3 Circular dichroism

Circular dichroism (CD) spectroscopy is a technique which measures the differences in the absorption of left and right handed circularly polarised light ΔA (= $A_{Left} - A_{Right}$), which arises because of structural asymmetry of the chromophores (either peptide bonds or the aromatic amino acids). In a well defined ordered structure the spectrum produces positive and negative peaks, while in the absence of an ordered structure the CD signal is zero. Although the technique only gives low-resolution structural information, it has the following advantages: CD spectra are very sensitive to changes in molecular conformation, only small amounts of material are required, and a wide range of solvent conditions can easily be examined. CD spectroscopy can be used

to investigate the secondary structure of proteins or to detect secondary and tertiary structural changes caused by variations in e.g. pH. It can also be used to monitor protein denaturation bought about by changes in temperature or addition of chemical denaturants such as urea. To determine the secondary structure content of proteins, CD is measured in the far-UV spectral region (190-250 nm) where the peptide bond is the major chromophore. The usefulness of CD derives from the fact that the intense CD bands of peptide bonds are very different in both shape and intensity for different secondary structural elements (Johnson, 1990; Rodger and Ismail, 2000; Sreerama and Woody, 2000).

The Beer-Lambert law for absorbance is:

$$A = \varepsilon_m * C * l \qquad [4]$$

where A is the absorbance, ε_m is the molar extinction coefficient (M^{-1} cm^{-1}), C is the protein concentration (M) and l is the path length (cm).

The CD equivalent of this equation is:

$$\Delta\varepsilon_m = \frac{\Delta A}{C * l} \qquad [5]$$

where $\Delta\varepsilon_m = (\varepsilon_{Left} - \varepsilon_{Right})$ is the molar CD extinction coefficient.

CD intensities in the far-UV region are usually presented on a mean residue basis as $\Delta\varepsilon_{MRW}$, where $\Delta\varepsilon_{MRW}$ is equal to $\Delta\varepsilon_m$ divided by the number of residues. Different secondary structures (α-helix, β-sheet and random coil) have different CD spectra. The α-helix has a positive peak at 197 nm and negative ones at 207 nm and 222 nm. The β-sheet generally has a positive peak at 196 nm and a negative one at 210-218 nm. The random coil has a weak positive peak at around 212 nm and a strong negative one at 195 nm. From the CD spectra, the fraction of each of the secondary structure elements present in a protein can be determined. However, although CD spectroscopy can determine the percentage of the different secondary structures, it cannot determine which residues are involved in which specific secondary structure. The secondary structure content is estimated using a database of CD spectra of known proteins (Yang

et al., 1986), and secondary structure contents that were derived from their X-ray structures. The secondary structure content of a protein is determined by fitting to the appropriate combination of spectra of proteins with known structure.

In order to determine the thermal stability of a protein, changes in the CD spectra with increasing temperature can be measured. Although measurements are generally performed by monitoring at a single wavelength, it can be useful to record spectra at higher temperatures to examine how much residual structure remains following unfolding.

For all measurements the protein samples were extensively dialysed overnight at 4 °C in buffer H, and the protein concentration used per experiment was 0.15 mg/ml. In collaboration with Dr. Stephen. Martin, NIMR, London, CD spectra were measured between 190 nm – 260 nm on a Jasco J-715 spectropolarimeter using 1 mm fused silica cuvettes at 25 °C. Multiple scans were averaged and the appropriate buffer blanks were subtracted. The secondary structure contents were determined using the fitting programs CONTIN, SELCON, CDSSTR (Sreerama and Woody, 2000). Thermal denaturation curves were recorded by measuring the CD signal continuously at 224 nm over the ranges of 20 °C - 80 °C in sealed 1 mm cuvettes. The temperature was increased at 1 degree/minute using the manufacturer's Peltier thermal controller. The curve was smoothed using a moving polynomial (Savitzky and Golay, 1964), and the T_m values were determined from the first derivative of the smoothed unfolding curve.

2.5 Western blotting

Proteins for western blotting were separated using SDS-PAGE and then transferred onto a suitable dimension polyvinyidene difluoride membrane (pore size 0.45 μM) (Millipore) by electroblotting in a tank (GE Healthcare) at 50 V for 1 hr in buffer 1. Once the transfer was complete, the membrane was blocked overnight in 20 ml of buffer 3 at RT, washed twice for 5 mins in 20 ml of buffer 2 at RT and then twice for 5 mins in 20 ml of buffer 4 at RT. The membrane was incubated in 20 ml of buffer 2 containing 1:20,000 dilution of the anti-GST HRP (horseradish peroxidase) conjugated antibody (Sigma) and then washed 5 times for 5 mins each in 20 ml of buffer 2 at RT. The membrane was incubated for 5 mins in 5 ml of a 1:1 ratio of the two solutions (enhancer solution and peroxide solution) provided in the West Pico Chemiluminescent Substrate Kit (Pierce) and then developed using an X-ray film (Kodak).

Buffer 1

10 mM CAPS (pH 11.0)

10 % methanol

Buffer 2

50 mM NaCl

20 mM Tris (pH 7.5)

0.05 % Tween-20

0.2 % Triton X 100

Buffer 3

Buffer 2 plus 3 % BSA

Buffer 4

100 mM NaCl

10 mM Tris (pH 7.5)

2.6 Lipid sedimentation assays

2.6.1 Liposome production

All lipids used were bought as solids and solubilised in chloroform to a final concentration of 10 mg/ml, apart from PtdIns(3,4)P_2 which was made to a final concentration of 1 mg/ml stock (due to the limited quantity provided by the manufacturer). All stocks were stored at -20 °C in glass vials (1.8 ml Wheaton glass vial) which had been pre-rinsed with chloroform. Liposomes were prepared on ice by mixing lipids at the following concentrations: 50 % phosphatidylcholine (PC), 40 % phosphatidylethanolamine (PE), 5 % phosphatidylserine (PS) and 5 % PtdIns(3,4)P_2 in a total volume of 200 µl. 200 µl of methanol was added to give a final reaction volume of 400 µl. Parallel to this, a control was prepared by omitting PtdIns(3,4)P_2 and substituting the volume with chloroform. The lipid mixture was protonated prior to use by adding 1 M HCl to a final concentration of 0.1 % i.e. 400 µl chloroform, 400 µl methanol and 4.6 µl of 1 M HCl. The samples were sonicated briefly for 5-10 seconds in a bath sonicator and allowed to stand for 15 mins at RT. The mixtures were dried under nitrogen to form a thin lipid film in the glass vial. The dried pellets were resuspended to a final concentration of 1 mg/ml in filtered sample buffer composed of 20 mM Hepes (pH 7.5), 100 mM NaCl, 1 mM DTT and 1 mM EDTA. The resuspended lipids were left to hydrate for 1 hr at RT, gently agitating by bath sonication every 10 mins for 5-10 sec. The lipid mixes were further mixed in the bath sonicator until a homogenous suspension was formed (approximately 2-4 mins). To fully form the vesicles 4-6 brief pulses using a small 3.2 mm sonicator probe were applied (2 sec sonication and 2 sec rest).

2.6.2 Liposome binding assay

Reaction mixtures were prepared on ice in polycarbonate centrifuge tubes (Beckman). 50 µl of the 1 mg/ml stock liposomes were mixed with 40 µl of the liposome buffer (sample buffer plus 1 mM $MgCl_2$) and 5-10 µl of the purified protein (15 µM final protein concentration). The samples were mixed repeatedly with a pipette and incubated on ice for 15 mins. The liposomes were sedimented by centrifugation at 140,000 g (Beckman TLA100 ultracentrifuge) at 4 °C for 15 mins. The supernatant was

carefully removed and transferred to a separate vial, and the liposome pellets were resuspended in 100 µl of liposome buffer (it is important to solubilise the pellet in an equal volume as the supernatant). 10 µl of sample were incubated with 5 µl of 2 X SDS loading buffer and the samples were heated at 100 °C for 2 mins. Equal volumes of pellet and supernatant (15 µl) were loaded onto a NOVEX 4-12 % Bis-Tris SDS-PAGE gel and separated at 200 V constant current for 1 hr, then visualised with SimplyBlue SafeStain.

2.6.3 Adjustments to improve the lipid sedimentation assay

Due to problems with the experimental protocol various adjustments were made to maximise binding.

Adjustment 1:
-Include 10 % cholesterol in liposome mix
-Use speedvac for further evaporation

Adjustment 2:
-Use 5 % PA instead of 5 % PS
-Use 2 ml glass vials for liposome production (Chromacol)
-Produce multilameller vesicles (MLV's) by vortexing instead of sonication

Adjustment 3:
-Increase PA and PtdIns(3,4)P_2 concentration to 10 %
-Use 2 ml glass vials for liposome production (Chromacol)
-Use a freeze drier from E-C Modulyo for solvent evaporation

2.7 PIP (PtdIns(3,4)P_2) bead binding assay

PIP beads are agarose beads that have PtdIns(3,4)P_2 covalently attached. 50 µl slurry of beads was pelleted at 1000 rpm for 1 min at 4 °C and the storage solution was discarded. The beads were washed in 50 µl of binding buffer containing 10 mM Hepes (pH 7.4), 150 mM NaCl and 0.25 % NONIDET P-40 (NP-40). The supernatant was discarded and the beads were resuspended in 50 µl of the binding buffer. 5 µg of protein was added and incubated at 4 °C for 3 hrs on a rocking device. The beads were washed five times with ten bed volumes of binding buffer by centrifugation at 1000 rpm for 1

min at 4 °C. The beads were pelleted by centrifugation, the supernatant was discarded and an equal volume (50 µl) of 2 X SDS loading buffer was added. The samples were mixed and incubated at 100 °C for 2 mins. 20 µl of the samples were separated on a NOVEX 4-12 % Bis-Tris SDS-PAGE gel, at 200 V constant current for 1 hr. They were visualised with either SimplyBlue SafeStain or electroblotted for western blot analysis. Control PIP beads were also provided by the manufacturer without PtdIns(3,4)P_2 coupled and were run parallel to the assay to ensure that any binding observed was not due to non-specific binding to the agarose beads.

2.8 Fluorescence spectroscopy

Fluorescence spectroscopy experiments were carried out to determine binding affinities for complexes between a fluoresceine labelled $p22^{phox}$ derived peptide (peptide 3, Appendix: A4) and $p47^{phox}$ proteins. Changes in peptide fluorescence were monitored at 525 nm upon excitation at 429 nm. In addition, binding affinities for complex formation between a 35-mer peptide derived from the polybasic region of $p47^{phox}$ (peptide 1, Appendix: A4) and $p47^{phox}$ tandem SH3 domain proteins was measured by following changes in tryptophan fluorescence at 320 nm upon excitation at 295 nm.

Stocks of the fluorescein labelled $p22^{phox}$ peptide and the $p47^{phox}$ 35-mer polybasic peptide were made in 20 mM Hepes (pH 7.5). The protein samples and working solutions of peptides were made in buffer H. The pH of the buffers was adjusted depending on the pI of the individual proteins to one unit above or below the pI. All experiments were carried out at 20 °C. For each experiment the peptide or protein to be placed into the cuvette was diluted to a final concentration of 1.0 µM. An amount of protein or peptide was also added to the component that was to be titrated to maintain a 1.0 µM concentration of fluorescent material (to account for dilution effects). The sample was titrated into the cuvette and allowed to equilibrate for 3 min after each addition before the reading was taken. All experiments were repeated at least 3 times and the data were fitted to a quadratic equation (equation 12) using the program GraFit (version 5). Control experiments were performed where buffer H was titrated into component A, to ensure that the fluorescence observed in experimental assays was not due to artifactual background signal.

2.9 Isothermal titration calorimetry

Isothermal titration calorimetry (ITC) experiments were carried out to determine binding affinities for complexes between $p47^{phox}$ proteins and $p67^{phox}(SH3)_B$. Heat changes were monitored at 15 °C. In addition, complex formation for $p22^{phox}$ derived peptide (peptide 2, Appendix: A4) or the $p47^{phox}$ 35-mer polybasic region peptide (peptide 1, Appendix: A4) with $p47^{phox}$ tandem SH3 domain proteins were determined. Heat changes were monitored at 18 °C. Protein samples were dialysed overnight at 4 °C in buffer H using a dialysis membrane with an appropriate MWCO (Slide-a-Lyzer, Pierce). Due to the small molecular weights of the peptides used, dialysis was not feasible. In this case the peptides were diluted with the experimental buffer. The pH of the buffers were adjusted depending on the pI of the individual proteins and to one unit above or below the pI. The protein samples were centrifuged for 10 min at 4 °C to pellet any aggregated protein. The volumes of proteins required to load the instruments were 2.2 ml for the cell, and 600 µl for the syringe, which were degassed under vacuum for 10 min. The cell and syringe were washed thoroughly with filtered dH_20 and then with buffer H. The cell was filled using a 2.5 ml syringe by carefully introducing the sample gradually from bottom to top, avoiding the introduction of air bubbles. Typically 250 – 400 µM of ligand was titrated into 25 – 40 µM protein in the cell (varied depending on the affinity of the interaction). Heats of dilution in control experiments were determined by titration of the syringe component into buffer H. The heats of dilution were subtracted from the raw data before fitting to the quadratic equation shown in equation 19, using the evaluation software supplied by the manufacturer (Microcal Origin version 5.0).

The parameters shown in Table 10 were employed for all ITC experiments undertaken. To compensate for losses/dilutions from the tip of the syringe during the experimental set-up, the first injection of all ITC experiments was of a smaller volume (2 µl). Data from this first injection were removed from the final curve fitting analysis and all experiments were repeated at least three times.

Table 10: **ITC experimental parameters.**

Parameter	Value
Number of injections	30
Cell temperature (°C)	X
Reference power (μCal/sec)	15
Initial delay (sec)	300
Syringe concentration (mM)	Y
Cell concentration (mM)	Z
Stirring speed (rpm)	310
Injection volume (μl)	1 • 2 μl 29 • 10μl
Injection spacing (sec)	300
Feedback mode	High

The reference power is a small amount of power that is continuously supplied to the reference cell heater. The cell temperature is the temperature of the experiment. The initial delay is the time from the start of the experimental data collection time until the 1st injection. The injection spacing is the time between each injection and should be chosen such that the signal has returned to baseline before the next injection. A high feedback mode gives the fastest response time (VP-ITC user manual, 2004).

2.10 Quantitative analysis of protein-ligand interactions

In principle there are two different approaches in which protein-ligand interactions can be quantified. The first approach measures the concentration of bound and free ligand directly. Examples of such techniques include ultrafiltration, gel filtration, ultracentrifugation, flow and equilibrium dialysis. The second approach is based on inferring concentration changes in free or bound ligand from the variation in some physical property of the system. Examples of such techniques include optical spectroscopy (fluorescence, circular dichroism, and absorbance), NMR, and isothermal titration calorimetry. In these methods the measured signal is related to changes in concentration. The interaction of a protein with a ligand is represented as:

$$P + L \Leftrightarrow PL \quad \text{with} \quad K_d = \frac{[P][L]}{[PL]} \qquad \textbf{[6]}$$

Substituting the mass balance relationship, $P_T = [PL] + [P]$ and $L_T = [PL] + [L]$ gives equations 7 and 8:

where P_T is the total protein concentration (free and bound), and L_T is the total ligand concentration (free and bound)

Substitution of the expressions for P and L into equation 6 gives:

$$K_d = \frac{([P_T] - [PL])([L_T] - [PL])}{[PL]} \qquad \textbf{[7]}$$

$$K_d[PL] = P_T L_T - [PL]([P_T] + [L_T]) + [PL]^2 \qquad \textbf{[8]}$$

thus,

$$[PL]^2 - [PL](P_T + L_T + K_d) + P_T L_P = 0 \qquad \textbf{[9]}$$

[PL] is given by the solution of the quadratic equation, where:

$$[PL] = \frac{(P_T + L_T + K_d) - \sqrt{(P_T + L_T + K_d)^2 - 4P_T L_T}}{2} \qquad \textbf{[10]}$$

2.11 Quantitative techniques used in this study

In this study ITC was chosen as the principle method for characterising protein-protein and protein-peptide interactions. A single ITC experiment simultaneously determines a range of parameters (binding affinity, stoichiometry and thermodynamic parameters), without having to modifying the proteins under investigation. However, the method requires large amounts of proteins and in some instances using ITC was not a feasible option due to poor protein yield and stability. In this case fluorescence spectroscopy was used as an alternative technique.

2.11.1 Fluorescence spectroscopy

Fluorescence spectroscopy is a highly sensitive technique that only requires small amounts of protein and therefore is often used to quantitate protein-ligand interactions. The fluorescence can arise from intrinsic natural fluorophores or extrinsic fluorescent probes. The fluorescence of proteins can be characterised by their excitation and emission spectra, the quantum yield (ratio of photons emitted to those absorbed) and anisotropy or polarisation values. The spectral properties depend on the atomic environment of the fluorophore and its accessibility to the solvent, which can change upon interaction with ligands. The changes measured can be used to quantify the interactions and determine binding affinities, as was done in this study. Thus, fluorescence spectroscopy provides a sensitive means to characterise proteins and their interactions (Lakowicz, 1999; Ninfa and Ballou, 1998; Szabo, 2000).

Substances which display fluorescence can be divided into naturally occurring intrinsic fluorophores and into extrinsic fluorophores that are added to otherwise non-fluorescent samples. Intrinsic fluorophores include cofactors such as NADH or FAD and proteins. Fluorescence observed in proteins derives from the aromatic side chains of the amino acids: tryptophan, tyrosine and phenylalanine. The emission maximum of free tyrosine is ~ 303 nm and this is generally the same for tyrosine in a protein. In contrast, whilst the emission maximum of free tryptophan is ~ 355 nm, a tryptophan in a protein can emit anywhere from 313-355 nm, depending on the polarity of the environment. In proteins containing all three amino acids, fluorescence is almost always dominated by tryptophan because its extinction coefficient is significantly higher than that of tyrosine and phenylalanine. In addition, the fluorescence of phenylalanine and tyrosine can be quenched via energy transfer to tryptophan.

The use of intrinsic fluorescence for quantifying protein/protein or protein/peptide interaction is only feasible if one of the binding partners does not contain any tryptophan residues. If they are present in both, then titration of the second component may lead to severe background fluorescence, which can be difficult to subtract. If this is the case then the use of extrinsic fluorescent probes for monitoring complex formation may be a better alternative. Frequently used extrinsic fluorescent probes include fluorescein and rhodamine. These extrinsic labels are most often covalently attached to either cysteine residues, to the amino groups of lysine residues or to the N-terminus of peptides. However, introducing these probes at a specific site in larger proteins can be difficult, as proteins often contain more than one cysteine or lysine residue. Although these excess residues can be removed by mutagenesis, the effect on stability and activity of the protein must be examined. Furthermore, if extrinsic labels are introduced it has to be ensured that the label does not interfere with the interaction under investigation.

2.11.1.1 Physical principles

The production of fluorescence is generally a three step process i) absorption, ii) vibrational relaxation back down to ground vibrational levels and iii) emission. This phenomenon is schematically described by the Jablonski diagram (Figure 27). Absorption of energy takes the molecule from a low vibrational level of the ground electronic state (S_o) to a higher vibrational level of the first excited state (S_1) or a second excited state (S_2). After reaching one of the higher vibrational energy levels of the excited state, the molecule loses excess vibrational energy by collision and falls to the lowest vibrational level of that state (internal conversion). This loss of energy through collision gives rise to the 'Stokes shift'. From here the molecules eventually revert back to any of the vibrational levels of S_o, emitting energy in the form of fluorescence. In addition to fluorescence, phosphorescence can take place where the molecules enter a triplet state (T_1) (Figure 27). The energy emitted from T_1 to S_o as phosphorescence results in longer wavelengths relative to fluorescence. Fluorescence emission can take place within 10^{-9}-10^{-6} seconds, whereas phosphorescence emission takes place within 10^{-4}-10^{2} seconds.

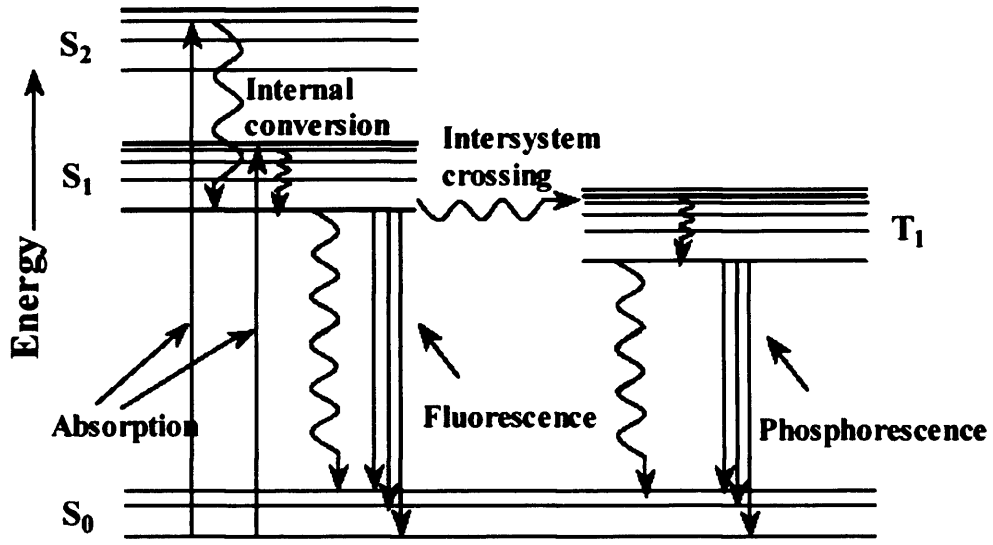

Figure 27: **Jablonski diagram**. This diagram shows the different energy levels and processes in an electronically excited molecule. Indicated are the ground state (S_o), first excited state (S_1), second excited state (S_2) and triplet state (T_1) (taken and adapted from Szabo, 2000).

2.11.1.2 Instrumentation

All experiments undertaken in this study were carried out using a PC1 photon counting spectroflurometer (ISS, USA). Figure 28 shows a schematic diagram of a typical fluorescence spectrophotometer. The instrument contains a xenon lamp, which provides a high intensity light at wavelengths ranging from 200 nm-1000 nm. The beam splitter splits the light into two, where one beam passes through the sample and the other through a reference cell. The instrument also contains two monochromators, one of which selects the appropriate excitation wavelength (λ_{EX}) from the light source and the other the appropriate emission (λ_{EM}) wavelength. The photon intensity is detected by a photomultiplier and converted into an electrical signal (Lakowicz, 1999).

2.11.1.3 Determining the spectral parameters for the binding experiment

In order to obtain data of sufficient quality to quantitate a protein-ligand interaction, a significant change in the fluorescence signal is required upon complex formation. The largest change in signal may not necessarily occur at the emission maximum (E_{max}) of the isolated protein or ligand, as this may shift upon complex formation. Therefore, correctly selecting the appropriate wavelength at which complex formation is followed is crucial. This selection can easily be made by recording spectra of the protein or ligand on its own, and of the protein/ligand complex. The emission wavelength should then be chosen such that the differences in signal between the free and bound state are maximal. A typical protein emission spectrum is shown in Figure 29. The $p47^{phox}$ tandem SH3 domain protein (which contains five tryptophan residues) is present in the cuvette at a concentration of 1 μM. Upon addition of a 20-fold excess of the $p47^{phox}$ 35-mer polybasic peptide (which contains no tryptophan residues), the fluorescence signal increases and the emission maximum shifts from 340 nm to 320 nm. The biggest increase is observed at 320 nm and therefore all titrations were carried out at this emission wavelength.

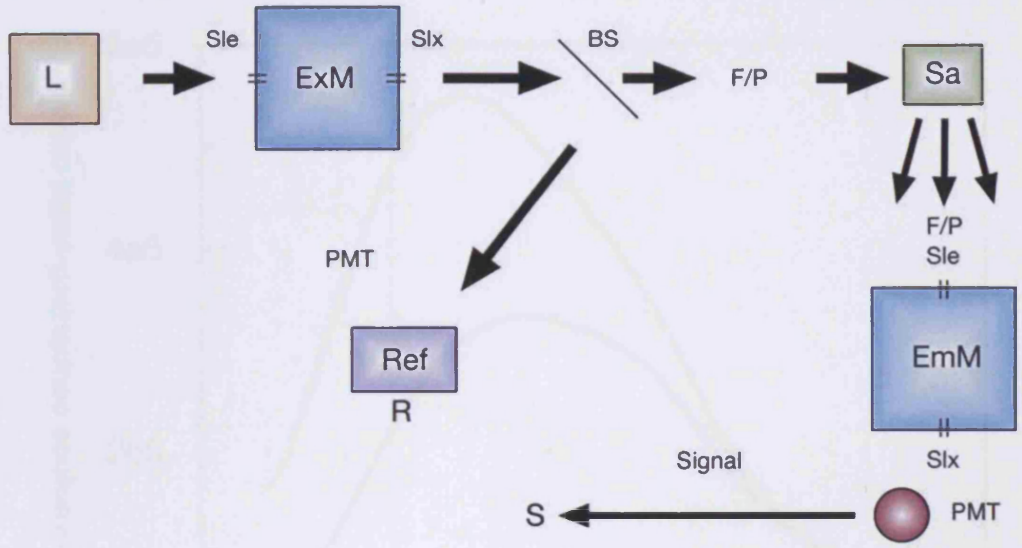

Figure 28: **A schematic diagram of a typical fluorescence spectrophotometer**. L represents the light source, ExM is the excitation monochromator, which selects the appropriate excitation wavelength. BS is the beam splitter which splits the light into two, where one beam passes through the sample and the other through the reference. F/P is the filter or polarizer (polarizers are used to measure the fluorescence anisotropy). Sa is the sample holder, EmM is the excitation monochromator which selects the appropriate emission wavelength. PMT are the photomultiplier tubes which detect photons and convert them to an electrical signal. SLe and SLx are the entrance end exit slits of the monochromators; respectively. S and R are the sample and reference fluorescence signals; respectively (taken and adapted from Szabo, 2000).

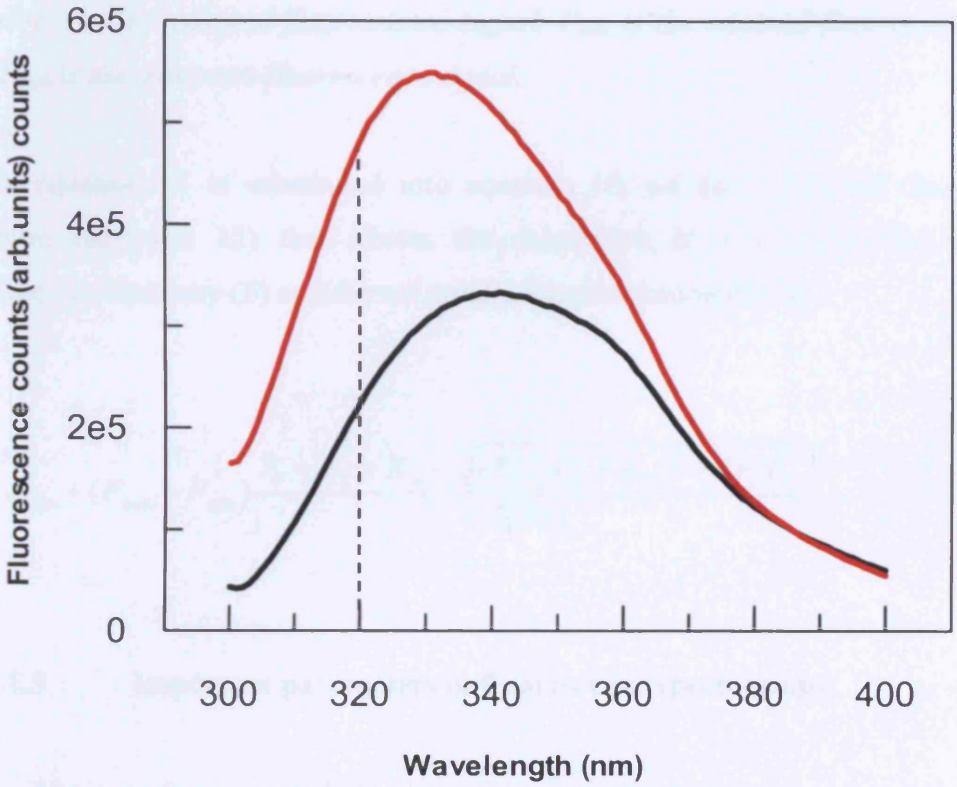

Figure 29: Change in fluorescence intensity and emission maximum upon complex formation (intrinsic tryptophan fluorescence). $P47^{phox}$Wild-$type_{tandem}$ (aa 156-285) (black line) contains five tryptophan residues. Addition of excess peptide ($p47^{phox}$ 35-mer polybasic region peptide) leads to an increase in fluorescence intensity by approximately 2-fold (red line) and the fluorescence maximum shifts from 340 nm to 320 nm upon complex formation (broken black line).

2.11.1.4 Curve fitting

The concentration of complex formed is given by the ratio of the measured change in fluorescence to the amplitude:

$$[PL] = \frac{(F - F_{min})[P_T]}{(F_{min} - F_{max})} \quad \textbf{[11]}$$

where F is the measured fluorescence signal, F_{min} is the minimal fluorescence signal and F_{max} is the maximum fluorescence signal.

When equation 11 is substituted into equation 10, we get a form of the quadratic equation (equation 12) that allows the calculation of a K_d from the measured fluorescence intensity (F) at different protein/ligand concentrations:

$$F = F_{min} + (F_{max} - F_{min}) \frac{P_T + L_T + K_d - \sqrt{(P_T + L_T + K_d)^2 - 4P_T L_T}}{2[PL]} \quad \textbf{[12]}$$

2.11.1.5 Important parameters in fluorescence spectroscopy

Various factors need to be taken into consideration when planning a fluorescence spectroscopy experiment (reviewed by Lakowicz, 1999 and Szabo, 2000). For example changes in temperature affect the viscosity of the medium and hence collision of fluorophore and solvent molecules. Therefore, fluorescence is temperature dependent and it is essential that the reactant solutions used have reached their final temperature prior to the start of measurements, especially those on ice. Thermostatted cell holders are recommended. As fluorescence titrations are an equilibrium assay one needs to ensure that the samples are at equilibrium i.e. the fluorescence signal remains constant during recording. It may be necessary to wait for a few minutes prior to recording the data. Furthermore, it is essential to determine the concentrations of both reactants precisely. The concentration of the cuvette reactant should be the lowest concentration possible, which reduces not only the material used, but also possible

inner-filter effects. However, the concentration must not be too low as loss of material through binding to the walls of the cuvette can occur.

Proteins should be a pure as possible to prevent non-specific interactions and samples should be free of impurities such as dust (samples should be filtered or centrifuged). In addition, buffers of the highest quality should be used, which do not absorb light in the wavelength range of the experiment.

If an unexpected decrease in fluorescence signal is observed, then it is important to check that long exposure to light (photobleaching) or mechanical stress due to stirring (stability) is not the cause. To check for photobleaching one can measure the signal first continuously without stirring and then mix the sample. This will lead to an increase in signal as new molecules will get into the light path, if the fluorescence decrease is due to photobleaching. If photobleaching is a problem this can be reduced by lowering the light intensity or by closing the shutter during measurements. If photobleaching is ruled out then the decrease in signal could be due to mechanical stress, in which case the speed of the stirrer should be lowered. Another possible reason could be loss of protein due to adherence to the cuvette walls, in which case changing buffer conditions would be suitable or perhaps coating the cuvette with a detergent such as Tween 20 to minimise protein sticking.

2.11.2 Isothermal titration calorimetry

Isothermal titration calorimetry (ITC) is a powerful technique used for the study of protein-ligand interactions and can be applied to interactions involving proteins, lipids, carbohydrates, nucleic acids, metal ions and others (reviewed in the VP-ITC user manual; (Ladbury, 2004; Leavitt and Freire, 2001; Perozzo et al., 2004; Pierce et al., 1999). It is a thermodynamic technique that monitors the heat that accompanies a binding reaction. Upon complex formation heat can either be released (exothermic reaction) or absorbed (endothermic reaction) and the amount of heat released or absorbed is directly proportional to the amount of bound ligand. A single binding experiment simultaneously determines the thermodynamic properties including the binding constant (K_a), enthalpy change ($\Delta H°$), and stoichiometry (n) (Wiseman et al., 1989). Using the determined values of ΔH and K_a, a full thermodynamic profile can be elucidated, where the Gibbs free energy of the reaction ($\Delta G°$) and the entropy change ($\Delta S°$) can be derived. The association constant K_a is related to the Gibbs free energy by the following relationship:

$$\Delta G° = -RT \ln K_a \qquad \textbf{[13]}$$

where R is the universal gas constant (1.987 cal K^{-1} mol^{-1}), and T is the absolute temperature in Kelvin (0 °C = 273.15 K).

$\Delta G°$ can also be expressed in terms of $\Delta H°$ and $\Delta S°$ by the relationship:

$$\Delta G° = \Delta H° - T\Delta S° \qquad \textbf{[14]}$$

If the experiments are repeated over a range of different temperatures, the heat capacity associated ($Cp°$) with the reaction can also be determined since,

$$\Delta Cp° = \frac{\partial \Delta H°}{\partial T} \qquad \textbf{[15]}$$

The Gibbs free energy change ($\Delta G°$) is a measure of the chemical potential of a reaction and is a combination of changes in the enthalpy ($\Delta H°$) and entropy ($\Delta S°$) during a reaction. $\Delta H°$ reflects the formation/breaking of hydrogen bonds, van der

Waals interactions and salt bridges. These components produce either favourable or unfavourable contributions to the free energy. Generally, ΔS^{o} represents all the other positive and negative forces which contribute to the free energy. The total entropy change is expressed by several contributing effects, but mainly solvation entropy (complex formation may be accompanied by desolvation, whereby water is released, resulting in favourable gains in ΔS). Conformational entropy also contributes to the total entropy change, but usually contributes unfavourably (complex formation may reduce the rotational degrees of freedom) (Perozzo et al., 2004). The thermodynamic profile derived from ITC experiments can be used to complement a crystal or NMR structure to characterise the activity and function of proteins and their ligands.

2.11.2.1 Instrumentation

All calorimetric experiments in this study were carried out using a Microcal VP-ITC instrument (Microcal Inc, Northamton USA). Figure 30 shows a schematic diagram of the VP-ITC unit. The instrument consists of two cells, the sample and reference cells. The sample cell holds the protein of interest and the reference cell holds either buffer solution or water. Both cells are kept at thermal equilibrium throughout the experiment and are enclosed in an adiabatic outer shield (jacket). The spinning syringe contains the second component (ligand), which is injected serially into the sample cell to give a thermal titration curve. Figure 31 shows a typical output obtained for the titration of a peptide into protein. Enthalpic changes are measured as heat change per unit time (μcal/s) that must be added to maintain zero temperature difference between the two cells, at the designated temperature of the experiment. Reactions resulting in the evolution of heat (exothermic) cause a negative change in DP power (differential power between the reference and sample cell), as less DP feedback is required to keep the cells at thermal equilibrium. The opposite is observed for endothermic reactions, where additional energy to the sample cell is required to maintain equal temperatures in both cells. Each peak corresponds to the amount of heating/cooling required to compensate for the heat generated/absorbed upon each addition of the ligand. The heat absorbed/released upon each injection (Q_i) is proportional to i) the amount of ligand that binds in that particular injection ($v \times \Delta L_i$) and ii) the binding enthalpy for that reaction:

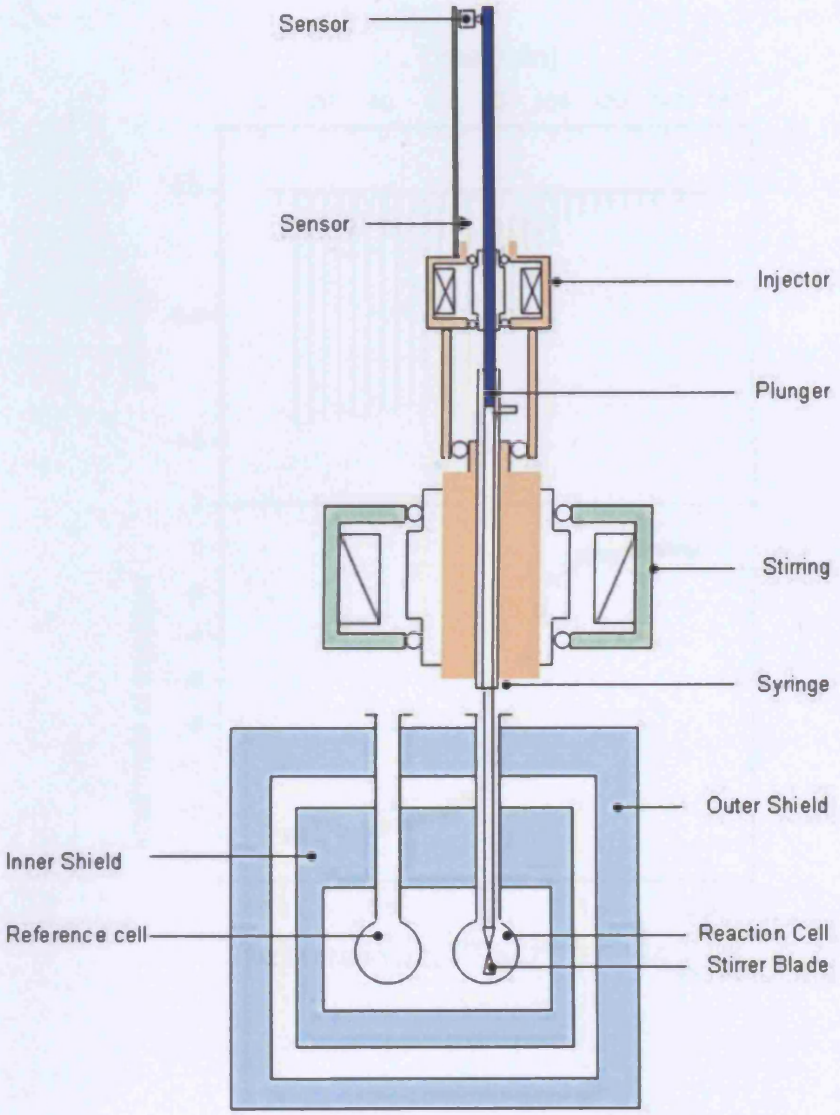

Figure 30: **Schematic diagram of the VP-ITC Unit (Microcal).** Taken and adapted from the Microcal VP-ITC user manual, 2004.

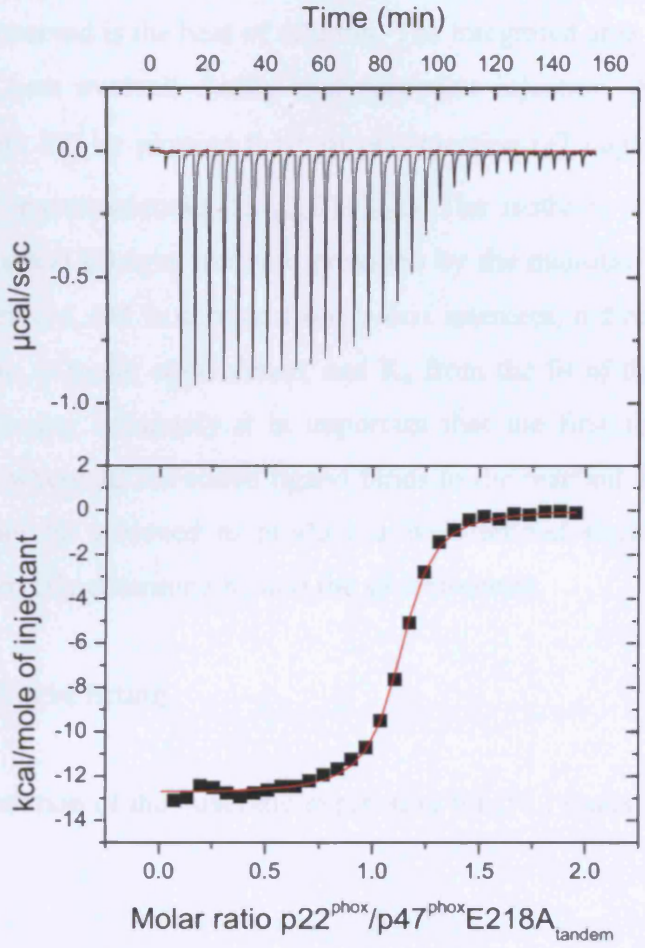

Figure 31: Example ITC data for the titration of 29 µM $p47^{phox}E218E_{tandem}$ with 250 µM $p22^{phox}$ peptide. The upper figure shows the power (µcal/sec) versus time. At each injection an exothermic spike is observed. The area under the spike is proportional to the heat of binding. The lower figure shows the amount of heat measured, normalized to the number of moles of injected $p22^{phox}$ peptide (kcal/mol) (peptide 2) versus the molar ratio of cumulative $p22^{phox}$ peptide added to $p47^{phox}E218E_{tandem}$.

$$Qi = v \times \Delta H \times \Delta Li \qquad [16]$$

where v is the reaction volume of the experimental cell.

The size of the peaks decrease as the binding sites on the macromolecule in the cell become saturated, and once the sample cell reactant is fully saturated by the ligand, then any heat observed is the heat of dilution. The integrated area under each peak gives the amount of heat evolved during that particular injection. A binding isotherm is generated (Figure 31) by plotting the heat per injection (Q_i) against the molar ratio of the ligand and macromolecule ($[L]_{total}/[M]_{total}$). The isotherm is fitted using a linear least-squares method (Origin software provided by the manufacturer) from which ΔH, K_a and n are derived. ΔH is derived from y-axis intercept, n from the inflection of the binding isotherm at molar equivalence, and K_a from the fit of the curve. To determine the binding enthalpy accurately it is important that the first few injections define a baseline region where all the added ligand binds to the reactant. Furthermore, complete saturation should be achieved to produce a well-defined sigmoidal curve, which is important to correctly determine K_a and the stoichiometry.

2.11.2.2 Curve fitting

Differentiation of the quadratic expression for [PL] (equation 10) with respect to L_{tot} gives:

$$\frac{d[PL]}{d[L_{tot}]} = \frac{1}{2} + \frac{1-(1-r)/2-L_r/2}{\sqrt{L_r^2 - 2L_r(1-r)+(1-r)^2}} \qquad [17]$$

where r is equal to K_d/PT and L_r is equal to L_{tot}/P_{tot}

The change in the concentration of PL can be related to the heat by:

$$dQ = d[PL] \times \Delta H \times v \qquad [18]$$

where ΔH is the enthalpy of binding, v is the reaction cell volume and Q is the heat change evolved from the reaction.

Then substitution of equation 17 into 18 yields the final equation:

$$\frac{1}{v(dQ/dL_{tot})} = \Delta H\left(\frac{1}{2} + \frac{1-(1+r)/2-L_r/2}{\sqrt{L_r 2 - 2L_r(1-r)+(1+r)^2}}\right) \qquad \textbf{[19]}$$

Equation 19 describes the curve, which represents binding isotherms for a single-site interaction (Wiseman et al., 1989). The micro-calorimeter measures the differential heat dQ/dL_{tot}.

2.11.2.3 Concentration requirements

The concentration of the cell reactant required depends on the strength of the interaction to be measured. The optimal amount of cell reactant can be determined using the unitless C parameter. The C parameter is the concentration ratio of the cell reactant divided by the K_d and defines the shape of the binding isotherm.

$$C = K_a[M_{tot}]n \qquad \textbf{[20]}$$

where K_a is the binding association constant, M_{tot} is the total macromolecule cell concentration, and n is the stoichiometry.

It is crucial to determine the correct cell reactant concentration required for the experiment. If the concentration is too low (C<1) the isotherm curve becomes very shallow, where the drop at equivalence point broadens and the intercept at the Y axis is lower than the true ΔH°. The sigmoidal curve loses its characteristic shape thereby making it extremely difficult to determine the K_d, molar ratio and ΔH° (Figure 32). If the concentration is too high (C>1000), the molar ratio and ΔH° can be easily determined but the K_d cannot, as at the transition region the sigmoidal curve becomes rectangular in shape with too few points collected near equivalence. The height of the curve corresponds to ΔH° and the sharp drop occurs at the stoichiometric equivalence point (n). Hence, reactions with large K_a values should be studied at low macromolecule concentration and the opposite is true for low K_a values. Ideally, one should use cell reactant concentrations where the C values are 10-500, and the syringe reactant concentration should be 10-20-fold greater than that of the cell concentration.

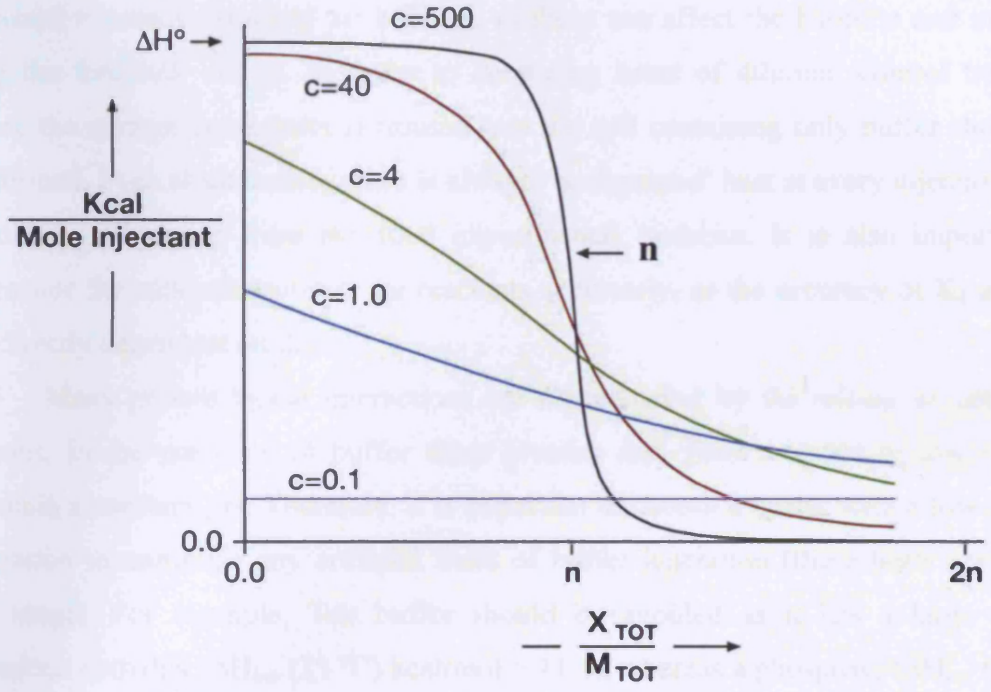

Figure 32: Binding isotherms at various C parameter values. When the cell reactant is too low (C<1), the data shape is shallow which makes it difficult to determine the K_d and $\Delta H°$ accurately. When the cell reactant is too high (C>500) then there is insufficient information at the transition region to determine the K_d. The optimal C values are between 10 and 500. Taken and adapted from the Microcal VP-ITC user manual, 2004.

2.11.2.4 Important parameters in ITC

Various factors need to be taken into consideration when planning an ITC experiment. For example, it is essential that the cell and syringe solutions be precisely chemically (pH and solvent components) matched as even small differences can cause background heats of mixing, thereby masking the heat of binding for the reaction. In order to avoid this, extensive dialysis of both reactants is critical to match the components. Furthermore, all samples should be filtered or centrifuged to remove aggregate particles. Prior to loading the cell and syringe materials, both have to be degassed to remove residual air bubbles, as these can affect the baseline and interfere with the feedback circuit. In order to determine heats of dilution, control titrations where the syringe component is titrated into the cell containing only buffer should be performed. Even at saturation, there is always 'background' heat at every injection. This should be subtracted from the final experimental isotherm. It is also important to determine the concentrations of the reactants accurately, as the accuracy of K_d and ΔH are directly dependent on this.

Many protein-ligand interactions are accompanied by the release or uptake of protons. In the presence of buffer these protons are either released or absorbed to maintain a constant pH. Therefore, it is important to choose a buffer with a low heat of ionization to minimize any artificial heats of buffer ionization (these heats are in the kcal/range). For example, Tris buffer should be avoided as it has a large proton ionization enthalpy (ΔH_{ion} (25 °C) kcal/mol = 11.4), whereas a phosphate (ΔH_{ion} (25 °C) kcal/mol = 0.9) or Hepes buffer (ΔH_{ion} (25 °C) kcal/mol = 5.7) are well suited.

If no change in signal is observed during a titration this may be due to the affinity being too weak for the relative concentrations used. In this case, the reactant concentrations should be increased by ~ 10-fold to amplify the signal. Alternatively, the temperature can be changed by 5-10 °C in either direction, as ΔH is temperature dependent and coincidently might be zero at a given temperature. If the binding observed is too tight then lowering the reactant concentrations, particularly the cell reactant may be better. Alternatively, the temperature can be increased as this often causes affinities to become weaker, which is particularly true for exothermic reactions. The opposite is true for endothermic reactions where decreasing the temperature can weaken affinities.

CHAPTER THREE

3.0 Phosphorylation of $p47^{phox}$ and NADPH oxidase activation

$P47^{phox}$ is phosphorylated on eleven serine residues of which eight are required for activation of the NADPH oxidase (Ago et al., 1999; el Benna et al., 1994; El Benna et al., 1996; Faust et al., 1995; Groemping et al., 2003; Inanami et al., 1998; Johnson et al., 1998). Five of these serine residues are located within the polybasic region (S303, 304, 315, 320 and 328), and the remaining three are located at the extreme C-terminus (S359, 370 and 379), a region that interacts with $p67^{phox}$ (Finan et al., 1994; Lapouge et al., 2002; Leto et al., 1994). Many studies have shown that phosphorylation of the serine residues within the polybasic region is important for the transformation of the inactive, auto-inhibited state into the active state (Ago et al., 1999; el Benna et al., 1994; El Benna et al., 1996; Groemping et al., 2003). Although Ago and colleagues showed that phosphorylation of the C-terminal serine residues S359, 370 and 379 do not directly promote binding of $p47^{phox}$ to $p22^{phox}$, it is not known whether they synergise with the polybasic region, to contribute to the interaction (Ago et al., 1999). In addition, the potential effects of such phosphorylation events on the interaction with other oxidase components such as $p67^{phox}$ have not been directly characterised. Until now the effect of these phosphorylation events have mainly been conducted with respect to superoxide production or membrane translocation of $p47^{phox}$ (Faust et al., 1995; Johnson et al., 1998).

This chapter describes experiments to investigate the effect that phosphorylation of the C-terminal serine residues S359, 370 and 379 may have on the formation of the active conformation of $p47^{phox}$ and the subsequent interaction with $p22^{phox}$, the association with $p67^{phox}$ and on the interaction with phosphatidylinositols.

3.1 The effect of p47^{phox} C-terminal phosphorylation on its interaction with p22^{phox}

3.1.1 Overview and aims

As shown in Figure 7, serine residues 359, 370 and 379 are remote from the polybasic, auto-inhibitory region. Hence, phosphorylation of these residues would not be expected to have a direct effect on the release of the auto-inhibited conformation as observed for serine residues 303-328. Interestingly however, a detailed quantitative analysis of the interaction between p22^{phox} and p47^{phox} showed, that the binding affinity of a p22^{phox}-derived peptide for a mutant in which all five serine residues in the polybasic region had been substituted with glutamates was 20-fold weaker than for the isolated tandem SH3 domains (Groemping et al., 2003). This discrepancy could suggest that glutamate residues are not ideal mimics of phosphoserines and therefore cannot support the formation of the fully active form of p47^{phox}. Alternatively though, this observation raises the possibility that phosphorylation of these serine residues alone may not support the fully active conformation of the protein, and that phosphorylation of the remaining three serine residues in the C-terminal region of the protein may act synergistically and induce conformational changes that promote the interaction with p22^{phox}. This possibility was tested using mutants of p47^{phox} in which a varying numbers of serine residues have been replaced by glutamates and their interaction with a fluorescein labelled p22^{phox}-derived peptide was followed by fluorescence spectroscopy.

3.1.2 Results

Two plasmids containing the serine to glutamate mutations S303, 304, 315, 320 and 328E (pGEX-p47^{phox}S5E) and S359, 370 and 379E (pGEX-p47^{phox}S3E), in the full-length construct were already available (Groemping et al., 2003; Lapouge and Rittinger, unpublished results). PGEX-p47^{phox}S5E mimics phosphorylation of serine residues in the polybasic region, whereas pGEX-p47^{phox}S3E mimics phosphorylation within the C-terminal region. These mutant plasmids were used to construct a plasmid containing all eight serine to glutamate substitutions (pGEX-p47^{phox}S8E) as described in section 2.2.1. The phosphorylation mimics p47^{phox}S8E, p47^{phox}S5E, p47^{phox}S3E as well as p47^{phox}Wild-type and the isolated tandem SH3 domains i.e. p47^{phox}Wild-type$_{tandem}$ (aa

156-285) were purified to homogeneity. Their binding to a fluoresceine labelled $p22^{phox}$ derived peptide (hereafter called $p22^{phox*}$ peptide) was measured using fluorescence spectroscopy. In addition circular dichroism (CD) spectroscopy was used to determine if the introduction of these mutations had any effect on the secondary structure of the proteins or on their thermal stability. The methods used in these studies are described in chapter 2 of the Materials and Method section.

3.1.2.1 Protein expression and purification

Proteins were expressed in a soluble form in *E.coli* under similar conditions and in similar amounts as $p47^{phox}$Wild-type, with the exception of $p47^{phox}$S8E (see section 3.1.2.2). They were purified by affinity chromatography on glutathione sepharose, followed by either ion-exchange or size exclusion chromatography after protease cleavage of the GST-tag. Figure 33 shows the purity of the proteins used for the fluorescence titrations. All the proteins ran as single bands at their expected molecular weights (~ 45 kDa), and could be easily concentrated to 500 μM - 1 mM apart from $p47^{phox}$S8E, which aggregated above 250 μM. The identities of the purified proteins were confirmed by electrospray mass spectrometry.

3.1.2.2 Cloning and purification of $p47^{phox}$S8E

The full-length plasmid containing eight serine to glutamate mutations (pGEX-$p47^{phox}$S8E) was constructed as described in section 2.2.1. Initial attempts to express and purify the protein yielded a mixture of the full-length protein (aa 1-390, 45 kDa) and a shorter, C-terminally deleted variant (aa 1-354, 41 kDa) (as determined by mass spectrometry, data not shown). The separation of full-length and degraded protein proved impossible using anion exchange chromatography, due to the similarities in pI (9.1 and 8.6, respectively) (Figures 34 A and B). Gel filtration chromatography could also not be used to separate the two proteins, due to the small difference in molecular weight. Therefore, to allow purification of the full-length protein, a His_6-tag was engineered onto the C-terminus of pGEX-$p47^{phox}$S8E by PCR. The resulting protein was well expressed (Figure 35) in *E.coli* and largely soluble. A first purification step was carried out using glutathione sepharose 4B to capture the full-length as well as C-

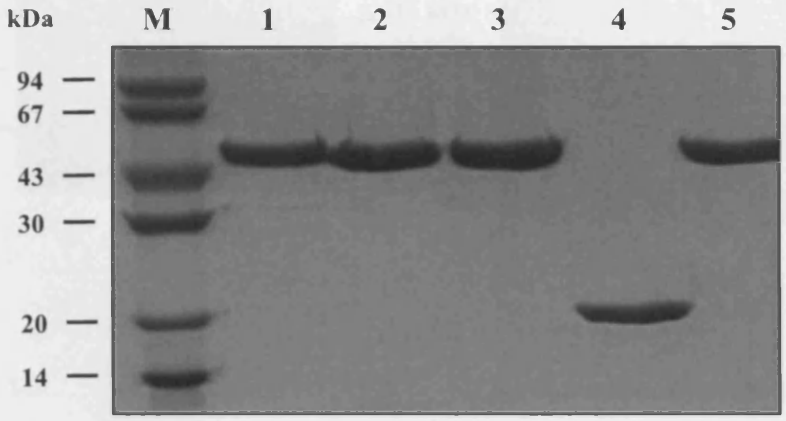

Figure 33: SDS-PAGE of proteins used for fluorescence spectroscopy experiments. Analysis of the purity of $p47^{phox}$Wild-type and mutants of $p47^{phox}$ that mimic serine phosphorylation. 5 µg of protein were loaded per lane.

M:	Low molecular weight marker (GE Healthcare)	
1:	$p47^{phox}$ S8E (S303, 304, 315, 320, 328, 359, 370 and 379E)	(46 kDa)
2:	$p47^{phox}$ S5E (S303, 304, 315, 320, 328E)	(45 kDa)
3:	$p47^{phox}$ S3E (S359, 370 and 379E)	(45 kDa)
4:	$p47^{phox}$ $Wild\text{-}type_{tandem}$ (aa 156-285)	(15 kDa)
5:	$p47^{phox}$ Wild-type	(45 kDa)

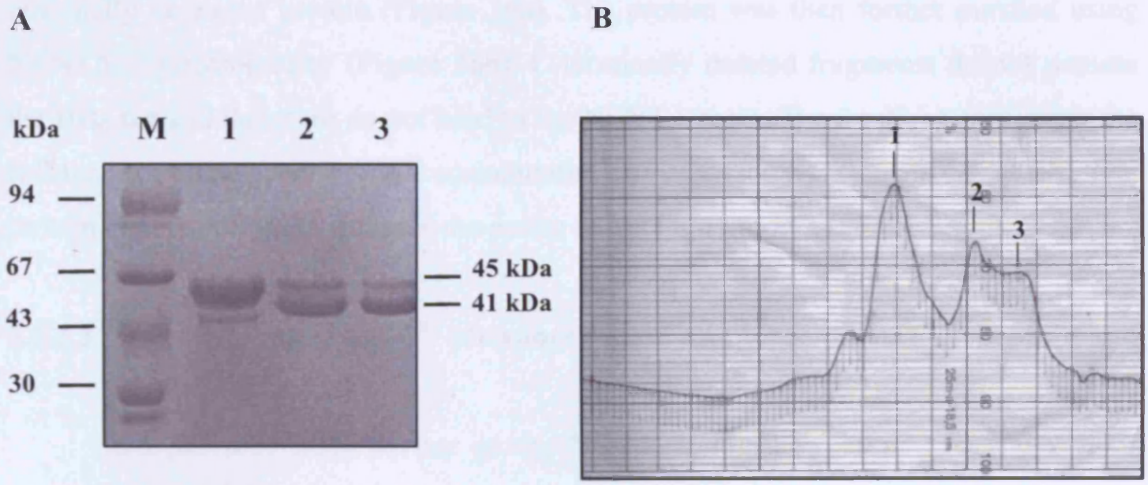

Figure 34: Purification of p47^{phox}S8E by anion exchange chromatography. A. SDS gel. Lanes 1, 2 and 3 show the fractions collected during the NaCl gradient. Two bands are observed running at 45 kDa (full-length p47^{phox}) and 41 kDa (C-terminally deleted variant of p47^{phox}). M: low molecular weight marker (GE Healthcare). B. Shows the corresponding chromatogram. Peaks 1, 2 and 3 correspond to lanes 1, 2 and 3 in Figure 29A.

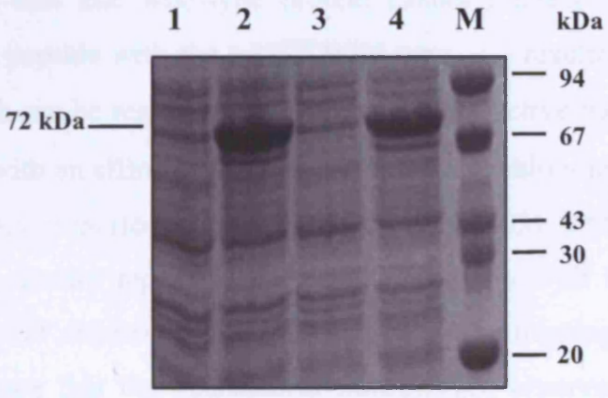

Figure 35: IPTG induction of p47^{phox}S8E-His$_6$. SDS-PAGE analysis of cell lysates before and after IPTG induction (2 different colonies). Lanes 1 and 3: cells before induction, 2 and 4: 3 hrs after induction with 1 mM IPTG. Molecular weight of GST-p47^{phox}S8E-His$_6$ is 72 kDa. M: low molecular weight marker (GE Healthcare).

terminally degraded protein (Figure 36a). The protein was then further purified using Ni-NTA chromatography (Figure 36b). C-terminally deleted fragments do not possess the His_6-tag and therefore do not bind to the Ni-NTA resin. The fractions containing the full-length protein were pooled, concentrated and analysed by SDS-PAGE at different protein concentrations to monitor the purity of the final product (Figure 36c).

3.1.2.3 Binding of $p47^{phox}$ phosphorylation mimics to the $p22^{phox}$ peptide

In a previous study by our group, the interaction between $p22^{phox}$ and various mutants of $p47^{phox}$ was quantified using fluorescence spectroscopy. The change in fluorescence of a fluorescein labelled $p22^{phox*}$ peptide upon addition of increasing amounts of $p47^{phox}$ was followed. In contrast, attempts to measure this interaction by ITC were unsuccessful because the heat change upon complex formation proved too small to allow a reliable determination of the affinity and enthalpy of the interaction (Groemping et al., 2003). For this reason, the fluorescent approach was chosen in the present work to characterise the potential effect of phosphorylation of C-terminal serine residues on the interaction with $p22^{phox}$ (peptide 3, Appendix: A4). Results of the fluorescence spectroscopy experiments are summarised in Table 11.

In accordance with earlier studies, titration of the $p22^{phox*}$ peptide with $p47^{phox}$Wild-type did not result in any significant changes in fluorescence intensity, supporting the fact that wild-type protein cannot interact with $p22^{phox}$. In contrast, titration of the peptide with the $p47^{phox}$Wild-$type_{tandem}$ resulted in a binding affinity of 0.56 μM, which can be regarded to represent to fully active state, and $p47^{phox}$S5E bound to the peptide with an affinity of 5.7 μM. All of these values are in good agreement with those previously reported (Groemping et al., 2003) and were used as control experiments to ensure reproducibility and familiarity with the experimental system. Additional control experiments were carried out by titrating buffer into the $p22^{phox*}$ peptide, to ensure that the decrease in fluorescence observed was due to binding of peptide to protein, and not an artefact.

To determine whether phosphorylation of the $p47^{phox}$ C-terminal serine residues S359, 370, 379 alone had any effect on the interaction with $p22^{phox}$, the peptide was titrated with the triple phosphorylation mimic $p47^{phox}$S3E. However, no change in fluorescence was detected, indicating that these mutations alone do not relieve auto-inhibition. Nevertheless, it is conceivable that phosphorylation of these residues may act

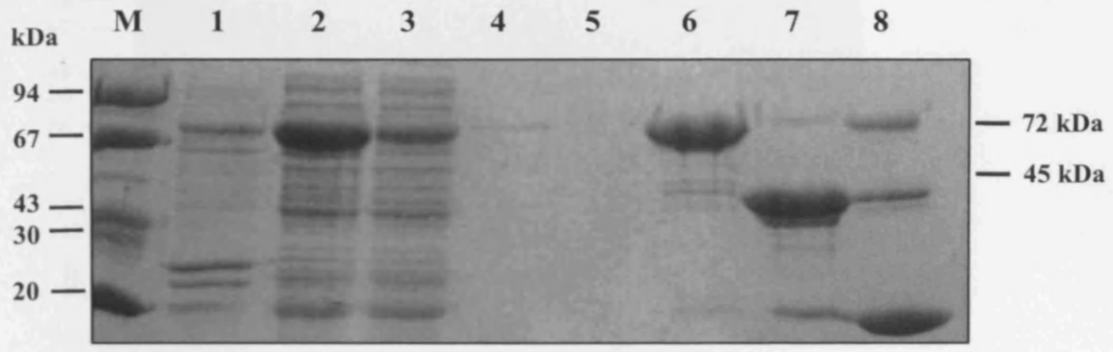

Figure 36a: Purification of $p47^{phox}$S8E-His_6 by affinity chromatography on glutathione sepharose.

M: Low molecular weight marker (GE Healthcare)
1: Pellet
2: Supernatant
3: Flow through
4: Wash with high salt buffer B
5: Wash with low salt buffer C
6: GST beads before 3C protease cleavage
7: Elution after 3C protease cleavage
8: GST beads after cleavage

For composition of buffers refer to Appendix: A4

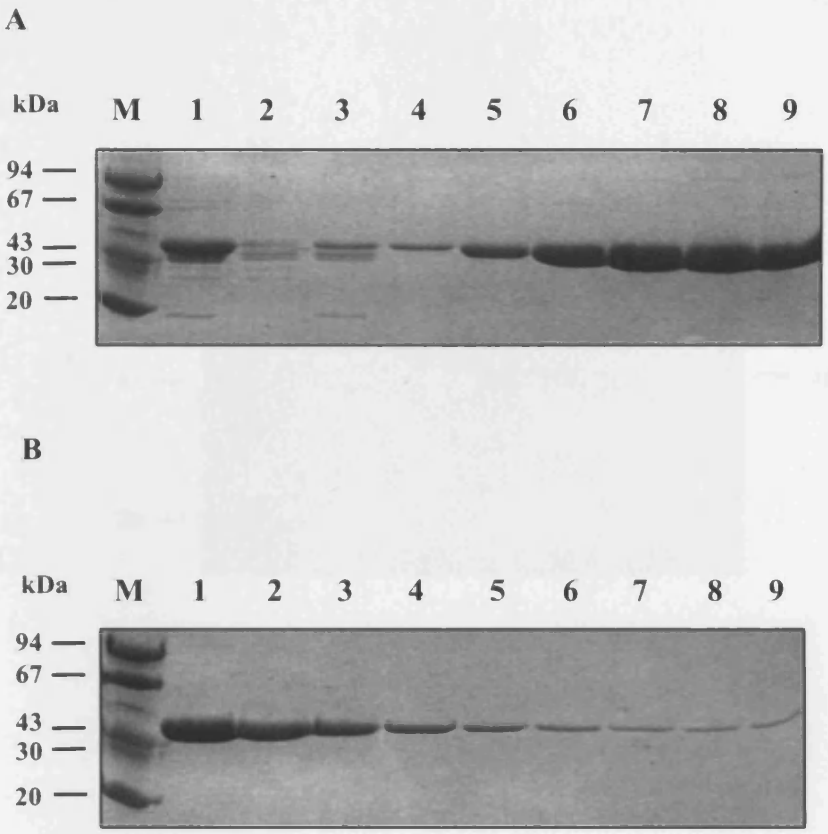

Figure 36b: Further purification of p47^{phox}S8E-His$_6$ using Ni-NTA chromatography.

A

M: Low molecular weight marker (GE Healthcare)

1: Load (protein eluted from the glutathione sepharose column)

2: Flow through

3: Wash with buffer D (containing 20 mM imidazole- refer to Appendix: A4)

4-9: Elution of pure protein during a linear imidazole gradient (20 mM-1 M)

B

M: Low molecular weight marker (GE Healthcare)

1-9: Elution of pure protein (continues from Figure 31b,A)

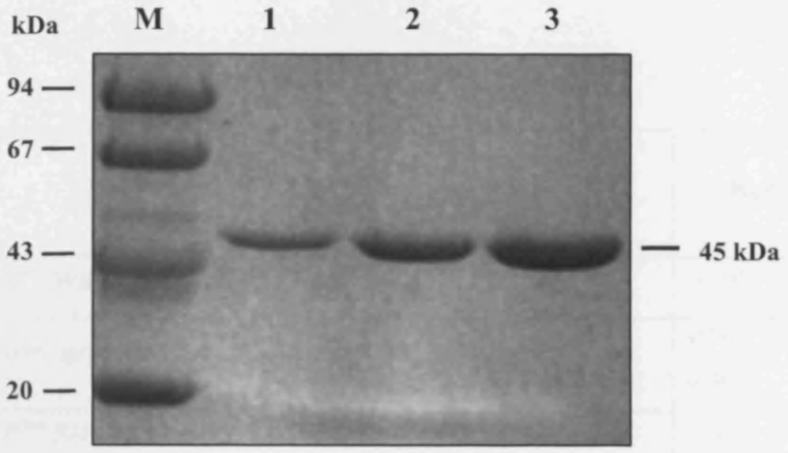

Figure 36c: **Purity of $p47^{phox}$S8E-His_6.** Analysis of the purity of $p47^{phox}$S8E-His_6. Various concentrations were loaded and a single band was observed at the expected molecular weight (45 kDa).

M: Low molecular weight marker (GE Healthcare)

1: 2 µg

2: 5 µg

3: 10 µg

N.B. **For purposes of simplicity, $p47^{phox}$S8E-His_6 hereafter will be referred to as $p47^{phox}$S8E.**

Table 11: Dissociation constants for the complexes formed between the $p47^{phox}$ phosphorylation mimics and the 16-mer fluorescein labelled $p22^{phox}$ peptide.

$p47^{phox}$ protein	K_d (μM)
$p47^{phox}$ Wild-type	> 500
$p47^{phox}$ Wild-type$_{tandem}$	0.56 ± 0.03 0.40
$p47^{phox}$ S3E (S359, 370, 379E)	> 500
$p47^{phox}$ S5E (S303, 304, 315, 320, 328E)	5.7 ± 0.08 8.0
$p47^{phox}$ S8E (S303, 304, 315, 320, 328, 359, 370, 379E)	4.7 ± 0.07

Fluorescence experiments were carried out in buffer H (pH according to the individual proteins, and to one unit above or below the pI). The $p47^{phox}$ proteins were titrated at increasing concentrations into the cuvette containing 1 μM of the fluorescein labelled $p22^{phox}$ peptide. Results shown in blue are those reported previously (Groemping et al., 2003). Values are the mean of at least three independent experiments. The errors (±) are the standard deviation of the mean. These errors are surprisingly small and while they attest to the high reproducibility of the system, they nevertheless certainly underestimate the real error of the experiments. For this reason it seems more realistic to assume an error of at least 10 % that is composed of errors in the pipettes and the determination of protein concentrations.

synergistically with phosphorylation of serine residues in the polybasic region, to promote the interaction with $p22^{phox}$. To investigate this possibility, binding studies using $p47^{phox}$S8E were carried out. However, this protein bound with an affinity of 4.7 μM to the $p22^{phox*}$ peptide, which is not significantly different from that obtained for $p47^{phox}$S5E. Figure 37 shows representative fluorescence titrations for the binding of the $p47^{phox}$ phosphorylation mimics to $p22^{phox}$. These results suggest that phosphorylation of the C-terminal serine residues S359, 370 and 379 do not synergise with phosphorylation of the serine residues located within the polybasic region, to destabilise the auto-inhibited conformation of $p47^{phox}$.

3.1.2.4 Circular dichroism measurements of the $p47^{phox}$ phosphorylation mutants

Circular dichroism (CD) spectroscopy was used to determine the secondary structure content and the thermal stability of the proteins under investigation, as described in section 2.4.3. Figure 38 shows the CD spectra for the different proteins, which are all similar to $p47^{phox}$Wild-type, thereby confirming that any changes observed in the binding affinities are not solely due to changes in secondary structure. Small variations in intensity were observed, probably deriving from small errors in the determination of protein concentration and are not significant. The secondary structure content of these proteins was calculated from the CD spectra using the methods described by Sreerama and Woody, 2000. For example, the secondary structure content of $p47^{phox}$S5E which is listed in Table 12 is similar to $p47^{phox}$Wild-type. The thermal stability of the proteins was assessed by measuring changes in ellipticity at 210 nm with increasing temperature (20 °C - 80 °C). Figure 39 shows the thermal scans for the different proteins. The $p47^{phox}$S3E mutant protein behaved similar to $p47^{phox}$Wild-type, while $p47^{phox}$S5E and $p47^{phox}$S8E showed unfolding/precipitation at lower temperatures (6 - 8 °C) than $p47^{phox}$Wild-type. This suggests that these mutations somewhat destabilise the protein. However, the stability of these mutant proteins is not changed in the temperature range in which they were used for binding studies (20 °C). All the reactions were reversible.

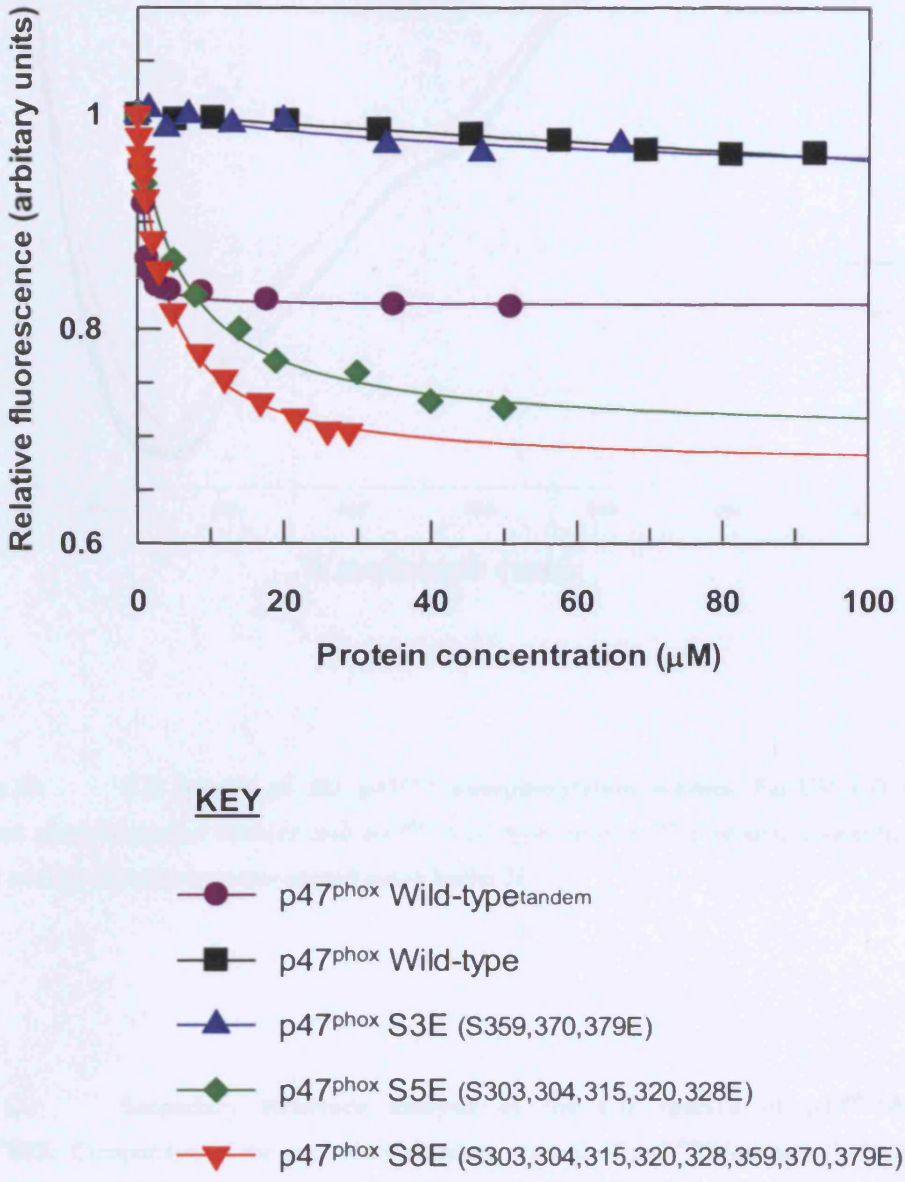

Figure 37: Fluorescence titrations for the binding of $p47^{phox}$ phosphorylation mimics to the fluorescein labelled $p22^{phox}$ peptide. Similar to $p47^{phox}$Wild-type, $p47^{phox}$S3E does not show any significant changes in fluorescence intensity upon addition of the $p22^{phox*}$ peptide. Working solutions of protein and peptide were made in buffer H and all titrations were carried out at 20 °C.

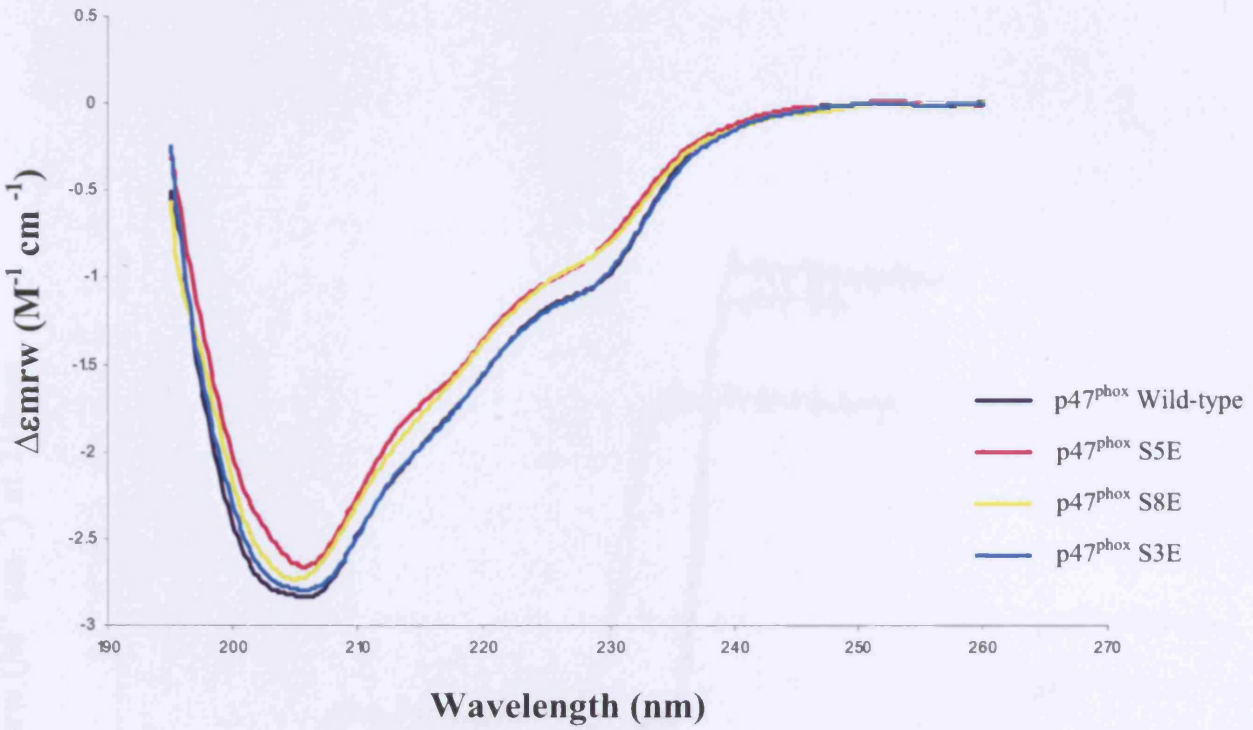

Figure 38: CD spectra of the p47^{phox} phosphorylation mimics. Far-UV CD spectra of the different phosphorylation mimics and p47^{phox}Wild-type protein. The protein concentration was 0.15 mg/ml and the experiments were carried out in buffer H.

Table 12: Secondary structure analysis of the CD spectra of p47^{phox}Wild-type and p47^{phox}S5E. Comparison of the secondary structure content of p47^{phox}Wild-type (WT) and p47^{phox}S5E (S5E), as calculated using the programs CONTIN, SELCON and CDSSTR (Sreerama and Woody, 2000). The secondary structure content of the other mutant proteins was similar to wild-type protein and within the acceptable 10 % error margin.

Program	α-helix (%)		β-sheet (%)		Turn (%)		Random (%)	
	WT	S5E	WT	S5E	WT	S5E	WT	S5E
CONTIN	14	17	37	35	23	26	26	22
SELCON	12.7	10	39	36	24.1	27.5	24.2	26.5
CDSSTR	13.8	17.7	36	37	25.2	22	25	23.3

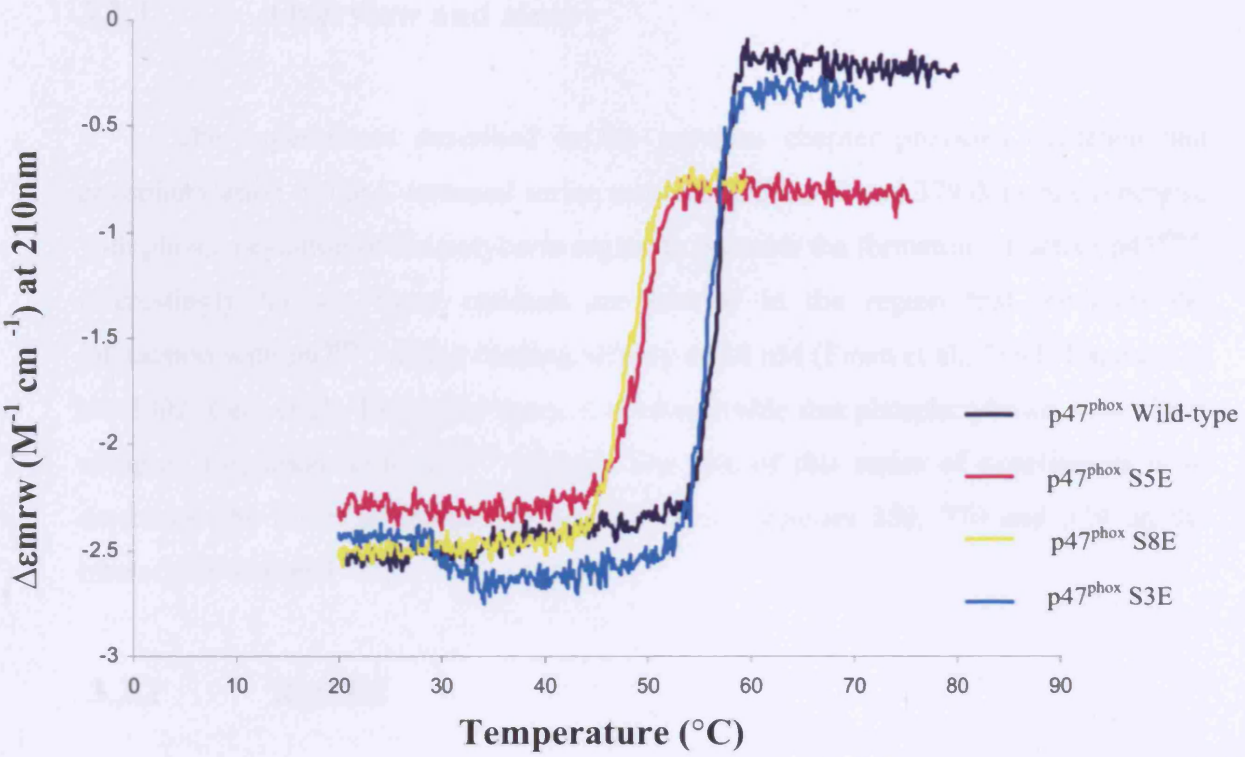

Figure 39: Thermal denaturation curves for the p47^{phox} phosphorylation mimics. The ellipticity at 210 nm was continuously measured as the temperature was increased from 20 °C – 80 °C. The protein concentration was 0.15 mg/ml and the experiments were carried out in buffer H.

3.2 The effect of C-terminal $p47^{phox}$ phosphorylation on its interaction with $p67^{phox}$

3.2.1 Overview and aims

The experiments described in the previous chapter provided evidence that phosphorylation of the C-terminal serine residues S359, 370 and 379 does not synergise with phosphorylation of the polybasic region to promote the formation of active $p47^{phox}$. Interestingly though, these residues are located in the region that mediates the interaction with $p67^{phox}$ with a binding affinity of 20 nM (Finan et al., 1994; Lapouge et al., 2002; Leto et al., 1994) and hence it is conceivable that phosphorylation may affect complex formation with $p67^{phox}$ instead. The aim of this series of experiments is to determine the effect of phosphorylation of serine residues 359, 370 and 379 on the interaction with $p67^{phox}$.

3.2.2 Results

The overall approach taken for this study was similar to that described in the previous chapter, using substitution of serine with glutamate residues to mimic phosphoserines. Various plasmids containing serine to glutamate mutations in the full-length construct were already available at the beginning of this study. These plasmids include the individual mutants; pGEX-$p47^{phox}$S359E and pGEX-$p47^{phox}$S370E, the double mutant; pGEX-$p47^{phox}$S359/370E, as well as those described in section 3.1. In addition, site-directed mutagenesis was used to construct the individual mutant pGEX-^{phox}S379E within the full-length construct. A full-length plasmid containing $p67^{phox}$, as well as the isolated second SH3 domain of $p67^{phox}$ ($p67^{phox}(SH3)_B$) were also already available.

3.2.2.1 Protein expression and purification

All proteins were expressed and purified in a soluble form in *E.coli* under similar conditions and in similar amounts as the wild-type protein (apart from $p47^{phox}$S8E). The proteins were purified by affinity chromatography on glutathione sepharose, followed by either ion-exchange or size exclusion chromatography after

protease or thrombin cleavage of the GST-tag. Figures 40 A and B show the purity of the proteins used for the various ITC experiments. All the proteins ran as single bands at their expected molecular weights and could be easily concentrated to 500 μM - 1 mM other than $p47^{phox}$S8E. The identities of the purified proteins were verified by electrospray mass spectrometry.

3.2.2.2 Binding of C-terminal $p47^{phox}$ phosphorylation mimics to $p67^{phox}$

The use of fluorescence spectroscopy to monitor complex formation between $p67^{phox}$ and $p47^{phox}$ was not feasible as both proteins contain tryptophan residues, which would interfere with the use of protein fluorescence as a signal. Similarly, the introduction of an extrinsic fluorophore at a specific site in a protein the size of $p67^{phox}$ or $p47^{phox}$ is difficult and can give rise to numerous problems. For this reason ITC was chosen to characterise the interaction between the $p47^{phox}$ phosphorylation mimics and $p67^{phox}$. This technique has the advantage that in addition to the binding constant, it also allows the determination of the stoichiometry of the interaction as well as the thermodynamic parameters ΔG, ΔH and $T\Delta S$. In previous studies where the interaction between $p47^{phox}$ and $p67^{phox}$ was investigated, the experiments were carried out in the following manner: full-length $p47^{phox}$ was placed in the syringe as it is very stable and can be highly concentrated, while full-length $p67^{phox}$ was placed in the cell (due to its lower protein yield and stability) (Lapouge et al., 2000). Unfortunately, such an experimental design was not possible in this case as $p47^{phox}$S8E also has problems with poor protein yield and stability. To circumvent this problem it was decided to carry out all binding experiments using only the C-terminal SH3 domain of $p67^{phox}$ ($p67^{phox}(SH3)_B$), as it is well established that this domain is sufficient to fully reconstitute the interaction with $p47^{phox}$ (Kami et al., 2002; Lapouge et al., 2002). $P67^{phox}(SH3)_B$ can be produced in large quantities and is very stable at higher concentrations and was hence used as the syringe component. Control experiments were carried out to ensure reproducibility and to confirm that only $p67^{phox}(SH3)_B$ is involved in the interaction. ITC experiments were performed in which wild-type $p47^{phox}$ was titrated with full-length-$p67^{phox}$ or isolated $p67^{phox}(SH3)_B$. The K_d values measured were identical (38 nM for both), which supports the previous observations. The binding affinities and thermodynamic parameters of complex formation between the different $p47^{phox}$ phosphorylation mimics and $p67^{phox}$ were measured at 15 °C. Results for the

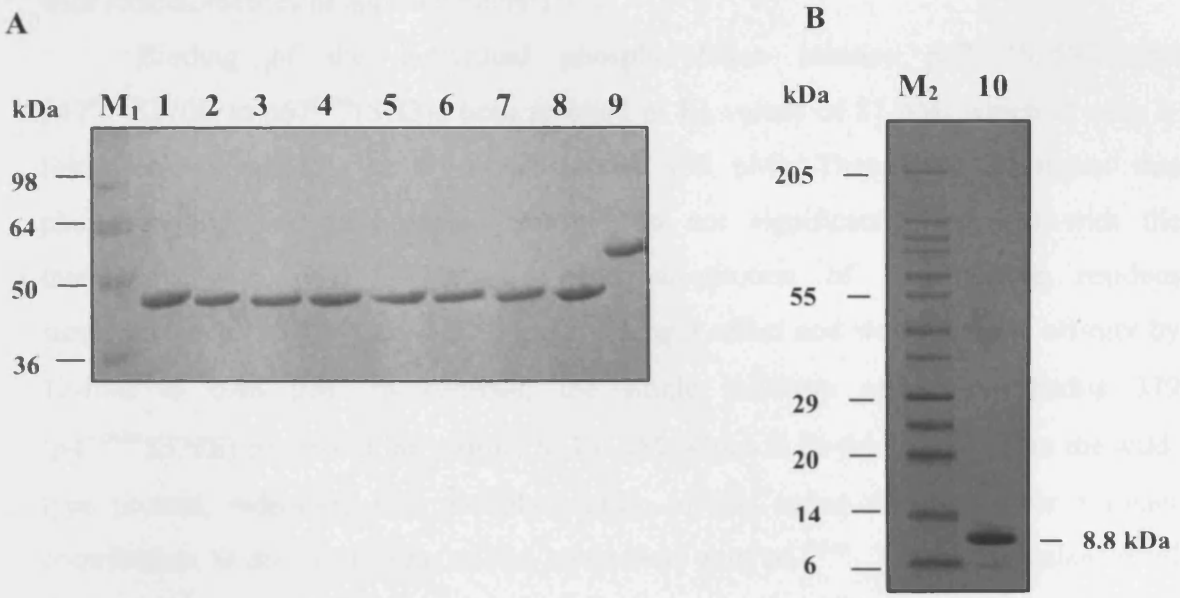

Figure 40: SDS-PAGE of proteins used for ITC experiments. A. Analysis of the purity of $p67^{phox}$Wild-type and $p47^{phox}$Wild-type proteins, plus $p47^{phox}$ phosphorylation mimics. 3 µg were loaded per lane. B. Analysis of the purity of $p67^{phox}(SH3)_B$. 4 µg was loaded.

M_1:	Low molecular weight marker (GE Healthcare)	
M_2:	High molecular weight marker (Sigma)	
1:	$p47^{phox}$ Wild-type	(45 kDa)
2:	$p47^{phox}$ S359E	(45 kDa)
3:	$p47^{phox}$ S370E	(45 kDa)
4:	$p47^{phox}$ S359/370E	(45 kDa)
5:	$p47^{phox}$ S379E	(45 kDa)
6:	$p47^{phox}$ S3E (S359, 370 and 379E)	(45 kDa)
7:	$p47^{phox}$ S5E (S303, 304, 315, 320 and 328E)	(45 kDa)
8:	$p47^{phox}$ S8E (S303, 304, 315, 320, 328, 359, 370 and 379E)	(46 kDa)
9:	$p67^{phox}$ Wild-type	(60 kDa)
10:	$p67^{phox}$ $(SH3)_B$ (aa 243-297)	(8.8 kDa)

ITC experiments are summarised in Table 13. All binding reactions were exothermic with stoichiometries of approximately 1:1.

Binding of the individual phosphorylation mimics $p47^{phox}$S359E and $p47^{phox}$S370E to $p67^{phox}(SH3)_B$ both resulted in K_d values of 81 nM, which is only 2-fold weaker than for the wild-type protein (38 nM). These results suggest that phosphorylation of these serine residues do not significantly interfere with the interaction with $p67^{phox}$. However, the substitution of both serine residues simultaneously ($p47^{phox}$S359/370E) had a stronger effect and weakened the affinity by 12-fold to 0.48 μM. In contrast, the single mutation of serine residue 379 ($p47^{phox}$S379E) decreased the affinity to 1.0 μM, which is 26-fold weaker than the wild-type protein, indicating that phosphorylation of this serine residue makes a major contribution to the weakening of the interaction with $p67^{phox}$. The combination of all three mutations ($p47^{phox}$S3E) led to a further decrease in affinity to 2.4 μM, 63-fold weaker than between the wild-type proteins.

Although the interaction between $p47^{phox}$ and $p67^{phox}$ only involves the C-terminal region of $p47^{phox}$, it may be possible that phosphorylation of serine residues within the polybasic region may induce conformational changes in the C-terminal region and thereby influence the affinity for $p67^{phox}$. For this reason, the interaction between $p47^{phox}$S5E and $p67^{phox}(SH3)_B$ was investigated. The two proteins interact with an affinity of 61 nM, which is not significantly different from that of wild-type protein (38 nM), suggesting that phosphorylation of serine residues 303, 304, 315, 320 and 328 does not fundamentally effect the interaction with $p67^{phox}$. To further investigate whether phosphorylation of these serine residues acts synergistically with the phosphorylation of the serine residues located around the C-terminal proline rich region, binding of $p47^{phox}$S8E to $p67^{phox}(SH3)_B$ was measured. A K_d value of 2.9 μM was obtained, which is almost identical to that of $p47^{phox}$S3E, clearly indicating that the interaction with $p67^{phox}$ is only modified by phosphorylation of serine residues 359, 370 and 379. Figure 41 shows representative titration curves for these interactions.

Interestingly, although the affinity of $p67^{phox}$ for $p47^{phox}$S359/370E and $p47^{phox}$S379E is lower than for wild-type $p47^{phox}$, the enthalpy for complex formation actually increased for these two complexes, accompanied by compensating less favourable entropy changes. That may suggest that additional interactions take place in these complexes that are not observed between the wild-type proteins and that restrict the conformational flexibility of the complex. However, a similar increase in ΔH is not

Table 13: Thermodynamic values for the titration of $p67^{phox}(SH3)_B$ into $p47^{phox}$ phosphorylation mimics.

$p47^{phox}$ protein	K_d (nM)	ΔH (kcal/mol)	TΔS (kcal/mol)	ΔG (kcal/mol)
WT *	37 ± 4.1	-3.86 ±0.11	5.90 ± 0.06	-9.78 ± 0.45
WT	35 ± 3.2	-6.2 ± 0.03	3.62 ± 0.1	-9.82 ± 0.05
S359E	59.7 ± 1.1	-6.02 ± 0.19	3.54 ± 0.03	-9.56 ± 0.2
S370E	79 ± 2.1	-6.51 ± 0.02	2.85 ± 0.1	-9.36 ± 0.2
S359, 370E	475 ± 5	-7.72 ± 0.06	0.62 ± 0.09	-8.34 ± 0.05
S379E	965 ± 50	-8.37 ± 0.27	-0.43 ± 0.1	-7.94 ± 0.4
S3E	2450 ± 50	-5.63 ± 0.33	1.76 ± 0.2	-7.40 ± 0.65
S5E	64.7 ± 3.5	-6.25 ± 0.01	3.21 ± 0.11	-9.46 ± 0.42
S8E	2850 ± 50	-4.60 ± 0.06	2.71 ± 0.08	-7.31 ± 0.05

ITC experiments were carried out in buffer H (pH according to the individual proteins, and to one unit above or below the pI) at 15 °C. $P47^{phox}$ proteins in the cell were used at concentrations in the range of 25-40 μM. $P67^{phox}(SH3)_B$ was titrated at concentrations of 250-400 μM. Titration of full-length $p67^{phox}$ into wild-type $p47^{phox}$ protein is shown by an asterisk (*). The binding stoichiometry values (n) ranged from 0.9-1.1.Values are the mean of at least three independent experiments. The errors (±) are the standard deviation of the mean. As discussed in Table 11 the error values on these experiments are extremely low, due to the very good reproducibility of the system. Nevertheless, it seems more appropriate to assume an error of around 10 % that is contributed to mainly by pipetting errors during the determination of protein concentrations.

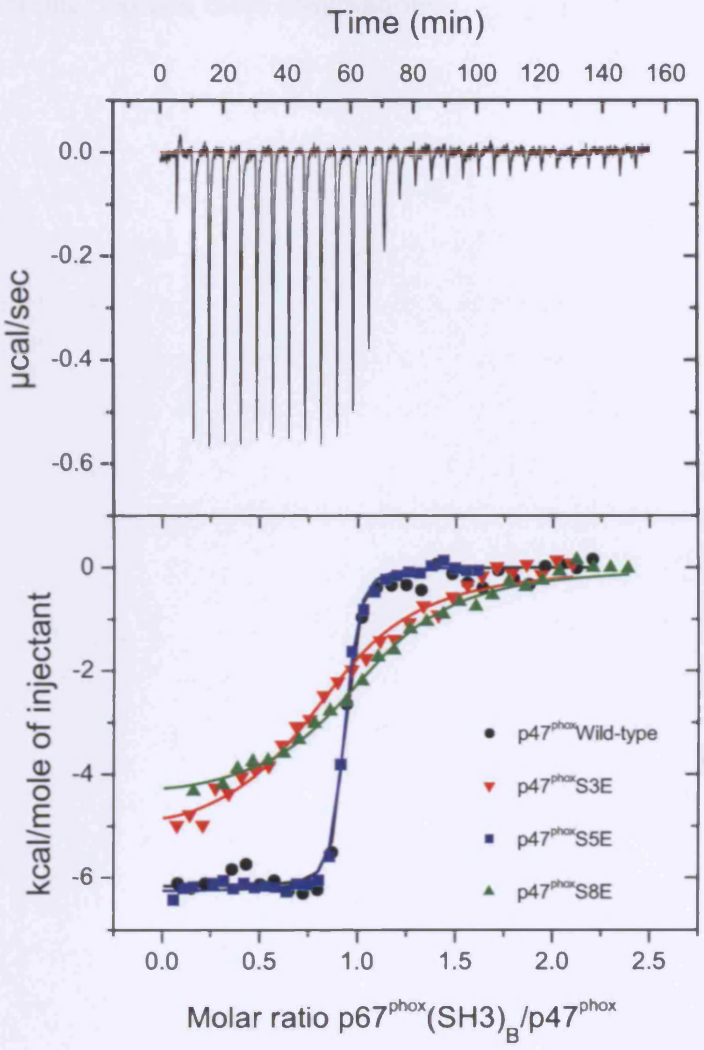

Figure 41: Complex formation between $p67^{phox}(SH3)_B$ and different $p47^{phox}$ proteins. ITC measurements of complex formation between $p67^{phox}(SH3)_B$ and $p47^{phox}$Wild-type, $p47^{phox}$S3E (S359/379E), $p47^{phox}$S5E (S303/328E) and $p47^{phox}$S8E (S303/379E). Upper part, raw data of the titration of $p47^{phox}$Wild-type (33 µM) with $p67^{phox}(SH3)_B$ (321 µM). Lower part, integrated heat changes corrected for the heats of dilution and fitted curve, based on a single-site binding model. All experiments were carried out at 15 °C in buffer H.

observed for binding of the triple mutant, $p47^{phox}$S3E, which on the other hand somewhat questions this idea. Further studies such as the crystal structure of the individual $p47^{phox}$ phosphorylation mutants in complex with $p67^{phox}(SH3)_B$ are now required to further explain these observations.

3.3 The effect of C-terminal $p47^{phox}$ phosphorylation on its interaction with PtdIns(3,4)P_2

3.3.1 Overview and aims

The cytosolic NADPH oxidase proteins $p40^{phox}$ and $p47^{phox}$ each contain a PX domain in their respective N-termini. PX domains are lipid interaction modules, which are found in a variety of proteins that associate with cell membranes (section 1.4.4). Unlike the $p40^{phox}$ PX domain, which specifically binds to PtdIns(3)P (Ago et al., 2001; Bravo et al., 2001; Ellson et al., 2001; Kanai et al., 2001), the $p47^{phox}$ PX domain can interact with a variety of phosphoinositides (Ago et al., 2001; Kanai et al., 2001; Zhan et al., 2002), but preferentially binds PtdIns(3,4)P_2 (Kanai et al., 2001; Karathanassis et al., 2002). In addition, the $p47^{phox}$ PX domain has been proposed to contain a second lipid binding pocket, which is speculated to recognise anionic phospholipids such as phosphatidylserine (PS) or phosphatidic acid (PA) to increase membrane affinity (Karathanassis et al., 2002).

The interaction of the $p47^{phox}$ PX domain with membrane phospholipids aids the association of the cytoplasmic trimeric complex ($p47^{phox}$-$p67^{phox}$-$p40^{phox}$) with the membrane to form the active NADPH oxidase complex. However, during the inactive state of the enzyme, the $p47^{phox}$ PX domain only very weakly binds lipids, due to auto-inhibitory interactions of the PX domain with the remainder of the protein (Ago et al., 2003; Karathanassis et al., 2002). Two studies have shown that mutant proteins in which phosphorylation of various serine residues have been mimicked by glutamates, specifically of 303, 304, 328 located in the polybasic region of $p47^{phox}$ and of S303, 304, 328, 359, 370 (Ago et al., 2003; Karathanassis et al., 2002) increase the lipid-binding capability of the PX domain. However, it is not clear whether phosphorylation of the C-terminal serine residues S359, 370 and 379 really contributes to this event. This chapter describes experiments aimed at investigating the effect that phosphorylation of the C-terminal serine residues may have on restoring lipid binding to the PX domain in the context of the full-length protein.

3.3.2 Results

In order to determine the effects of $p47^{phox}$ phosphorylation on binding to PtdIns(3,4)P_2, the following phosphorylation mimics were tested: $p47^{phox}$S3E, $p47^{phox}$S5E and $p47^{phox}$S8E. The full-length $p47^{phox}$ protein was used as a negative control, while the isolated $p47^{phox}$ PX domain was used as a positive control, which should show maximum binding. Parallel to this, the PH domain of the TAPP1 (tandem PH domain containing protein) protein was used as an additional positive control, as this PH domain is known to interact specifically with PtdIns(3,4)P_2 with high affinity (Dowler et al., 2000; Kimber et al., 2002; Thomas et al., 2001). Two different protein-lipid pull down methods were used to determine lipid binding i) lipid sedimentation assays and ii) the use of PIP beads (PtdIns(3,4)P_2 coated agarose beads). The methods used in these studies are described in chapter 2 of the Materials and Methods section.

3.3.2.1 Lipid sedimentation assays

Initial binding experiments were carried out according to the protocol published by Karathanassis and colleagues, with minor modifications. Briefly, lipid concentrations were used at 50 % PC, 40 % PE, 5 % PS and 5 % PtdIns(3,4)P_2. The lipid mix was protonated with HCl, sonicated, dried under nitrogen, resuspended in buffer and then further sonicated to form the liposomes (Karathanassis et al., 2002). Subsequent modifications made to this protocol included omitting the protonation procedure as pre-protonated PtdIns(3,4)P_2 were employed, and lipid concentrations were used at 42 % PE, 42 % PC, 6 % PS and 10 % PtdIns(3,4)P_2. Initially only three different proteins were tested to establish the protocol, including full-length $p47^{phox}$, isolated $p47^{phox}$ PX domain and $p47^{phox}$S5E (intermediate binding should be expected). However, no convincing binding for the $p47^{phox}$ PX domain and $p47^{phox}$S5E could be observed. Increasing the protein concentration also did not aid lipid binding (data not shown). Due to these problems Roger Williams at the MRC-LMB, Cambridge, who published the above protocol was contacted, and it was decided to carry out the assay under his supervision. It was suggested to use the PH domain of the TAPP1 protein as an additional positive control, as it specifically binds to PtdIns(3,4)P_2 with a high affinity (Thomas et al., 2001). In addition, adjustment 1 to the protocol was made (section 2.6.3). Negative controls were also performed i) using lipid samples in the absence of PtdIns(3,4)P_2 and ii) where the liposomes were omitted. The results showed only

minimal binding of the PH domain of the TAPPI protein to PtdIns(3,4)P_2 (Figure 42). No binding of the full-length $p47^{phox}$ protein to PtdIns(3,4)P_2 was observed, as expected, and insignificant amounts were apparent in the negative control lanes. Nevertheless, no binding was observed for the isolated $p47^{phox}$ PX domain and only a small amount of binding observed for the phosphorylation mimic $p47^{phox}$S5E. These results were in contrast to previous results, in which the isolated PX domain was fully lipid bound and hence in the pellet (Ago et al., 2003; Karathanassis et al., 2002). The experiment was repeated back in the host laboratory using a new batch of purified $p47^{phox}$ PX domain protein to ensure that the previous problems were not due to faulty protein preparation. However, no binding could be observed, not even for the PH domain of TAPP1 protein (data not shown). It was hypothesised that the thickness of the glass vials in which the liposomes were being produced (Wheaton 1 ml vials) may not have allowed the pulses of the bath sonicator to penetrate through efficiently thus affecting vesicle production. Therefore, it was suggested to use thinner glass vials (Chromacol 2 ml vials), the same as those used in the LMB laboratory. However, upon repeating the experiment the assay once again proved unsuccessful (data not shown). The use of 5 % PA in place of 5 % PS was tested as this may aid lipid binding, because PA is more negatively charged than PS, and therefore might bind to the 'basic' pocket of the $p47^{phox}$ PX domain more tightly. Again no binding of the isolated $p47^{phox}$ PX domain was observed (data not shown). An increase in centrifugation time to ensure that the vesicles are fully sedimented, again failed to show any binding of the $p47^{phox}$ PX domain.

The lipid sedimentation assays described so far involved the production of unilameller vesicles (SUV's), formed through lipid sonication. Multilameller vesicles (MLV's) produced through lipid vortexing are believed to sediment more efficiently, and therefore the use of MLV's parallel to the use of SUV's was also tested (adjustment 2 of the protocol, section 2.6.3), but again no binding was observed (data not shown). Further analysis of the protocol suggested that drying of the lipids under nitrogen may not have been sufficient enough to remove all traces of organic solvents, thereby affecting binding. A final experiment was carried out (adjustment 3 of the protocol, section 2.6.3) using the isolated $p47^{phox}$ PX domain, with concentrations of PA and PtdIns(3,4)P_2 increased to 10 %,

Figure 42: Binding of p47^{phox} proteins to liposomes. Binding of p47^{phox} proteins to PtdIns(3,4)P_2. 15 μM total protein was incubated with liposomes containing PC:PE:PS: PtdIns(3,4)P_2 (50:40:5:5), PC:PE:PS (50:40:5) and a negative control without PtdIns(3,4)P_2. PtdIns(3,4)P_2 indicated by an asterisk (*) was kindly donated by Roger Williams, MRC-LMB, Cambridge. The PH domain of the TAPP1 protein was used as a positive control. P and S indicate 'pellet' and 'supernatant' after centrifugation; respectively. Samples were analysed by SDS-PAGE and stained with the SimplyBlue SafeStain.

and with the lipids further dried in a freezdryer for 2 hrs after initial drying under nitrogen. However, even after all these modifications to the protocol described above, we still could not observe any evidence for an interaction between the $p47^{phox}$ PX domain and PtdIns(3,4)P_2 (Figure 43).

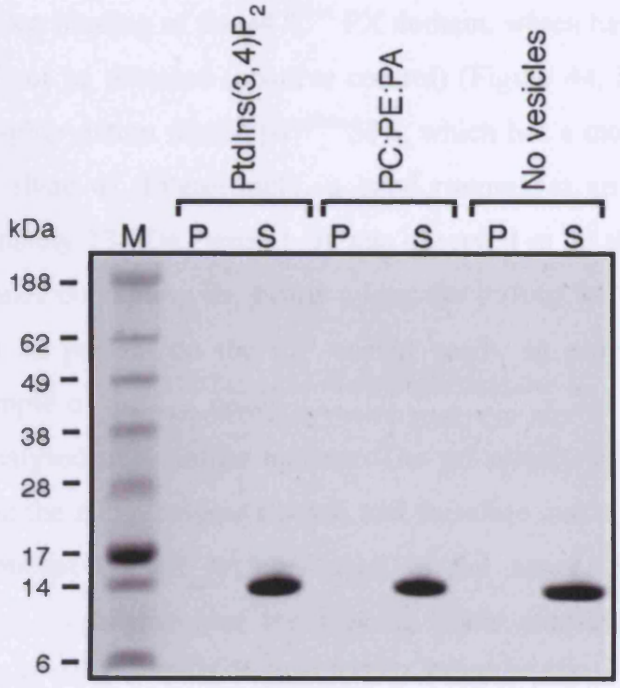

Figure 43: Binding of the p47^{phox} PX domain to liposomes. 15 μM protein was incubated with vesicles containing PC:PE:PA:PtdIns(3,4)P_2 (40:40:10:10), PC:PE:PA (40:40:10) and a control test minus the vesicles. Lipid samples were dried under nitrogen and further dried in a freedryer for 2 hrs. M: molecular weight marker (SeeBlue marker, Invitrogen). P and S indicate 'pellet' and 'supernatant' after centrifugation, respectively. Samples were analysed by SDS-PAGE and stained with SimplyBlue SafeStain.

3.3.2.2 PIP bead assay

After lipid sedimentation assays failed to show convincing binding to the positive controls $p47^{phox}$ PX domain and the TAPP1 PH domain, agarose beads coated with PtdIns(3,4)P_2 were used as an alternative method to detect protein-lipid interactions. However, binding of the $p47^{phox}$ PX domain, which has a molecular weight of 15.7 kDa could not be detected (positive control) (Figure 44, lane1). Similarly, no binding of the phosphorylation mimic $p47^{phox}$S5E, which has a molecular weight of 45 kDa was detected (lane 4). Interestingly, a band running at an apparent molecular weight of approximately 13 kDa (lanes 1-6) was observed in all the experiments apart from the control lanes containing the beads minus the PtdIns(3,4)P_2, suggesting that a contaminant might be present on the PIP coated beads. In order to investigate this further, a clean sample of the test beads was run on a Novex Bis-Tris SDS-PAGE gel (Figure 45) and analysed in a similar manner. The gel clearly shows that the 13 kDa protein is present in the manufacturer's beads and therefore, not a possible degradation product or contaminant of the proteins used in the assay. After contacting the manufacturer it was established that the agarose beads contained covalently linked streptavidin, which is used to bind PtdIns(3,4)P_2. Streptavidin is a tetrameric protein with a molecular weight of 52.8 kDa. Upon treatment of the beads with a denaturant such as SDS the tetramer is dissociated, releasing a steptavidin monomer with a molecular weight of 13.2 kDa, which corresponds exactly to the band observed.

The absence of binding of the $p47^{phox}$ PX domain to the PIP beads raised the question about the sensitivity of the assay. Although 5 μg of protein was used in each test of which approximately 1 μg was loaded onto the SDS gel, possibly only a fraction of the proteins may have bound to the PIP beads. If the affinity was weak then binding may have been too low to be detected using the SimplyBlue SafeStain. Although the manufacturer's protocol suggests that Coomasie staining can be used for protein visualization, we decided to measure the minimal amount of protein ($p47^{phox}$ full-length and the isolated $p47^{phox}$ PX domain) that can be detected with the SimplyBlue SafeStain.

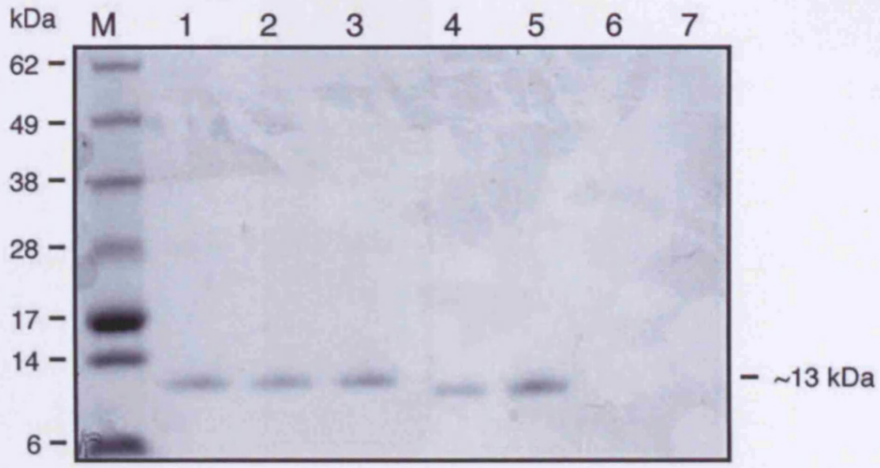

Figure 44: Binding of $p47^{phox}$ protein to PtdIns(3,4)P_2 coated PIP beads. A band is observed running at approximately 13 kDa for all the proteins (lanes 1-5) excluding the controls (lanes 6 and 7). 20 µl of samples were loaded per lane.

M: Molecular weight marker (SeeBlue marker, Invitrogen)

1: $p47^{phox}$ PX domain

2: $p47^{phox}$ full-length protein

3: $p47^{phox}$S3E (S359, 370 and 379E)

4: $p47^{phox}$S5E (S303, 304, 315, 320 and 328E)

5: $p47^{phox}$S8E (S303, 304, 315, 320, 328, 359, 370 and 379E)

6: Control beads plus the $p47^{phox}$ PX domain

7: Control beads plus the $p47^{phox}$ full-length wild-type protein

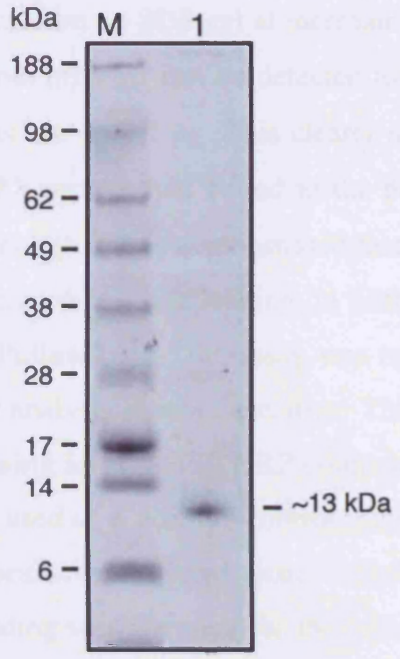

Figure 45: SDS-PAGE analysis of PtdIns(3,4)P_2 coated PIP beads. 20 µl of unused PtdIns(3,4)P_2 coated PIP beads were loaded onto a Novex Bis-Tris SDS gel. Lane 1: streptavidin monomer running at approximately 13 kDa. M: molecular weight marker (SeeBlue marker, Invitrogen).

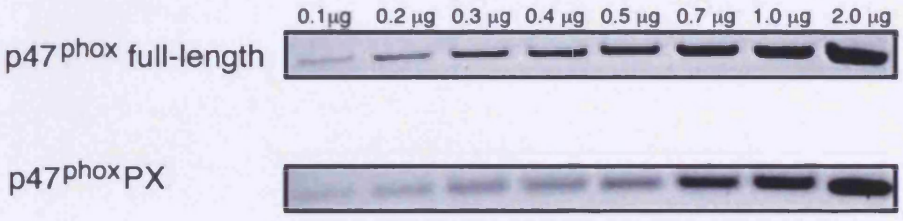

Figure 46: P47^{phox} full-length and p47^{phox} PX domain proteins at increasing concentrations. SDS-PAGE analysis shows that both proteins can be visualised at concentrations as low as 0.2 µg by using the SimplyBlue SafeStain.

The proteins were analysed on an SDS gel at increasing concentrations (0.1 μg - 2 μg). Figure 46 shows that both proteins can be detected using the SimplyBlue SafeStain at protein concentrations as low as 0.2 μg. This clearly indicates that even if only a tenth of the isolated $p47^{phox}$ PX protein had bound to the beads, then this would have been apparent on the gel. Although it was demonstrated that concentrations as low as 0.2 μg could be detected by SimplyBlue SafeStaining, to further investigate the binding of the $p47^{phox}$ proteins to the PtdIns(3,4)P_2, the assay was repeated and analysed by western blotting, as this form of analysis is more sensitive. The proteins were purified as GST-fusions and visualised using an anti-GST HRP-conjugated antibody. The PH domain of the TAPP1 protein was used as a positive control. Figure 47 clearly shows that the PH domain bound to the beads as expected (lane 6-upperband). By comparison, only a marginal amount of binding was apparent for the isolated $p47^{phox}$ PX domain (lane 1), where maximum binding should be observed and the phosphorylation mutant $p47^{phox}$S5E (lane 4), where intermediate binding should be observed. No binding was observed for the phosphorylation mimic $p47^{phox}$S8E. This experiment shows that this assay works well for the PH domain, which has a high affinity for PtdIns(3,4)P_2. However, it appears that the assay may not work well for proteins that have a lower affinity for lipids such as the $p47^{phox}$ proteins.

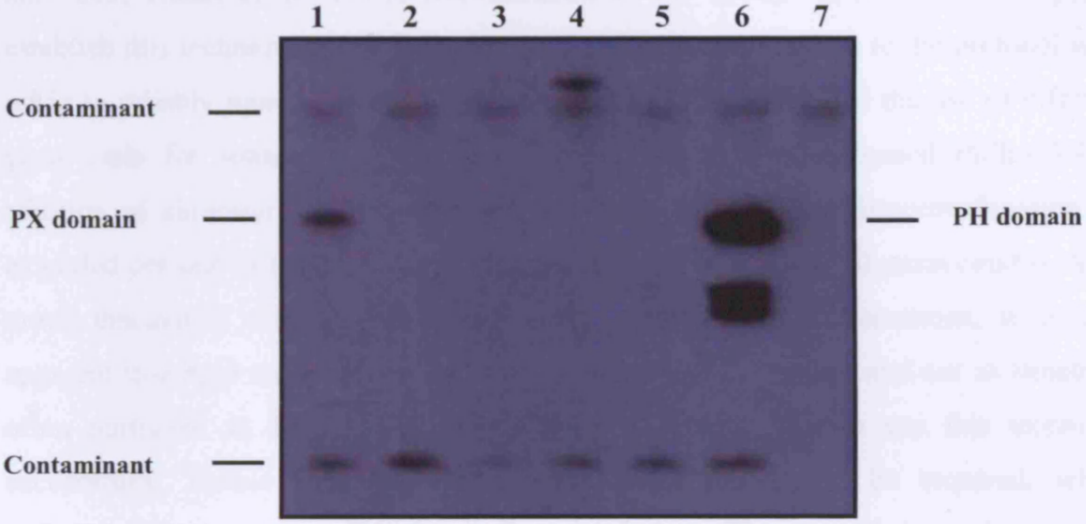

Figure 47: Western blot analysis of the binding of $p47^{phox}$ proteins to PtdIns(3,4)P_2 coated PIP beads.

1: $p47^{phox}$ PX domain
2: $p47^{phox}$ full-length wild-type
3: $p47^{phox}$S3E (S359, 370 and 379E)
4: $p47^{phox}$S5E (S303, 304, 315, 320 and 328E)
5: $p47^{phox}$S8E (S303, 304, 315, 320, 328, 359, 370 and 379E)
6: PH domain of TAPP1
7: Control beads containing the $p47^{phox}$ PX domain (minus PtdIns(3,4)P_2)

N.B. The PH domain of the TAPP1 protein is temperature sensitive and degrades after thawing on ice (lane 6, lower bands show the degraded protein).

3.3.3 Summary of lipid binding assays

This lipid sedimentation protocol has been used by a number of groups with minor modifications to study the interaction between $p47^{phox}$ and various lipids (Ago et al., 2003; Kanai et al., 2001; Karathanassis et al., 2002). After initial attempts to establish this technique proved unsuccessful, different adjustments to the protocol were made to reliably monitor protein-lipid interactions. These included the use of different glass vials for sonication, the use of protonated and un-protonated PtdIns(3,4)P_2, addition of cholesterol, production of SUV's and MLV's and ultracentrifugation for extended periods of time. Despite these changes the assays proved unsuccessful. After much discussion with experts in the field of protein-lipid interactions, it became apparent that lipid sedimentation assays are rather difficult to use and not as simple as often portrayed in the literature. This suggested to us that to use this technique successfully, further work to optimise the conditions would be required, which unfortunately was not possible due to time restrictions. The most likely explanation for the absence of protein in the pelleted fractions is that the vesicles may not have formed efficiently, possibly due to insufficient sonification or the presence of trace organic solvents. Alternatively, it is possible that binding did take place but that the vesicles did not sedimented efficiently, and would need to be made heavier, for example through the use of brominated lipids or the inclusion of sucrose into the vesicles.

Similarly, binding experiments using PtdIns(3,4)P_2 coated agarose beads also proved unsuccessful. Phosphoinositide coated agarose beads have been used previously to detect lipid binding to PH domains (Rao et al., 1999) but not to PX domains. In accordance, control experiments with the TAPP1 PH domain showed a clear interaction with the PIP beads. PH domains predominantly recognize the head group of phosphatidylinositols, and do not require additional lipids for this interaction. In contrast, the PX domain of $p47^{phox}$ has been suggested to require the presence of PA or PS for maximum binding to occur (Karathanassis et al., 2002). This may explain why only extremely weak binding was observed in these experiments, and indicates that this technique is not suitable to detect PX domain-lipid interactions.

3.4 Discussion

The activation and assembly of the NADPH oxidase is a complex process that is regulated by reversible protein-protein interactions, multiple phosphorylation events and association with membrane bound phospholipids. A central player in this regulatory network is the $p47^{phox}$ subunit, which is on one hand responsible for maintaining the trimeric $p40^{phox}$-$p67^{phox}$-$p47^{phox}$ complex cytosolic during the resting state, and on the other hand for translocating it to the membrane bound flavocytochrome after appropriate activation. To perform these tasks $p47^{phox}$ adopts two different conformations: a resting, auto-inhibited conformation and an active, open form. To switch between these two states, the protein undergoes a major conformational change that is induced by phosphorylation of eight serine residues (Ago et al., 1999; el Benna et al., 1994; El Benna et al., 1996; Faust et al., 1995; Groemping et al., 2003; Inanami et al., 1998; Johnson et al., 1998). Five of these serine residues, 303, 304, 315, 320 and 328, are found in the auto-inhibitory polybasic region, while S359, 370 and 379 are located in the extreme C-terminus adjacent to a proline-rich motif. Most studies have concentrated on the effect of phosphorylation events in the polybasic region of $p47^{phox}$ (Ago et al., 2003; Ago et al., 1999; Groemping et al., 2003; Inanami et al., 1998; Karathanassis et al., 2002), and little attention has been paid to the phosphorylation of those serine residues located adjacent to the proline-rich region. Here we investigated the effect of phosphorylation of serine residues 359, 370 and 379 on the interaction with $p22^{phox}$ and $p67^{phox}$ as well as on binding to phosphatidylinositols.

Unfortunately, it is not possible to produce $p47^{phox}$ that is specifically phosphorylated at a given position, as most kinases that phosphorylate $p47^{phox}$ do so on multiple serine residues. Furthermore, these phosphorylation events are often not stoichiometric, and result in a mixture of proteins with different degrees of phosphorylation at different residues, that cannot be separated by chromatographic methods. For this reason it was decided to substitute those serines that become phosphorylated by glutamate residues, which are similar in charge and conformation to a phosphoserine, and are often used as mimics of serine phosphorylation. The validity of such an approach is supported by a number of studies, that have shown that these kind of mutant $p47^{phox}$ proteins can induce activation of the NADPH oxidase (Ago et al., 1999; Groemping et al., 2003; Karathanassis et al., 2002).

3.4.1 C-terminal $p47^{phox}$ phosphorylation does not affect the interaction with $p22^{phox}$

The isolated tandem SH3 domains of $p47^{phox}$ ($p47^{phox}$Wild-$type_{tandem}$) are thought to represent the open, fully active conformation of $p47^{phox}$, which is able to interact with $p22^{phox}$ with high affinity (Groemping et al., 2003). Experiments to investigate the contribution of individual serine residues within the auto-inhibitory polybasic region to the activation process, has shown that a protein in which all five serine residues have been substituted by glutamates is able to bind to $p22^{phox}$. However, this interaction occurs 20-fold weaker than the interaction with the tandem SH3 domain construct (Groemping et al., 2003). This discrepancy in affinity suggests that this penta-phosphorylated mutant does not represent the fully active state of $p47^{phox}$. This could be simply due to glutamate residues not being ideal phosphorylation mimics. Alternatively though, it may suggest that phosphorylation of the C-terminal serine residues play a role in the activation process.

To investigate the latter possibility, it was first tested if the triple mutant $p47^{phox}$S3E, in which S359, 370 and 379 had been simultaneously substituted by glutamate residues, is able to interact with the $p22^{phox*}$ peptide. However, no binding was observed, clearly indicating that phosphorylation of the C-terminal serine residues is not sufficient to destabilise the auto-inhibited conformation of the protein. Next, to determine whether phosphorylation of the C-terminal serine residues acts in a synergistic fashion with serine residues within the polybasic region, binding measurements with a mutant that mimicks phosphorylation of all eight serine residues were performed. However, this mutant displayed a similar binding affinity as $p47^{phox}$S5E, which clearly shows that phosphorylation of the $p47^{phox}$ C-terminal region does not contribute to the interaction with $p22^{phox}$. Therefore, the difference in binding affinity for $p22^{phox}$ between $p47^{phox}$S5E and $p47^{phox}$Wild-$type_{tandem}$, is most likely due to the fact that glutamate residues are not fully effective in mimicking phosphorylation. This interpretation is further supported by the CD spectroscopy data, which show that $p47^{phox}$S5E and $p47^{phox}$S8E unfolded/precipitated at lower temperatures than $p47^{phox}$S3E, which behaved similar to the wild-type protein. This suggests that phosphorylation of the polybasic region has a destabilising effect on the protein, that is not replicated or increased by phosphorylation of the C-terminal serine residues.

3.4.2 C-terminal $p47^{phox}$ phosphorylation weakens the interactions with $p67^{phox}$

The results from section 3.1 have clearly shown that phosphorylation of the C-terminal serine residues (S359, 370 and 379) does not contribute to the formation of active $p47^{phox}$. However, their location within the $p67^{phox}$-binding region (Kami et al., 2002) suggests another function: the regulation of complex formation with $p67^{phox}$. To investigate this possibility, the relevant phosphorylation mimics were used to quantify the interaction with $p67^{phox}$ by ITC. Most of the binding measurements were carried out using the isolated $p67^{phox}(SH3)_B$ domain instead of the full-length protein, as this fragment is more stable and hence better suited for ITC experiments. This is a valid approach as other studies (Lapouge et al., 2002) as well as control experiments carried out in this work, have shown that the interaction between $p47^{phox}$ and $p67^{phox}$ only requires the second SH3 domain of the latter, for the formation of a tight complex.

Substitution of the individual serine residues only showed a significant effect on complex formation in the case of $p47^{phox}$S379E, which reduced the affinity for $p67^{phox}$ 26-fold. This observation can be rationalised by the recently solved NMR structure of $p67^{phox}(SH3)_B$ in complex with the C-terminal region of $p47^{phox}$, which shows that S359 and S370 are solvent exposed and do not form part of the binding interface (Kami et al., 2002) (Figure 48, A). Thus, phosphorylation would not be expected to directly affect the protein-peptide interface. In contrast, the hydroxyl group of S379 forms a hydrogen bond with the carboxyl group of glutamate 496. This thereby stabilises the complex and suggests that introduction of a negatively charged phosphate group at this position would lead to charge repulsion, and steric clashes (Figure 48, B). Interestingly, despite the absence of a significant reduction in binding affinity for the individual phosphorylation mimics $p47^{phox}$S359E and $p47^{phox}$S370E, the simultaneous phosphorylation of both residues ($p47^{phox}$S359/370E) weakened the interaction 12-fold. At present the reason for this is not clear, and we can only speculate that the sum of two negatively charged residues may induce conformational changes in this region, and thereby interfere with complex formation. A similar observation was made with the construct in which all three serine residues were substituted simultaneously ($p47^{phox}$S3E). This further supports the notion that simultaneous phosphorylation of S359 or S370 may alter the conformation of $p47^{phox}$, and

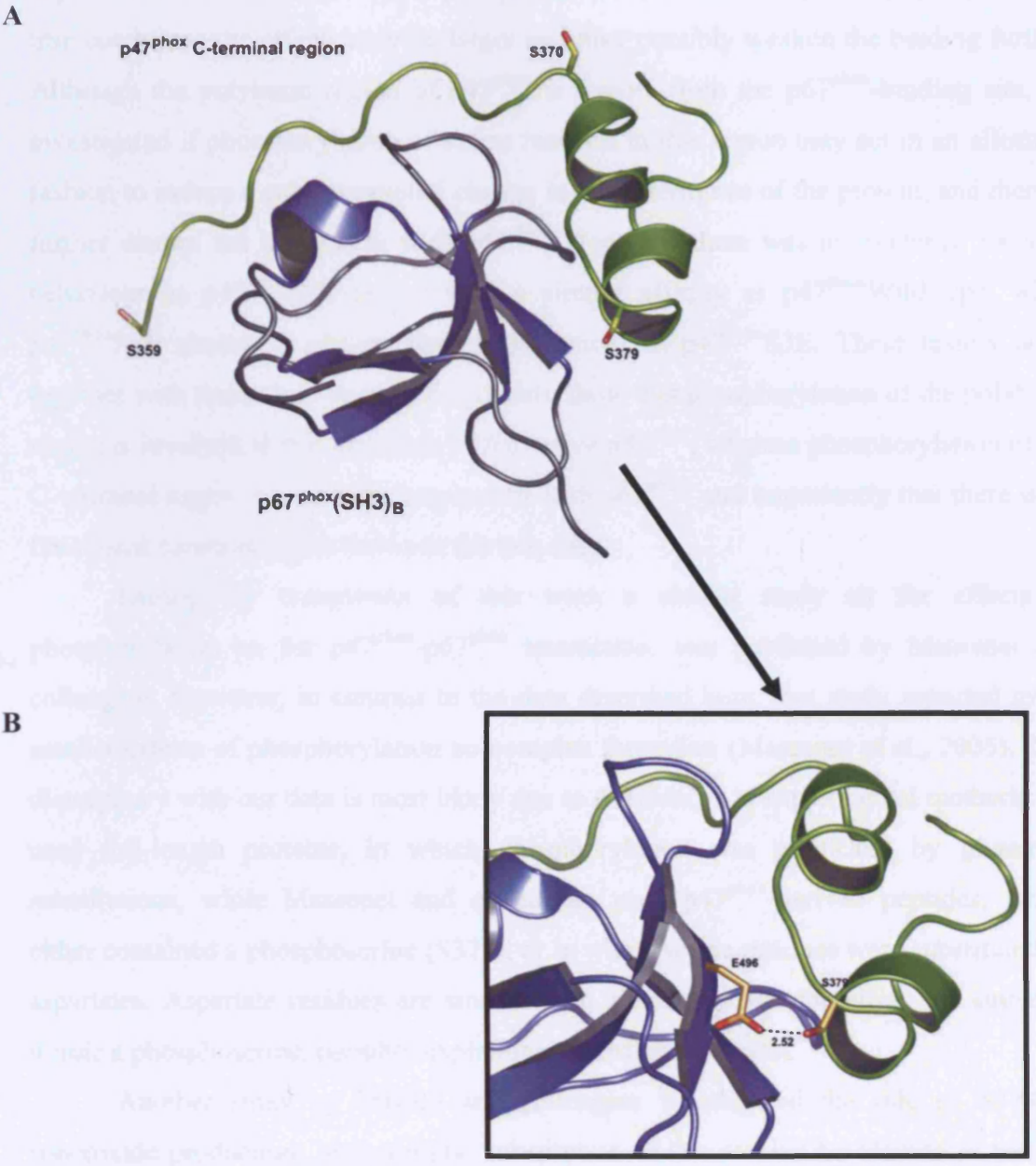

Figure 48: **The C-terminal region of $p47^{phox}$ interacts with $p67^{phox}(SH3)_B$.** A. $P67^{phox}(SH3)_B$ is shown in blue and the C-terminal region of the $p47^{phox}$ in green. Phosphorylation sites (S359, 370 and 379) are shown as yellow sticks. B. A magnification of the hydrogen bond interaction between S379 ($p47^{phox}$) and E496 ($p67^{phox}$). The hydrogen bond distance is in Å. PDB identifier 1K4U (Kami et al., 2002).

thus enhances the effect of a phosphoserine at position 379. Furthermore, it has to be kept in mind that in these studies phosphoserines have been mimicked, and that under true conditions the effects may be larger and may possibly weaken the binding further. Although the polybasic region of $p47^{phox}$ is remote from the $p67^{phox}$-binding site, we investigated if phosphorylation of serine residues in this region may act in an allosteric fashion to induce a conformational change in the C-terminus of the protein, and thereby further disrupt the interaction with $p67^{phox}$. However, there was no evidence for such behaviour as $p47^{phox}$S5E bound with a similar affinity as $p47^{phox}$Wild-type, while $p47^{phox}$S8E showed a similar binding behaviour to $p47^{phox}$S3E. These results taken together with those from section 3.1, clearly show that phosphorylation of the polybasic region is involved in the formation of the active $p47^{phox}$, whereas phosphorylation of the C-terminal region weakens the interaction with $p67^{phox}$, and importantly that there is no functional communication between the two sites.

During the completion of this work a similar study on the effects of phosphorylation on the $p47^{phox}$-$p67^{phox}$ interaction, was published by Massenet and colleagues. However, in contrast to the data described here, that study reported much smaller effects of phosphorylation on complex formation (Massenet et al., 2005). This discrepancy with our data is most likely due to differences in experimental methods: we used full-length proteins, in which phosphorylation was mimicked by glutamate substitutions, while Massenet and colleagues used $p47^{phox}$-derived peptides, which either contained a phosphoserine (S379), or in which serine residues were substituted by aspartates. Aspartate residues are smaller than glutamates and therefore less suited to mimic a phosphoserine, possibly explaining the different results.

Another study by Mizuki and colleagues investigated the role of S379 in superoxide production. Interestingly, substitution of this residue by alanine as well as glutamate severely reduced superoxide production (Mizuki et al., 2005). This observation supports the important role of Ser379 in complex formation with $p67^{phox}$. It shows that disruption of the $Ser379_{p47}$-$E496_{p67}$ hydrogen bond, either by removal of the serine side chain or its phosphorylation, severely interferes with superoxide production thus consistent with our data. This is most likely due to interference with translocation of $p67^{phox}$ to the membrane.

3.4.3 Possible model for phosphorylation-induced changes in NADPH oxidase assembly

Many researchers believe that during the inactive state of the NADPH oxidase some $p47^{phox}$ exists in complex with $p67^{phox}$ and $p40^{phox}$ as a tight hetero-trimer (Park et al., 1992; Someya et al., 1993; Wientjes et al., 1993), where the C-terminal region of $p47^{phox}$ is bound to $p67^{phox}$ (Finan et al., 1994; Kami et al., 2002; Lapouge et al., 2002). However, more recently this model has been challenged, when it was reported that only $p67^{phox}$ and $p40^{phox}$ exist in a complex, and that $p47^{phox}$ associates at a later stage with this dimer in what could be seen as the first step in the activation process (Brown et al., 2003) (refer to section 1.3.2. for further details). This observation is rather surprising, given that in their un-phosphorylated forms, $p47^{phox}$ and $p67^{phox}$ interact tightly with an affinity of 20 nM (Lapouge et al., 2002). In order to explain this observation, additional proteins or ligands or possibly posttranslational modifications that interfere with complex formation would be required. The results presented from our current study are extremely interesting in light of these developments, and may help reconcile the conflicting data that are currently in the literature. In the resting state, the C-terminal region of $p47^{phox}$ may have a basal level of phosphorylation that interferes with the interaction with $p67^{phox}$. This may occur either directly or possibly due to the recruitment of another protein, that specifically binds the phosphorylated form. De-phosphorylation of $p47^{phox}$ by an as yet unknown phosphatase would then constitute the first step in the activation of the NADPH oxidase, and allow the formation of the $p47^{phox}$-$p67^{phox}$-$p40^{phox}$ complex. This process may then be followed by phosphorylation of the remaining serine residues to form the active form of $p47^{phox}$, and induce translocation to the membrane where it binds to $p22^{phox}$. This in turn may bring $p67^{phox}$ into close proximity to $gp91^{phox}$ and its binding partner Rac, to activate the production of superoxide radicals.

Such a role for phosphorylation of S359, 370 and 379 seems more likely than the model suggested by Babior and co-workers, in which phosphorylation of S359 and 370 preceeds all other phosphorylation events. It was suggested that this leads to translocation of the cytoplasmic complex to the membrane, where phosphorylation of the remaining serine residues would occur (Johnson et al., 1998). This model is at odds with all the available structural and biochemical data on phosphorylation induced changes in the conformation of $p47^{phox}$ and is very difficult to rationalize at present.

CHAPTER FOUR

4.0 The superSH3 domain as a novel protein-protein interaction module

The tandem SH3 domains of $p47^{phox}$ ($SH3_A$ and $SH3_B$) work in coordination to form a single ligand binding site of high affinity, for either the $p47^{phox}$ polybasic region or $p22^{phox}$ (Groemping et al., 2003; Yuzawa et al., 2004a; Yuzawa et al., 2004b). This conformation is known as the superSH3 domain and has been proposed to be a general, novel protein-protein interaction module (Groemping et al., 2003). The correct positioning of $SH3_A$ and $SH3_B$ with respect to one another within the superSH3 domain is important for the formation of a high affinity ligand binding surface. The formation of the $p47^{phox}$ superSH3 domain is dependent on two structural features, the covalent linker connecting the two SH3 domains and a conserved 'GWW' motif located in each n-Src loop and adjoining β-strands βC. This region is where the two SH3 domains are closest and make contacts across the domain interface (Groemping et al., 2003). There are a number of proteins in the SMART nrdb (http://smart.embl-heidelberg.de/) that contain multiple SH3 domains harbouring 'GWW' motifs. So far, none of these proteins have been specifically tested for their ability to form a superSH3 domain. Nevertheless, for at least two of these proteins, FISH and CIN85, biochemical data have been published that suggest that adjacent SH3 domains in these proteins do cooperate in some form for ligand binding (Abram et al., 2003; Kowanetz et al., 2003). These observations support the proposal that the superSH3 domain may indeed be a novel signal transduction module.

This chapter describes experiments designed to better understand the structural features that allow a pair of adjacent SH3 domains to cooperate in a stable fashion and form a superSH3domain.

4.1 Sequence requirements of the linker for the formation of the superSH3 domain

4.1.1 Overview and aims

It has previously been shown by our group that the covalent linker between $SH3_A$ and $SH3_B$ ($_{213}$LDSPDETEDPEPNYA$_{227}$) is absolutely essential for the formation of the superSH3 domain, as no interaction between the two individual domains is detected in free solution (Groemping et al., 2003). Furthermore, this linker makes a number of hydrogen bonds with the remainder of the protein in the auto-inhibited state that are believed to be important for the structural integrity of this conformation. Some of these interactions are made by backbone carbonyls and amide groups in the linker, whilst others are made by the carbonyls of the side-chains of E218, E220 and D221, and may hence provide specificity to the formation of the superSH3 domain. Other linker features that could be important for correctly orientating the SH3 domains for the interaction with their ligands are the specific length of the linker (15 amino acids), and the presence of three proline residues at positions 216, 222 and 224 that could provide a certain degree of structural constraint.

An understanding of the contribution of these linker features to the formation and stabilisation of the $p47^{phox}$ superSH3 domain, would not only be useful for a better general understanding of this novel structural arrangement, but may also help to predict which proteins may behave in a similar fashion. Therefore, this study was aimed at describing how strict the structural requirements are in the context of linker length, flexibility and composition for the formation of the superSH3 domain in the auto-inhibited and active states of $p47^{phox}$.

4.1.2 Results

In order to determine the importance of specific hydrogen bonds between the linker and the two SH3 domains, the hydrogen bond-forming residues E218, E220 and D221 were substituted by alanine (pGEX-$p47^{phox}$E218A, pGEX-$p47^{phox}$E220A and pGEX-$p47^{phox}$D221A) using site-directed mutagenesis. In addition, a triple mutant containing all three substitutions was constructed (pGEX-$p47^{phox}$D/E3A) (refer to

Figure 20 for interactions made by these residues). To investigate the effect of linker length on the superSH3 domain, the length was decreased by removing amino acid A227 (pGEX-p47^{phox}A1^{-}), and increased by the addition of one (pGEX-p47^{phox}A1^{+}) or two (pGEX-p47^{phox}A2^{+}) alanine residues adjacent to A227. Flexibility of the linker was increased by substituting P216, P222 and P224 with alanine residues, to make the triple mutant pGEX-p47^{phox}3PA. All of these mutations were introduced in the tandem SH3 domains (aa 156-285), hereafter designated as e.g. p47^{phox}3PA$_{tandem}$. The mutant proteins were tested in two different contexts: i) their interaction with the p47^{phox} 35-mer peptide derived from the polybasic region, representing the auto-inhibited state and ii) their interaction with a p22^{phox}-derived peptide (hereafter called p22^{phox} peptide), representing the active state. Furthermore, the two triple mutations, pGEX-p47^{phox}D/E3A and pGEX-p47^{phox}3PA, were introduced into the construct representing the auto-inhibited core, comprising the tandem SH3 domains plus the polybasic region (aa 156-340), hereafter designated as p47^{phox}D/E3A$_{auto}$ and p47^{phox}3PA$_{auto}$. These constructs were used to test whether increasing linker flexibility, or removal of stabilising hydrogen bonds could destabilise the auto-inhibited conformation, but still allow binding to the p22^{phox} peptide (representing the active state).

ITC studies were performed to determine the binding affinities and thermodynamic parameters of complex formation. In addition, circular dichroism (CD) spectroscopy was used to determine if the mutations introduced any changes to the secondary structure of the mutant proteins. Furthermore, the thermal stability of those mutant proteins that showed the largest changes in binding affinity was determined by CD spectroscopy, to ensure that a reduction in binding is not due to increased instability of the proteins under investigation. The methods for these techniques are fully described in chapter 2 of the Materials and Methods section.

4.1.2.1 Expression and purification of p47^{phox}D/E3A$_{auto}$ and p47^{phox}3PA$_{auto}$

The auto-inhibited core construct containing the triple D/E to A mutations (p47^{phox}D/E3A$_{auto}$) was grown and expressed under standard conditions (see Materials and Methods). Although the protein was highly over-expressed, purification proved unsuccessful as the majority of the protein was insoluble (Figure 49A, lane 1). Growth and induction conditions were varied in an attempt to obtain soluble material. However, slower cell growth in LB media as apposed to TB, and growth and protein induction at

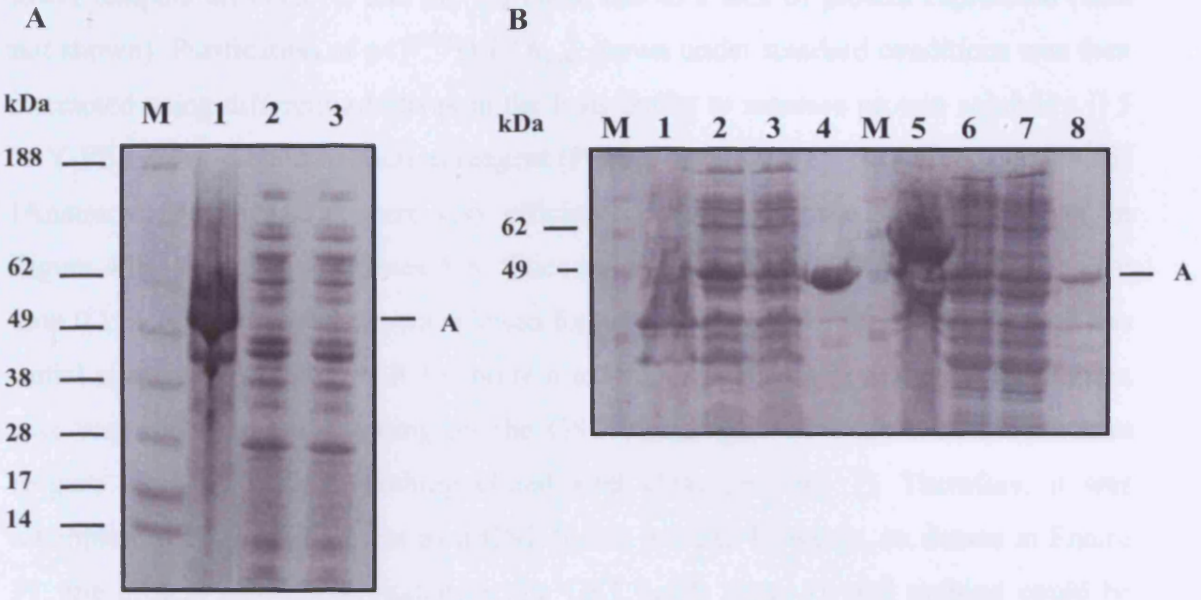

Figure 49: **Expression and purification of $p47^{phox}D/E3A_{auto}$.**

A: Purification using standard lysis buffer

M: Molecular weight marker (SeeBlue marker, Invitrogen)
1: Pellet
2: Supernatant
3: Flow through

B: Solubilisation of $p47^{phox}D/E3A_{auto}$ using standard lysis buffer plus 5 % Y-PER or 0.1 % BOG

M: Molecular weight marker (SeeBlue marker, Invitrogen)
1: Pellet
2: Supernatant
3: Flow through
4: GST beads

5 % Y-PER

5: Pellet
6: Supernatant
7: Flow through
8: GST beads

0.1 % BOG

A: $p47^{phox}D/E3A_{auto}$ (47.1 kDa)

lower temperatures (16 °C and 20 °C) failed due to a lack of protein expression (data not shown). Purification of $p47^{phox}D/E3A_{auto}$ grown under standard conditions was then attempted using different additives in the lysis buffer to increase protein solubility i) 5 % Y-PER yeast protein extraction reagent (Pierce) or ii) 0.1 % β-octylglucoside (BOG) (Anatrace). Both reagents were very efficient in solubilising the protein as shown in Figure 49B, lanes 1-4 and lanes 5-8. Since the use of 5 % Y-PER was more effective than 0.1 % BOG, this reagent was chosen for subsequent purification trials. Despite this initial success in using Y-PER for protein extraction, the untagged protein in solution was very unstable, precipitating on the GST beads upon cleavage with 3C-protease (Figure 50, lane 8) with nothing eluted after cleavage (lane 7). Therefore, it was attempted to purify the mutant as a GST-fusion protein. However, as shown in Figure 51, the protein again precipitated on the GST beads (lane 8), and nothing could be eluted with 15 mM reduced glutathione (lane 7). Similar results were observed with the use of 0.1 % BOG (data not shown).

Unfortunately, the auto-inhibited core construct containing the triple proline mutations ($p47^{phox}3PA_{auto}$), behaved in a similar manner and purification was also unsuccessful despite similar optimisation and solubilisation attempts (data not shown). Based on the insolubility of these auto-inhibited core region proteins, no attempt was made to make a linker length mutant in this construct as similar results were anticipated. Overall, these results show that increasing the linker flexibility and removing the stabilising hydrogen bonds has a detrimental effect on the stability and most likely the folding of the superSH3 domain in the auto-inhibited state.

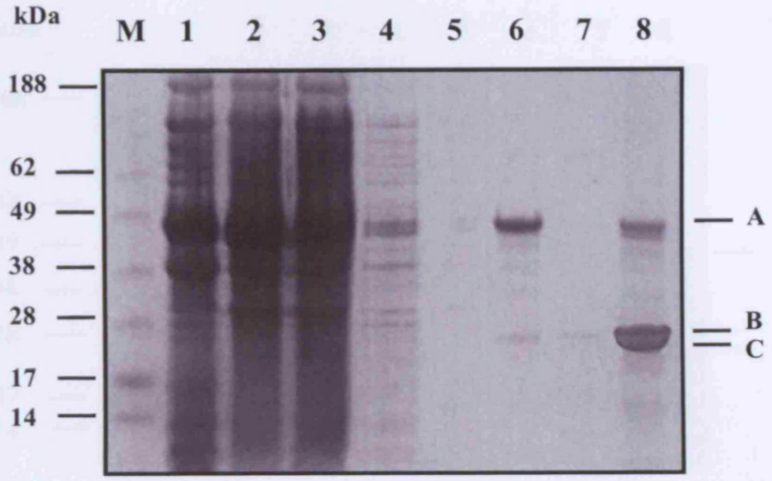

Figure 50: **Purification of $p47^{phox}D/E3A_{auto}$ using 5 % Y-per and cleavage with 3C protease.**

M: Molecular weight marker (SeeBlue marker, Invitrogen)

1: Pellet

2: Supernatant

3: Flow through

4: Wash with high salt buffer B

5: Wash with low salt buffer C

6: GST beads before 3C protease cleavage

7: Elution after cleavage

8: GST beads after overnight cleavage

A: **$p47^{phox}D/E3A_{auto}$-GST fusion (47.1 kDa)**

B: **GST (26 kDa)**

C: **$p47^{phox}D/E3A_{auto}$ (21.6 kDa)**

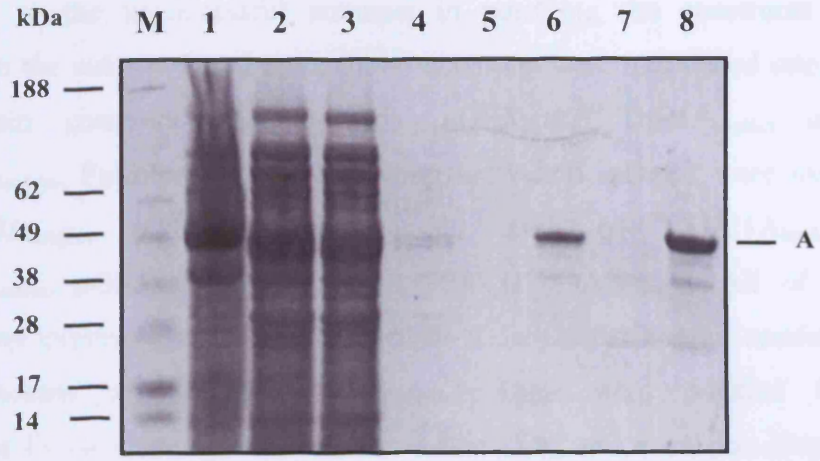

Figure 51: Purification of p47^{phox}D/E3A$_{auto}$ as a GST-fusion.

M: Molecular weight marker (SeeBlue marker, Invitrogen)

1: Pellet

2: Supernatant

3: Flow through

4: Wash with high salt buffer B (pH 7.5)

5: Wash with low salt buffer C (pH 7.5)

6: GST beads before elution with 15 mM reduced glutathione

7: Elution with 15 mM reduced glutathione

8: GST beads after elution

A: p47^{phox}D/E3A$_{auto}$ GST-fusion (47.1 kDa)

4.1.2.2 Expression and purification of $p47^{phox}$ linker mutants in the tandem SH3 domains

Due to the unsuccessful attempts in purifying the constructs with triple mutations in the auto-inhibited core, these mutations were introduced into the tandem SH3 domain construct (aa 156-285): pGEX-$p47^{phox}$D/E3A$_{tandem}$ and pGEX-$p47^{phox}$3PA$_{tandem}$. Furthermore, the following individual mutants were made: pGEX-$p47^{phox}$E218A$_{tandem}$, pGEX-$p47^{phox}$E220A$_{tandem}$, pGEX-$p47^{phox}$D221A$_{tandem}$, pGEX-$p47^{phox}$A1$^{-}_{tandem}$, pGEX-$p47^{phox}$A1$^{+}_{tandem}$, pGEX-$p47^{phox}$A2$^{+}_{tandem}$. All of the mutant proteins were expressed in a soluble form in *E.coli*, under similar conditions and in similar amounts as $p47^{phox}$Wild-type$_{tandem}$. They were purified by affinity chromatography on glutathione sepharose, followed by size exclusion chromatography after protease cleavage of the GST-tag. Figures 52A and 52B show the purity of the different mutant proteins used for the ITC experiments as determined by SDS-PAGE. All the proteins ran as single bands at their expected molecular weights (15.2 kDa - 15.5 kDa) and could be easily concentrated to 500 μM- 1mM. The identities of the purified proteins were confirmed by electrospray mass spectrometry.

CD spectroscopy showed that the mutations did not affect the secondary structure of the proteins. Figure 53 shows a typical CD spectrum for $p47^{phox}$E218A$_{tandem}$, which is similar to that of $p47^{phox}$Wild-type$_{tandem}$. The secondary structure content of $p47^{phox}$E218A$_{tandem}$ is listed in Table 14 and is similar to $p47^{phox}$Wild-type$_{tandem}$ (Sreerama and Woody, 2000) (refer to Appendix: A6 for the spectra of the other mutant proteins). In addition, the thermal stability of $p47^{phox}$D/E3A$_{tandem}$, $p47^{phox}$E218A$_{tandem}$ and $p47^{phox}$3PA$_{tandem}$ was checked by CD spectroscopy, which showed that the insertion of these mutations did not affect the structural integrity of the resulting proteins (also in Appendix: A6).

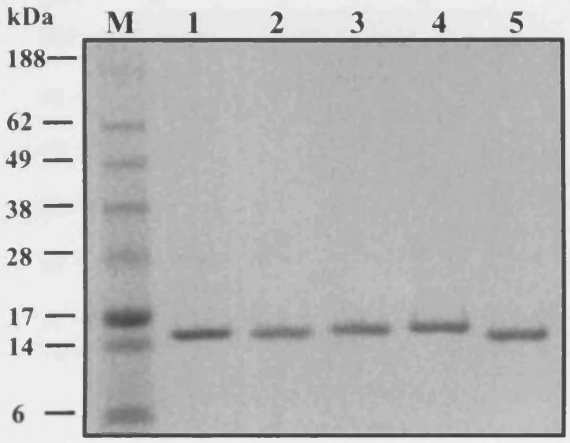

Figure 52A: SDS-PAGE gel of $p47^{phox}$ linker mutants in the tandem SH3 domains. Analysis of the purity of the $p47^{phox}$ linker proteins used for the ITC experiments. 3-5 μg were loaded and a single band is observed at the corresponding molecular weights.

M:	Molecular weight marker (SeeBlue marker, Invitrogen)	
1:	$p47^{phox}$Wild-type$_{tandem}$	(15.4 kDa)
2:	$p47^{phox}$A1$^{-}_{tandem}$	(15.3 kDa)
3:	$p47^{phox}$A1$^{+}_{tandem}$	(15.5 kDa)
4:	$p47^{phox}$A2$^{+}_{tandem}$	(15.5 kDa)
5:	$p47^{phox}$3PA$_{tandem}$	(15.3 kDa)

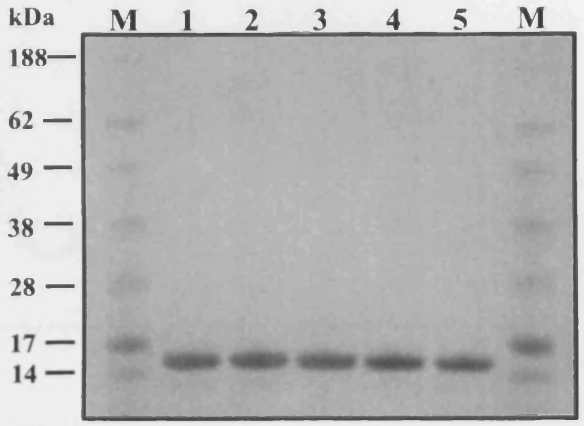

Figure 52B: SDS-PAGE gel of $p47^{phox}$ linker mutants in the tandem SH3 domains. Analysis of the purity of the $p47^{phox}$ linker proteins used for the ITC experiments. 3-5 µg were loaded and a single band is observed at the corresponding molecular weights.

M:	Molecular weight marker (SeeBlue marker, Invitrogen)	
1:	$p47^{phox}$ Wild-type$_{tandem}$	(15.4 kDa)
2:	$p47^{phox}$E218A$_{tandem}$	(15.3 kDa)
3:	$p47^{phox}$E220A$_{tandem}$	(15.3 kDa)
4:	$p47^{phox}$D221A$_{tandem}$	(15.4 kDa)
5:	$p47^{phox}$D/E3A$_{tandem}$	(15.2 kDa)

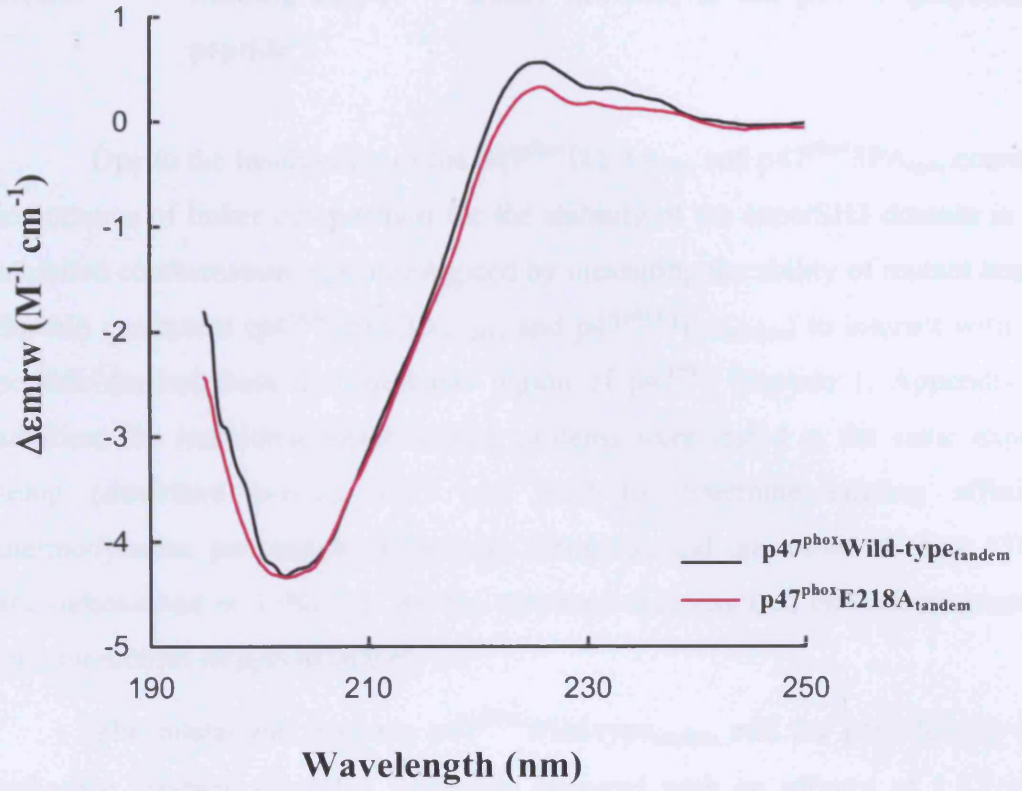

Figure 53: **CD spectra of p47^{phox}Wild-type$_{tandem}$ and p47^{phox}E218A$_{tandem}$.** Far-UV CD spectra of p47^{phox}Wild-type$_{tandem}$ and p47^{phox}E218A$_{tandem}$ (aa 156-285). The protein concentration was 0.15 mg/ml, and the experiments were carried out in buffer H.

Table 14: **Secondary structure analysis of the CD spectra of p47^{phox}Wild-type$_{tandem}$ and p47^{phox}E218A$_{tandem}$.** Comparison of the secondary structure content of p47^{phox}Wild-type$_{tandem}$ (WT) and p47^{phox}E218A$_{tandem}$ (E218E), as calculated using the programs CONTIN, SELCON and CDSSTR (Sreerama and Woody, 2000).

Program	α-helix (%)		β-sheet (%)		Turn (%)		Random (%)	
	WT	E218A	WT	E218A	WT	E218A	WT	E218A
CONTIN	6.1	6.3	41.5	34.9	26.6	22.6	25.8	36.2
SELCON	7.3	5.2	38.9	34.4	26.5	22.7	27.3	37.7
CDSSTR	6.9	7.6	40.6	32.9	26.2	23.1	26.3	36.4

4.1.2.3 Binding of $p47^{phox}$ linker mutants to the $p47^{phox}$ polybasic region peptide

Due to the insolubility of the $p47^{phox}D/E3A_{auto}$ and $p47^{phox}3PA_{auto}$ constructs, the importance of linker composition for the stability of the superSH3 domain in the auto-inhibited conformation was investigated by measuring the ability of mutant tandem SH3 domain constructs ($p47^{phox}D/E3A_{tandem}$ and $p47^{phox}3PA_{tandem}$) to interact with a 35-mer peptide derived from the polybasic region of $p47^{phox}$ (peptide 1, Appendix: A4). In addition, the individual linker mutant proteins were tested in the same experimental setup (described below). ITC was used to determine binding affinities and thermodynamic parameters of complex formation and the results of these ITC studies are summarised in Table 15. All the titrations demonstrated exothermic reactions and stoichiometries of approximately 1:1.

The interaction between $p47^{phox}Wild\text{-}type_{tandem}$ and the peptide was used as a reference titration. Complex formation occurred with an affinity of 1.12 μM and a binding enthalpy of -17.8 kcal/mol, which is in close agreement with data previously reported by our group (Groemping et al., 2003) (Table 15). ITC experiments with the individual hydrogen bond forming mutants $p47^{phox}E220A_{tandem}$ and $p47^{phox}D221A_{tandem}$ gave K_d values of 3.12 μM and 2.69 μM, respectively, which are only ~ 2-fold weaker than $p47^{phox}Wild\text{-}type_{tandem}$. $P47^{phox}E218A_{tandem}$ showed the most significant change of all the individual mutant proteins with a reduction in affinity to 5.76 μM, approximately 5-fold weaker than $p47^{phox}Wild\text{-}type_{tandem}$. Surprisingly though, the simultaneous replacement of all three residues ($p47^{phox}D/E3A_{tandem}$) did not reduce the binding affinity any further (5.76 μM). This suggests that slight structural arrangements may take place in this mutant protein, that could allow the formation of other compensating interactions.

The replacement of three proline residues in the linker ($p47^{phox}3PA_{tandem}$) had a similarly minor effect on complex formation with the polybasic peptide (2.0 μM), just as the shortening or lengthening of the linker. $P47^{phox}A1^{-}_{tandem}$, $p47^{phox}A1^{+}_{tandem}$ and $p47^{phox}A2^{+}_{tandem}$ bound with K_d values of 2.81 μM, 1.62 μM and 3.32 μM, respectively, which is only 2-3-fold weaker than $p47^{phox}Wild\text{-}type_{tandem}$. A typical titration curve for complex formation between $p47^{phox}A1^{-}_{tandem}$ and the polybasic peptide is shown in Figure 54, and the thermodynamic parameters are listed in Table 15.

Table 15: Binding affinities and thermodynamic parameters for titration of the $p47^{phox}$ linker mutants with the $p47^{phox}$ polybasic region peptide.

Protein	K_d (μM)	ΔH (kcal/mol)	TΔS (kcal/mol)	ΔG (kcal/mol)
$p47^{phox}$ Wild-type$_{tandem}$	1.12 ± 0.07	-17.8 ± 0.56	-9.86 ± 0.5	-7.95 ± 0.1
$p47^{phox}$ E218A$_{tandem}$	5.76 ± 0.2	-17.1 ± 1.0	-10.1 ± 0.71	-6.99 ± 0.09
$p47^{phox}$ E220A$_{tandem}$	3.12 ± 0.65	-19.1 ± 0.55	-11.8 ± 0.5	-7.34 ± 0.05
$p47^{phox}$ D221A$_{tandem}$	2.69 ± 0.75	-14.5 ± 0.05	-7.03 ± 0.35	-7.45 ± 0.39
$p47^{phox}$ D/E3A$_{tandem}$	5.76 ± 0.05	-15.5 ± 0.15	-8.54 ± 0.15	-6.99 ± 0.15
$p47^{phox}$ A1$^{-}_{tandem}$	2.81 ± 0.15	-11.3 ± 0.65	-3.86 ± 0.3	-7.4 ± 0.09
$p47^{phox}$ A1$^{+}_{tandem}$	1.62 ± 0.12	-12.1 ± 0.09	-4.36 ± 0.05	-7.73 ± 0.03
$p47^{phox}$ A2$^{+}_{tandem}$	3.32 ± 0.2	-11.9 ± 0.2	-4.59 ± 0.09	-7.31 ± 0.08
$p47^{phox}$ 3PA$_{tandem}$	2.0 ± 0.03	-12.3 ± 0.1	-4.69 ± 0.1	-7.6 ± 0.02

ITC experiments were performed in buffer H (pH according to the individual proteins, and to one unit above or below the pI) at 18 °C. Proteins in the cell (aa 156-285) were used at concentrations in the range of 27-43 μM. The $p47^{phox}$ 35-mer polybasic region peptide was titrated at concentrations of 250-400 μM. Values are the mean of at least three independent experiments. The errors (±) are the standard deviation of the mean. The binding stoichiometry values (n) ranged from 0.9-1.1. As discussed in the previous tables, these errors are small due to good reproducibility of the system. However, it seems more appropriate to assume an error of around 10 % derived from pipetting errors during protein concentration determination.

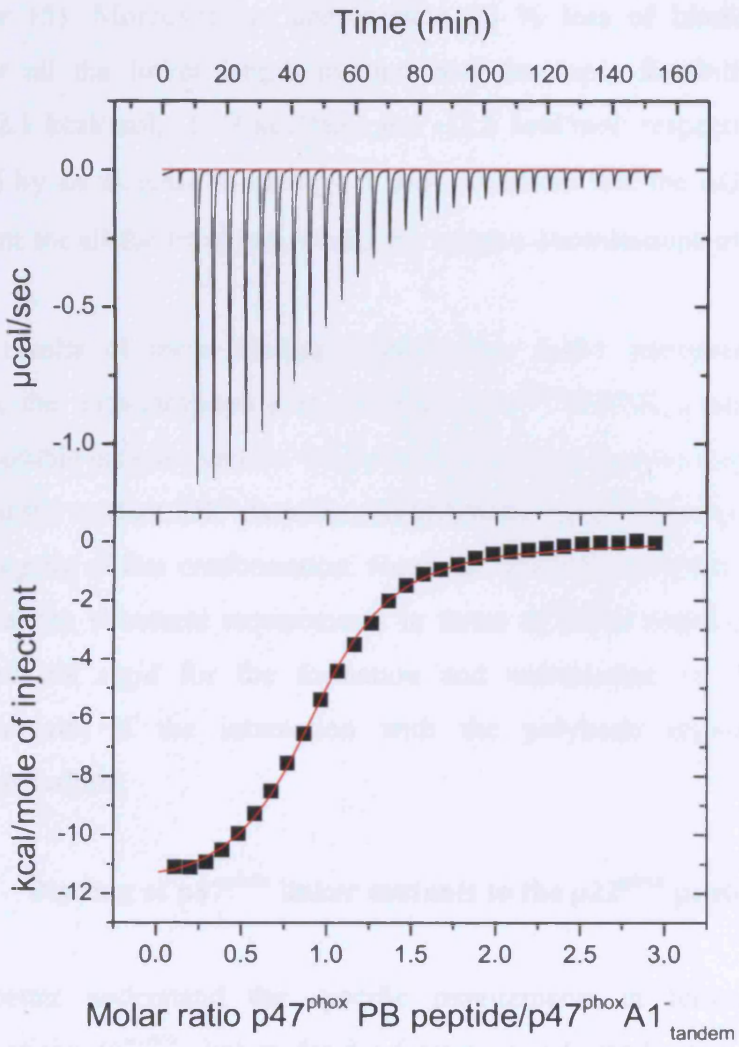

Figure 54: Characterisation of the interaction between the $p47^{phox}$ 35-mer polybasic peptide and $p47^{phox}A1^{-}_{tandem}$. The upper plot shows the raw data for the titration of the polybasic peptide (351 µM) into $p47^{phox}A1^{-}_{tandem}$ (27 µM). The lower plot shows the isotherm after subtraction of the heats of dilution. The data were fitted to a single-site binding model. Experiments were carried out in buffer H at 18 °C.

Interestingly, in spite of only minor changes in affinity and hence in free energy (ΔG), pronounced changes in the relative contributions of ΔH and $T\Delta S$ were observed, particularly for $p47^{phox}E220A_{tandem}$. Substitution of glutamate 220 resulted in a gain in binding enthalpy, with a compensating less favourable change in the $T\Delta S$ value (Table 15). Moreover, an approximate 30 % loss of binding enthalpy was observed for all the linker length mutants and the triple flexibility mutant (-11.3 kcal/mol, -12.1 kcal/mol, -11.9 kcal/mol and -12.3 kcal/mol; respectively), which was compensated by an increase in entropy. Figure 55 shows that the ΔG values remained fairly constant for all the titrations, whilst the relative contributions of ΔH and $T\Delta S$ are varied.

The results of these binding studies were rather unexpected as the triple mutations in the auto-inhibited core construct ($p47^{phox}D/E3A_{auto}$ and $p47^{phox}3PA_{auto}$) produced insoluble protein (section 4.1.2.1). This indicates that the interactions between the linker and the tandem SH3 domains and polybasic region are very important for the structural integrity of this conformation. However, given the titrations described above it appears that the structural requirements in terms of linker composition, length and flexibility are not rigid for the formation and stabilisation of the auto-inhibited superSH3 domain, if the interaction with the polybasic region occurs in an intermolecular fashion.

4.1.2.4 Binding of $p47^{phox}$ linker mutants to the $p22^{phox}$ peptide

To better understand the specific requirements in terms of length and composition of the $p47^{phox}$ linker, for the formation and stabilisation of the superSH3 domain in the active state, complex formation between the tandem SH3 domain constructs and the $p22^{phox}$ peptide (peptide 2, Appendix: A1) was studied by ITC. The results of these titrations are summarised in Table 16. All the binding reactions were exothermic with stoichiometries of approximately 1:1.

As described previously, the binding of $p47^{phox}Wild\text{-}type_{tandem}$ to the $p22^{phox}$ peptide was used as a reference. Binding occurred with an affinity of 0.14 μM and a binding enthalpy of -11.8 kcal/mol, which is in close agreement with data previously published by our group (Groemping et al., 2003). Binding experiments using the individual hydrogen bond forming mutant proteins $p47^{phox}E218A_{tandem}$, $p47^{phox}E220A_{tandem}$ and $p47^{phox}D221A_{tandem}$ showed only marginal changes in binding

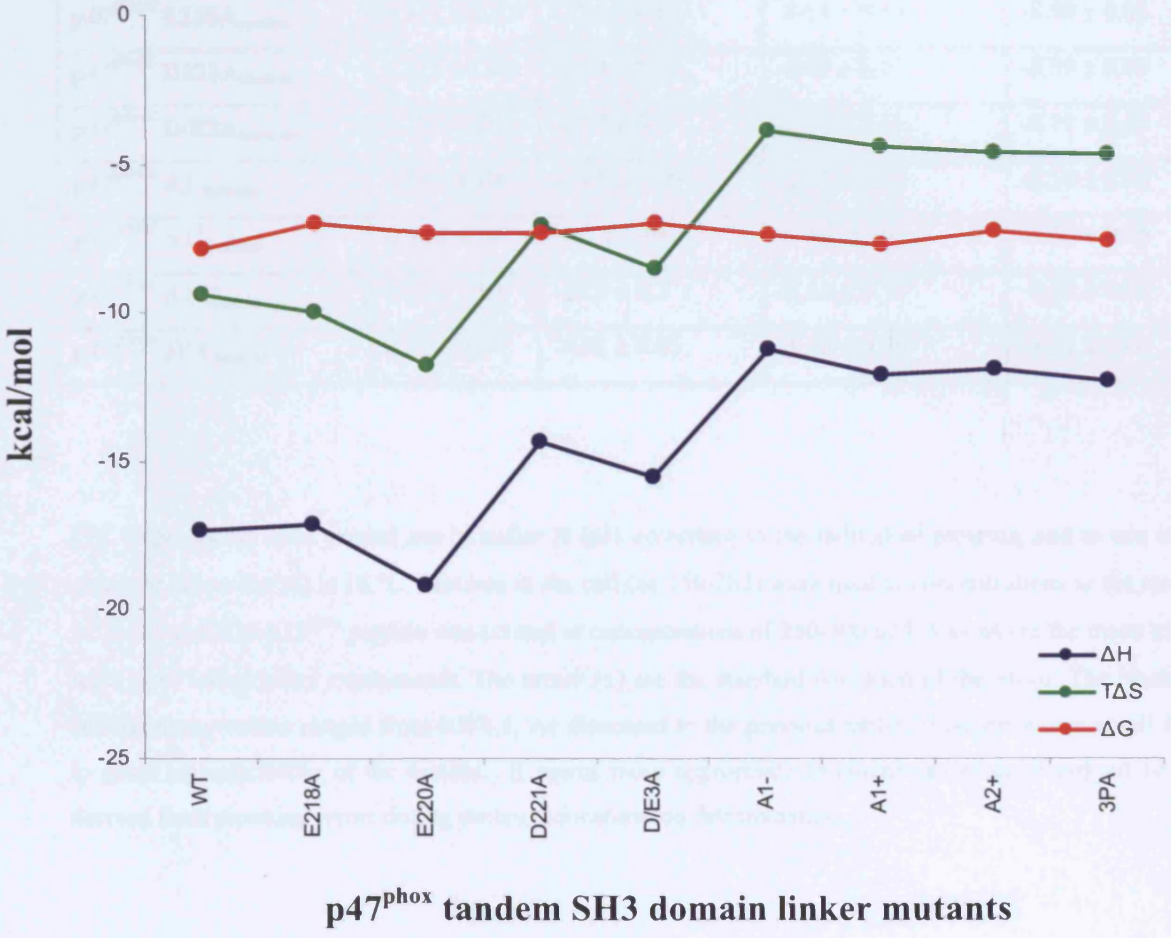

Figure 55: Thermodynamic profile of the complexes between the $p47^{phox}$ tandem SH3 domain linker mutants and the $p47^{phox}$ 35-mer polybasic region peptide. Graph illustrating that ΔG (red) values remain relatively similar for all the complexes, owing to compensating changes in the enthalpic (ΔH) (blue) and entropic (TΔS) (green) contributions.

Table 16: Binding affinities and thermodynamic parameters for the interaction of the $p47^{phox}$ linker mutants with the 16-mer $p22^{phox}$ peptide.

Protein	K_d (μM)	ΔH (kcal/mol)	TΔS (kcal/mol)	ΔG (kcal/mol)
$p47^{phox}$ Wild-type$_{tandem}$	0.14 ± 0.04	-11.8 ± 0.3	-2.65 ± 0.35	-9.15 ± 0.05
$p47^{phox}$ E218A$_{tandem}$	0.218 ±0.07	-13.0 ± 0.25	-4.14 ± 0.55	-8.90 ± 0.13
$p47^{phox}$ E220A$_{tandem}$	0.211 ± 0.03	-12.4 ± 0.15	-3.55 ± 0.15	-8.90 ± 0.03
$p47^{phox}$ D221A$_{tandem}$	0.219 ±0.07	-10.9 ± 0.03	-2.03 ± 0.17	-8.89 ± 0.09
$p47^{phox}$ D/E3A$_{tandem}$	0.29 ± 0.01	-11.2 ± 0.5	-2.45 ± 0.5	-8.71 ± 0.03
$p47^{phox}$ A1$^{-}_{tandem}$	0.54 ± 0.08	-10.5 ± 0.09	-2.13 ± 0.08	-8.36 ± 0.08
$p47^{phox}$ A1$^{+}_{tandem}$	0.38 ± 0.06	-9.2 ± 0.05	-0.66 ± 0.05	-8.56 ± 0.06
$p47^{phox}$ A2$^{+}_{tandem}$	0.33 ± 0.05	-10.3 ± 0.3	-1.66 ± 0.35	-8.64 ± 0.05
$p47^{phox}$ 3PA$_{tandem}$	0.56 ± 0.05	-9.81 ± 0.05	-1.48 ± 0.09	-8.33 ± 0.06

ITC Experiments were carried out in buffer H (pH according to the individual proteins, and to one unit above or below the pI) at 18 °C. Proteins in the cell (aa 156-285) were used at concentrations in the range of 25-40 μM. The $p22^{phox}$ peptide was titrated at concentrations of 250-400 μM. Values are the mean of at least three independent experiments. The errors (±) are the standard deviation of the mean. The binding stoichiometry values ranged from 0.9-1.1. As discussed in the previous tables, these errors are small due to good reproducibility of the system. It seems more appropriate to assume an error of around 10 % derived from pipetting errors during protein concentration determination.

affinities (~ 0.2 μM) compared to $p47^{phox}$Wild-$type_{tandem}$ (0.14 μM). Similarly, the triple mutant $p47^{phox}$D/E3A_{tandem} only showed a small decrease in binding affinity (0.29 μM). These results suggest that these hydrogen bond forming residues may not play an important role in the stabilisation of the superSH3 domain in the active state. Shortening the linker by one amino acid ($p47^{phox}A1^{-}_{tandem}$) had one of the strongest effects on the interaction, and led to a 4-fold decrease in binding affinity (0.54 μM). The titration curve for this reaction is shown in Figure 56. $P47^{phox}A1^{+}_{tandem}$ bound with an affinity of 0.38 μM, ~ 3-fold weaker than $p47^{phox}$Wild-$type_{tandem}$, while $p47^{phox}A2^{+}_{tandem}$ gave a K_d value of 0.33 μM. Experiments using the triple flexibility mutant protein $p47^{phox}$3PA_{tandem} weakened the affinity 4-fold to 0.56 μM. Overall, these data suggest that increasing or decreasing the length of the linker by one or two amino acids, or increasing the linker flexibility has only a limited effect on the formation of the active superSH3 domain. Intriguingly, the substitution of either E218 or E220 ($p47^{phox}$E218A_{tandem} and $p47^{phox}$E220A_{tandem}) made complex formation between the mutant proteins and the $p22^{phox}$ peptide energetically more favourable (13.0 kcal/mol and -12.4 kcal/mol; respectively) (Figure 57 and Table 16), suggesting that slight rearrangements in these constructs may have allowed the formation of novel hydrogen bonds.

As observed already for the intermolecular interaction of these mutant proteins with the polybasic peptide, it appears that the structural requirements for the formation of the superSH3 domain in the active state of $p47^{phox}$, in terms of linker composition, length and flexibility are not very strict.

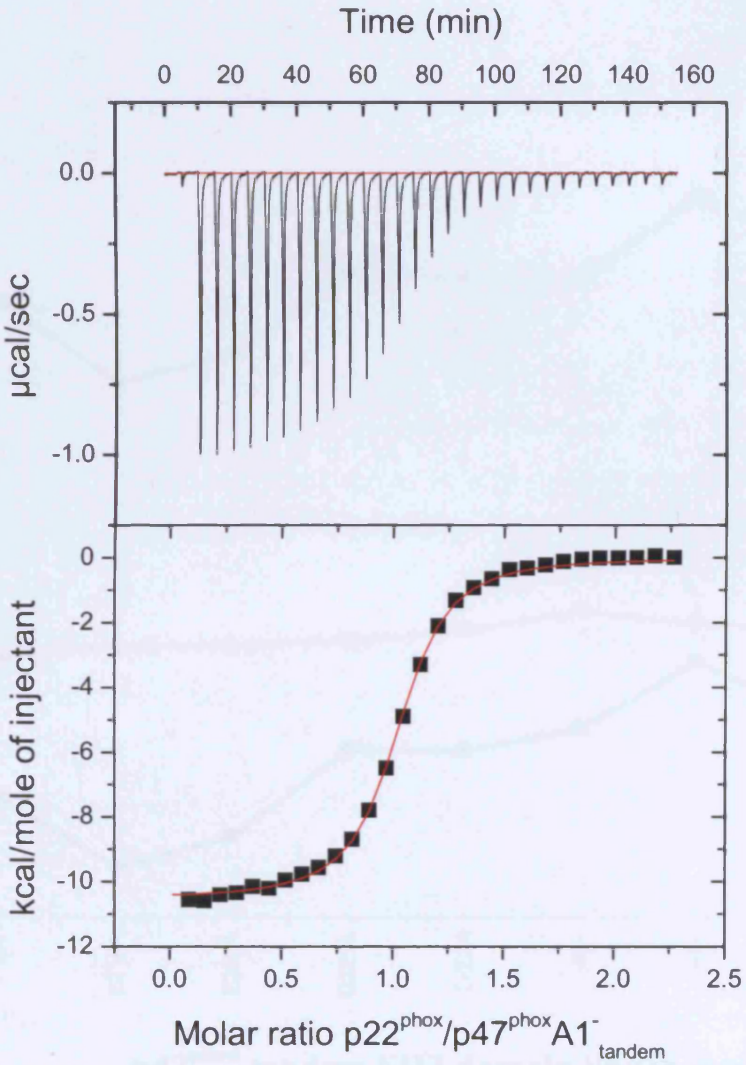

Figure 56: Characterisation of the interaction between the $p22^{phox}$ peptide and $p47^{phox}A1^{-}_{tandem}$. The upper plot shows the raw data for the titration of the $p22^{phox}$ peptide (350 µM) into $p47^{phox}A1^{-}_{tandem}$ (35 µM). The lower plot shows the binding isotherm after subtraction of the heats of dilution. The data were fitted to a single-site binding model. Experiments were carried out in buffer H at 18 °C.

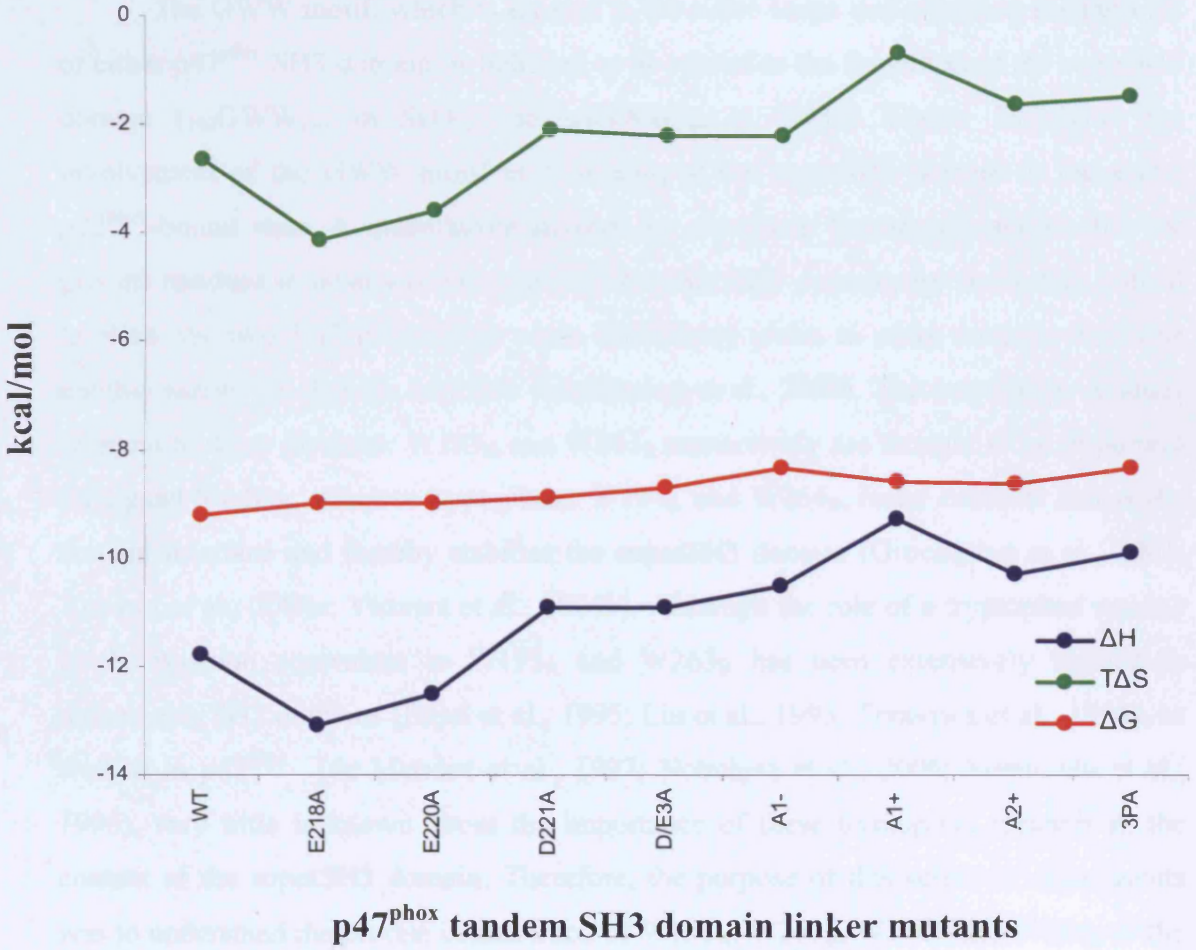

Figure 57: Thermodynamic profile of the interaction between the p47^{phox} tandem SH3 domain linker mutants and the p22^{phox} peptide. Graph illustrating that ΔG (red) values remain relatively similar for all the complexes, owing to compensating changes in the enthalpic (ΔH) (blue) and entropic (TΔS) (green) contributions.

4.2 The role of the GWW motif in the formation of the superSH3 domain

4.2.1 Overview and aims

The GWW motif, which is located in the n-Src loops and adjoining β-strand βC of either $p47^{phox}$ SH3 domain, is believed to be central to the formation of the superSH3 domain ($_{192}GWW_{194}$ in $SH3_A$ and $_{262}GWW_{264}$ in $SH3_B$). Figure 58 shows the involvement of the GWW motif in formation of the superSH3 domain in the active $p22^{phox}$-bound state. A quantitative analysis by our group has already shown that the glycine residues in positions 192 and 262 in either SH3 domain, are absolutely critical to allow the two SH3 domains to come sufficiently close, to make contacts with one another across the domain interface (Groemping et al., 2003). The tryptophan residues adjacent to these glycines: $W193_A$ and $W263_B$ respectively are thought to be important for ligand binding, whereas tryptophans $W194_A$ and $W264_B$, make contacts across the domain interface and thereby stabilise the superSH3 domain (Groemping et al., 2003; Yuzawa et al., 2004a; Yuzawa et al., 2004b). Although the role of a tryptophan residue in the position equivalent to $W193_A$ and $W263_B$ has been extensively studied in monomeric SH3 domains (Erpel et al., 1995; Liu et al., 1993; Terasawa et al., 1994), as well as in $p47^{phox}$ (de Mendez et al., 1997; Nobuhisa et al., 2006; Sumimoto et al., 1996), very little is known about the importance of these tryptophan residues in the context of the superSH3 domain. Therefore, the purpose of this series of experiments was to understand the precise contribution of $W193_A$, $W263_B$, $W194_A$ and $W264_B$ to the stability and ligand binding properties of the $p47^{phox}$ superSH3 domain.

4.2.2 Results

The importance of $W193_A$ and $W263_B$ in ligand binding is well documented in the case of single SH3 domains (de Mendez et al., 1997; Nobuhisa et al., 2006; Sumimoto et al., 1996). It is not known however if they play the same role in the context of the superSH3 domain, and whether the presence of additional contacts outside the conserved ligand binding site (at least in the auto-inhibited state) may be able to compensate for the loss of this tryptophan. Most previous studies investigated

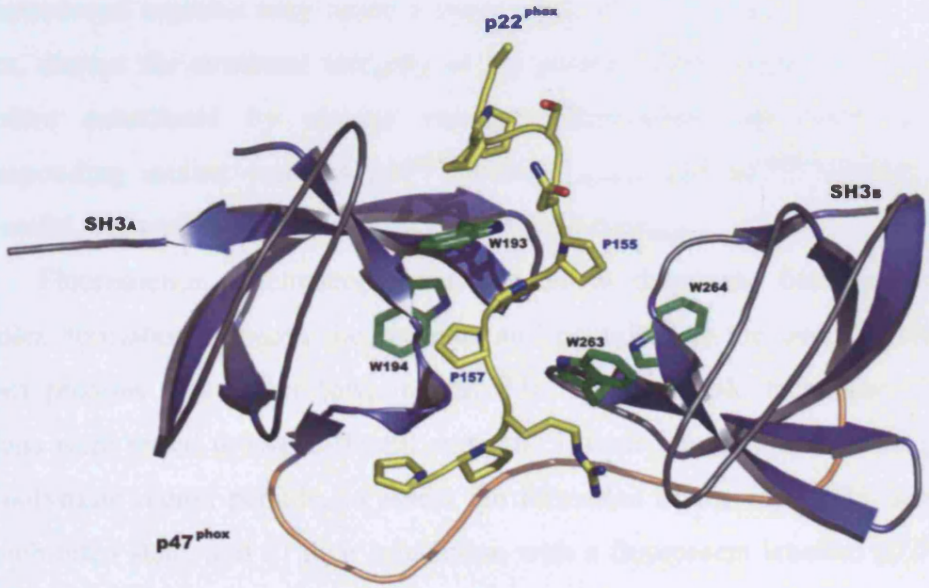

Figure 58: The GWW motif in the n-Src loops of p47^{phox} is central to the formation of a superSH3 domain. The p47^{phox} superSH3 domain in complex with the p22^{phox} peptide. The tandem SH3 domains of p47^{phox} are shown in blue, the linker in orange and the p22^{phox} peptide in yellow stick format. P47^{phox} GWW motif residues involved in ligand binding (W193$_A$ and W263$_B$) and stabilisation (W194$_A$ and W264$_B$) are shown as green sticks. PDB identifier 1OV3 (Groemping et al., 2003).

the role of $W193_A$ and $W263_B$ in either superoxide formation or membrane translocation using a substitution with arginine (de Mendez et al., 1997; Sumimoto et al., 1996). The same substitution was made here to maintain consistency and allow comparison of our binding studies with the previous functional studies. All mutations were introduced into the tandem SH3 domain construct (aa 156-285). Expression and purification of $p47^{phox}W193R_{A\text{-}tandem}$ and $p47^{phox}W263R_{B\text{-}tandem}$ presented few problems, other than a lower yield of protein than for $p47^{phox}Wild\text{-}type_{tandem}$. In contrast, $p47^{phox}W194R_{A\text{-}tandem}$ and $p47^{phox}W264R_{B\text{-}tandem}$ were expressed in an insoluble form (data not shown). A possible explanation for this behaviour is that the long side chain of the introduced arginine may cause a steric clash with the opposing SH3 domain and hence, disrupt the structural integrity of the protein. These tryptophan residues were therefore substituted by alanine residues. Expression and purification of the corresponding mutant proteins $p47^{phox}W194A_{A\text{-}tandem}$ and $p47^{phox}W264A_{B\text{-}tandem}$ was successful, but with lower yields than $p47^{phox}Wild\text{-}type_{tandem}$.

Fluorescence spectroscopy was chosen to determine binding affinities for complex formation between the proteins and peptides, as the overall yield of these mutant proteins was rather low, making ITC an unsuitable technique. The mutant proteins were tested in two different contexts: i) their interaction with the $p47^{phox}$ 35-mer polybasic region peptide, to assess the formation of the superSH3 domain in the auto-inhibited state, and ii) their interaction with a fluorescein labelled $p22^{phox}$ peptide ($p22^{phox*}$ peptide), to assess the formation of the superSH3 domain in the active state. The interaction with the polybasic peptide was followed using the intrinsic fluorescence of tryptophan residues in the tandem SH3 domains (peptide 1, refer to Appendix: A4), as this peptide was not fluorescently labelled, nor contained tryptophan residues. The interaction with the $p22^{phox}$ derived peptide was measured following changes in the extrinsic fluorescein fluorescence (peptide 3, refer to Appendix: A4).

Furthermore, potential changes in the secondary structure content of the mutant proteins were determined by CD spectroscopy. In addition, for those mutant proteins which showed the largest effects on binding affinity, the thermal stability was also determined to ensure that the reduction in binding was not due to increased instability of the proteins under investigation. The methods for these techniques are fully described in chapter 2 of the Materials and Methods section.

4.2.2.1 Expression and purification of the $p47^{phox}$ GWW motif mutants

The mutant proteins $p47^{phox}W193R_{A\text{-}tandem}$, $p47^{phox}W263R_{B\text{-}tandem}$, $p47^{phox}W194A_{A\text{-}tandem}$ and $p47^{phox}W264A_{B\text{-}tandem}$ were expressed in a soluble form, but at lower yields than $p47^{phox}Wild\text{-}type_{tandem}$. They were purified by affinity chromatography on glutathione sepharose, followed by size exclusion chromatography after protease cleavage of the GST-tag. Figure 59 shows the purity of the proteins used for the fluorescence titration experiments, as determined by SDS-PAGE. All proteins ran as single bands at their expected molecular weights (~ 15.3 kDa), and their identity was verified by electrospray mass spectrometry. Moreover, CD spectroscopy showed that none of the mutations had any affects on protein folding. Figure 60 shows a typical CD spectrum for $p47^{phox}W263R_{B\text{-}tandem}$, which is similar to that of $p47^{phox}Wild\text{-}type_{tandem}$. Table 17 shows the corresponding secondary structure content of $p47^{phox}W263R_{B\text{-}tandem}$,which is similar to $p47^{phox}Wild\text{-}type_{tandem}$ (Sreerama and Woody, 2000) (refer to Appendix: A6 for the CD spectra of the other mutant proteins). In addition, the thermal stability of $p47^{phox}W193R_{A\text{-}tandem}$ and $p47^{phox}W263R_{B\text{-}tandem}$ was checked by CD spectroscopy, which showed that the mutations did not affect the structural integrity of the proteins (also in Appendix: A6).

4.2.2.2 Complex formation between the GWW motif tryptophan mutants and the $p47^{phox}$ polybasic region peptide

The results of the fluorescence titrations are summarised in Table 18. The use of intrinsic fluorescence as a signal to monitor protein-ligand interactions is a powerful technique, that sometimes can provide structural clues about the complex under investigation. The technique is extremely sensitive and as a consequence is also prone to artefacts, especially when ligand binding results in a decrease of the fluorescence signal. To ensure that the signal changes monitored upon addition of the peptide are only due to complex formation, the interaction between $p47^{phox}Wild\text{-}type_{tandem}$ and the $p47^{phox}$ 35-mer polybasic region peptide was used as a control and reference experiment. Complex formation occurred with a binding affinity of 1.1 μM, which is in close agreement with that previously reported by our group using ITC (1.5 μM) (Groemping et al., 2003). Titrations of buffer into peptide were also performed as an

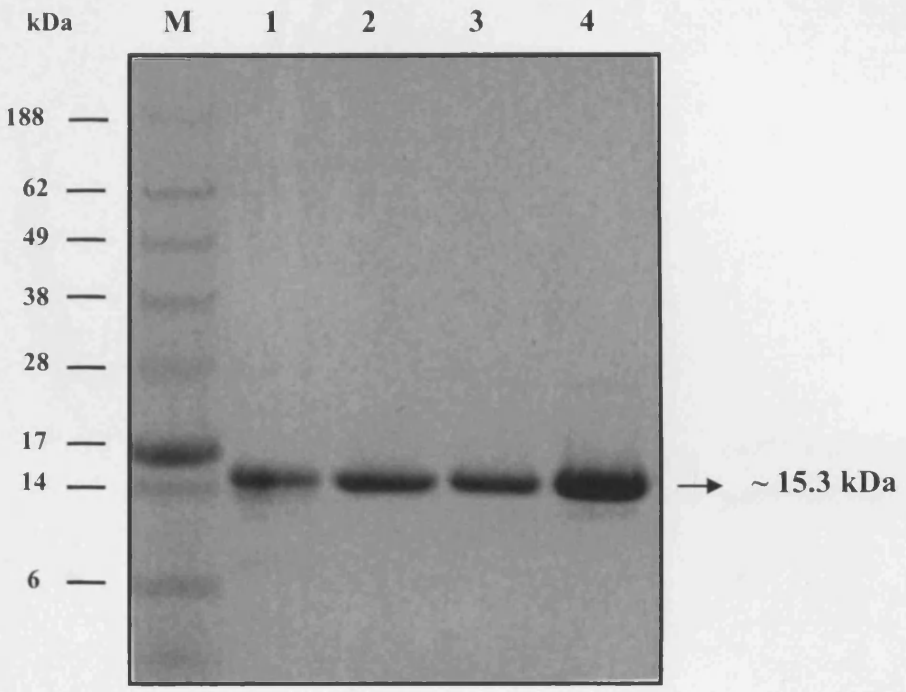

Figure 59: SDS-PAGE of the p47^{phox} GWW motif mutant proteins used for fluorescence spectroscopy experiments. 4-12 % Bis-Tris Novex SDS-PAGE analysis of the p47^{phox} GWW (aa 156-285) motif tryptophan mutants used in these experiments. All proteins are approximately 15.3 kDa.

M: Molecular weight marker (SeeBlue marker, Invitrogen)

1: p47^{phox}W193R$_{A\text{-tandem}}$

2: p47^{phox}W194A$_{B\text{-tandem}}$

3: p47^{phox}W263R$_{A\text{-tandem}}$

4: p47^{phox}W264A$_{B\text{-tandem}}$

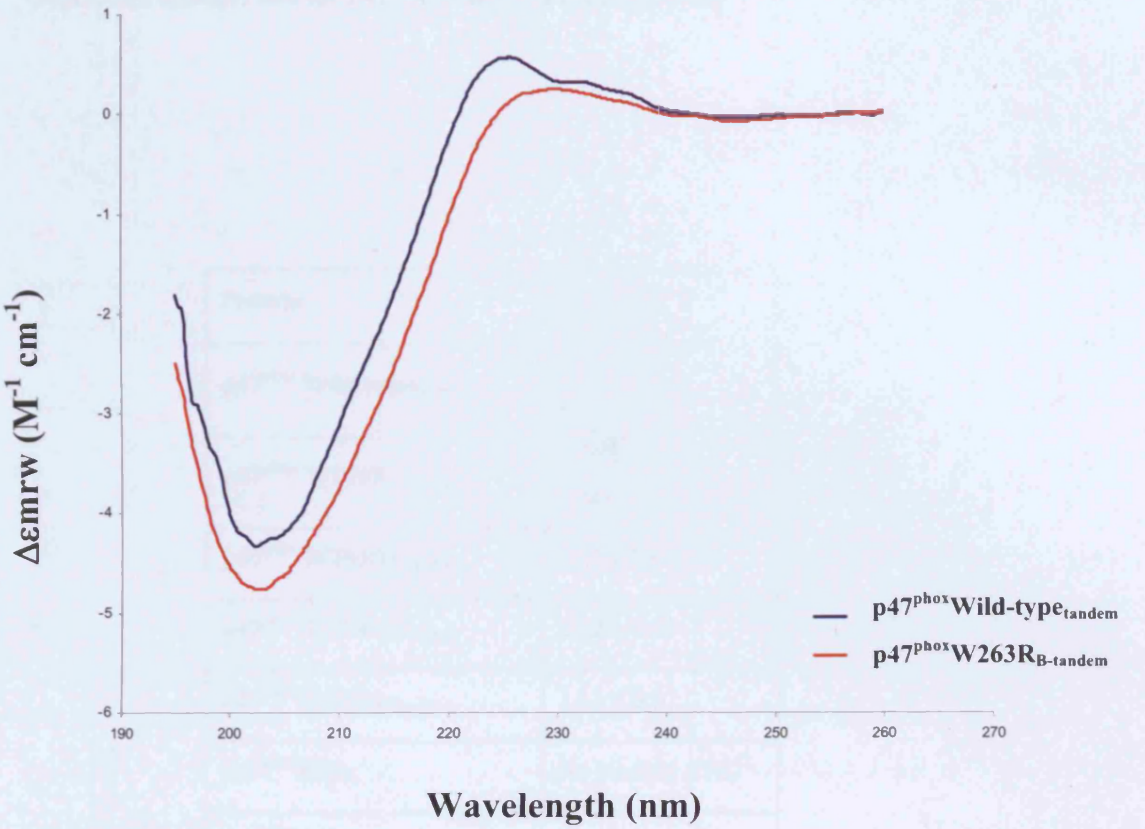

Figure 60: **CD spectra of p47^{phox}Wild-type$_{tandem}$ and p47^{phox}W263R$_{B\text{-}tandem}$.** Far-UV CD spectra of p47^{phox}Wild-type$_{tandem}$ and p47^{phox}W263R$_{B\text{-}tandem}$ (aa 156-285). The protein concentration was 0.15 mg/ml, and the experiments were carried out in buffer H.

Table 17: **Secondary structure analysis of the CD spectra of p47^{phox}Wild-type$_{tandem}$ and p47^{phox}W263R$_{B\text{-}tandem}$.** Comparison of the secondary structure content of p47^{phox}Wild-type$_{tandem}$ (WT) and p47^{phox}W263RB$_{tandem}$ (W263R$_B$), as calculated using the programs CONTIN, SELCON and CDSSTR (Sreerama and Woody, 2000).

Program	α-helix (%)		β-sheet (%)		Turn (%)		Random (%)	
	WT	W263R$_B$	WT	W263R$_B$	WT	W263R$_B$	WT	W263R$_B$
CONTIN	6.1	5.3	41.5	32.8	26.6	23.5	25.8	38.4
SELCON	7.3	7.8	38.9	34.0	26.5	22.5	27.3	35.7
CDSSTR	6.9	7.2	40.6	31.7	26.2	22.9	26.3	38.2

Table 18: Dissociation constants for the complexes formed between the $p47^{phox}$ GWW motif tryptophan mutants and the $p47^{phox}$ 35-mer PB region peptide.

Protein	K_d (μM)
$p47^{phox}$ Wild-type$_{tandem}$	1.11± 0.9 1.5 *(ITC)*
$p47^{phox}$ W193R$_{A\text{-}tandem}$	> 500 > 500 *(ITC)*
$p47^{phox}$ W263R$_{B\text{-}tandem}$	4.11 ± 0.01
$p47^{phox}$ W194A$_{A\text{-}tandem}$	2.62 ± 0.03
$p47^{phox}$ W264A$_{B\text{-}tandem}$	1.12 ± 0.07
$p47^{phox}$SH3$_A$	No binding *(ITC)*
$p47^{phox}$SH3$_B$	No binding *(ITC)*

Experiments were carried out in buffer H (pH according to the individual proteins, and to one unit above or below the pI) at 20 °C. The $p47^{phox}$ 35-mer polybasic region peptide was titrated at increasing concentrations into a cuvette containing 1 μM of either $p47^{phox}$Wild-type$_{tandem}$, or the GWW motif tryptophan mutants (aa 156-285). Previous results from our group are shown in blue. $P47^{phox}$ SH3$_A$ (aa 159-212) and $p47^{phox}$ SH3$_B$ (aa 228-284) are the isolated SH3 domains (Groemping et al., 2003). Values taken are the mean of at least three independent experiments. The errors (±) are the standard deviation of the mean. As discussed in the previous tables, these errors are small due to good reproducibility of the system. However, it seems more appropriate to assume an error of around 10 % derived from pipetting errors and protein concentration determination.

additional control, to ensure that any changes in fluorescence observed were not an artefact. Titration of the peptide into $p47^{phox}W193R_{A\text{-}tandem}$ did not produce any significant changes in fluorescence intensity, suggesting that no binding takes place. On the other hand, mutation of this tryptophan residue in $SH3_B$ ($p47^{phox}W263R_{B\text{-}tandem}$) resulted in a slight decrease in fluorescence, that was sufficient to determine a dissociation constant of 4.1 μM, ~ 3-fold weaker than $p47^{phox}Wild\text{-}type_{tandem}$. Figure 61 shows the fluorescence titration curves for the titration of $p47^{phox}W193R_{A\text{-}tandem}$ and $p47^{phox}W263R_{A\text{-}tandem}$ with the polybasic peptide. As the measurements in this section rely on changes in tryptophan fluorescence, we thought it important to rule out the possibility that the absence of a fluorescence signal for the $p47^{phox}W193R_{A\text{-}tandem}$ titration, may be solely due to the removal of tryptophan residue 193. Therefore, additional ITC experiments were carried out to further investigate this interaction by titrating the polybasic peptide into $p47^{phox}W193R_{A\text{-}tandem}$ at 18 °C. However, the heat change of this reaction was rather small (-2.31 kcal/mol) and the data quite noisy, thereby making the data difficult to fit reliably (data not shown). The experiment was repeated at 12 °C in the hope that the heat capacity of this binding reaction is such that ΔH might be bigger at this given temperature (section 2.11.2.4). Unfortunately, the heat change again was too small and the data quality not sufficient to allow a reliable fit (-3.32 kcal/mol, data not shown). Based on these titrations we estimate the binding affinity to be more than 500 μM. This result further supports the fluorescence data and suggests that upon removal of $W193_A$ binding to the polybasic peptide does not take place. Together, these observations suggest that in the context of the inactive, auto-inhibited state, $W193R_A$ appears to be much more important for ligand binding than $W263R_B$. This is somewhat surprising given that unlike in the active state, neither SH3 domain is capable of binding to the polybasic peptide on its own (Groemping et al., 2003).

Mutation of $W194_A$ ($p47^{phox}W194A_{A\text{-}tandem}$) only slightly disrupted the interaction with the polybasic peptide (2.6 μM), while removal of $W264_B$ ($p47^{phox}W264A_{B\text{-}tandem}$) had no effect at all on complex formation (1.1 μM). Figure 62 shows the fluorescence titration curves for these interactions. These data indicate that $W194_A$ and $W264_B$ are not important in the stabilisation of the superSH3 domain conformation in the inactive, auto-inhibited state.

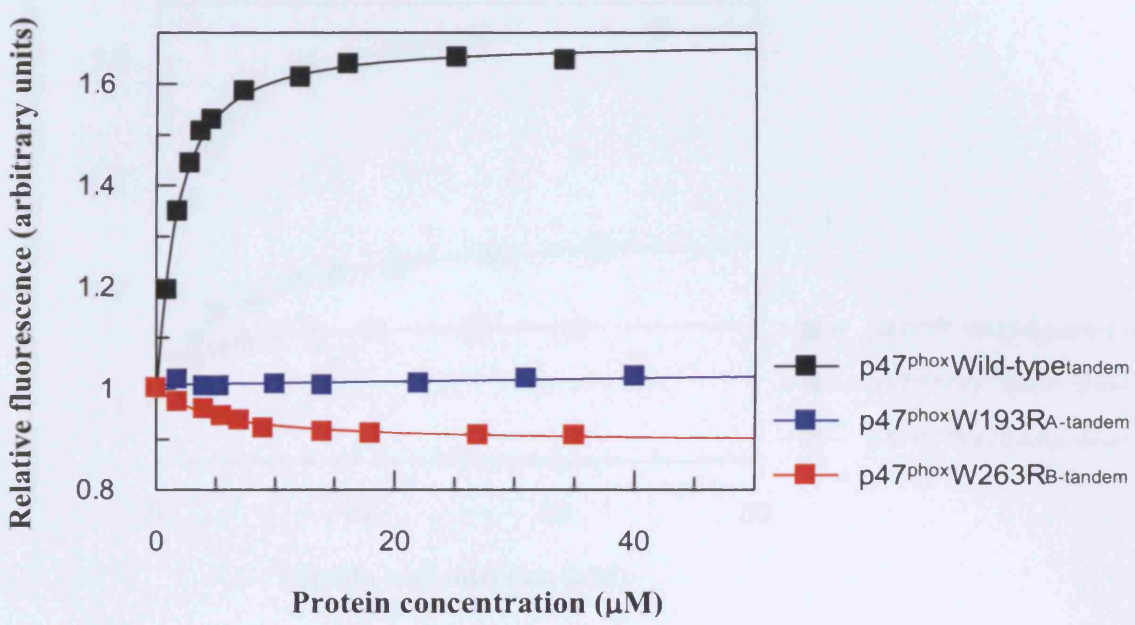

Figure 61: Fluorescence titrations of the interactions the between $p47^{phox}W193R_{A\text{-}tandem}$ and $p47^{phox}W263R_{B\text{-}tandem}$ with the $p47^{phox}$ 35-mer PB region peptide. $P47^{phox}W193R_{A\text{-}tandem}$ shows no change in fluorescence intensity, indicative of no binding. The titrations were carried out 20 °C in buffer H.

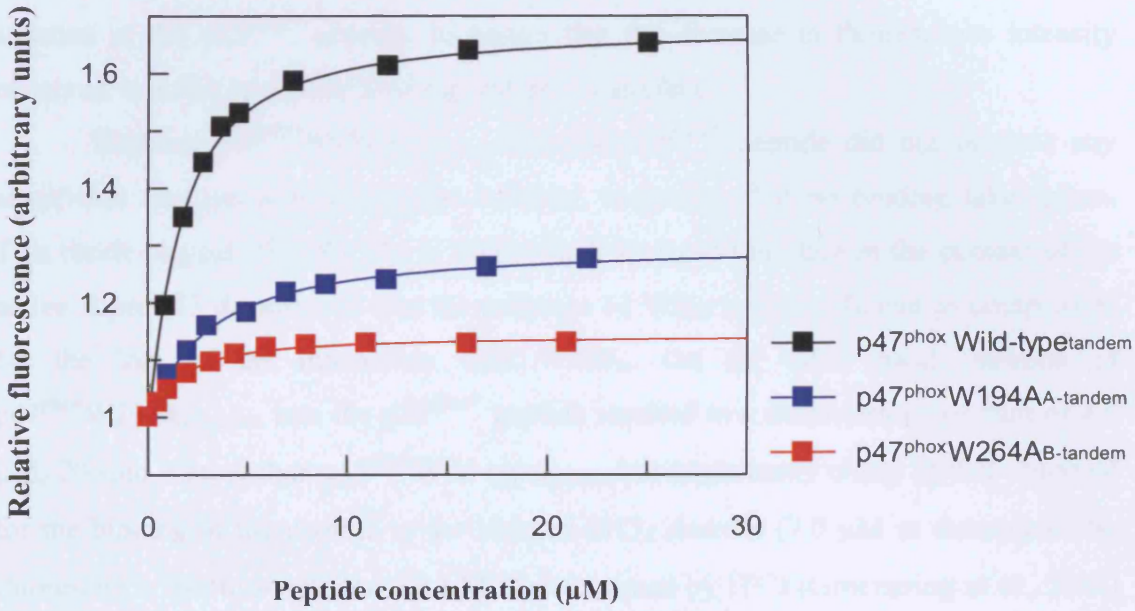

Figure 62: Fluorescence titrations of the interactions between $p47^{phox}W194A_{A\text{-}tandem}$ and $p47^{phox}W264A_{B\text{-}tandem}$ with the $p47^{phox}$ 35-mer PB region peptide. The titrations were carried out at 20 °C in buffer H.

4.2.2.3 Complex formation between the GWW motif tryptophan mutants and the $p22^{phox}$* peptide

The results of the fluorescence titrations are summarised in Table 19. As before, the titration of the $p47^{phox}$Wild-$type_{tandem}$ protein into the $p22^{phox*}$ peptide was used as a reference experiment. This complex represents the fully active state, and produces the highest affinity observed. The dissociation constant obtained (0.2 μM) was reproducible and is in close agreement with that previously obtained by our group (Groemping et al., 2003). In addition, control experiments were carried out where buffer was titrated into a solution of the $p22^{phox*}$ peptide, to ensure that the decrease in fluorescence intensity observed was due to peptide binding and not an artefact.

Titration $p47^{phox}W193R_{A\text{-}tandem}$ into the $p22^{phox*}$ peptide did not produce any significant changes in fluorescence intensity, indicating that no binding takes place. This result suggests that $W193_A$ is also critical for ligand binding in the context of the active superSH3 domain and that the presence of $SH3_B$ is not sufficient to compensate for the loss of the interaction with $W193_A$. On the other hand, titration of $p47^{phox}W263R_{B\text{-}tandem}$ into the $p22^{phox*}$ peptide resulted in a dissociation constant of 4.0 μM, 20-fold weaker than $p47^{phox}$Wild-$type_{tandem}$, but importantly closer to that observed for the binding of the peptide to the isolated $SH3_A$ domain (7.0 μM as determined by fluorescence spectroscopy and 3.4 μM as determined by ITC) (Groemping et al., 2003) (Table 19). Figure 63 shows the fluorescence titration curves for the binding of $p47^{phox}W193R_{A\text{-}tandem}$, and $p47^{phox}W263R_{B\text{-}tandem}$ to the $p22^{phox*}$ peptide. Together, these observations suggest that the role of the first tryptophan residue within the G<u>W</u>W motif is conserved and identical to that of this tryptophan in isolated SH3 domains (de Mendez et al., 1997; Nobuhisa et al., 2006; Sumimoto et al., 1996).

On the other hand, substitution of $W194_A$ and $W264_B$ had a smaller effect: $p47^{phox}W194A_{A\text{-}tandem}$ interacted with the $p22^{phox*}$ peptide with a K_d of 1.3 μM, which is only about 6-fold weaker than $p47^{phox}$Wild-$type_{tandem}$, while $p47^{phox}W264A_{B\text{-}tandem}$ bound 8-fold weaker with an affinity of 1.6 μM. Figure 64 shows the fluorescence titration curves for the binding of $p47^{phox}W194A_{A\text{-}tandem}$ and $p47^{phox}W264A_{B\text{-}tandem}$ to the $p22^{phox*}$ peptide. These data suggest that the individual removal of these tryptophan residues that are not directly involved in ligand binding, only partially disrupts the interaction between the two SH3 domains. However, some cooperativity between the domains is preserved as the interaction with the $p22^{phox*}$ peptide is still stronger than that of isolated $SH3_A$.

Table 19: Dissociation constants for the complexes formed between the $p47^{phox}$ GWW motif tryptophan mutants and the 16-mer fluorescein labelled $p22^{phox}$ peptide.

Protein	K_d (μM)
$p47^{phox}$ Wild-type$_{tandem}$	0.21 ± 0.01 0.19 *(ITC)* 0.4 *(Fluorescence spectroscopy)*
$p47^{phox}$ W193R$_{A\text{-}tandem}$	> 500
$p47^{phox}$ W263R$_{A\text{-}tandem}$	4.01 ± 0.04
$p47^{phox}$ W194A$_{B\text{-}tandem}$	1.33 ± 0.07
$p47^{phox}$ W264A$_{B\text{-}tandem}$	1.62 ± 0.04
$p47^{phox}$ SH3$_A$	3.4 *(ITC)* 7.0 *(Fluorescence spectroscopy)*
$p47^{phox}$ SH3$_B$	No binding *(ITC)*

Experiments were carried out in buffer H (pH according to the individual proteins, and to one unit above or below the pI) at 20 °C. $P47^{phox}$ Wild-type$_{-tandem}$ and the GWW tryptophan motif mutants (aa 156-285) were titrated at increasing concentrations into a cuvette containing a 1 μM solution of the $p22^{phox*}$ peptide. Previous results from our group are shown in blue. $P47^{phox}$ SH3$_A$ (aa 159-212) and $p47^{phox}$ SH3$_B$ (aa 228-284) are the isolated SH3 domains (Groemping et al., 2003). Values shown are the mean of at least three independent experiments. The errors (±) are the standard deviation of the mean. As discussed in the previous tables, these errors are small due to good reproducibility of the system. It seems more appropriate to assume an error of around 10 % derived from pipetting errors and protein concentration determination.

NOTE

The affinity of $p47^{phox}$Wild-type$_{tandem}$ for the $p22^{phox*}$ peptide determined in these experiments is reproducibly higher than that observed in previous experiments (section 3.1.3.3). This is most likely due to the fact that the two different sets of experiments were carried out using two different peptide stock solutions, derived from two different peptide syntheses. Importantly though, within each set of experiments the same peptide stock was used, and hence the differences in affinities observed are reliable and internally consistent.

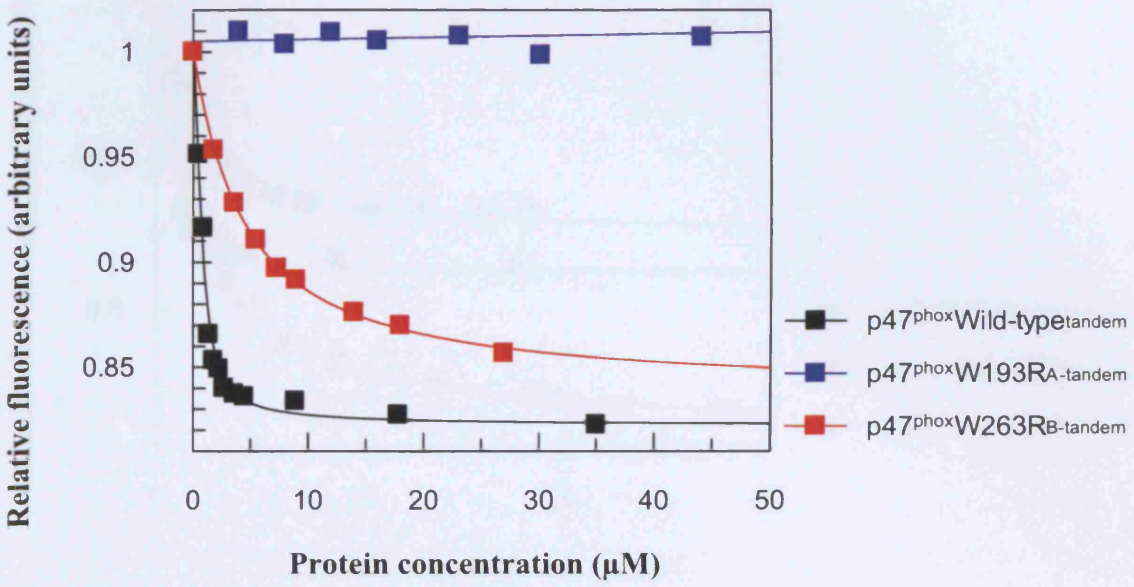

Figure 63: Fluorescence titrations of the interactions between $p47^{phox}W193R_{A\text{-}tandem}$ and $p47^{phox}W263R_{B\text{-}tandem}$ with the 16-mer fluoresceine labelled $p22^{phox}$ peptide. $P47^{phox}W193R_{A\text{-}tandem}$ does not produce any significant change in fluorescence intensity of the $p22^{phox}$* peptide, indicative of no binding. Titrations were carried out at 20 °C in buffer H.

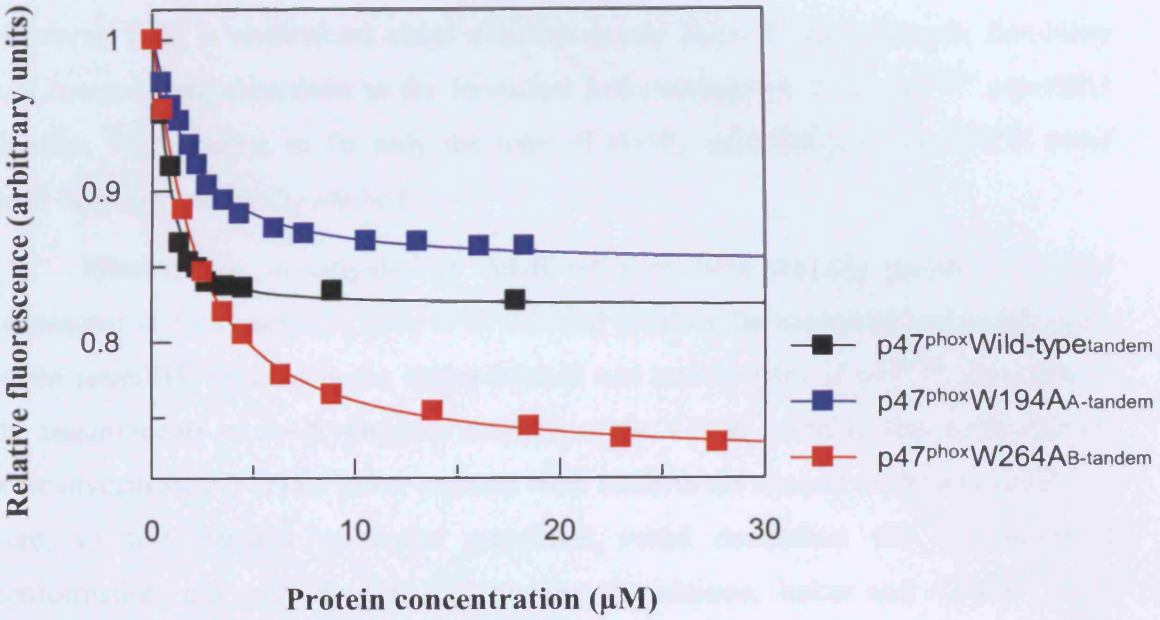

Figure 64: Fluorescence titrations of the interaction between $p47^{phox}W194A_{A\text{-}tandem}$ and $p47^{phox}W264A_{B\text{-}tandem}$ and the 16-mer fluoresceine labelled $p22^{phox}$ peptide. Titrations were carried out at 20 °C in buffer H.

4.3 Discussion

The coordinated action of the $p47^{phox}$ $SH3_A$ and $SH3_B$ domains produce a single ligand binding site of high affinity, and this conformation is referred to as the 'superSH3' domain. Biochemical studies (Groemping et al., 2003) as well as structural data (Groemping et al., 2003; Yuzawa et al., 2004a; Yuzawa et al., 2004b) show that the linker connecting $SH3_A$ and $SH3_B$, as well as the conserved 'GWW' motif located in the n-Src loops are central to the formation of this novel conformation (Figure 58). However, little is understood about whether certain linker features (length, flexibility and composition) contribute to the formation and stabilisation of the $p47^{phox}$ superSH3 domain. Furthermore, so far only the roles of $G192_A$ and $G262_B$ in the GWW motif have been systematically studied.

Here it was investigated in detail whether there are any precise structural constraints in the linker, that have to be fulfilled to allow the formation and stabilisation of the superSH3 domain in the auto-inhibited and active states of $p47^{phox}$. In addition, the requirements of the tryptophan residues of the GWW motif in this conformation were investigated. Various linker mutants were made in the context of the auto-inhibited core, to test whether particular mutations could destabilise the auto-inhibited conformation, but still allow $p22^{phox}$ binding. In addition, linker and 'GWW' motif mutants were made in the context of the tandem SH3 domains and their ability to form a superSH3 domain and accommodate either the $p47^{phox}$ polybasic peptide or $p22^{phox}$-derived peptide was also tested.

4.3.1 The structural requirements for the $p47^{phox}$ linker are strict in the context of the auto-inhibited core

Linker length and flexibility have been shown to play important roles in systems where a tight control of protein activity is achieved through intramolecular protein-protein interactions. Examples of such proteins include the Src family of non-receptor protein-tyrosine kinases (Hofmann et al., 2005). The activity of Src kinases is regulated by two intramolecular interactions. These involve the binding of the SH2 domain to a C-terminal phosphotyrosine and association of the SH3 domain with the SH2-kinase linker (Sicheri et al., 1997; Williams et al., 1997; Xu et al., 1997). Activation of the

enzyme is achieved in part by de-phosphorylation of the phosphotyrosine (as well as by competition with high affinity SH2 and SH3 domain ligands) and the subsequent disruption of the SH2 domain mediated interaction. However, a study by Kuriyan and colleagues has shown that increasing the flexibility of the SH2-SH3 domain linker can also relieve auto-inhibition and induce kinase activation. This highlights the importance of the SH2-SH3 domain linker in maintaining auto-inhibition (Young et al., 2001).

In this study we wanted to test whether specific linker features are also important for maintaining the auto-inhibited conformation of $p47^{phox}$. The interactions made between the linker and the tandem SH3 domains as well as the polybasic region in the inactive state are much more extensive than those made in the active state with either $SH3_A$ or $SH3_B$ domains and the $p22^{phox}$ peptide (Groemping et al., 2003; Yuzawa et al., 2004a; Yuzawa et al., 2004b). This suggests that the linker requirements may be stricter in the auto-inhibited than in the active state. To test these possibilities, two different triple mutations were introduced into the auto-inhibited core construct i) mutations disrupting the formation of specific hydrogen bonds ($p47^{phox}D/E3A_{auto}$) and ii) where the flexibility of the linker is increased through the removal of proline residues ($p47^{phox}3PA_{auto}$). Intriguingly, both of the resulting mutant proteins were insoluble, strongly supporting the notion that maintaining a certain degree of constraint is important for the formation of the auto-inhibited superSH3 domain, and that an increase in linker flexibility may interfere with proper protein folding. Nevertheless, in contrast to our results there has been a previous report where partial purification of the full-length protein with the following mutations in the linker region (D217A/E218A/E223A) appeared successful (Peng et al., 2003). However, it is important to note that only the substitution of E218 is identical between the two constructs. The other two substituted residues, D217 and E223 do not form hydrogen bonds with the tandem SH3 domains. In fact, E223 is solvent exposed and its removal would not be expected to have any effect. Nevertheless, D217 forms a hydrogen bond with the backbone amide group of K317 in the polybasic region and its removal may weaken the intramolecular interaction. Although it is impossible to know for sure why the two constructs behave so differently, it is possible that the use of a baculovirus expression system, which was used by Peng and colleagues may be better suited for expression of these mutants than the bacterial system used here. This may explain the different stabilities observed. Nevertheless, it seems likely that the removal of five hydrogen bonds in our construct may have interfered with correct protein folding, possibly even in an insect cell-based expression system. Therefore, we believe that the results from our study strongly indicate that the

structural requirements of the $p47^{phox}$ linker are strict in the context of the auto-inhibited superSH3 domain.

4.3.2 The structural requirements for the $p47^{phox}$ linker are more flexible for binding to ligands in an intermolecular interaction

As it was impossible to produce soluble proteins to study linker mutants in the context of the auto-inhibited core construct, we decided to introduce the corresponding mutants into the tandem SH3 domain construct and investigate the interaction with the $p47^{phox}$ 35-mer polybasic peptide to mimic the auto-inhibited conformation. Somewhat unexpectedly, soluble protein was obtainable for all the mutants tested. Even more surprisingly, given the insolubility of the $p47^{phox}$D/E3A_{auto} and $p47^{phox}$3PA_{auto} constructs, complex formation between these mutants, and the polybasic peptide was only weakened to a relatively small degree, with a maximum 5-fold decrease in affinity for $p47^{phox}$E218A_{tandem} and $p47^{phox}$D/E3A_{tandem}. A similar observation was made for the interaction with the $p22^{phox}$ derived peptide: neither mutation tested resulted in a significant loss of binding affinity, and most mutants only reduced the strength of complex formation 2-3 fold. The strongest effect observed for this interaction was with those mutants that had either a decreased linker length ($p47^{phox}$A1$^{-}_{tandem}$) or increased flexibility (0.56 μM): both mutants bound the $p22^{phox}$ peptide only 4-fold weaker than $p47^{phox}$Wild-type$_{tandem}$. During the writing of thesis a similar study on the effects of varying the length of $p47^{phox}$ linker on $p22^{phox}$ binding and superoxide production was published. Using pull-down assays, Nobuhisa and colleagues showed that shortening or lengthening the linker by 2-6 amino acids had little effect on complex formation with $p22^{phox}$ and NADPH oxidase activity. Similar results were obtained upon the removal of the hydrogen bond forming residues E220 and D221 (Nobuhisa et al., 2006). This study unlike that by Peng and colleagues further supports our data, and clearly shows that mutating the linker has little effect on the formation and stabilisation of the superSH3 domain in the active state of $p47^{phox}$.

Taken together, these results clearly show that there is a significant difference of the effect of linker mutations depending if the superSH3 domain is involved in an intra- or intermolecular interaction. In the case of an intermolecular interaction, as exemplified by the complexes with the polybasic and $p22^{phox}$-derived peptides, there

seems to be a lot of flexibility with regards to sequence and the linker appears to only play a role in physically connecting the two domains. At first, this seems somewhat surprising as the linker is involved in a number of specific interactions with the two SH3 domains, especially in the auto-inhibited state (see Figure 20) and one would assume that the loss of these interactions may seriously interfere with ligand binding. However, it is possible that in the case of an intermolecular interaction, there is sufficient flexibility in the system to allow the two SH3 domains to cooperate and form a superSH3 domain under a variety of conditions. This is probably due to the fact that many other interactions take place between the tandem SH3 domains and the peptides. These may compensate for those interactions lost through mutations in the linker and may otherwise stabilise the superSH3 domain conformation. This does not appear to be the case for an intramolecular interaction. The insolubility of the mutants tested strongly indicates that in such a case the structural constraints of the linker are much more rigid, and are likely important to allow the correct folding of the superSH3 domain containing protein. This is particularly interesting in light of the fact that the non-phagocytic $p47^{phox}$ homologue NOXO1 does not contain the 3 proline residues present in the linker of the phagocytic protein, nor the hydrogen bond forming residues E218 or D221. Indeed, this protein is currently not believed to adopt a similar auto-inhibited conformation. On the other hand, the interaction of NOXO1 with $p22^{phox}$ also appears to occur in the superSH3 domain conformation (Dutta & Rittinger, unpublished result), supporting the idea that the precise composition of the linker is not as important for an intermolecular interaction with an external ligand.

Altogether, these data suggest that the chemical nature of the linker is important in the context of an intramolecular interaction, as interactions between the linker and the two SH3 domains may be required for the correct folding of the protein. On the other hand, linker requirements appear to be significantly less stringent for intermolecular interactions, where this increased flexibility may be important to allow the accommodation of a number of different targets.

4.3.3 $W193_A$ is more important for ligand binding than $W263_B$, in both the active and auto-inhibited states

The tryptophan residues of each SH3 domain in positions 193_A and 263_B are fully conserved among the family of SH3 domains and are directly involved in ligand binding (Larson and Davidson, 2000). Mutagenesis studies in $p47^{phox}$ have shown that

$W193_A$ plays a crucial role in $p22^{phox}$ binding. Substitution of the tryptophan to arginine completely disrupts complex formation of the isolated $SH3_A$ domain with $p22^{phox}$ and interferes with superoxide production plus membrane translocation of the mutant, full-length protein. In contrast, mutation of its equivalent residue in $SH3_B$ has little effect (de Mendez et al., 1997; Sumimoto et al., 1996). Here we have investigated the effect of mutating these residues in the tandem SH3 domain construct on their ability to interact with the polybasic and $p22^{phox}$-derived peptides. When interpreting the results from these studies it is important to keep in mind that isolated $SH3_A$ is able to interact with the $p22^{phox}$ peptide with an affinity of 3.4 μM (fluorescence spectroscopy), whilst $SH3_B$ cannot (Groemping et al., 2003). However, neither isolated SH3 domain can form a stable complex with the polybasic region (Groemping et al., 2003). Mutation of $W193_A$ ($p47^{phox}W193R_{A\text{-}tandem}$) completely abrogated complex formation with the $p22^{phox}$ peptide, while the equivalent mutation in $SH3_B$ ($p47^{phox}W263R_{B\text{-}tandem}$) reduced the affinity of the mutant protein for $p22^{phox}$ to that of isolated $SH3_A$. These results show that in the active superSH3 domain, both $W193_A$ and $W263_B$ behave the same as in the isolated SH3 domains (de Mendez et al., 1997; Sumimoto et al., 1996). As binding to $p22^{phox}$ is dominated by the interaction with $SH3_A$ (for details see section 1.6.2.2), removal of $W193_A$ is detrimental to the interaction, while the equivalent mutation in $SH3_B$ merely reduces the affinity to that of isolated $SH3_A$.

The precise role of $W193_A$ and $W263_B$ in the auto-inhibited state is not clear at present. In this study we found the binding behaviour of the polybasic region to be similar to that of $p22^{phox}$, which was rather unexpected given that isolated $SH3_A$ is not able to interact with this region (Groemping et al., 2003). Substitution of $W193_A$ to arginine abolished the interaction with the polybasic peptide, judging by the absence of a change in intrinsic fluorescence. However, as the absence of a signal change could potentially be due to the removal of $W193_A$, whose fluorescence may dominate the signal observed, the interaction was also probed by ITC. No convincing binding was observed, which is in good agreement with the fluorescence data. These results suggest that although the interactions between isolated $SH3_A$ and the polybasic region are not sufficient to allow the formation of a stable complex (Groemping et al., 2003), the hydrogen bonds and hydrophobic interactions made by $W193_A$ are absolutely crucial for ligand binding in the superSH3 domain. In contrast, $W263_B$ does not appear to significantly contribute to the ligand binding properties of the superSH3 domain, as its removal only weakened the interaction with the polybasic peptide 2-fold. These findings

are extremely interesting as it suggests that $SH3_A$ plays a more dominant role in the auto-inhibited state than previously assumed.

4.3.4 $W194_A$ and $W264_B$ are only important for the stabilisation of the superSH3 domain in the active state

Residues $W194_A$ and $W264_B$ are not directly involved in interactions with neither $p22^{phox}$ nor the polybasic region. Instead these residues have been proposed to contribute to the stabilisation of the superSH3 domain through the formation of inter-SH3 domain hydrogen bonds in the auto-inhibited and active states (Groemping et al., 2003; Yuzawa et al., 2004a; Yuzawa et al., 2004b). However, the data presented here show that removal of either residue has only a marginal effect on the interaction with the polybasic peptide, indicating that in the auto-inhibited state the loss of an interdomain interaction can easily be compensated for by the extensive network of interaction formed between the tandem SH3 domains, the linker and polybasic region of the protein (Groemping et al., 2003; Yuzawa et al., 2004a; Yuzawa et al., 2004b). In the active state, both tryptophan residues form water-mediated hydrogen bonds across the domain interface, while many of the additional interactions that stabilise the auto-inhibited conformation are missing. Accordingly, substitution of either $W194_A$ or $W264_B$ to alanine has a stronger effect and reduces the affinity for $p22^{phox}$ by 6-fold and 8-fold, respectively. Interestingly, these binding affinities are closer to those observed for the wild-type isolated $SH3_A$ domain (Groemping et al., 2003) and suggest that either residue is required to ensure that a stable superSH3 domain is formed that can bind its target ligands with high affinity. Removal of either tryptophan will induce sufficient flexibility into the system to disrupt some of the cooperativity of the two domains, thereby creating a situation where the interaction with $SH3_A$ dominates complex formation and the supporting effect of $SH3_B$ is partially lost.

Taken together, these studies show that the two SH3 domains of $p47^{phox}$ that cooperate to form the superSH3 domain make different contributions to the ligand binding capability of this domain. In both the auto-inhibited and the active states, $SH3_A$ plays a much more important role in ligand binding and accordingly the removal of $W193_A$, which is conserved in all SH3 domains (Larson and Davidson, 2000), has a major effect on affinity. The significance of tryptophans 194 and 264 depends more on the context of the interaction: in the auto- inhibited state, where a large number of

contacts are made between the tandem SH3 domains and the polybasic region outside of the core binding region, either of these tryptophans plays only a minor role in the stabilisation of the superSH3 domain. However, in the active state, where many of these interactions are lost, the interdomain contacts made by these tryptophan residues become more important and are required for the formation of a high affinity ligand binding site.

4.3.5 Are there other proteins that may form a superSH3 domain?

The results from section 4.1 and 4.2 clearly indicate that the requirements for the formation and stability of a superSH3 domain in terms of linker composition and the presence of a 'GWW' motif are not overly stringent, suggesting that other proteins may also be capable of forming such a conformation. The precise nature of the linker appears to be more important for an intramolecular interaction and hence might limit the type of proteins that are able to use the superSH3 domain to regulate protein activity through auto-inhibition. The linker appears to be less important for intermolecular interactions, which on the other hand may have stricter requirements for the presence of the 'GWW' motif. Furthermore, our data also show the relative contribution of the two SH3 domains to ligand binding does not have to be equal thereby probably extending the type of proteins that could adopt this conformation.

Interactions mediated by SH3 domains can be relatively weak and non-specific (Chen et al., 1993) and the superSH3 domain conformation might be a mechanism to achieve additional specificity and affinity in these interactions while simultaneously retaining a certain degree of flexibility for the accommodation of ligands with different binding properties. There are many other proteins such as CIN85 (Abram et al., 2003) and FISH (Kowanetz et al., 2003) that contain multiple, adjacent SH3 domains. These proteins often act as adaptors or scaffolds to allow the formation of large, multi-protein complexes. Binding studies have shown that the SH3 domains of these proteins cooperate for ligand binding. For example, CIN85 contains three SH3 domains and although the individual SH3 domains are capable of binding their target ligands with micromolar affinities, the extended structure of two or three SH3 domains significantly increases the affinity (Kowanetz et al., 2003). Further studies are now required to gain a better insight into the role of this novel protein-protein interaction domain in other biological systems.

CHAPTER FIVE

5.0 Final discussion and concluding remarks

This study focuses on two different aspects of NADPH oxidase activity: i) the functional role of phosphorylation of serine residues in the C-terminal region of $p47^{phox}$ in the assembly process and ii) the structural requirements for the formation and stabilisation of the superSH3 domain in the auto-inhibited and active states of $p47^{phox}$.

5.1 $P47^{phox}$ phosphorylation and NADPH oxidase activation

$P47^{phox}$ is the most extensively phosphorylated subunit of the NADPH oxidase. A total of eleven serine residues have been identified as targets of phosphorylation, of which only eight appear to be required for enzyme activation (Ago et al., 1999; el Benna et al., 1994; El Benna et al., 1996; Faust et al., 1995; Groemping et al., 2003; Inanami et al., 1998; Johnson et al., 1998). Five of these residues are located within the polybasic, auto-inhibitory region (S303, 304, 315, 320 and 328), while the remaining three are located adjacent to the C-terminal proline-rich region (S359, 370 and 379), the region which otherwise mediates the interaction with $p67^{phox}$ (Figure 19) (Finan et al., 1994; Kami et al., 2002; Lapouge et al., 2002; Leto et al., 1994). Phosphorylation of serine residues within the polybasic region, in particular of S303, 304 and 328 relieves the auto-inhibited conformation of $p47^{phox}$ and allows binding to $p22^{phox}$, thereby promoting superoxide production (Ago et al., 1999; Groemping et al., 2003). In contrast, phosphorylation of the C-terminal serine residues (S359, 370 and 370) alone appears not to be sufficient to promote an interaction between $p47^{phox}$ and $p22^{phox}$ (Ago et al., 1999). However, it has never been investigated if phosphorylation events within the C-terminal region can synergise with phosphorylation of the polybasic region, and thereby contribute to the disruption of the auto-inhibited state and promote NADPH oxidase assembly.

To address this issue phosphorylation mimics were produced (by the substitution of serine for glutamate residues) and their ability to interact with a fluoresceine labelled $p22^{phox}$-derived peptide was investigated. These experiments demonstrated that a triple C-terminal phosphorylation mimic (S359, 370 and 379E) fails to relieve auto-inhibition and allow interaction with $p22^{phox}$, in support of the previous findings by Ago and colleagues. Furthermore, this study revealed that a mutant protein mimicking

phosphorylation of the entire protein (S303, 304, 315, 320, 328, 359, 370 and 379E) behaves similarly with respect to the interaction with $p22^{phox}$, to a protein where only phosphorylation of the polybasic region has been mimicked (S303, 304, 315, 320 and 328E). These results clearly demonstrate that phosphorylation of the C-terminal serine residues do not synergise with phosphorylation of the polybasic region to weaken the intramolecular interaction between the tandem SH3 domains and the polybasic region, and allow an interaction with the flavocytochrome. This raises the question about the functional role of these C-terminal phosphorylation events and their effect on superoxide production. It would be very interesting to directly compare these three different phosphorylation mimics in cell free activation assays, to test their ability to support the production of superoxide. Should the $p47^{phox}$S5E and $p47^{phox}$S8E mutant proteins behave in a similar manner as observed in our binding studies, this would indicate that phosphorylation of the C-terminal serine residues may be an unspecific "by-product" of phosphorylation of the auto-inhibitory region. On the other hand, should there be clear differences in the activity of these two proteins as very recently suggested by Mizuki and colleagues, then this would point towards a functional role that is currently not understood.

In respect to this, it is important to take into consideration that the C-terminal serine residues of $p47^{phox}$ are located within a region that is known to bind with high affinity to the C-terminal SH3 domain of $p67^{phox}$ (Finan et al., 1994; Kami et al., 2002; Lapouge et al., 2002; Leto et al., 1994). Hence, it is possible that C-terminal phosphorylation of $p47^{phox}$ may be involved in regulating this interaction instead. The same approach of employing phosphorylation mimics was used to test this hypothesis and it was shown that C-terminal phosphorylation of $p47^{phox}$ indeed weakens the interaction with $p67^{phox}$. In particular, phosphorylation of S379 appears to play a central role. However, as observed for the release of the auto-inhibited conformation, there is no synergistic interplay between phosphorylation of serine residues in the polybasic and the C-terminal region, suggesting that both events are functionally independent. During the completion of this work, similar studies were published which support our findings and further show that phosphorylation of S379 severely affects NADPH oxidase activity (Massenet et al., 2005; Mizuki et al., 2005). The possibility that phosphorylation directly targets the $p47^{phox}$-$p67^{phox}$ interaction is at first glance rather surprising, given that the translocation mechanism requires a tightly associated $p47^{phox}$-$p67^{phox}$-$p40^{phox}$ complex (Lapouge et al., 2002; Park et al., 1992; Someya et al., 1993; Wientjes et al., 1993), to co-migrate as a whole to the membrane for enzyme activation. However, it

may help to explain the recent findings by Brown and colleagues, that $p47^{phox}$ is in fact not associated with the $p67^{phox}$-$p40^{phox}$ complex under resting conditions (Brown et al., 2003). Based on these data we propose the following model for phosphorylation-induced changes in NADPH oxidase assembly (Figure 65). Briefly, in the inactive state of the enzyme only $p67^{phox}$ and $p40^{phox}$ exist in a complex. The C-terminal region of $p47^{phox}$ may have a basal level of phosphorylation, which prevents complex formation with $p67^{phox}$ and/or possibly provides a binding site for another, yet unidentified regulatory protein. De-phosphorylation of the C-terminal region would constitute the first step in the activation process, allowing the formation of the trimeric $p47^{phox}$-$p67^{phox}$-$p40^{phox}$ complex. This is then followed by phosphorylation of the serine residues in the polybasic region to induce the active form of $p47^{phox}$, which can then migrate to the membrane, in complex with $p67^{phox}$ and $p40^{phox}$ and bind to $p22^{phox}$ (discussed in more detail in section 3.4.3).

The role of $p40^{phox}$ in NADPH oxidase activity remains controversial (Ellson et al., 2006; Grizot et al., 2001; Kuribayashi et al., 2002; Sathyamoorthy et al., 1997; Tsunawaki et al., 1996). The $p40^{phox}$ SH3 domain has been reported to be another binding partner for the C-terminal proline-rich region of $p47^{phox}$ and was speculated to compete with the $p67^{phox}$ C-terminal SH3 domain for binding. However, the binding affinity of the $p47^{phox}$-$p67^{phox}$ interaction is much higher than that for the $p47^{phox}$-$p40^{phox}$ interaction, which makes a direct competition very unlikely (Fuchs et al., 1996; Grizot et al., 2001; Lapouge et al., 2002; Wientjes et al., 1996). However, it is interesting to note that $p40^{phox}$ becomes phosphorylated on two sites: threonine 154, which is close to the SH3 domain and serine 315, which is located in the C-terminal portion (Bouin et al., 1998). Although the role of these phosphorylation events has not been investigated so far, it is tempting to speculate that phosphorylation, particularly of threonine 154, may induce conformational changes within the SH3 domain, thereby raising the affinity of $p40^{phox}$ for $p47^{phox}$ and allowing it to compete directly with $p67^{phox}$. This could be investigated in future work by carrying out quantitative binding assays between phosphorylated $p40^{phox}$ and $p47^{phox}$. $P67^{phox}$ is also phosphorylated on one major site: threonine 233 (Forbes et al., 1999). Interestingly, this residue is located within a PR region adjacent to the N-terminal SH3 domain of $p67^{phox}$, both of which have unknown functions in the regulation of NADPH oxidase activity. Future work should now be directed towards determining whether phosphorylation of this residue triggers any conformational changes within $p67^{phox}$ that may influence its interaction

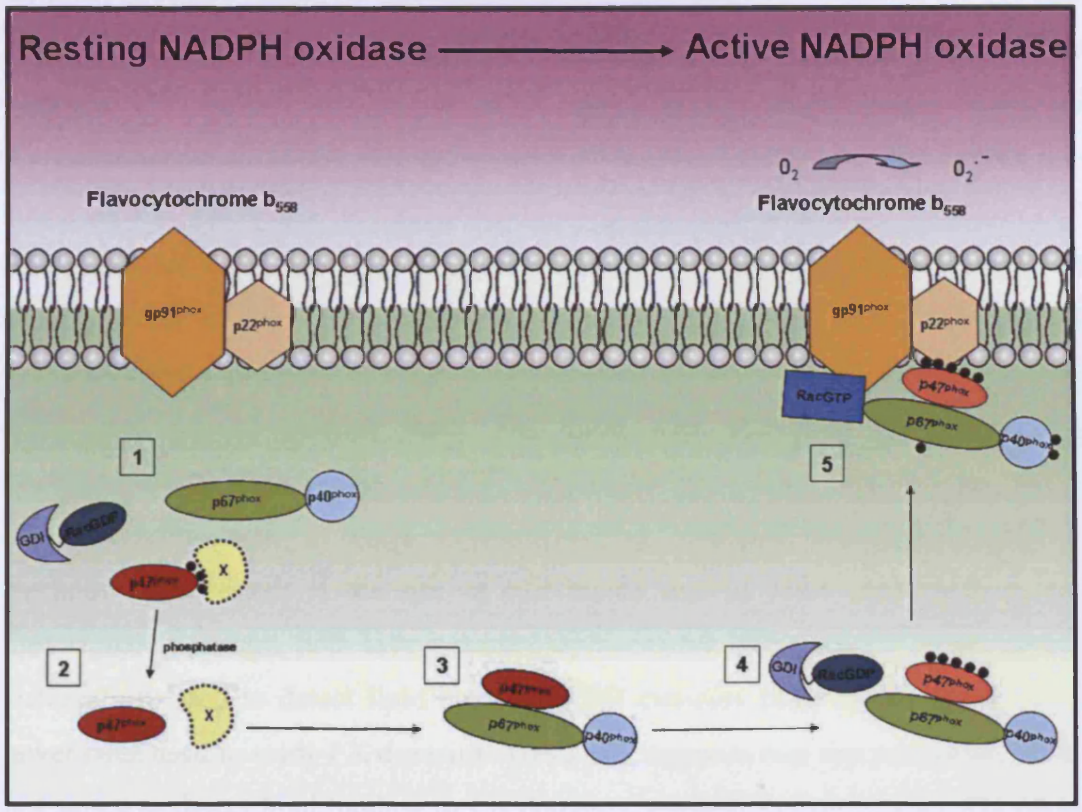

Figure 65: Proposed model for NADPH oxidase activation. Resting state (1): during the resting state of NADPH oxidase the C-terminal serine residues of $p47^{phox}$ (S359, S370 and S379) have a basal level of phosphorylation, possibly due to binding with a yet unknown protein (represented as X), which interferes with the interaction with $p67^{phox}$. De-phosphorylation (2): $p47^{phox}$ C-terminal serine residues become dephosphorylated which constitutes the first step in the activation of the NADPH oxidase. Complex formation (3): de-phosphorylation releases the unknown protein making $p47^{phox}$ available to bind the $p67^{phox}$-$p40^{phox}$ complex to form the $p47^{phox}$-$p67^{phox}$-$p40^{phox}$ trimer. Phosphorylation (4): the process is then followed by phosphorylation of serine residues (S303, S304, S315, S320 and S328) within the polybasic region of $p47^{phox}$ to give the active form of $p47^{phox}$. Translocation (5): phosphorylation induces translocation of $p47^{phox}$ to the membrane where it binds to $p22^{phox}$ thereby bringing $p67^{phox}$ and $p40^{phox}$ into close proximity to $gp91^{phox}$, and its binding partner Rac to activate the production of $O_2^{\cdot -}$.

with other NADPH oxidase components, such as $p47^{phox}$, $p40^{phox}$ or $gp91^{phox}$. Such studies could help to produce a better and more complete understanding of how phosphorylation regulates the assembly and ultimately activity of the multi-protein NADPH oxidase complex.

In the present study it was also attempted to investigate the effect of $p47^{phox}$ C-terminal phosphorylation on lipid binding to $p47^{phox}$. In the resting state, the PX domain of $p47^{phox}$ is not fully accessible for lipid binding due to an intramolecular interaction between this domain and an unknown region of the protein (Ago et al., 2003; Karathanassis et al., 2002). The intramolecular binding target for the PX domain is most likely part of the auto-inhibitory segment, as phosphorylation of the polybasic region, particularly of S303, 304 and 328, exposes the PX domain and restores maximum lipid binding (Ago et al., 2003; Karathanassis et al., 2002). It is not clear however, if phosphorylation of the C-terminal serine residues (S359, 370 and 379) plays a role in this event. In the present study this issue was addressed by testing various phosphorylation mimicking $p47^{phox}$ mutants, for their ability to bind to phosphatidylinositols. In these experiments two different protein-lipid pull down methods were tested: i) the use of PIP beads and ii) lipid sedimentation assays. Unfortunately though, both assays proved unsuccessful. Although PIP beads have been successfully used to detect lipid binding to PH domains (Rao et al., 1999), they had never been used to study PX domains. This study suggests that this particular method is not suited to detect lipid binding to PX domains, possibly because unlike PH domains, PX domains require more than just the lipid head group to form a tight interaction. In contrast, lipid sedimentation assays have previously been used successfully for the study of $p47^{phox}$ (Ago et al., 2003; Kanai et al., 2001; Karathanassis et al., 2002), so it was rather surprising when this assay failed to work in this study. The most likely explanation for this being, that the lipid vesicles may not have sedimented efficiently. In future studies the vesicles should therefore be made heavier either by including sucrose (Suire et al., 2002) or using brominated lipids (Tortorella and London, 1994). Other experimental approaches that could be adopted, include lipid overlay assays (Dowler et al., 2000; Kanai et al., 2001) or possibly surface plasmon resonance (Karathanassis et al., 2002). The latter technique is known to be quite difficult to use, however, would have the major advantage over all the other methods described here as it provides quantitative binding data.

5.2 The superSH3 domain as a novel protein interaction module

A number of studies have shown that, although $p22^{phox}$ can interact with the isolated $SH3_A$ domain of $p47^{phox}$ (de Mendez et al., 1997; Groemping et al., 2003; Sumimoto et al., 1996), binding is significantly increased in the presence of $SH3_B$ (de Mendez et al., 1997; Groemping et al., 2003). Biochemical and especially structural studies have uncovered that this high affinity is mediated by the formation of a 'superSH3' domain, where the conserved ligand binding sites of $SH3_A$ and $SH3_B$ are juxtaposed and work in coordination, a conformation that is also observed in the auto-inhibited state (Figures 8 and 10) (Groemping et al., 2003; Yuzawa et al., 2004a; Yuzawa et al., 2004b). It has been proposed that the linker connecting the two SH3 domains and a 'GWW' motif located in each n-Src loop of either SH3 domain are central to the formation of this superSH3 domain, which is believed to constitute a general protein interaction module (Groemping et al., 2003). However, little is known about how stringent the structural requirements are for the formation and stabilisation of this novel conformation, both in the auto-inhibited and active states of $p47^{phox}$. In the present study these requirements were investigated by introducing a number of mutations into the tandem SH3 domains and testing their ability to interact either with a peptide derived from the polybasic region or a $p22^{phox}$-derived peptide. Furthermore, a subset of mutants were made within the auto-inhibited core construct of $p47^{phox}$ to mimic the behaviour of full-length, auto-inhibited $p47^{phox}$. These studies demonstrate that the chemical nature (length, flexibility and composition) of the linker is critical in the auto-inhibited state, where the composition and length of the linker may be important for the correct folding of the protein. In contrast, the structural requirements are significantly less stringent for the formation of the superSH3 domain, when tested in the context of binding to the polybasic and $p22^{phox}$-peptides. These data strongly suggest that the identity of the linker is important in the context of intramolecular interactions, but that more variations in the linker can be tolerated for the formation of intermolecular complexes. Such an increased flexibility may be important to allow a variety of proteins containing tandem SH3 domains, to form a superSH3 domain and accommodate different targets. An interesting study at this point would be to ascertain what the minimum and maximum linker lengths and flexibility are for the formation of this novel conformation. This could be conducted by using deletion mutants (of greater length than

those used in this study) and linker glycine mutants, in conjunction with quantitative binding assays.

Furthermore, in this study the precise role of the tryptophan residues in the GWW motif for the stabilisation and ligand binding properties of the superSH3 domain was tested. The first tryptophan residue in this motif is known to be absolutely crucial for ligand binding in isolated SH3 domains (de Mendez et al., 1997; Hata et al., 1998; Sumimoto et al., 1996). The results presented here indicate that it plays the same role in the active, $p22^{phox}$ -bound state where removal of $W193_A$ completely disrupts complex formation, while removal of $W263_B$ reduces the affinity for the $p22^{phox}$-peptide to that of isolated $SH3_A$. Similar effects on binding to the polybasic peptide were observed. These experiments showed that both in the auto-inhibited and active states of $p47^{phox}$, $SH3_A$ plays a more dominant role in ligand binding than $SH3_B$.

$W194_A$ and $W264_B$ are believed to contribute to the stabilisation of the superSH3 domain due to the formation of interdomain hydrogen bonds (Groemping et al., 2003; Yuzawa et al., 2004a; Yuzawa et al., 2004b). Nevertheless, we show here that these interactions are not important for the stabilisation of the superSH3 domain in the auto-inhibited state. Upon removal of either of these residues the affinity for the polybasic region is maintained, possibly due to the large number of stabilising contacts made outside the core binding region. In contrast, interactions made by $W194_A$ and $W264_B$ become more important in the active state, as many of the stabilising peptide-tandem SH3 domain interactions seen in the auto-inhibited state are missing. Individual mutations of these residues to alanine reduce the affinity for $p22^{phox}$ by 6-fold and 8-fold, respectively. An interesting experiment to do at this point would be to mutate both $W194_A$ and $W264_B$ simultaneously, to determine whether this may reduce the affinity for $p22^{phox}$ to that observed for the isolated wild-type $SH3_A$ domain.

Altogether, our data indicate that the requirements for the formation and stabilisation of a superSH3 domain are not extremely strict, in terms of linker composition and the presence of the GWW motif. However, there are interesting differences in the requirements depending if the superSH3 domain/target interaction occurs in an intra- or intermolecular manner. In the case of an intramolecular interaction, the linker composition becomes more important, whilst the presence of the tryptophans in the GWW motif is less important. In contrast, intermolecular interactions made by the superSH3 domain, allow a great deal of flexibility in terms of linker length and composition, but rely more on interactions made by the tryptophan residues to achieve a high-affinity interaction. This suggests that other proteins that contain

multiple SH3 domains, separated by variable linkers, may also form such a conformation to achieve additional specificity and affinity. It is now important to test some of these proteins for their ability to adopt a superSH3 domain, in particular for those proteins where data have already shown that their SH3 domains cooperate somehow for ligand binding (Abram et al., 2003; Kowanetz et al., 2003). This would establish if this domain arrangement is indeed a general novel protein-protein interaction module.

REFERENCES

Abo, A., Pick, E., Hall, A., Totty, N., Teahan, C. G., and Segal, A. W. (1991). Activation of the NADPH oxidase involves the small GTP-binding protein p21rac1. Nature *353*, 668-670.

Abo, A., Webb, M. R., Grogan, A., and Segal, A. W. (1994). Activation of NADPH oxidase involves the dissociation of p21rac from its inhibitory GDP/GTP exchange protein (rhoGDI) followed by its translocation to the plasma membrane. Biochem J *298 Pt 3*, 585-591.

Abram, C. L., Seals, D. F., Pass, I., Salinsky, D., Maurer, L., Roth, T. M., and Courtneidge, S. A. (2003). The adaptor protein fish associates with members of the ADAMs family and localizes to podosomes of Src-transformed cells. J Biol Chem *278*, 16844-16851.

Aderem, A., and Ulevitch, R. J. (2000). Toll-like receptors in the induction of the innate immune response. Nature *406*, 782-787.

Ago, T., Kuribayashi, F., Hiroaki, H., Takeya, R., Ito, T., Kohda, D., and Sumimoto, H. (2003). Phosphorylation of p47phox directs phox homology domain from SH3 domain toward phosphoinositides, leading to phagocyte NADPH oxidase activation. Proc Natl Acad Sci U S A *100*, 4474-4479.

Ago, T., Nunoi, H., Ito, T., and Sumimoto, H. (1999). Mechanism for phosphorylation-induced activation of the phagocyte NADPH oxidase protein p47(phox). Triple replacement of serines 303, 304, and 328 with aspartates disrupts the SH3 domain-mediated intramolecular interaction in p47(phox), thereby activating the oxidase. J Biol Chem *274*, 33644-33653.

Ago, T., Takeya, R., Hiroaki, H., Kuribayashi, F., Ito, T., Kohda, D., and Sumimoto, H. (2001). The PX domain as a novel phosphoinositide- binding module. Biochem Biophys Res Commun *287*, 733-738.

Ahluwalia, J., Tinker, A., Clapp, L. H., Duchen, M. R., Abramov, A. Y., Pope, S., Nobles, M., and Segal, A. W. (2004). The large-conductance Ca2+-activated K+ channel is essential for innate immunity. Nature *427*, 853-858.

Ahmed, S., Prigmore, E., Govind, S., Veryard, C., Kozma, R., Wientjes, F. B., Segal, A. W., and Lim, L. (1998). Cryptic Rac-binding and p21(Cdc42Hs/Rac)-activated kinase phosphorylation sites of NADPH oxidase component p67(phox). J Biol Chem *273*, 15693-15701.

Alloul, N., Gorzalczany, Y., Itan, M., Sigal, N., and Pick, E. (2001). Activation of the superoxide-generating NADPH oxidase by chimeric proteins consisting of segments of the cytosolic component p67(phox) and the small GTPase Rac1. Biochemistry *40*, 14557-14566.

Ambruso, D. R., Knall, C., Abell, A. N., Panepinto, J., Kurkchubasche, A., Thurman, G., Gonzalez-Aller, C., Hiester, A., deBoer, M., Harbeck, R. J., *et al.* (2000). Human neutrophil immunodeficiency syndrome is associated with an inhibitory Rac2 mutation. Proc Natl Acad Sci U S A *97*, 4654-4659.

Antal-Szalmas, P. (2000). Evaluation of CD14 in host defence. Eur J Clin Invest *30*, 167-179.

Apostolopoulos, V., and McKenzie, I. F. (2001). Role of the mannose receptor in the immune response. Curr Mol Med *1*, 469-474.

Aratani, Y., Koyama, H., Nyui, S., Suzuki, K., Kura, F., and Maeda, N. (1999). Severe impairment in early host defense against Candida albicans in mice deficient in myeloperoxidase. Infect Immun *67*, 1828-1836.

Aratani, Y., Kura, F., Watanabe, H., Akagawa, H., Takano, Y., Suzuki, K., Maeda, N., and Koyama, H. (2000). Differential host susceptibility to pulmonary infections with bacteria and fungi in mice deficient in myeloperoxidase. J Infect Dis *182*, 1276-1279.

Babior, B. M., Curnutte, J. T., and Kipnes, R. S. (1975). Biological defense mechanisms. Evidence for the participation of superoxide in bacterial killing by xanthine oxidase. J Lab Clin Med *85*, 235-244.

Babior, B. M., and Kipnes, R. S. (1977). Superoxide-forming enzyme from human neutrophils: evidence for a flavin requirement. Blood *50*, 517-524.

Babior, B. M., Kipnes, R. S., and Curnutte, J. T. (1973). Biological defense mechanisms. The production by leukocytes of superoxide, a potential bactericidal agent. J Clin Invest *52*, 741-744.

Baggiolini, M., Hirsch, J. G., and De Duve, C. (1969). Resolution of granules from rabbit heterophil leukocytes into distinct populations by zonal sedimentation. J Cell Biol *40*, 529-541.

Bainton, D. F. (1993). Neutrophilic leukocyte granules: from structure to function. Adv Exp Med Biol *336*, 17-33.

Baldridge, C. W., and Gerard, R. W. (1933). The extra respiration of phagocytosis. Am J Physiol *103*, 235.

Banchereau, J., Briere, F., Caux, C., Davoust, J., Lebecque, S., Liu, Y. J., Pulendran, B., and Palucka, K. (2000). Immunobiology of dendritic cells. Annu Rev Immunol *18*, 767-811.

Bashford, D., Chothia, C., and Lesk, A. M. (1987). Determinants of a protein fold. Unique features of the globin amino acid sequences. J Mol Biol *196*, 199-216.

Bateman, A., Coin, L., Durbin, R., Finn, R. D., Hollich, V., Griffiths-Jones, S., Khanna, A., Marshall, M., Moxon, S., Sonnhammer, E. L., *et al.* (2004). The Pfam protein families database. Nucleic Acids Res *32*, D138-141.

Belaaouaj, A., McCarthy, R., Baumann, M., Gao, Z., Ley, T. J., Abraham, S. N., and Shapiro, S. D. (1998). Mice lacking neutrophil elastase reveal impaired host defense against gram negative bacterial sepsis. Nat Med *4*, 615-618.

Bertin, J., Nir, W. J., Fischer, C. M., Tayber, O. V., Errada, P. R., Grant, J. R., Keilty, J. J., Gosselin, M. L., Robison, K. E., Wong, G. H., *et al.* (1999). Human CARD4 protein is a novel CED-4/Apaf-1 cell death family member that activates NF-kappaB. J Biol Chem *274*, 12955-12958.

Biberstine-Kinkade, K. J., DeLeo, F. R., Epstein, R. I., LeRoy, B. A., Nauseef, W. M., and Dinauer, M. C. (2001). Heme-ligating histidines in flavocytochrome b(558): identification of specific histidines in gp91(phox). J Biol Chem *276*, 31105-31112.

Bouin, A. P., Grandvaux, N., Vignais, P. V., and Fuchs, A. (1998). p40(phox) is phosphorylated on threonine 154 and serine 315 during activation of the phagocyte NADPH oxidase. Implication of a protein kinase c-type kinase in the phosphorylation process. J Biol Chem *273*, 30097-30103.

Boyton, R. J., and Openshaw, P. J. (2002). Pulmonary defences to acute respiratory infection. Br Med Bull *61*, 1-12.

Braff, M. H., and Gallo, R. L. (2006). Antimicrobial peptides: an essential component of the skin defensive barrier. Curr Top Microbiol Immunol *306*, 91-110.

Bravo, J., Karathanassis, D., Pacold, C. M., Pacold, M. E., Ellson, C. D., Anderson, K. E., Butler, P. J., Lavenir, I., Perisic, O., Hawkins, P. T., *et al.* (2001). The crystal structure of the PX domain from p40(phox) bound to phosphatidylinositol 3-phosphate. Mol Cell *8*, 829-839.

Bromberg, Y., and Pick, E. (1984). Unsaturated fatty acids stimulate NADPH-dependent superoxide production by cell-free system derived from macrophages. Cell Immunol *88*, 213-221.

Brown, G. E., Stewart, M. Q., Liu, H., Ha, V. L., and Yaffe, M. B. (2003). A novel assay system implicates PtdIns(3,4)P(2), PtdIns(3)P, and PKC delta in intracellular production of reactive oxygen species by the NADPH oxidase. Mol Cell *11*, 35-47.

Bundgaard, J. R., Sengelov, H., Borregaard, N., and Kjeldsen, L. (1994). Molecular cloning and expression of a cDNA encoding NGAL: a lipocalin expressed in human neutrophils. Biochem Biophys Res Commun *202*, 1468-1475.

Capron, M. (1991). Eosinophils and parasites. Ann Parasitol Hum Comp *66 Suppl 1*, 41-45.

Cech, P., and Lehrer, R. I. (1984). Phagolysosomal pH of human neutrophils. Blood *63*, 88-95.

Chang, Y. C., Segal, B. H., Holland, S. M., Miller, G. F., and Kwon-Chung, K. J. (1998). Virulence of catalase-deficient aspergillus nidulans in p47(phox)-/- mice. Implications for fungal pathogenicity and host defense in chronic granulomatous disease. J Clin Invest *101*, 1843-1850.

Chaplin, D. D. (2006). 1. Overview of the human immune response. J Allergy Clin Immunol *117*, S430-435.

Chen, J. K., Lane, W. S., Brauer, A. W., Tanaka, A., and S.L.Schreiber (1993). Biased Combinatorial Libraries: Novel Ligands for the SH3 Domian of Phosphatidylionositol 3-Kinase. J Am Chem soc *115*, 12591-12592.

Chothia, C., Gelfand, I., and Kister, A. (1998). Structural determinants in the sequences of immunoglobulin variable domain. J Mol Biol *278*, 457-479.

Corvera, S., D'Arrigo, A., and Stenmark, H. (1999). Phosphoinositides in membrane traffic. Curr Opin Cell Biol *11*, 460-465.

Cross, A. R., Curnutte, J. T., and Heyworth, P. G. (1996a). Hematologically important mutations: the autosomal recessive forms of chronic granulomatous disease. Blood Cells Mol Dis *22*, 268-270.

Cross, A. R., Curnutte, J. T., Rae, J., and Heyworth, P. G. (1996b). Hematologically important mutations: X-linked chronic granulomatous disease. Blood Cells Mol Dis *22*, 90-95.

Cross, A. R., Rae, J., and Curnutte, J. T. (1995). Cytochrome b-245 of the neutrophil superoxide-generating system contains two nonidentical hemes. Potentiometric studies of a mutant form of gp91phox. J Biol Chem *270*, 17075-17077.

D'Andrea, L. D., and Regan, L. (2003). TPR proteins: the versatile helix. Trends Biochem Sci *28*, 655-662.

Dalgarno, D. C., Botfield, M. C., and Rickles, R. J. (1997). SH3 domains and drug design: ligands, structure, and biological function. Biopolymers *43*, 383-400.

Dang, P. M., Babior, B. M., and Smith, R. M. (1999). NADPH dehydrogenase activity of p67PHOX, a cytosolic subunit of the leukocyte NADPH oxidase. Biochemistry *38*, 5746-5753.

Dang, P. M., Cross, A. R., and Babior, B. M. (2001). Assembly of the neutrophil respiratory burst oxidase: a direct interaction between p67PHOX and cytochrome b558. Proc Natl Acad Sci U S A *98*, 3001-3005.

Das, A. K., Cohen, P. W., and Barford, D. (1998). The structure of the tetratricopeptide repeats of protein phosphatase 5: implications for TPR-mediated protein-protein interactions. Embo J *17*, 1192-1199.

de Mendez, I., Homayounpour, N., and Leto, T. L. (1997). Specificity of p47phox SH3 domain interactions in NADPH oxidase assembly and activation. Mol Cell Biol *17*, 2177-2185.

DeLeo, F. R., Burritt, J. B., Yu, L., Jesaitis, A. J., Dinauer, M. C., and Nauseef, W. M. (2000). Processing and maturation of flavocytochrome b558 include incorporation of heme as a prerequisite for heterodimer assembly. J Biol Chem *275*, 13986-13993.

DeLeo, F. R., Yu, L., Burritt, J. B., Loetterle, L. R., Bond, C. W., Jesaitis, A. J., and Quinn, M. T. (1995). Mapping sites of interaction of p47-phox and flavocytochrome b with random-sequence peptide phage display libraries. Proc Natl Acad Sci U S A *92*, 7110-7114.

Dexter, T. M., and Spooncer, E. (1987). Growth and differentiation in the hemopoietic system. Annu Rev Cell Biol *3*, 423-441.

Didsbury, J., Weber, R. F., Bokoch, G. M., Evans, T., and Snyderman, R. (1989). rac, a novel ras-related family of proteins that are botulinum toxin substrates. J Biol Chem *264*, 16378-16382.

Diebold, B. A., and Bokoch, G. M. (2001). Molecular basis for Rac2 regulation of phagocyte NADPH oxidase. Nat Immunol *2*, 211-215.

Diekmann, D., Abo, A., Johnston, C., Segal, A. W., and Hall, A. (1994). Interaction of Rac with p67phox and regulation of phagocytic NADPH oxidase activity. Science *265*, 531-533.

Dill, K. A. (1990). Dominant forces in protein folding. Biochemistry *29*, 7133-7155.

Dinauer, M. C. (2005). Chronic granulomatous disease and other disorders of phagocyte function. Hematology (Am Soc Hematol Educ Program), 89-95.

Dinauer, M. C., Pierce, E. A., Erickson, R. W., Muhlebach, T. J., Messner, H., Orkin, S. H., Seger, R. A., and Curnutte, J. T. (1991). Point mutation in the cytoplasmic domain of the neutrophil p22-phox cytochrome b subunit is associated with a nonfunctional NADPH oxidase and chronic granulomatous disease. Proc Natl Acad Sci U S A *88*, 11231-11235.

Dowler, S., Currie, R. A., Campbell, D. G., Deak, M., Kular, G., Downes, C. P., and Alessi, D. R. (2000). Identification of pleckstrin-homology-domain-containing proteins with novel phosphoinositide-binding specificities. Biochem J *351*, 19-31.

Dunne, D. W., Resnick, D., Greenberg, J., Krieger, M., and Joiner, K. A. (1994). The type I macrophage scavenger receptor binds to gram-positive bacteria and recognizes lipoteichoic acid. Proc Natl Acad Sci U S A *91*, 1863-1867.

Dusi, S., Donini, M., and Rossi, F. (1996). Mechanisms of NADPH oxidase activation: translocation of p40phox, Rac1 and Rac2 from the cytosol to the membranes in human neutrophils lacking p47phox or p67phox. Biochem J *314 (Pt 2)*, 409-412.

el Benna, J., Faust, L. P., and Babior, B. M. (1994). The phosphorylation of the respiratory burst oxidase component p47phox during neutrophil activation. Phosphorylation of sites recognized by protein kinase C and by proline-directed kinases. J Biol Chem *269*, 23431-23436.

El Benna, J., Faust, R. P., Johnson, J. L., and Babior, B. M. (1996). Phosphorylation of the respiratory burst oxidase subunit p47phox as determined by two-dimensional phosphopeptide mapping. Phosphorylation by protein kinase C, protein kinase A, and a mitogen-activated protein kinase. J Biol Chem *271*, 6374-6378.

Ellson, C. D., Davidson, K., Ferguson, G. J., O'Connor, R., Stephens, L. R., and Hawkins, P. T. (2006). Neutrophils from p40phox-/- mice exhibit severe defects in NADPH oxidase regulation and oxidant-dependent bacterial killing. J Exp Med *203*, 1927-1937.

Ellson, C. D., Gobert-Gosse, S., Anderson, K. E., Davidson, K., Erdjument-Bromage, H., Tempst, P., Thuring, J. W., Cooper, M. A., Lim, Z. Y., Holmes, A. B., *et al.* (2001). PtdIns(3)P regulates the neutrophil oxidase complex by binding to the PX domain of p40(phox). Nat Cell Biol *3*, 679-682.

Elsbach, P. (1998). The bactericidal/permeability-increasing protein (BPI) in antibacterial host defense. J Leukoc Biol *64*, 14-18.

Erpel, T., Superti-Furga, G., and Courtneidge, S. A. (1995). Mutational analysis of the Src SH3 domain: the same residues of the ligand binding surface are important for intra- and intermolecular interactions. Embo J *14*, 963-975.

Ezekowitz, R. A., Sastry, K., Bailly, P., and Warner, A. (1990). Molecular characterization of the human macrophage mannose receptor: demonstration of multiple carbohydrate recognition-like domains and phagocytosis of yeasts in Cos-1 cells. J Exp Med *172*, 1785-1794.

Faust, L. R., el Benna, J., Babior, B. M., and Chanock, S. J. (1995). The phosphorylation targets of p47phox, a subunit of the respiratory burst oxidase. Functions of the individual target serines as evaluated by site-directed mutagenesis. J Clin Invest *96*, 1499-1505.

Fedoroff, O. Y., Townson, S. A., Golovanov, A. P., Baron, M., and Avis, J. M. (2004). The structure and dynamics of tandem WW domains in a negative regulator of notch signaling, Suppressor of deltex. J Biol Chem *279*, 34991-35000.

Feller, S. M., Ren, R., Hanafusa, H., and Baltimore, D. (1994). SH2 and SH3 domains as molecular adhesives: the interactions of Crk and Abl. Trends Biochem Sci *19*, 453-458.

Feng, S., Chen, J. K., Yu, H., Simon, J. A., and Schreiber, S. L. (1994). Two binding orientations for peptides to the Src SH3 domain: development of a general model for SH3-ligand interactions. Science *266*, 1241-1247.

Feng, S., Kasahara, C., Rickles, R. J., and Schreiber, S. L. (1995). Specific interactions outside the proline-rich core of two classes of Src homology 3 ligands. Proc Natl Acad Sci U S A *92*, 12408-12415.

Fernandez, H. N., Henson, P. M., Otani, A., and Hugli, T. E. (1978). Chemotactic response to human C3a and C5a anaphylatoxins. I. Evaluation of C3a and C5a leukotaxis in vitro and under stimulated in vivo conditions. J Immunol *120*, 109-115.

Finan, P., Shimizu, Y., Gout, I., Hsuan, J., Truong, O., Butcher, C., Bennett, P., Waterfield, M. D., and Kellie, S. (1994). An SH3 domain and proline-rich sequence mediate an interaction between two components of the phagocyte NADPH oxidase complex. J Biol Chem *269*, 13752-13755.

Finkel, T. (2003). Oxidant signals and oxidative stress. Curr Opin Cell Biol *15*, 247-254.

Forbes, L. V., Truong, O., Wientjes, F. B., Moss, S. J., and Segal, A. W. (1999). The major phosphorylation site of the NADPH oxidase component p67phox is Thr233. Biochem J *338 (Pt 1)*, 99-105.

Freeman, J. L., Abo, A., and Lambeth, J. D. (1996). Rac "insert region" is a novel effector region that is implicated in the activation of NADPH oxidase, but not PAK65. J Biol Chem *271*, 19794-19801.

Freeman, J. L., Kreck, M. L., Uhlinger, D. J., and Lambeth, J. D. (1994). Ras effector-homologue region on Rac regulates protein associations in the neutrophil respiratory burst oxidase complex. Biochemistry *33*, 13431-13435.

Freeman, J. L., and Lambeth, J. D. (1996). NADPH oxidase activity is independent of p47phox in vitro. J Biol Chem *271*, 22578-22582.

Fruman, D. A., Rameh, L. E., and Cantley, L. C. (1999). Phosphoinositide binding domains: embracing 3-phosphate. Cell *97*, 817-820.

Fuchs, A., Dagher, M. C., Faure, J., and Vignais, P. V. (1996). Topological organization of the cytosolic activating complex of the superoxide-generating NADPH-oxidase. Pinpointing the sites of interaction between p47phoz, p67phox and p40phox using the two-hybrid system. Biochim Biophys Acta *1312*, 39-47.

Galli, S. J. (2000). Mast cells and basophils. Curr Opin Hematol *7*, 32-39.

Galli, S. J., Gordon, J. R., and Wershil, B. K. (1991). Cytokine production by mast cells and basophils. Curr Opin Immunol *3*, 865-872.

Gallin, J. I., Buescher, E. S., Seligmann, B. E., Nath, J., Gaither, T., and Katz, P. (1983). NIH conference. Recent advances in chronic granulomatous disease. Ann Intern Med *99*, 657-674.

Golde, D. W. (1991). The stem cell. Sci Am *265*, 86-93.

Gordon, S. (1995). The macrophage. Bioessays *17*, 977-986.

Gorzalczany, Y., Sigal, N., Itan, M., Lotan, O., and Pick, E. (2000). Targeting of Rac1 to the phagocyte membrane is sufficient for the induction of NADPH oxidase assembly. J Biol Chem *275*, 40073-40081.

Govindaraj, S., and Poulos, T. L. (1995). Role of the linker region connecting the reductase and heme domains in cytochrome P450BM-3. Biochemistry *34*, 11221-11226.

Grizot, S., Grandvaux, N., Fieschi, F., Faure, J., Massenet, C., Andrieu, J. P., Fuchs, A., Vignais, P. V., Timmins, P. A., Dagher, M. C., and Pebay-Peyroula, E. (2001). Small angle neutron scattering and gel filtration analyses of neutrophil NADPH oxidase cytosolic factors highlight the role of the C-terminal end of p47phox in the association with p40phox. Biochemistry *40*, 3127-3133.

Groemping, Y., Lapouge, K., Smerdon, S. J., and Rittinger, K. (2003). Molecular basis of phosphorylation-induced activation of the NADPH oxidase. Cell *113*, 343-355.

Hampton, M. B., Kettle, A. J., and Winterbourn, C. C. (1998). Inside the neutrophil phagosome: oxidants, myeloperoxidase, and bacterial killing. Blood *92*, 3007-3017.

Han, C. H., Freeman, J. L., Lee, T., Motalebi, S. A., and Lambeth, J. D. (1998). Regulation of the neutrophil respiratory burst oxidase. Identification of an activation domain in p67(phox). J Biol Chem *273*, 16663-16668.

Han, C. H., and Lee, M. H. (2000). Activation domain in P67phox regulates the steady state reduction of FAD in gp91phox. J Vet Sci *1*, 27-31.

Harper, A. M., Chaplin, M. F., and Segal, A. W. (1985). Cytochrome b-245 from human neutrophils is a glycoprotein. Biochem J *227*, 783-788.

Harper, A. M., Dunne, M. J., and Segal, A. W. (1984). Purification of cytochrome b-245 from human neutrophils. Biochem J *219*, 519-527.

Hata, K., Ito, T., Takeshige, K., and Sumimoto, H. (1998). Anionic amphiphile-independent activation of the phagocyte NADPH oxidase in a cell-free system by p47phox and p67phox, both in C terminally truncated forms. Implication for regulatory Src homology 3 domain-mediated interactions. J Biol Chem *273*, 4232-4236.

Hawkins, P. T., Davidson, K., and Stephens, L. R. (2007). The role of PI3Ks in the regulation of the neutrophil NADPH oxidase. Biochem Soc Symp, 59-67.

Hayakawa, T., Suzuki, K., Suzuki, S., Andrews, P. C., and Babior, B. M. (1986). A possible role for protein phosphorylation in the activation of the respiratory burst in

human neutrophils. Evidence from studies with cells from patients with chronic granulomatous disease. J Biol Chem *261*, 9109-9115.

Hayashi, F., Means, T. K., and Luster, A. D. (2003). Toll-like receptors stimulate human neutrophil function. Blood *102*, 2660-2669.

Hegvold, A. B., and Gabrielsen, O. S. (1996). The importance of the linker connecting the repeats of the c-Myb oncoprotein may be due to a positioning function. Nucleic Acids Res *24*, 3990-3995.

Henderson, L. M., Chappell, J. B., and Jones, O. T. (1987). The superoxide-generating NADPH oxidase of human neutrophils is electrogenic and associated with an H+ channel. Biochem J *246*, 325-329.

Heyneman, R. A., and Vercauteren, R. E. (1984). Activation of a NADPH oxidase from horse polymorphonuclear leukocytes in a cell-free system. J Leukoc Biol *36*, 751-759.

Heyworth, P. G., Bohl, B. P., Bokoch, G. M., and Curnutte, J. T. (1994). Rac translocates independently of the neutrophil NADPH oxidase components p47phox and p67phox. Evidence for its interaction with flavocytochrome b558. J Biol Chem *269*, 30749-30752.

Heyworth, P. G., and Cross, A. R. (2002). Chronic granulomatous disease mutations and the PX domain. Nat Cell Biol *4*, E110.

Heyworth, P. G., Cross, A. R., and Curnutte, J. T. (2003). Chronic granulomatous disease. Curr Opin Immunol *15*, 578-584.

Heyworth, P. G., Curnutte, J. T., Nauseef, W. M., Volpp, B. D., Pearson, D. W., Rosen, H., and Clark, R. A. (1991). Neutrophil nicotinamide adenine dinucleotide phosphate oxidase assembly. Translocation of p47-phox and p67-phox requires interaction between p47-phox and cytochrome b558. J Clin Invest *87*, 352-356.

Heyworth, P. G., Curnutte, J. T., Noack, D., and Cross, A. R. (1997). Hematologically important mutations: X-linked chronic granulomatous disease--an update. Blood Cells Mol Dis *23*, 443-450.

Heyworth, P. G., Knaus, U. G., Settleman, J., Curnutte, J. T., and Bokoch, G. M. (1993). Regulation of NADPH oxidase activity by Rac GTPase activating protein(s). Mol Biol Cell *4*, 1217-1223.

Hirano, T., Kinoshita, N., Morikawa, K., and Yanagida, M. (1990). Snap helix with knob and hole: essential repeats in S. pombe nuclear protein nuc2+. Cell *60*, 319-328.

Hiroaki, H., Ago, T., Ito, T., Sumimoto, H., and Kohda, D. (2001). Solution structure of the PX domain, a target of the SH3 domain. Nat Struct Biol *8*, 526-530.

Hoebe, K., Janssen, E., and Beutler, B. (2004). The interface between innate and adaptive immunity. Nat Immunol *5*, 971-974.

Hoffman, G. R., Nassar, N., and Cerione, R. A. (2000). Structure of the Rho family GTP-binding protein Cdc42 in complex with the multifunctional regulator RhoGDI. Cell *100*, 345-356.

Hofmann, G., Schweimer, K., Kiessling, A., Hofinger, E., Bauer, F., Hoffmann, S., Rosch, P., Campbell, I. D., Werner, J. M., and Sticht, H. (2005). Binding, domain orientation, and dynamics of the Lck SH3-SH2 domain pair and comparison with other Src-family kinases. Biochemistry *44*, 13043-13050.

Holmes, B., Page, A. R., and Good, R. A. (1967). Studies of the metabolic activity of leukocytes from patients with a genetic abnormality of phagocytic function. J Clin Invest *46*, 1422-1432.

Honbou, K., Minakami, R., Yuzawa, S., Takeya, R., Suzuki, N. N., Kamakura, S., Sumimoto, H., and Inagaki, F. (2007). Full-length p40phox structure suggests a basis for regulation mechanism of its membrane binding. Embo J *26*, 1176-1186.

Hulo, N., Bairoch, A., Bulliard, V., Cerutti, L., De Castro, E., Langendijk-Genevaux, P. S., Pagni, M., and Sigrist, C. J. (2006). The PROSITE database. Nucleic Acids Res *34*, D227-230.

Inanami, O., Johnson, J. L., McAdara, J. K., Benna, J. E., Faust, L. R., Newburger, P. E., and Babior, B. M. (1998). Activation of the leukocyte NADPH oxidase by phorbol ester requires the phosphorylation of p47PHOX on serine 303 or 304. J Biol Chem *273*, 9539-9543.

Inohara, N., Koseki, T., del Peso, L., Hu, Y., Yee, C., Chen, S., Carrio, R., Merino, J., Liu, D., Ni, J., and Nunez, G. (1999). Nod1, an Apaf-1-like activator of caspase-9 and nuclear factor-kappaB. J Biol Chem *274*, 14560-14567.

Ishida, K., Takeshige, K., Takasugi, S., and Minakami, S. (1989). GTP-dependent and -independent activation of superoxide producing NADPH oxidase in a neutrophil cell-free system. FEBS Lett *243*, 169-172.

Ito, T., Matsui, Y., Ago, T., Ota, K., and Sumimoto, H. (2001). Novel modular domain PB1 recognizes PC motif to mediate functional protein-protein interactions. Embo J *20*, 3938-3946.

Iyer, G. Y. N., Islam, M. F., and Quastel, J. H. (1961). Biochemical aspects of phagocytosis. Nature *192*, 535-541.

Janeway, C., Traverns, P., Walport, M., and Shlomchik, M. (2001). Immunobiology, 5th edn (New York Garland Science).

Janeway, C. A., Jr. (2001). How the immune system works to protect the host from infection: a personal view. Proc Natl Acad Sci U S A *98*, 7461-7468.

Johnson, J. L., Park, J. W., Benna, J. E., Faust, L. P., Inanami, O., and Babior, B. M. (1998). Activation of p47(PHOX), a cytosolic subunit of the leukocyte NADPH oxidase. Phosphorylation of ser-359 or ser-370 precedes phosphorylation at other sites and is required for activity. J Biol Chem *273*, 35147-35152.

Johnson, W. C., Jr. (1990). Protein secondary structure and circular dichroism: a practical guide. Proteins *7*, 205-214.

Joseph, G., and Pick, E. (1995). "Peptide walking" is a novel method for mapping functional domains in proteins. Its application to the Rac1-dependent activation of NADPH oxidase. J Biol Chem *270*, 29079-29082.

Jozic, D., Cardenes, N., Deribe, Y. L., Moncalian, G., Hoeller, D., Groemping, Y., Dikic, I., Rittinger, K., and Bravo, J. (2005). Cbl promotes clustering of endocytic adaptor proteins. Nat Struct Mol Biol.

Jung, V., Wei, W., Ballester, R., Camonis, J., Mi, S., Van Aelst, L., Wigler, M., and Broek, D. (1994). Two types of RAS mutants that dominantly interfere with activators of RAS. Mol Cell Biol *14*, 3707-3718.

Kami, K., Takeya, R., Sumimoto, H., and Kohda, D. (2002). Diverse recognition of non-PxxP peptide ligands by the SH3 domains from p67(phox), Grb2 and Pex13p. Embo J *21*, 4268-4276.

Kanai, F., Liu, H., Field, S. J., Akbary, H., Matsuo, T., Brown, G. E., Cantley, L. C., and Yaffe, M. B. (2001). The PX domains of p47phox and p40phox bind to lipid products of PI(3)K. Nat Cell Biol *3*, 675-678.

Karathanassis, D., Stahelin, R. V., Bravo, J., Perisic, O., Pacold, C. M., Cho, W., and Williams, R. L. (2002). Binding of the PX domain of p47(phox) to phosphatidylinositol 3,4-bisphosphate and phosphatidic acid is masked by an intramolecular interaction. Embo J *21*, 5057-5068.

Kimber, W. A., Trinkle-Mulcahy, L., Cheung, P. C., Deak, M., Marsden, L. J., Kieloch, A., Watt, S., Javier, R. T., Gray, A., Downes, C. P., *et al.* (2002). Evidence that the tandem-pleckstrin-homology-domain-containing protein TAPP1 interacts with Ptd(3,4)P2 and the multi-PDZ-domain-containing protein MUPP1 in vivo. Biochem J *361*, 525-536.

Kitano, H., and Oda, K. (2006). Robustness trade-offs and host-microbial symbiosis in the immune system. Mol Syst Biol *2*, 2006 0022.

Klebanoff, S. J. (1967a). Iodination of bacteria: a bactericidal mechanism. J Exp Med *126*, 1063-1078.

Klebanoff, S. J. (1967b). A peroxidase-mediated antimicrobial system in leukocytes. J Clin Invest *46*, 1478.

Klebanoff, S. J. (1968). Myeloperoxidase-halide-hydrogen peroxide antibacterial system. J Bacteriol *95*, 2131-2138.

Klebanoff, S. J. (1974). Role of the superoxide anion in the myeloperoxidase-mediated antimicrobial system. J Biol Chem *249*, 3724-3728.

Klebanoff, S. J., and White, L. R. (1969). Iodination defect in the leukocytes of a patient with chronic granulomatous disease of childhood. N Engl J Med *280*, 460-466.

Knaus, U. G., Heyworth, P. G., Evans, T., Curnutte, J. T., and Bokoch, G. M. (1991). Regulation of phagocyte oxygen radical production by the GTP-binding protein Rac 2. Science *254*, 1512-1515.

Koga, H., Terasawa, H., Nunoi, H., Takeshige, K., Inagaki, F., and Sumimoto, H. (1999). Tetratricopeptide repeat (TPR) motifs of p67(phox) participate in interaction with the small GTPase Rac and activation of the phagocyte NADPH oxidase. J Biol Chem *274*, 25051-25060.

Kolset, S. O., and Gallagher, J. T. (1990). Proteoglycans in haemopoietic cells. Biochim Biophys Acta *1032*, 191-211.

Kowanetz, K., Szymkiewicz, I., Haglund, K., Kowanetz, M., Husnjak, K., Taylor, J. D., Soubeyran, P., Engstrom, U., Ladbury, J. E., and Dikic, I. (2003). Identification of a novel proline-arginine motif involved in CIN85-dependent clustering of Cbl and down-regulation of epidermal growth factor receptors. J Biol Chem *278*, 39735-39746.

Kuribayashi, F., Nunoi, H., Wakamatsu, K., Tsunawaki, S., Sato, K., Ito, T., and Sumimoto, H. (2002). The adaptor protein p40(phox) as a positive regulator of the superoxide-producing phagocyte oxidase. Embo J *21*, 6312-6320.

Ladbury, J. E. (2004). Application of isothermal titration calorimetry in the biological sciences: things are heating up! Biotechniques *37*, 885-887.

Lakowicz, J. (1999). Principles of Fluorescence Spectroscopy, 2nd edn (New York: Kluwer Academic/Plenum Publishers).

Lambeth, J. D. (2000). Regulation of the phagocyte respiratory burst oxidase by protein interactions. J Biochem Mol Biol *33*, 427-439.

Lanier, L. L. (1998). NK cell receptors. Annu Rev Immunol *16*, 359-393.

Lapouge, K., Smith, S. J., Groemping, Y., and Rittinger, K. (2002). Architecture of the p40-p47-p67phox complex in the resting state of the NADPH oxidase. A central role for p67phox. J Biol Chem *277*, 10121-10128.

Lapouge, K., Smith, S. J., Walker, P. A., Gamblin, S. J., Smerdon, S. J., and Rittinger, K. (2000). Structure of the TPR domain of p67phox in complex with Rac.GTP. Mol Cell *6*, 899-907.

Larson, S. M., and Davidson, A. R. (2000). The identification of conserved interactions within the SH3 domain by alignment of sequences and structures. Protein Sci *9*, 2170-2180.

Leavitt, S., and Freire, E. (2001). Direct measurement of protein binding energetics by isothermal titration calorimetry. Curr Opin Struct Biol *11*, 560-566.

Lehrer, R. I., Hanifin, J., and Cline, M. J. (1969). Defective bactericidal activity in myeloperoxidase-deficient human neutrophils. Nature *223*, 78-79.

Leto, T. L., Adams, A. G., and de Mendez, I. (1994). Assembly of the phagocyte NADPH oxidase: binding of Src homology 3 domains to proline-rich targets. Proc Natl Acad Sci U S A *91*, 10650-10654.

Leto, T. L., Lomax, K. J., Volpp, B. D., Nunoi, H., Sechler, J. M., Nauseef, W. M., Clark, R. A., Gallin, J. I., and Malech, H. L. (1990). Cloning of a 67-kD neutrophil oxidase factor with similarity to a noncatalytic region of p60c-src. Science *248*, 727-730.

Leusen, J. H., Bolscher, B. G., Hilarius, P. M., Weening, R. S., Kaulfersch, W., Seger, R. A., Roos, D., and Verhoeven, A. J. (1994a). 156Pro-->Gln substitution in the light chain of cytochrome b558 of the human NADPH oxidase (p22-phox) leads to defective translocation of the cytosolic proteins p47-phox and p67-phox. J Exp Med *180*, 2329-2334.

Leusen, J. H., de Boer, M., Bolscher, B. G., Hilarius, P. M., Weening, R. S., Ochs, H. D., Roos, D., and Verhoeven, A. J. (1994b). A point mutation in gp91-phox of cytochrome b558 of the human NADPH oxidase leading to defective translocation of the cytosolic proteins p47-phox and p67-phox. J Clin Invest *93*, 2120-2126.

Levay, P. F., and Viljoen, M. (1995). Lactoferrin: a general review. Haematologica *80*, 252-267.

Lim, W. A., and Richards, F. M. (1994). Critical residues in an SH3 domain from Sem-5 suggest a mechanism for proline-rich peptide recognition. Nat Struct Biol *1*, 221-225.

Lim, W. A., Richards, F. M., and Fox, R. O. (1994). Structural determinants of peptide-binding orientation and of sequence specificity in SH3 domains. Nature *372*, 375-379.

Liu, X., Marengere, L. E., Koch, C. A., and Pawson, T. (1993). The v-Src SH3 domain binds phosphatidylinositol 3'-kinase. Mol Cell Biol *13*, 5225-5232.

Lomax, K. J., Leto, T. L., Nunoi, H., Gallin, J. I., and Malech, H. L. (1989). Recombinant 47-kilodalton cytosol factor restores NADPH oxidase in chronic granulomatous disease. Science *245*, 409-412.

Ma, Y. G., Cho, M. Y., Zhao, M., Park, J. W., Matsushita, M., Fujita, T., and Lee, B. L. (2004). Human mannose-binding lectin and L-ficolin function as specific pattern recognition proteins in the lectin activation pathway of complement. J Biol Chem *279*, 25307-25312.

Mandell, G. L. (1974). Bactericidal activity of aerobic and anaerobic polymorphonuclear neutrophils. Infect Immun *9*, 337-341.

Manser, E., Loo, T. H., Koh, C. G., Zhao, Z. S., Chen, X. Q., Tan, L., Tan, I., Leung, T., and Lim, L. (1998). PAK kinases are directly coupled to the PIX family of nucleotide exchange factors. Mol Cell *1*, 183-192.

Massenet, C., Chenavas, S., Cohen-Addad, C., Dagher, M. C., Brandolin, G., Pebay-Peyroula, E., and Fieschi, F. (2005). Effects of p47phox C terminus phosphorylations on binding interactions with p40phox and p67phox. Structural and functional comparison of p40phox and p67phox SH3 domains. J Biol Chem *280*, 13752-13761.

Mayer, B. J. (2001). SH3 domains: complexity in moderation. J Cell Sci *114*, 1253-1263.

Mayer, B. J., and Eck, M. J. (1995). SH3 domains. Minding your p's and q's. Curr Biol *5*, 364-367.

Mayer, B. J., Hamaguchi, M., and Hanafusa, H. (1988). A novel viral oncogene with structural similarity to phospholipase C. Nature *332*, 272-275.

Meischl, C., and Roos, D. (1998). The molecular basis of chronic granulomatous disease. Springer Semin Immunopathol *19*, 417-434.

Messina, C. G., Reeves, E. P., Roes, J., and Segal, A. W. (2002). Catalase negative Staphylococcus aureus retain virulence in mouse model of chronic granulomatous disease. FEBS Lett *518*, 107-110.

Metchnikoff, E. (1905). Immunity in Infective Diseases (Cambridge: Cambridge University Press).

Mizuki, K., Takeya, R., Kuribayashi, F., Nobuhisa, I., Kohda, D., Nunoi, H., Takeshige, K., and Sumimoto, H. (2005). A region C-terminal to the proline-rich core of p47phox regulates activation of the phagocyte NADPH oxidase by interacting with the C-terminal SH3 domain of p67phox. Arch Biochem Biophys *444*, 185-194.

Mongiovi, A. M., Romano, P. R., Panni, S., Mendoza, M., Wong, W. T., Musacchio, A., Cesareni, G., and Di Fiore, P. P. (1999). A novel peptide-SH3 interaction. Embo J *18*, 5300-5309.

Moore, P. L., Bank, H. L., Brissie, N. T., and Spicer, S. S. (1978). Phagocytosis of bacteria by polymorphonuclear leukocytes. A freeze-fracture, scanning electron microscope, and thin-section investigation of membrane structure. J Cell Biol *76*, 158-174.

Morgan, B. P., Marchbank, K. J., Longhi, M. P., Harris, C. L., and Gallimore, A. M. (2005). Complement: central to innate immunity and bridging to adaptive responses. Immunol Lett *97*, 171-179.

Muller-Eberhard, H. J. (1988). Molecular organization and function of the complement system. Annu Rev Biochem *57*, 321-347.

Nakamura, R., Sumimoto, H., Mizuki, K., Hata, K., Ago, T., Kitajima, S., Takeshige, K., Sakaki, Y., and Ito, T. (1998). The PC motif: a novel and evolutionarily conserved sequence involved in interaction between p40phox and p67phox, SH3 domain-containing cytosolic factors of the phagocyte NADPH oxidase. Eur J Biochem *251*, 583-589.

Nauseef, W. M. (1988). Myeloperoxidase deficiency. Hematol Oncol Clin North Am *2*, 135-158.

Nauseef, W. M., Volpp, B. D., McCormick, S., Leidal, K. G., and Clark, R. A. (1991). Assembly of the neutrophil respiratory burst oxidase. Protein kinase C promotes

cytoskeletal and membrane association of cytosolic oxidase components. J Biol Chem *266*, 5911-5917.

Neilands, J. B. (1995). Siderophores: structure and function of microbial iron transport compounds. J Biol Chem *270*, 26723-26726.

Ninfa, A. J., and Ballou, D. P. (1998). Fundamental Laboratory Approaches for Biochemistry AND Biotechnology (Maryland: Fitzgerald Science Press, Inc).

Nisimoto, Y., Motalebi, S., Han, C. H., and Lambeth, J. D. (1999). The p67(phox) activation domain regulates electron flow from NADPH to flavin in flavocytochrome b(558). J Biol Chem *274*, 22999-23005.

Noack, D., Rae, J., Cross, A. R., Ellis, B. A., Newburger, P. E., Curnutte, J. T., and Heyworth, P. G. (2001). Autosomal recessive chronic granulomatous disease caused by defects in NCF-1, the gene encoding the phagocyte p47-phox: mutations not arising in the NCF-1 pseudogenes. Blood *97*, 305-311.

Noble, M. E., Musacchio, A., Saraste, M., Courtneidge, S. A., and Wierenga, R. K. (1993). Crystal structure of the SH3 domain in human Fyn; comparison of the three-dimensional structures of SH3 domains in tyrosine kinases and spectrin. Embo J *12*, 2617-2624.

Nobuhisa, I., Takeya, R., Ogura, K., Ueno, N., Kohda, D., Inagaki, F., and Sumimoto, H. (2006). Activation of the superoxide-producing phagocyte NADPH oxidase requires co-operation between the tandem SH3 domains of p47phox in recognition of a polyproline type II helix and an adjacent alpha-helix of p22phox. Biochem J *396*, 183-192.

Nunoi, H., Rotrosen, D., Gallin, J. I., and Malech, H. L. (1988). Two forms of autosomal chronic granulomatous disease lack distinct neutrophil cytosol factors. Science *242*, 1298-1301.

Ogura, K., Nobuhisa, I., Yuzawa, S., Takeya, R., Torikai, S., Saikawa, K., Sumimoto, H., and Inagaki, F. (2005). NMR solution structure of the tandem SH3 domains of p47phox complexed with a p22phox derived proline-rich peptide. J Biol Chem.

Ogura, Y., Inohara, N., Benito, A., Chen, F. F., Yamaoka, S., and Nunez, G. (2001). Nod2, a Nod1/Apaf-1 family member that is restricted to monocytes and activates NF-kappaB. J Biol Chem *276*, 4812-4818.

Ottinger, E. A., Botfield, M. C., and Shoelson, S. E. (1998). Tandem SH2 domains confer high specificity in tyrosine kinase signaling. J Biol Chem *273*, 729-735.

Palucka, K., and Banchereau, J. (1999). Dendritic cells: a link between innate and adaptive immunity. J Clin Immunol *19*, 12-25.

Park, J. W., Ma, M., Ruedi, J. M., Smith, R. M., and Babior, B. M. (1992). The cytosolic components of the respiratory burst oxidase exist as a M(r) approximately 240,000 complex that acquires a membrane-binding site during activation of the oxidase in a cell-free system. J Biol Chem *267*, 17327-17332.

Parkos, C. A., Allen, R. A., Cochrane, C. G., and Jesaitis, A. J. (1987). Purified cytochrome b from human granulocyte plasma membrane is comprised of two polypeptides with relative molecular weights of 91,000 and 22,000. J Clin Invest *80*, 732-742.

Parkos, C. A., Dinauer, M. C., Jesaitis, A. J., Orkin, S. H., and Curnutte, J. T. (1989). Absence of both the 91kD and 22kD subunits of human neutrophil cytochrome b in two genetic forms of chronic granulomatous disease. Blood *73*, 1416-1420.

Parkos, C. A., Dinauer, M. C., Walker, L. E., Allen, R. A., Jesaitis, A. J., and Orkin, S. H. (1988). Primary structure and unique expression of the 22-kilodalton light chain of human neutrophil cytochrome b. Proc Natl Acad Sci U S A *85*, 3319-3323.

Pawson, T. (1995). Protein modules and signalling networks. Nature *373*, 573-580.

Pawson, T., and Nash, P. (2003). Assembly of cell regulatory systems through protein interaction domains. Science *300*, 445-452.

Peng, G., Huang, J., Boyd, M., and Kleinberg, M. E. (2003). Properties of phagocyte NADPH oxidase p47-phox mutants with unmasked SH3 (Src homology 3) domains: full reconstitution of oxidase activity in a semi-recombinant cell-free system lacking arachidonic acid. Biochem J *373*, 221-229.

Perozzo, R., Folkers, G., and Scapozza, L. (2004). Thermodynamics of protein-ligand interactions: history, presence, and future aspects. J Recept Signal Transduct Res *24*, 1-52.

Pierce, M. M., Raman, C. S., and Nall, B. T. (1999). Isothermal titration calorimetry of protein-protein interactions. Methods *19*, 213-221.

Plaut, M., Pierce, J. H., Watson, C. J., Hanley-Hyde, J., Nordan, R. P., and Paul, W. E. (1989). Mast cell lines produce lymphokines in response to cross-linkage of Fc epsilon RI or to calcium ionophores. Nature *339*, 64-67.

Poltorak, A., He, X., Smirnova, I., Liu, M. Y., Van Huffel, C., Du, X., Birdwell, D., Alejos, E., Silva, M., Galanos, C., *et al.* (1998). Defective LPS signaling in C3H/HeJ and C57BL/10ScCr mice: mutations in Tlr4 gene. Science *282*, 2085-2088.

Ponting, C. P. (1996). Novel domains in NADPH oxidase subunits, sorting nexins, and PtdIns 3-kinases: binding partners of SH3 domains? Protein Sci *5*, 2353-2357.

Ponting, C. P., Ito, T., Moscat, J., Diaz-Meco, M. T., Inagaki, F., and Sumimoto, H. (2002). OPR, PC and AID: all in the PB1 family. Trends Biochem Sci *27*, 10.

Prehoda, K. E., and Lim, W. A. (2001). The double life of PX domains. Nat Struct Biol *8*, 570-572.

Quinn, M. T., Mullen, M. L., and Jesaitis, A. J. (1992). Human neutrophil cytochrome b contains multiple hemes. Evidence for heme associated with both subunits. J Biol Chem *267*, 7303-7309.

Rao, V. R., Corradetti, M. N., Chen, J., Peng, J., Yuan, J., Prestwich, G. D., and Brugge, J. S. (1999). Expression cloning of protein targets for 3-phosphorylated phosphoinositides. J Biol Chem *274*, 37893-37900.

Reeves, E. P., Lu, H., Jacobs, H. L., Messina, C. G., Bolsover, S., Gabella, G., Potma, E. O., Warley, A., Roes, J., and Segal, A. W. (2002). Killing activity of neutrophils is mediated through activation of proteases by K+ flux. Nature *416*, 291-297.

Reeves, E. P., Nagl, M., Godovac-Zimmermann, J., and Segal, A. W. (2003). Reassessment of the microbicidal activity of reactive oxygen species and hypochlorous

acid with reference to the phagocytic vacuole of the neutrophil granulocyte. J Med Microbiol *52*, 643-651.

Reid, K. B. (1986). Activation and control of the complement system. Essays Biochem *22*, 27-68.

Reid, K. B., and Day, A. J. (1989). Structure-function relationships of the complement components. Immunol Today *10*, 177-180.

Ren, R., Mayer, B. J., Cicchetti, P., and Baltimore, D. (1993). Identification of a ten-amino acid proline-rich SH3 binding site. Science *259*, 1157-1161.

Roberts, A. W., Kim, C., Zhen, L., Lowe, J. B., Kapur, R., Petryniak, B., Spaetti, A., Pollock, J. D., Borneo, J. B., Bradford, G. B., *et al.* (1999). Deficiency of the hematopoietic cell-specific Rho family GTPase Rac2 is characterized by abnormalities in neutrophil function and host defense. Immunity *10*, 183-196.

Rodger, A., and Ismail, M. (2000). Introduction to circular Dichroism, In Spectrophotometry & Spectrofluorimetry, M. Gore, ed. (Oxford: Oxford University Press), pp. 99-139.

Rogan, M. P., Geraghty, P., Greene, C. M., O'Neill, S. J., Taggart, C. C., and McElvaney, N. G. (2006). Antimicrobial proteins and polypeptides in pulmonary innate defence. Respir Res *7*, 29.

Roos, D., de Boer, M., Kuribayashi, F., Meischl, C., Weening, R. S., Segal, A. W., Ahlin, A., Nemet, K., Hossle, J. P., Bernatowska-Matuszkiewicz, E., and Middleton-Price, H. (1996). Mutations in the X-linked and autosomal recessive forms of chronic granulomatous disease. Blood *87*, 1663-1681.

Rossi, F., and Zatti, M. (1964). Biochemical aspects of phagocytosis in polymorphonuclear leucocytes. NADH and NADPH oxidation by the granules of resting and phagocytizing cells. Experientia *20*, 21-23.

Rotrosen, D., Yeung, C. L., Leto, T. L., Malech, H. L., and Kwong, C. H. (1992). Cytochrome b558: the flavin-binding component of the phagocyte NADPH oxidase. Science *256*, 1459-1462.

Royer-Pokora, B., Kunkel, L. M., Monaco, A. P., Goff, S. C., Newburger, P. E., Baehner, R. L., Cole, F. S., Curnutte, J. T., and Orkin, S. H. (1986). Cloning the gene for an inherited human disorder--chronic granulomatous disease--on the basis of its chromosomal location. Nature *322*, 32-38.

Ryan, G. B., and Hurley, J. V. (1966). The chemotaxis of polymorphonuclear leucocytes towards damaged tissue. Br J Exp Pathol *47*, 530-536.

Sambrook, J., Fritsch, E., and Maniatis, T. (1989). Molecular Cloning, A Laboratory Manual, 2nd edn: (Cold Spring Harbor Laboratory Press).

Sarfstein, R., Gorzalczany, Y., Mizrahi, A., Berdichevsky, Y., Molshanski-Mor, S., Weinbaum, C., Hirshberg, M., Dagher, M. C., and Pick, E. (2004). Dual role of Rac in the assembly of NADPH oxidase, tethering to the membrane and activation of p67phox: a study based on mutagenesis of p67phox-Rac1 chimeras. J Biol Chem *279*, 16007-16016.

Sathyamoorthy, M., de Mendez, I., Adams, A. G., and Leto, T. L. (1997). p40(phox) down-regulates NADPH oxidase activity through interactions with its SH3 domain. J Biol Chem *272*, 9141-9146.

Savitzky, A., and Golay, M. (1964). Smoothing and Differentiation of Data by Simplified Least Squares Procedures. Analytical Chemistry *36*, 1627-1639.

Sbarra, A. J., and Karnovsky, M. L. (1959). The biochemical basis of phagocytosis. I. Metabolic changes during the ingestion of particles by polymorphonuclear leukocytes. J Biol Chem *234*, 1355-1362.

Scapini, P., Lapinet-Vera, J. A., Gasperini, S., Calzetti, F., Bazzoni, F., and Cassatella, M. A. (2000). The neutrophil as a cellular source of chemokines. Immunol Rev *177*, 195-203.

Scheffzek, K., Stephan, I., Jensen, O. N., Illenberger, D., and Gierschik, P. (2000). The Rac-RhoGDI complex and the structural basis for the regulation of Rho proteins by RhoGDI. Nat Struct Biol *7*, 122-126.

Scheufler, C., Brinker, A., Bourenkov, G., Pegoraro, S., Moroder, L., Bartunik, H., Hartl, F. U., and Moarefi, I. (2000). Structure of TPR domain-peptide complexes:

critical elements in the assembly of the Hsp70-Hsp90 multichaperone machine. Cell *101*, 199-210.

Schiffmann, E., Corcoran, B. A., and Wahl, S. M. (1975). N-formylmethionyl peptides as chemoattractants for leucocytes. Proc Natl Acad Sci U S A *72*, 1059-1062.

Schwandner, R., Dziarski, R., Wesche, H., Rothe, M., and Kirschning, C. J. (1999). Peptidoglycan- and lipoteichoic acid-induced cell activation is mediated by toll-like receptor 2. J Biol Chem *274*, 17406-17409.

Segal, A. W. (1987). Absence of both cytochrome b-245 subunits from neutrophils in X-linked chronic granulomatous disease. Nature *326*, 88-91.

Segal, A. W. (1996). The NADPH oxidase and chronic granulomatous disease. Mol Med Today *2*, 129-135.

Segal, A. W. (2005). How neutrophils kill microbes. Annu Rev Immunol *23*, 197-223.

Segal, A. W., Garcia, R. C., Harper, A. M., and Banga, J. P. (1983). Iodination by stimulated human neutrophils. Studies on its stoichiometry, subcellular localization and relevance to microbial killing. Biochem J *210*, 215-225.

Segal, A. W., Geisow, M., Garcia, R., Harper, A., and Miller, R. (1981). The respiratory burst of phagocytic cells is associated with a rise in vacuolar pH. Nature *290*, 406-409.

Segal, A. W., Heyworth, P. G., Cockcroft, S., and Barrowman, M. M. (1985). Stimulated neutrophils from patients with autosomal recessive chronic granulomatous disease fail to phosphorylate a Mr-44,000 protein. Nature *316*, 547-549.

Segal, A. W., and Jones, O. T. (1979). The subcellular distribution and some properties of the cytochrome b component of the microbicidal oxidase system of human neutrophils. Biochem J *182*, 181-188.

Segal, A. W., West, I., Wientjes, F., Nugent, J. H., Chavan, A. J., Haley, B., Garcia, R. C., Rosen, H., and Scrace, G. (1992). Cytochrome b-245 is a flavocytochrome containing FAD and the NADPH-binding site of the microbicidal oxidase of phagocytes. Biochem J *284 (Pt 3)*, 781-788.

Seino, K., and Taniguchi, M. (2004). Functional roles of NKT cell in the immune system. Front Biosci *9*, 2577-2587.

Sicheri, F., Moarefi, I., and Kuriyan, J. (1997). Crystal structure of the Src family tyrosine kinase Hck. Nature *385*, 602-609.

Sikorski, R. S., Boguski, M. S., Goebl, M., and Hieter, P. (1990). A repeating amino acid motif in CDC23 defines a family of proteins and a new relationship among genes required for mitosis and RNA synthesis. Cell *60*, 307-317.

Simonsen, A., and Stenmark, H. (2001). PX domains: attracted by phosphoinositides. Nat Cell Biol *3*, E179-182.

Smith, R. M., Connor, J. A., Chen, L. M., and Babior, B. M. (1996). The cytosolic subunit p67phox contains an NADPH-binding site that participates in catalysis by the leukocyte NADPH oxidase. J Clin Invest *98*, 977-983.

Someya, A., Nagaoka, I., and Yamashita, T. (1993). Purification of the 260 kDa cytosolic complex involved in the superoxide production of guinea pig neutrophils. FEBS Lett *330*, 215-218.

Sreerama, N., and Woody, R. (2000). Estimation of Protein Secondary Structure from Circular Dichroism Spectra: Comparison of CONTIN, SELCON, and CDSSTR Methods with an Expanded Reference Set. Anal Biochem *287*, 252-260.

Stahl, P. D., and Ezekowitz, R. A. (1998). The mannose receptor is a pattern recognition receptor involved in host defense. Curr Opin Immunol *10*, 50-55.

Stuart, L. M., and Ezekowitz, R. A. (2005). Phagocytosis: elegant complexity. Immunity *22*, 539-550.

Styrt, B., and Klempner, M. S. (1982). Internal pH of human neutrophil lysosomes. FEBS Lett *149*, 113-116.

Suire, S., Hawkins, P., and Stephens, L. (2002). Activation of phosphoinositide 3-kinase gamma by Ras. Curr Biol *12*, 1068-1075.

Sumimoto, H., Hata, K., Mizuki, K., Ito, T., Kage, Y., Sakaki, Y., Fukumaki, Y., Nakamura, M., and Takeshige, K. (1996). Assembly and activation of the phagocyte NADPH oxidase. Specific interaction of the N-terminal Src homology 3 domain of p47phox with p22phox is required for activation of the NADPH oxidase. J Biol Chem *271*, 22152-22158.

Sumimoto, H., Kage, Y., Nunoi, H., Sasaki, H., Nose, T., Fukumaki, Y., Ohno, M., Minakami, S., and Takeshige, K. (1994). Role of Src homology 3 domains in assembly and activation of the phagocyte NADPH oxidase. Proc Natl Acad Sci U S A *91*, 5345-5349.

Sumimoto, H., Sakamoto, N., Nozaki, M., Sakaki, Y., Takeshige, K., and Minakami, S. (1992). Cytochrome b558, a component of the phagocyte NADPH oxidase, is a flavoprotein. Biochem Biophys Res Commun *186*, 1368-1375.

Szabo, A. (2000). Fluorescence principles and measurments (Oxford: Oxford University Press).

Takai, Y., Sasaki, T., and Matozaki, T. (2001). Small GTP-binding proteins. Physiol Rev *81*, 153-208.

Takeda, K., and Akira, S. (2005). Toll-like receptors in innate immunity. Int Immunol *17*, 1-14.

Takeuchi, O., Hoshino, K., Kawai, T., Sanjo, H., Takada, H., Ogawa, T., Takeda, K., and Akira, S. (1999). Differential roles of TLR2 and TLR4 in recognition of gram-negative and gram-positive bacterial cell wall components. Immunity *11*, 443-451.

Taylor, W. R., Jones, D. T., and Segal, A. W. (1993). A structural model for the nucleotide binding domains of the flavocytochrome b-245 beta-chain. Protein Sci *2*, 1675-1685.

Terasawa, H., Kohda, D., Hatanaka, H., Tsuchiya, S., Ogura, K., Nagata, K., Ishii, S., Mandiyan, V., Ullrich, A., Schlessinger, J., and et al. (1994). Structure of the N-terminal SH3 domain of GRB2 complexed with a peptide from the guanine nucleotide releasing factor Sos. Nat Struct Biol *1*, 891-897.

Thomas, C. C., Dowler, S., Deak, M., Alessi, D. R., and van Aalten, D. M. (2001). Crystal structure of the phosphatidylinositol 3,4-bisphosphate-binding pleckstrin homology (PH) domain of tandem PH-domain-containing protein 1 (TAPP1): molecular basis of lipid specificity. Biochem J *358*, 287-294.

Thrasher, A. J., Keep, N. H., Wientjes, F., and Segal, A. W. (1994). Chronic granulomatous disease. Biochim Biophys Acta *1227*, 1-24.

Tkalcevic, J., Novelli, M., Phylactides, M., Iredale, J. P., Segal, A. W., and Roes, J. (2000). Impaired immunity and enhanced resistance to endotoxin in the absence of neutrophil elastase and cathepsin G. Immunity *12*, 201-210.

Tomlinson, S. (1993). Complement defense mechanisms. Curr Opin Immunol *5*, 83-89.

Tortorella, D., and London, E. (1994). Method for efficient pelleting of small unilamellar model membrane vesicles. Anal Biochem *217*, 176-180.

Tsunawaki, S., Kagara, S., Yoshikawa, K., Yoshida, L. S., Kuratsuji, T., and Namiki, H. (1996). Involvement of p40phox in activation of phagocyte NADPH oxidase through association of its carboxyl-terminal, but not its amino-terminal, with p67phox. J Exp Med *184*, 893-902.

Van Kaer, L., and Joyce, S. (2005). Innate immunity: NKT cells in the spotlight. Curr Biol *15*, R429-431.

Volpp, B. D., Nauseef, W. M., and Clark, R. A. (1988). Two cytosolic neutrophil oxidase components absent in autosomal chronic granulomatous disease. Science *242*, 1295-1297.

Wallach, T. M., and Segal, A. W. (1996). Stoichiometry of the subunits of flavocytochrome b558 of the NADPH oxidase of phagocytes. Biochem J *320 (Pt 1)*, 33-38.

Wientjes, F. B., Hsuan, J. J., Totty, N. F., and Segal, A. W. (1993). p40phox, a third cytosolic component of the activation complex of the NADPH oxidase to contain src homology 3 domains. Biochem J *296 (Pt 3)*, 557-561.

Wientjes, F. B., Panayotou, G., Reeves, E., and Segal, A. W. (1996). Interactions between cytosolic components of the NADPH oxidase: p40phox interacts with both p67phox and p47phox. Biochem J *317 (Pt 3)*, 919-924.

Williams, J. C., Weijland, A., Gonfloni, S., Thompson, A., Courtneidge, S. A., Superti-Furga, G., and Wierenga, R. K. (1997). The 2.35 A crystal structure of the inactivated form of chicken Src: a dynamic molecule with multiple regulatory interactions. J Mol Biol *274*, 757-775.

Wilson, M. I., Gill, D. J., Perisic, O., Quinn, M. T., and Williams, R. L. (2003). PB1 domain-mediated heterodimerization in NADPH oxidase and signaling complexes of atypical protein kinase C with Par6 and p62. Mol Cell *12*, 39-50.

Winkelstein, J. A., Marino, M. C., Johnston, R. B., Jr., Boyle, J., Curnutte, J., Gallin, J. I., Malech, H. L., Holland, S. M., Ochs, H., Quie, P., *et al.* (2000). Chronic granulomatous disease. Report on a national registry of 368 patients. Medicine (Baltimore) *79*, 155-169.

Wiseman, T., Williston, S., Brandts, J. F., and Lin, L. N. (1989). Rapid measurement of binding constants and heats of binding using a new titration calorimeter. Anal Biochem *179*, 131-137.

Wishart, M. J., Taylor, G. S., and Dixon, J. E. (2001). Phoxy lipids: revealing PX domains as phosphoinositide binding modules. Cell *105*, 817-820.

Wodnar-Filipowicz, A., Heusser, C. H., and Moroni, C. (1989). Production of the haemopoietic growth factors GM-CSF and interleukin-3 by mast cells in response to IgE receptor-mediated activation. Nature *339*, 150-152.

Xu, W., Harrison, S. C., and Eck, M. J. (1997). Three-dimensional structure of the tyrosine kinase c-Src. Nature *385*, 595-602.

Xu, X., Barry, D. C., Settleman, J., Schwartz, M. A., and Bokoch, G. M. (1994). Differing structural requirements for GTPase-activating protein responsiveness and NADPH oxidase activation by Rac. J Biol Chem *269*, 23569-23574.

Yamaguchi, T., Hayakawa, T., Kaneda, M., Kakinuma, K., and Yoshikawa, A. (1989). Purification and some properties of the small subunit of cytochrome b558 from human neutrophils. J Biol Chem *264*, 112-118.

Yang, J. T., Wu, C. S., and Martinez, H. M. (1986). Calculation of protein conformation from circular dichroism. Methods Enzymol *130*, 208-269.

Young, M. A., Gonfloni, S., Superti-Furga, G., Roux, B., and Kuriyan, J. (2001). Dynamic coupling between the SH2 and SH3 domains of c-Src and Hck underlies their inactivation by C-terminal tyrosine phosphorylation. Cell *105*, 115-126.

Yu, H., Rosen, M. K., Shin, T. B., Seidel-Dugan, C., Brugge, J. S., and Schreiber, S. L. (1992). Solution structure of the SH3 domain of Src and identification of its ligand-binding site. Science *258*, 1665-1668.

Yu, L., Quinn, M. T., Cross, A. R., and Dinauer, M. C. (1998). Gp91(phox) is the heme binding subunit of the superoxide-generating NADPH oxidase. Proc Natl Acad Sci U S A *95*, 7993-7998.

Yuzawa, S., Ogura, K., Horiuchi, M., Suzuki, N. N., Fujioka, Y., Kataoka, M., Sumimoto, H., and Inagaki, F. (2004a). Solution structure of the tandem Src homology 3 domains of p47phox in an autoinhibited form. J Biol Chem *279*, 29752-29760.

Yuzawa, S., Suzuki, N. N., Fujioka, Y., Ogura, K., Sumimoto, H., and Inagaki, F. (2004b). A molecular mechanism for autoinhibition of the tandem SH3 domains of p47phox, the regulatory subunit of the phagocyte NADPH oxidase. Genes Cells *9*, 443-456.

Zhan, Y., Virbasius, J. V., Song, X., Pomerleau, D. P., and Zhou, G. W. (2002). The p40phox and p47phox PX domains of NADPH oxidase target cell membranes via direct and indirect recruitment by phosphoinositides. J Biol Chem *277*, 4512-4518.

APPENDIX

A1 General reagents

Table 20: General reagents and suppliers.

REAGENT	SUPPLIER
40 % w/v acrylamide/bisacrylamide (37:5:1)	Bio-Rad
Agarose	Invitrogen
Ammonium persulfate (APS)	Bio-Rad
Ampicillin	Sigma
β-mercaptoethanol	Sigma
Benzamidine	Sigma
Bis/Tris pre-cast gels (NOVEX)	Invitrogen
Bovine serum albumin (BSA)	Sigma
Bromophenol blue	BDH
CAPS	Sigma
Chlorofom	Sigma
DTT	Sigma
EDTA	Sigma
Ethidium bromide	Bio-Rad
Ethanol	Fisher scientific
Glutathione sepharose 4B resin	Amersham biosciences
Glycerol	BDH AnalaR
Hepes	Calbiochem
HCl	Fisher Scientific
Imidazole	Fluka
IPTG	Biogene
Loading buffer (6 X) (for agarose gels)	Novagen
Low molecular weight protein marker	Amersham biosciences
MES SDS running buffer (10 X)	Invitrogen
Methanol	Fisher Scientific
Ni-NTA resin	Qiagen
NP-40	Sigma
PCR marker	Novagen
Protease inhibitor cocktail tablets (EDTA free)	Roche

Reduced glutathione	Sigma
SDS running buffer (10 X)	National diagnostics
SeaBlue Plus 2 marker	Invitrogen
Shrimp alkaline phosphatase	Roche
Simply blue safe stain	Invitrogen
Sodium chloride	BDH AnalaR
T4 DNA ligase	Promega
TE buffer	Qiagen
TEMED	Bio-Rad
Thrombin	Merck Biosciences
Tris	BDH AnalaR
Triton X-100	Sigma
Tween-20	Aldrich

A2 Media and cells

Media

Luria-Bertani broth/agar (LB)

Bactotryptone	10 g/L
Yeast extract	5 g/L
NaCl	10 g/L
Distilled water	1 litre

Terrific broth (TB) *Mix 900 ml of A with 100 ml of B*

Part A		*Part B*	
Tryptone	12 g/L	K_2HPO_4 (0.72 M)	12.5 g/L
Yeast extract	24 g/L	KH_2PO_4 (0.17 M)	2 g/L
Glycerol	4 ml/L	Distilled water	100 ml
Distilled water	900 ml		

Bacterial cell strains

All cell strains were purchased from Novagen. NovaBlue cells were used for initial cloning and plasmid purification and BLR21(DE3) cells were used for protein expression.

Table 21: Genotypes of *E.coli* cells strains.

***E. coli* cell strains**	**Genotype**
NovaBlue	endA1 hsdR17 ($r_{K12}^-m_{K12}^+$) supE44 thi-1 recA1 gyrA96 relA1 lac F'[$proA^+B^+$ $lacI^q$ ZΔM15::Tn10 (Tc^R)]
BL21(DE3)	F^- ompT $hsdS_B(r_B^-m_B)$ gal dcm (DE3)

A3 SDS-PAGE and agarose gels compositions

SDS gels

4 X sample buffer

0.5 M Tris (pH 6.8)

Glycerol (40 % v/v)

10 % (w/v) SDS

100 mM DTT

0.05 % (w/v) bromophenol blue

Resolving buffer

1.5 M Tris (pH 8.8)

0.15 % SDS

Stacking buffer

0.5 M Tris (pH 6.8)

0.15 % SDS

Table 22: Composition of a 12 % SDS gel.

Reagent	Volumes for resolving gel	Volumes for stacking gel
40 % Acrylamide Bis solution	3 ml	0.7 ml
Resolving buffer/stacking buffer	2.5 ml	1.25 ml
Distilled water	4.5 ml	3 ml
10 % APS	100 µl	50 µl
TEMED	10 µl	5 µl

Agarose gels

Table 23: Composition of a 1 % agarose gel.

Reagent	Volume
Agarose	1 g
1 X TAE (40 mM Tris Acetate (pH 7.7), 1 mM EDTA)	100 ml
Ethidium bromide (10 mg/ml)	2 µl

A4 Buffers and peptides

Buffer compositions

The pH of buffers was adjusted to be one unit above or below the pI of the protein.

Buffer A

50 mM Hepes
300 mM NaCl
4 mM DTT
2 mM EDTA
4 mM benzamidine
Two protease inhibitor cocktail tablets (per 200 ml buffer)

Buffer B

50 mM Hepes
1 M NaCl
4 mM DTT
2 mM EDTA
4 mM benzamidine

Buffer C

50 mM Hepes
50 mM NaCl
1 mM EDTA
4 mM DTT
(Add 15 mM reduced-glutathione for GST-fusion protein elution)

Buffer D

50 mM Hepes
300 mM NaCl
20 mM imidazole
5 mM β-mercaptoethanol

Buffer E

50 mM Hepes
300 mM NaCl
1 M imidazole
5 mM β-mercaptoethanol

Buffer F

50 mM Hepes
50 mM NaCl
1 mM EDTA
2 mM DTT

Buffer G

50 mM Hepes
500 mM NaCl
1 mM EDTA

Buffer H

50 mM Hepes
100 mM NaCl
1 mM EDTA

Peptides

Dr. W. Mawby, University of Bristol, UK prepared the 35-mer peptide representing the $p47^{phox}$ polybasic region (peptide 1) (aa 296-330). An 18-mer peptide representing the proline-rich region of $p22^{phox}$ was prepared by Peter Fletcher (NIMR) (peptide 2), plus an identical peptide with a fluoresceine label attached (peptide 3) (aa 149-166).

RGAPPRRSSIRNAHSIHQRSRKRLSQDAYRRNSVR (peptide 1)

KQPPSNPPPRPPAEARKK (peptide 2)

$^{\text{fluoresceine}}$**KQPPSNPPPRPPAEARKK** (peptide 3)

A5 Oligonucleotides

Table 24 shows the oligonucleotides used in this study. Substitution of a specific wild-type residue to a mutant residue e.g. Glu → Ala at position 218 is shown as E218A.

Table 24: Oligonucleotides used for the cloning of $p47^{phox}$ mutants.

$p47^{phox}$ mutants	Sense primer (5-3)	Antisense primer (3-5)	Codon substitution shown for sense strand
S8E-His_6	CCAAGCGGAAGCTGGC GTCTGCCGTCCACCACC ACCACCACCACTGAGC GGCCGCTAAACTAT	ATAGTTTAGCGGCCGC TCAGTGGTGGTGGTGG TGGTGGACGGCAGAC GCCAGCTTCCGCTTGG	Addition of His_6 tag onto the N-terminus of full-length $p47^{phox}$
S379E	CTCATCCTGAACCGCTG CGAGGAGAGCACCAAG CGGAAG	CTTCCGCTTGGTGCTC TCCTCGCAGCGGTTCA GGATGAG	AGC→GAG
W193R_A	GAAGAGCGAGAGCGGT CGGTGGTTCTGTCAGAT GAAAG	CTTTCATCTGACAGAA CCACCGACCGCTCTCG CTCTTC	TGG→CGG
W194R_A	GAGAAGAGCGAGAGCG GTTGGCGATTCTGTCAG ATGAAAGCAAAG	CTTTGCTTTCATCTGA CAGAATCGCCAACCG CTCTCGCTCTTCTC	TGG→CGA
W194A_A	AGCGAGAGCGGTTGGG CGTTCTGTCAGATGAAA	TTTCATCTGACAGAAC GCCCAACCGCTCTCGC T	TGG→GCG
W263R_B	CAAGCTCCTGGACGGCC GGTGGGTCATCAGGAA AG	CTTTCCTGATGACCCA CCGGCCGTCCAGGAG CTTG	TGG→CGG
W264R_B	CACAAGCTCCTGGACG GCTGGCGAGTCATCAG GAAAGACGACGTC	GACGTCGTCTTTCCTG ATGACTCGCCAGCCGT CCAGGAGCTTGTG	TGG→CGA
W264A_B	CTCCTGGACGGCTGGGC GGTCATCAGGAAAGAC	GTCTTTCCTGATGACC GCCCAGCCGTCCAGG AG	TGG→GCG

E218E	CTGGACAGTCCTGACGC GACGGAGGATCCTGA GCCCAACTATGC	GCATAGTTGGGCTCAG GATCCTCCGTCGCGTC AGGACTGTCCAG	GAG→GCG
E220A	GGACAGTCCTGACGAG ACCGCGGACCCTGAGC CCAACTATGC	GCATAGTTGGGCTCAG GGTCCGCGGTCTCGTC AGGACTGTCC	GAA→GCG
D221A	GGACAGTCCTGACGAG ACGGAAGCCCCTGAGC CCAACTATGC	GCATAGTTGGGCTCAG GGGCTTCCGTCTCGTC AGGACTGTCC	GAC→GCC
D/E3A	CTGGACAGTCCTGACGC GACGGCAGCCCCTGAG CCCAACTATGC	GCATAGTTGGGCTCAG GGGCTGCCGTCGCGTC AGGACTGTCCAG	GAG→GCG GAA→GCG GAC→GCC
3PA	CCCCTGGACAGTGCGG ACGAGACGGAAGACGC GGAGGCGAACTATGCA GGTGAG	CTCACCTGCATAGTTC GCCTCCGCGTCTTCCG TCTCGTCCGCACTGTC CAGGGG	CCT→GCG CCT→GCG CCC→GCG
A1$^-$	CCTGAGCCCAACTATGG TGAGCCATACGTC	GACGTATGGCTCACCA TAGTTGGGCTCAGG	GCA→deletion
A1$^+$	CCTGAGCCCAACTATGC AGCAGGTGAGCCATAC GTC	GACGTATGGCTCACCT GCTGCATAGTTGGGCT CAGG	Addition of two GCA's
A2$^+$	CCTGAGCCCAACTATGC AGCAGCAGGTGAGCCA TACGTC	GACGTATGGCTCACCT GCTGCTGCATAGTTGG GCTCAGG	Addition of two GCA

A6 Circular dichroism results

Circular dichroism measurements of the p47^{phox} linker and GWW motif mutants

Figure 66 shows CD spectra for the various p47^{phox} mutant proteins (tandem SH3 domain construct; aa 156-285) and p47^{phox}Wild-type$_{tandem}$. All the spectra show a minimum at approximately 203 nm and a maximum at approximately 223 nm, which is characteristic of a protein with a large β-sheet content. The secondary structure content of these proteins was calculated using the methods described by (Sreerama and Woody, 2000). Importantly, all the mutant proteins have a similar secondary structure content to p47^{phox}Wild-type$_{tandem}$ (within the acceptable 10 % error margin) indicating that changes in ligand binding are not solely due to a loss in secondary structure.

In comparison to p47^{phox}Wild-type$_{tandem}$, two triple mutant proteins: p47^{phox}D/E3A$_{tandem}$ and p47^{phox}3PA$_{tandem}$, and the individual mutant p47^{phox}E218A$_{tandem}$ showed the largest changes in binding affinity, upon binding to the p47^{phox} 35-mer polybasic region peptide and/or p22^{phox} peptide. Similar was observed for p47^{phox}W193R$_{A\text{-}tandem}$ and p47^{phox}W263R$_{B\text{-}tandem}$ on binding to the p22^{phox*} peptide. Thermal unfolding of these mutant proteins was measured at 224 nm with increasing temperature (20 °C-80 °C). Figure 67 shows the thermal scans for p47^{phox}D/E3A$_{tandem}$, p47^{phox}3PA$_{tandem}$, p47^{phox}E218A$_{tandem}$, p47^{phox}W193R$_{A\text{-}tandem}$ and p47^{phox}W263R$_{B\text{-}tandem}$. All the proteins have a similar mid-point for unfolding of approximately 53 °C, which were all reversible. This suggests that the mutations do not have any major effects on the thermal stability of the proteins.

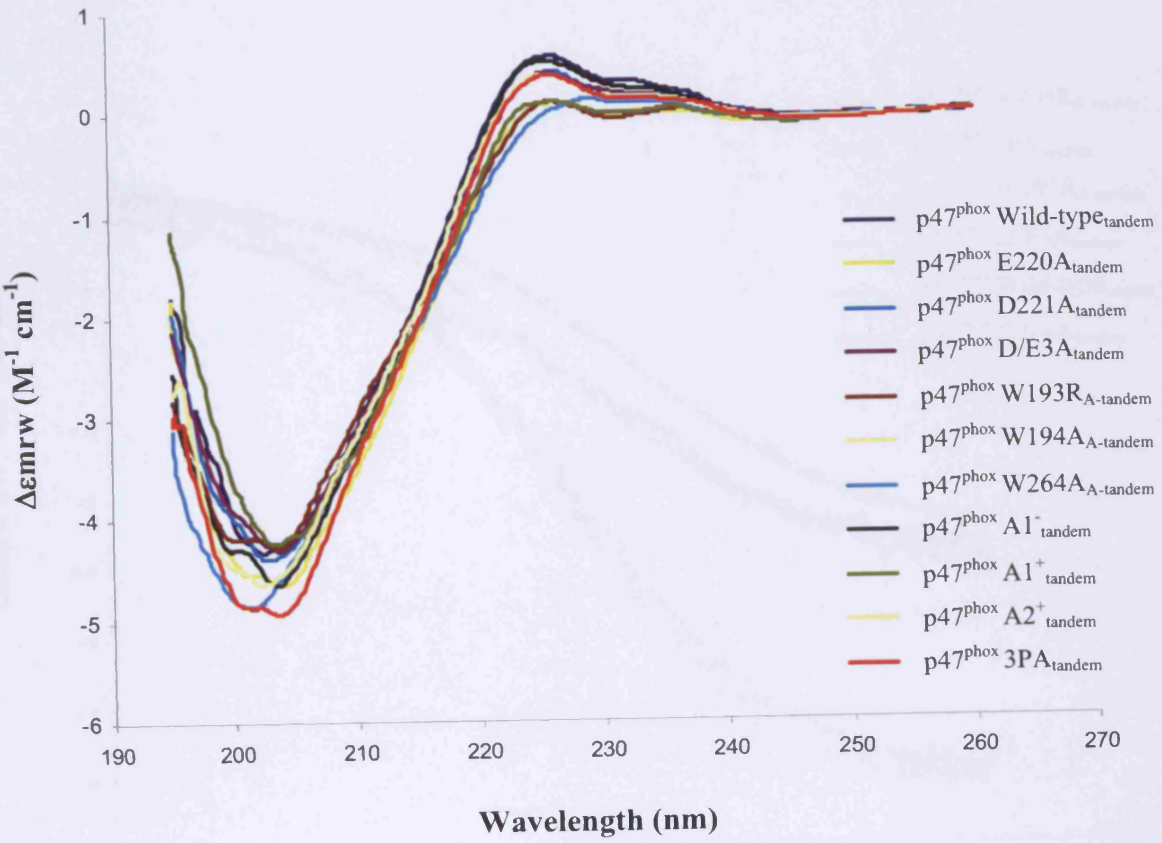

Figure 66: CD spectra of p47^{phox} tandem SH3 domain mutants. Far-UV CD spectra of the various p47^{phox} tandem SH3 domain mutants and p47^{phox}Wild-type$_{tandem}$ (aa 156-285). Spectra were taken in buffer H at a protein concentration of 0.15 mg/ml.

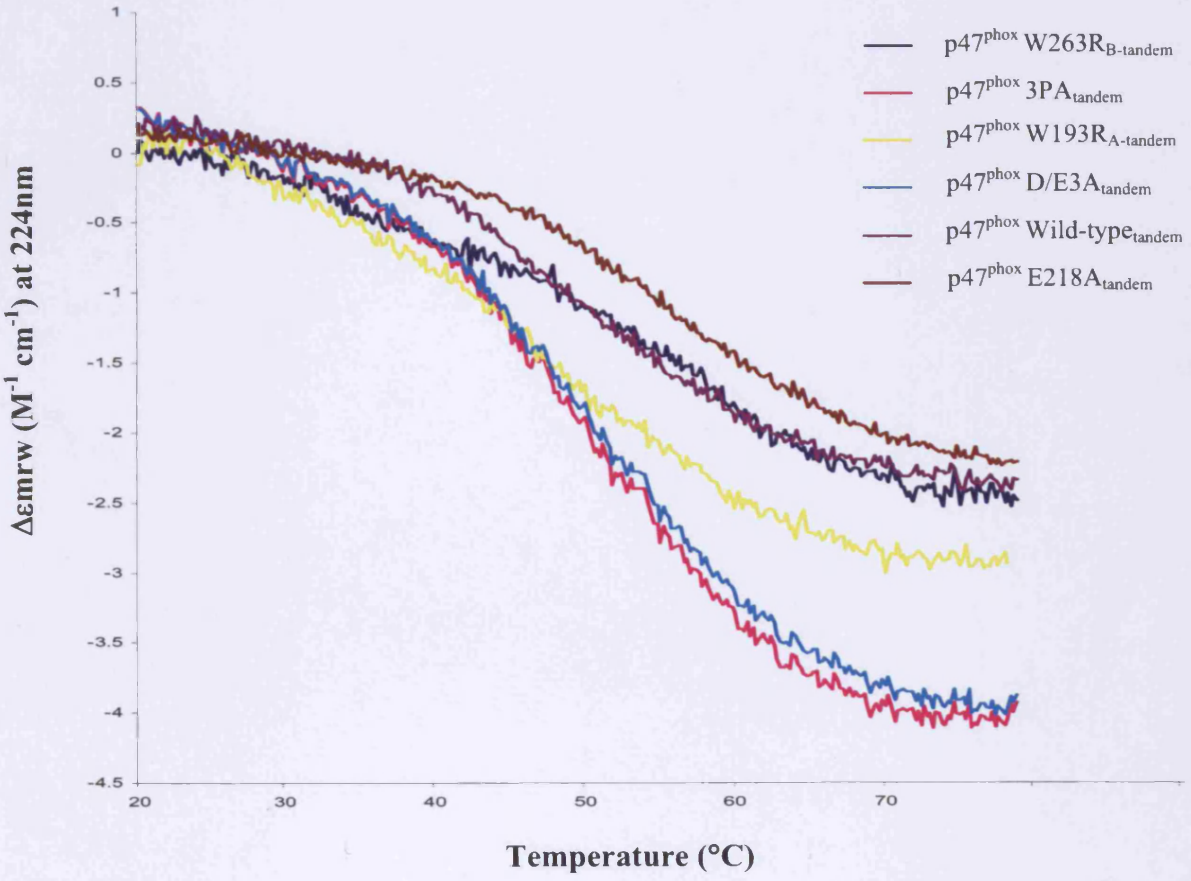

Figure 67: Thermal denaturation curves for p47^{phox} tandem SH3 domain mutants. The ellipiticity of the mutant proteins and p47^{phox}Wild-type$_{tandem}$ (aa 156-285) were continuously measured at 224 nm as the temperature was increased from 20 °C to 80 °C. The scans were measured in buffer H at a protein concentration of 0.15 mg/ml.